



From photon to product – Development and quantitative assessment of photosynthesis-driven oxygenase biocatalysis with cyanobacteria

Dissertation

Zur Erlangung des

Doktorgrades der Naturwissenschaften (Dr. rer.nat.)

der naturwissenschaftlichen Fakultät I – Biowissenschaften –

der Martin-Luther-Universität Halle-Wittenberg

Vorgelegt von

M.Sc. Adrian Tüllinghoff

Verteidigt am

23.05.2024

Gutachter:innen

Prof. Dr. Bruno Bühler

Prof. Dr. Markus Pietzsch

Prof. Dr. Julie Zedler

*Für Finja, Tarje, Hilja, Rune und allen Kindern:
Ihr verdient eine bessere Welt als diese.*

Acknowledgement

To finish a PhD is never an easy task. This is especially true when this stage of scientific career coincides with becoming a father of four. While this dual adventure made me fully alive the recent years, it is obvious that it would never have been possible without the continuous support of many people during the last months and years, whom I express my deepest gratitude.

My doctoral father, Bruno Bühler, I am deeply grateful for the scientific guidance, his sharp analytical mindset, his serenity, his tolerance to my errors, and his ruthlessly supportive attitude towards me and my project. Bruno, I am extremely lucky to have been part of your group, enabling me to mature both personally and scientifically in a constructive, warm, and joyful atmosphere. My supervisor, Jörg Toepel, I thank for his undaunted empathy, his pragmatic mindset, the invaluable motivation, but also his critical perspectives, shaping my way of thinking. Jörg, you could not only plant the fascination for photo-biotechnology in my heart, with your support it was fostered to flower – for sure better than my office plants.

My former Head of Department, Andreas Schmid, I thank for his visionary mindset and many fruitful discussions grinding my focus and my project. My present Head of Department, Hauke Harms, I thank for the constructive and open environment I could freely develop further. I thank all my colleagues from the former SOMA department, first and foremost, Sara, Samu, Fabi, Mahir, Hannah and Paul, for inspiration, motivation, constructive criticism, and a deep understanding of all ups and downs a PhD candidate feels. Thanks to all present and former members of the applied biocatalysis group – Caro, Diletta, Lisa, Tim, Sonja – for everlasting meetings and discussions and for never giving up on bringing (photo-)biotechnology further. I thank the technical staff, especially Daniel and Peter, but also Ron, Kristin, Pål, Jochen and Sebastian for all their support, advice and hands-on knowledge I received from you during the last years. Thanks to all (former) colleagues – Amadeus, Amelie, Anja, Anna, Artem, Bin, Caro R, Christian, Claudius, Corinna, Florian F, Franz, Franziska, Hans, Heiko, Inge, Isabel, Jacky, Jana, Jan-Hendrik, Jan-Simon, Jenny, Jens, Jianqi, Johanna, Johannes, Jonas, Juliane, Katharina, Katja, Laura, Linus, Lyn, Magda, Marcel, Maria, Martin (Wegner und Schirmer), Merle, Minmin, Moritz, Nina, Paul Bö, Robert, Rohan, Sabine, Selina, Seung Jae, Stephan, Susan, , Tillman, Valentina, Vincent, Vu – for a wonderful working environment, captivating due to openness, support, and a lot of fun while and after work.

I am deeply thankful for contribution from students under my supervision. Thank you, Maggie, for starting an exciting journey and for yielding my positive results during the first year. Thank you, Harcel, for your passion and your allegiance to my project bringing it a huge deal further. Thank you, Lieselotte, for your refreshing ideas and productive cooperation. Thanks also to Nina, Svea, Sonia, Bilkis, Florian, and Friederike for your time and effort, as well as all the

students in the practical course of applied biocatalysis, which was a pleasure to experience with you.

Persons external to UFZ accompanied me through the PhD period and supported me both directly and in the background. My advisor Peter Antes and my mentor Olaf Zenker I thank for their approachability and guidance. Youlia Spivak I thank for professional advices keeping me from falling to deep in my project and Eva Glanze I thank for excellent supervision to combine parenting and being a PhD. For scientific discussion and support I would like to acknowledge Julia und Thomas R, Michael, Marius, and Thomas Z. Last, I would like to express my gratitude to Cecilia for putting me on the scientific track, having been an exceptional mentor for gaining results and presenting them.

My parents Annette und HaJo and my sisters Ricarda and Cordula I am deeply thankful for your unconfined support, your respectful restraint, and your trust, never questioning that I will make it some day. I am sure that no word would be adequate to thank my marvelous wife Silja for her patience, her understanding, and almost unconditional loyalty to me and this project, being a big part of me in the last years. Silja, invisible in the lines and figures of my papers and writings, your support and love is and has been the fundament of my achievements. Finja und Tarje danke ich für ihr Lachen, ihre Herzlichkeit und ihre Neugier, und dafür, dass ihr mich jeden Tag aufs Neue herausfordert und mir unglaublich viel Freude bereitet. Und euch, Hilja und Rune, danke ich dafür, dass ihr mir ganz ohne Worte die Welt noch einmal neu erklärt und mir mit jedem Lächeln zeigt, dass die Wissenschaft doch nicht so wichtig ist, wie viele annehmen.

Preface

Since decades, the global surface temperature is on the rise. The Intergovernmental Panel on Climate Change describes this global warming, its causes, and its effects in regularly published reports. The latest Assessment Report elaborates on the newest research on global warming: Compared to 1850-1900, the global surface temperature has increased by 1.09 °C in 2011-2020, with an increase since 1970 being faster than in any other 50-year period during at least the last 2000 years.[1]

The effects already observed are tremendous:

“With high confidence, the climate change has caused widespread adverse impacts and related losses and damages to nature and people.”

Intergovernmental Panel on Climate Change Assessment report 6, Synthesis report

Among many others, this report subsumes dramatic loss of wild life, rising of sea levels, and ever more extreme weather situations threatening human life on earth.

Regarding the causes of climate change, there is no doubt: The main driver of global warming are human-caused greenhouse gas emissions, with the atmospheric carbon dioxide (CO₂) concentration accumulating to 410 ppm, which is with high confidence the highest value over the last two million years. In the face of destroying or own livelihood, actions to mitigate GHG emissions and thereby global warming were evolved and undertaken during the last decades, including policies and laws addressing mitigation. In this context, it is noteworthy that the costs for low to zero emission energy production have fallen by 55 to 85% (wind and solar energy, respectively) and that more and more low to zero emission production processes have been developed.[1]

Despite these promising developments, the assessment report unveils that the current mitigation as well as adaptation actions and policies are not sufficient to keep global warming below 1.5 °C in the 21st century. Clearly, innovative and disruptive technologies aiming for zero emission processes, or even better net CO₂ consumption, have to be developed to provide mankind with energy, food, and goods to ensure human life not only today but also in future.[1]

In this thesis, this general aim is tackled with a concrete idea, to come from photons to product or, in other words, to exploit the biochemical process of (oxygenic) photosynthesis for the biotechnological production of energy carriers and/or materials with sun light, CO₂, and H₂O as energy, carbon, and electron sources, respectively. The main research questions are how biotechnological reactions can efficiently be coupled to photosynthesis, with what efficiency energy in the form of activated electrons can be withdrawn, and which effects on the photosynthetic metabolism this implies.

Table of Content

Acknowledgement	I
Preface	III
Table of Content.....	IV
Summary	V
Zusammenfassung	VII
List of abbreviations	IX
Chapter 1 General Introduction.....	1
Chapter 2 Enlighting electron routes in oxyfunctionalizing <i>Synechocystis</i> sp. PCC 6803	21
Chapter 3 Maximizing photosynthesis-driven Baeyer-Villiger oxidation efficiency in recombinant <i>Synechocystis</i> sp. PCC 6803.....	32
Chapter 4 Light-driven redox biocatalysis on gram-scale in <i>Synechocystis</i> sp. PCC 6803 via an in vivo cascade.....	51
Chapter 5 From photons to product – a quantitative study on electron fluxes in oxygenase-active <i>Synechocystis</i> sp. PCC 6803	66
Chapter 6 General Discussion	86
References.....	105
Appendix	120

Summary

Since Earth formation, the sun has provided energy in abundance to our planet. Making direct use of this renewable resource will be key to replace an economy based on fossil resources by sustainable processes producing energy, food, and goods. Spread over all domains of life, photosynthesis is a natural process of light utilization. Evolved in cyanobacteria, oxygenic photosynthesis today is the most widespread type, combining the utilization of sunlight with exploiting water and CO₂ as electron and carbon sources, respectively.

The concept of photo-biotechnology is to use (oxygenic) photosynthesis for the light-driven production of energy carriers or materials. CO₂-valorization, the conversion of inorganic CO₂ to products with the help of phototrophic microorganisms, suffers from a limited CO₂-uptake rate. The coupling of redox enzymes to the photosynthetic light reaction constitutes a promising alternative as it allows for higher conversion rates and solar conversion efficiencies. Introducing and utilizing oxygenases in cyanobacteria is of particular interest, since the photosynthetic apparatus provides their co-substrates O₂ and reduction equivalents *in situ*.

In four research chapters, this thesis investigates the prerequisites and the efficiency of coupling oxygenases to the photosynthetic apparatus in *Synechocystis* sp. PCC 6803 (*Synechocystis*) with two heterologously expressed enzyme systems, a cytochrome P450 monooxygenase (CYP) and a Baeyer-Villiger monooxygenase (BVMO) from *Acidovorax* sp. CHX100. Reductant withdrawal rates for such redox biocatalysis on both short- and long-term and process stability are investigated as well as the physiology of the whole-cell catalyst.

Chapter 2 focuses on electron routes from photosystem I to a heterologously expressed CYP. *Synechocystis* strains harboring the oxygenase component of CYP alone or along with one or both components of its native electron transfer chain were generated and used to test, if host-intrinsic redox carriers can take over their function. We found an efficient electron coupling of host components to CYP, arguably realized by direct electron transfer from photosystem I to the ferredoxin of the native electron transfer chain. These findings promote understanding and simplification of electron transfer from the photosynthetic apparatus to heterologous redox enzymes.

As a second oxygenase system, BVMO was established in *Synechocystis* as described in **Chapter 3**. Limitations by enzyme level and reactant inhibition were overcome by expression system and reaction engineering. The optimized system enabled specific activities of up to $60.9 \pm 1.0 \text{ U g}_{\text{CDW}}^{-1}$ for the light-driven conversion of cyclohexanone to ϵ -caprolactone, unprecedentedly high for photosynthesis-driven oxygenase catalysis. Upon scale-up to 2-L-bioreactors, up to $1.3 \pm 0.1 \text{ g L}^{-1}$ ϵ -caprolactone were formed with product inhibition as key limitation, as it was confirmed by kinetic process modeling and simulation.

Chapter 4 deals with the extension of the BVMO system by a lactonase, resulting in a two-step *in vivo* redox cascade in *Synechocystis*. The lactonase was found to efficiently hydrolyze inhibiting ϵ -caprolactone to equally valuable 6-hydroxyhexanoic acid, thereby overcoming the key limitation. This allowed for light-driven formation of $3.1 \pm 0.1 \text{ g L}^{-1}$ ($6.8 \pm 0.2 \text{ g}$ in total) 6-hydroxyhexanoic acid at lab-scale, being eventually limited by the metabolic capacity for reductant supply. Quantifications of quantum usage and light conversion efficiency revealed that the biotransformation could tap otherwise unused photosynthetic potential.

The quantitative perspective is refined in **Chapter 5**: The physiological responses to the onset of an electron consumer, consisting of the developed *in vivo* cascade, were investigated under three different sink conditions. Continuous cultivations revealed a limited stability for the high rate supply of reduction equivalents. Distinct metabolic constraints affecting the long-term stability of electron withdrawal by the biotransformation are discussed, especially an NADPH/ATP imbalance, and optimization strategies for highly efficient and stable bioconversion driven by light, e.g., combined withdrawal of energy and reduction equivalents, are worked out.

In an overarching discussion (**Chapter 6**), the findings of this thesis are contextualized within biotechnological concepts and research. Particularly, light is discussed as a key parameter for photo-biotechnology, utilizing established concepts such as the window of operation. The feasibility of envisioned light-driven biotechnological processes is critically discussed, pinpointing possible applications as well as expected and necessary developments in the field. Thereby, and not least with the quantitative understanding of light-driven production processes, this thesis offers a framework for photo-biotechnology and its application in future.

Zusammenfassung

Seit ihrer Entstehung versorgt die Sonne unsere Erde mit Energie im Überschuss. Die Nutzung dieser erneuerbaren Energiequelle wird entscheidend sein, um die auf fossilen Rohstoffen aufgebaute Wirtschaft durch nachhaltige Prozesse zur Energiegewinnung und Herstellung von Nahrung und Gütern zu ersetzen. In allen Domänen des Lebens stellt die Photosynthese einen natürlichen Prozess der Lichtnutzung dar. Die in Cyanobakterien entstandene oxygene Photosynthese ist heute die verbreitetste Art; sie kombiniert die Nutzung von Sonnenlicht mit der Verwendung von Wasser und CO₂ als Elektronen- und Kohlenstoffquellen.

Photobiotechnologie beschreibt das Konzept, die (oxygene) Photosynthese für lichtgetriebenen Energiegewinnung oder Herstellungsprozesse zu nutzen. Die Wertschöpfung aus CO₂, bei dessen Umsetzung mit Hilfe von phototrophen Mikroorganismen kohlenstoffhaltige Produkte synthetisiert werden, ist durch geringe CO₂-Aufnahmeraten limitiert. Die Kopplung von Redoxenzymen an die photosynthetische Lichtreaktion stellt eine vielversprechende Alternative dar, da sie höhere Umsatzraten und Lichtnutzungseffizienzen ermöglicht. Das Einbringen und Nutzen von Oxygenasen in Cyanobakterien ist besonders interessant, weil der Photosyntheseapparat beide Co-substrate, O₂ und Reduktionsäquivalente, *in situ* bereitstellt.

In vier Forschungskapiteln untersucht diese Dissertation Voraussetzungen und Effizienz der Kopplung von Oxygenasen an den Photosyntheseapparat von *Synechocystis* sp. PCC 6803 (*Synechocystis*) mit Hilfe von zwei heterolog exprimierten Enzymsystemen, einer Cytochrom P450 Monooxygenase (CYP) und einer Baeyer-Villiger Monooxygenase (BVMO) von *Acidovorax* sp. CHX100. Die Rate, mit der Reduktionskraft kurz- und langfristig für Produktionsprozesse abgegriffen werden kann, und die Stabilität solche Prozesse sind neben der Physiologie der Ganzzell-Biokatalysatoren Schwerpunkte dieser Arbeit.

Die Elektronenrouten vom Photosystem I zur heterolog exprimierten CYP werden in **Kapitel 2** untersucht. *Synechocystis*-Stämme, die die Oxygenasekomponente der CYP alleine oder in Kombination mit einer oder beiden Komponenten der nativen CYP-Elektronentransportkette enthalten, wurden generiert und genutzt, um zu testen, ob Komponenten des Wirtsorganismus ihre Funktion übernehmen können. Dabei wurde ein effizienter Elektronenübertrag zur Oxygenasekomponente festgestellt, der offensichtlich durch direkten Elektronentransfer von Photosystem I zum Ferredoxin der nativen Elektronentransportkette realisiert wird. Diese Ergebnisse tragen zum Verständnis und zur Vereinfachung des Elektronentransfers vom Photosyntheseapparat zu heterologen Redoxenzymen bei.

Als zweites Oxygenasesystem wird in **Kapitel 3** die BVMO in *Synechocystis* etabliert. Einschränkungen durch das erreichte Proteinlevel und Inhibitionen durch Reaktanden wurden durch die Etablierung eines geeigneten Expressionssystems und reaktionstechnische

Lösungen überwunden. Unter optimalen Bedingungen wurden spezifische Aktivitäten von bis zu $60.9 \pm 1.0 \text{ U g}_{\text{CDW}}^{-1}$ für die licht-getriebene Umwandlung von Cyclohexanon zu ϵ -Caprolacton erzielt, was für lichtgetriebene Oxygenaseprozesse bislang unerreicht ist. In Skalierungsexperimenten konnte in 2-L-Bioreaktoren $1.3 \pm 0.1 \text{ g L}^{-1}$ ϵ -Caprolacton gebildet werden, mit Produktinhibierung als wohl entscheidende Limitierung, was durch kinetische Prozessmodellierung und -simulation bestätigt werden konnte.

Kapitel 4 behandelt die Erweiterung des BVMO Systems durch eine Laktonase, wodurch eine Zwei-Stufen-Kaskade *in vivo* in *Synechocystis* entwickelt wurde. Die Laktonase hydrolysiert das hemmende ϵ -Caprolacton zu ebenfalls nutzbarer 6-Hydroxyhexansäure und überwindet dabei die entscheidende Limitierung. Im Labormaßstab wurde damit die lichtgetriebene Bildung von $3.1 \pm 0.1 \text{ g L}^{-1}$ (insgesamt $6.8 \pm 0.2 \text{ g}$) 6-Hydroxyhexansäure erreicht, wobei die Kapazität des Stoffwechsels, Reduktionskraft bereitzustellen, letztlich limitierend war. Die Quantifizierung von Quantennutzung und Lichtnutzungseffizienz zeigte, dass die Biotransformation andernfalls verlorenes photosynthetisches Potenzial nutzt.

Die quantitative Perspektive wird in **Kapitel 5** ausgebaut: Die physiologische Reaktion auf das Anschalten einer elektronenverbrauchenden Biotransformation durch die entwickelte Zwei-Stufen-Kaskade wurde anhand von drei unterschiedlichen Elektronenabflussszenarien untersucht. Kontinuierliche Kultivierungen zeigten eine begrenzte Stabilität der hohen Zufuhr an Reduktionsäquivalenten hin zur Biotransformation. Diesbezüglich werden verschiedene metabolische Limitationen, im Speziellen ein NADPH/ATP-Ungleichgewicht, diskutiert und mögliche optimale Bedingungen für effiziente und stabile Biokonversion mit Licht als Energiequelle wie ein kombinierter Abzug von Energie und Reduktionsäquivalenten herausgearbeitet.

In der übergreifenden Diskussion (**Kapitel 6**) werden die Ergebnisse dieser Doktorarbeit in den Hintergrund biotechnologischer Konzepte und Forschung eingebettet. So wird beispielsweise das „Verfahrensfenster“ (*window of operation*) um das Licht als entscheidender Parameter für die Photobiotechnologie erweitert. Die Machbarkeit von angestrebten licht-getriebenen biotechnologischen Prozessen wird kritisch diskutiert und mögliche Anwendungen und zu erwartende und notwendige Entwicklungen im Feld aufgezeigt. Damit und nicht zuletzt mit dem quantitativen Verständnis von Licht-getriebenen Produktionsprozessen bietet diese Dissertation einen Rahmen für die Photobiotechnologie und ihre zukünftigen Anwendungen.

List of abbreviations

6-HA	6-hydroxy hexanoic acid
AEF	Alternative electron flow
ALE	Adaptive laboratory evolution
ATP, ADP	Adenosine triphosphate, adenosin diphosphate
B, k_B	By-product (formation rate)
BVMO	Baeyer-Villiger monooxygenase
camA, camB	Putidaredoxin, putidaredoxin reductase
Cas	CRISPR associated systems
CBB	Calvin-Benson-Bassham cycle
CDW	Cell dry weight
CET	Cyclic electron transfer
Chl- <i>a</i>	Chlorophyll- <i>a</i>
CHMO	Cyclohexanone monooxygenase
Chx	Cyclohexane
Cm	Chloramphenicol
CO ₂	Carbon dioxide
C-ol	Cyclohexanol
C-one	Cyclohexanone
Cox	Cytochrome c-oxidase
CRISPR(i)	Clustered regularly interspaced short palindromic repeats (interference)
Cyd	Cytochrome b/d-oxidase
CYP	Cytochrome P450 monooxygenase
Cyt b_6/f	Cytochrome b_6/f -complex
DCMU	3-(3,4-dichlorophenyl)-1,1-dimethylurea
DOC, pO ₂	Dissolved oxygen concentration
DSP	Downstream processing
ϵ -Cl	ϵ -caprolactone
E_k	Light saturation point
ETR	Electron transfer rate
Fd	Ferredoxin
Flv	Flavodiiron protein
FNR	Ferredoxin-NADPH-reductase
FP	Flat-panel
FTR	Ferredoxin-thioredoxin-reductase
GAPDH	Glycerinaldehyde-3-phosphate dehydrogenase
GC	Gas chromatography
HC	High carbon
HEPES	4-(2-hydroxyethyl)-1-piperazinethanesulfonic acid
HL	High light
hox	Native hydrogenase in <i>Synechocystis</i>
HPLC	High-pressure liquid chromatography
ISPR	<i>in situ</i> product removal
IPTG	Isopropyl- β -D-thiogalactopyranosid
K_i	Inhibitory constant

Km	Kanamycin
K_s	Substrate constant
LC	Low carbon
LEF	Linear electron flow
LL	Low light
$\log P_{o/w}$	Partitioning coefficient between octanol and water
NAD ⁺ /NADH	Nicotinamide adenine dinucleotide
NADP ⁺ /NADPH	Nicotinamide adenine dinucleotide phosphate
NarB	Nitrate reductase
NirA	Nitrite reductase
NPQ	Non-photochemical quenching
O ₂	Oxygen
OEC	Oxygen evolving complex
P, k_P	Product (formation rate)
PAM	Pulse amplitude modulation
PAR	Phototynthetically active radiation
PC	Plastocyanin
PETC	Photosynthetic electron transport chain
photo-STR	Stirred-tank photo-bioreactor
P _i	Inorganic phosphate
PKG	Phosphoglycerate kinase
<i>pmf</i>	Proton motive force
PQ/PQH ₂	Plastoquinone
PRK	Phosphoribulose kinase
PS I, PS II	Photosystem I, photosystem II
PTOX	Pastid terminal oxidase
PV	Photovoltaic
QE	Quantum efficiency regarding product formation
Q _{phar}	Photosynthetically absorbed quanta
Q _X , Q _P	Quantum demand for biomass, quantum demand for product formation
r _{AEF}	Alternative electron flux
r _C , r _N , r _{BT}	Electron flux towards carbon fixation, nitrogen assimilation, product formation
r _F	Maximum electron flux through PS II
ROS	Reactive oxygen species
Rubisco	Ribulose-1,5-bisphosphate-carboxylase-oxygenase
S	Substrate
SDS PAGE	Sodium dodecyl sulfate polyacrylamid gel electrophoresis
SirA	Sulfite reductase
SOD	Superoxide dismutase
TRL	Technology readiness level
Trx	Thioredoxin
TSP	Total soluble protein
U	Unit, $\mu\text{mol min}^{-1}$
v _{max}	Maximal velocity
wt	Wild type
X	Biomass
Φ_{PSII}	Effective quantum yield at PS II
Y _{P/S} , Y _{P/X}	Product yield on substrate, product yield on biomass

1 General Introduction

This introduction chapter comprises background information on (sun) light as energy source, photosynthesis and its evolutionary inventors, the phylum of cyanobacteria as promising the host organisms for photo-biotechnological processes. Principles, potentials, and limitations of photo-biotechnology will be looked at ending up with the scope covered by this thesis.

Parts of this chapter have been published in

Exploitation of hetero- and phototrophic metabolic modules for redox-intensive whole-cell biocatalysis

Eleni THEODOSIOU, Adrian TÜLLINGHOFF, Jörg TOEPEL, and Bruno BÜHLER

Frontiers in Bioengineering and Biotechnology, **2022**, 10:85575

<https://doi.org/10.3389/fbioe.2022.855715>

1.1 Photosynthesis: Generating products based on sunlight, water, and CO₂

1.1.1 Sunlight is an abundant energy resource for biological processes

The sun is one of the prerequisites for life on earth as it continuously provides a huge amount of energy to drive biological processes. The solar constant, putting the solar radiation provided to Earth in numbers, is 1361 W m^{-2} . [2] Assuming earth as an ideal sphere, the inconceivable amount of ca. 174 PW of solar radiation reaches the earth every hour. This approximately equals the global energy consumption of humankind in entire 2021 (168 PWh, [3]). This simplified calculation illustrates the tremendous potential of utilizing sunlight as energy source. In reality, due to earth rotation and albedo, [4] the radiation actually reaching the surface is reduced to maximally 236 W m^{-2} on a cloudless day.

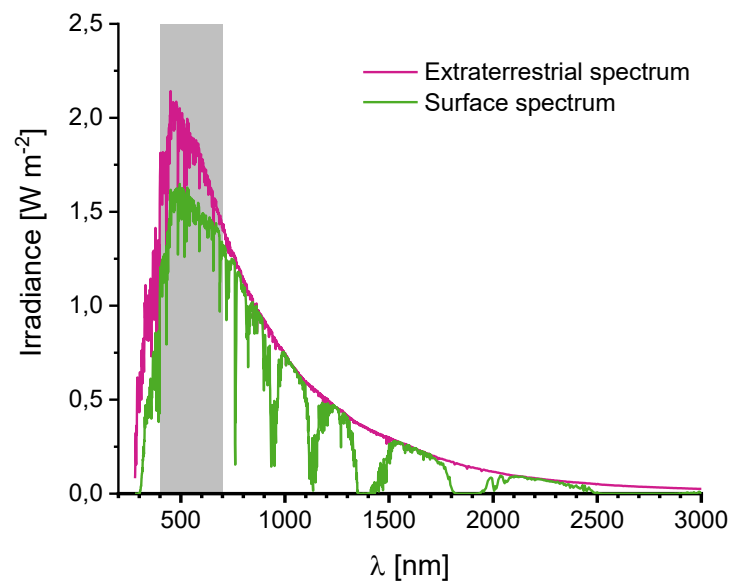


Figure 1: **Extraterrestrial (magenta) and surface (green) solar spectrum.** The standard extraterrestrial spectrum is used. [5] The depicted surface spectrum is the reference air mass 1.5 spectrum, with specified atmospheric conditions, described in detail in [6]. Photosynthetically active radiation is highlighted in grey.

The solar radiation covers a wavelengths range known as the solar spectrum. Plotting both the extraterrestrial and the surface spectrum as a function of the wavelengths from 300-3000 nm visualizes the differences caused by atmospheric absorption (Figure 1). The solar spectrum is categorized in different ranges, i.e., ultra-violet (<400 nm), visible (400-700 nm), and infrared light (>700 nm). In photo-biotechnology, the radiation between 400 and 700 nm is of interest, as only quanta of these wavelengths are used by standard oxygenic photosynthesis. Thus, this range is defined as photosynthetically active radiation (PAR); its integrated power accounts for about 43% of that of the total surface irradiation. Despite these deductions, the energy of PAR by far surpasses than the energy demand by humankind today. Therefore, it can only be deemed logical to use this abundant energy source to satisfy the global energy demand.

For energetic considerations, this work always refers to the unit $W\ m^{-2}$. However, having a close look at photosynthesis, it can be favorable to give information about the number of quanta per area, i.e. the photon flux density. Then, the unit $mol_{\text{photons}}\ m^{-2}\ s^{-1}$ will be used.

1.1.2 Oxygenic photosynthesis exploits water as abundant electron donor

Photosynthesis describes a process utilizing light energy to build up carbohydrates and finally biomass from CO_2 as carbon source. In a light-dependent reaction, light quanta are used to excite electrons in a photoactive biomolecule, a pigment, which can then reduce an electron acceptor leading to a charge separation. The excitation energy is typically transferred over several redox carriers in from of band gaps to finally reduce a stable electron acceptor, which can be used to drive reductive assimilation processes. The electrons to be excited thereby are derived from an electron donor, which is being oxidized in the process.[7]

Depending on the electron donor/source, different types of photosynthesis have evolved. Featured by plants, microalgae, and bacteria, oxygenic photosynthesis is the most widespread one. It uses water as electron donor, oxidizing it to molecular O_2 . The abundance of its main resources, namely sunlight, water, and carbon dioxide, explains its evolutionary success.[8] To be able to oxidize water, the combination of two photosystems in series is necessary, one photosystem (PS I) forming a reduction agent strong enough to reduce ferredoxin followed inter alia by electron transfer to $NADP^+$ and one photosystem (PS II) forming an oxidizing agent strong enough to oxidize water.

The first organisms known for the sequential linkage of two photosystems to drive oxygenic photosynthesis belong to the phylum of cyanobacteria. This evolution occurred at least 2.5 billion years ago, possibly even before,[9] and changed the face of planet dramatically in the great oxygenation event.[10] The concept of oxygenic photosynthesis, was retained in cyanobacteria and spread to the domain of eukaryotes by the endosymbiosis of cyanobacteria forming the ancestors of chloroplasts in micro- and macro-algae as well as higher plants.[11] Thus, cyanobacteria are considered classic model organisms to study the pivotal biochemical process of oxygenic photosynthesis.

1.1.3 Photosynthesis consists of two interconnected modules

Photosynthesis consists of two processes, which are interconnected:

- (1) The light-dependent reaction uses light energy to excite electrons derived from an electron donor, which is water in case of oxygenic photosynthesis being split into protons and O_2 by the action of four quanta. Electrons then are transferred to ferredoxin and $NADP^+$ via the photosynthetic electron transport chain (PETC) in the thylakoid membrane. This electron transfer via the PETC moreover is used to establish a proton

gradient, which is exploited to regenerate the intracellular energy carrier adenosine triphosphate (ATP).[12]

Incident light is absorbed by chlorophyll and accessory proteins, with phycobilisomes being a prominent antenna structure in cyanobacteria, consisting of the biliproteins phycoerythrin, phycocyanin and allophycocyanin.[13] These biliproteins coordinate covalently linked tetrapyrrole like phycoerythrobilin and phycocyanobilin, able to absorb quanta and transfer the excitation energy to adjacent accessory pigments. Thereby, the energy is channeled to chlorophyll-*a* (Chl-*a*) in the reaction centers, of PS II and PS I.[14, 15] Here, the excited Chl-*a* is either quenched by thermal dissipation, fluorescence, or energy transfer to another pigment, or it is photochemically used.[16] In the latter case, a charge separation occurs, reducing a primary acceptor molecule and leading to an oxidized Chl-*a* radical. In PS I, the oxidized Chl-*a* radical derives electrons from phycocyanin (see below), whereas PS II, derives them from water splitting in the oxygen evolving complex (OEC). Here, a cluster consisting of Mn and Ca, oxidizes water to protons and O₂ and stepwise transfers electrons via a tyrosine radical to the Chl-*a* in the reaction center.[17]

In the so-called linear electron flow (LEF, also called non cyclic electron flow, see Figure 2), electrons are further transferred from the reaction center of PS II via several redox partners to plastoquinone (PQ).[7] Its reduced form, hydroplastoquinone (PQH₂), can transfer electrons to the cytochrome b₆f-complex (Cyt b₆f).[12] This transmembrane protein complex is equipped with several cytochromes and translocates protons over the thylakoid membrane via the so-called Q-cycle.[18, 19] On the lumen side of the thylakoid membrane, soluble phycocyanin then transfers electrons from Cyt b₆f to PS I.[18] In its reaction center, absorbed quanta are again used to excite Chl-*a*. [20] Via Chl-*a*, phylloquinone, and Fe-S-centers,[15] electrons are then transferred to ferredoxin (Fd), the first stable electron acceptor of the PETC, being located in the cytosol. Ferredoxin-NADP⁺-reductase (FNR) oxidizes Fd to generate NADPH.[21] The sequential linkage of PS II and PS I and the orientation of the redox partners involved along the PETC[22] enables the coupling of water oxidation and NADP⁺ reduction according to the following stoichiometry:



Along the PETC, three components build up a pH gradient between lumen and stroma side: i) water-splitting in the OEC releases protons at the lumen side of the membrane, ii) PQ and Cyt b₆f translocate protons from the stroma side to the lumen side, and iii) reduction of NADP⁺ “binds” protons and reduces the proton concentration in the stroma. Both the H⁺ concentration gradient and the resulting electric field constitute a proton motive force (*pmf*). [23, 24] This *pmf* is used by the F₀F₁-ATPase to generate ATP out of adenosine diphosphate (ADP) and

inorganic phosphate (P_i), in a ratio of 3 ATP per 14 H^+ translocated from lumen to stroma.[18, 25]

(2) ATP and NADPH are used to assimilate CO_2 and form reduced triose-phosphate in the light-independent Calvin-Benson-Bassham (CBB) cycle.[26]

The light-dependent reaction generates energy in the form of ATP and reductive power in the form of NADPH to drive assimilatory processes, with the CBB cycle being the main consumer. The CBB cycle was found, proposed by, and named after M. Calvin, A. A. Benson, and J. A. Bassham in the 1950s.[26] It involves the coupling of relatively inert CO_2 to ribulose-1,5-bisphosphate by the enzyme ribulose-1,5-bisphosphate-carboxylase-oxgenase (Rubisco).[27] The resulting instable C6-intermediate decomposes to two 3-phospho-glycerate molecules,[27] which are phosphorylated by phosphoglycerate kinase (PKG) at the expense of ATP and reduced by glyceraldehyde-3-phosphate dehydrogenase (GAPDH) to triose-phosphates at the expense of NADPH. Then, re-arrangements catalyzed by aldolases, transketolases, epimerases, and isomerases, also operating the oxidative pentose phosphate cycle, yield ribulose-5-phosphate, which is phosphorylated by phosphoribulokinase (PRK) at the expense of ATP regenerating ribulose-1,5-bisphosphate,[28] being again substrate for CO_2 fixation by Rubisco. Overall, one triose-phosphate is formed from 3 CO_2 at the expense of 9 ATP and 6 NADPH.[26]

Hence, ATP and NADPH are required at a theoretical ratio of 1.5. In reality, other processes like photorespiration and N- and S-assimilation, but also amino acid synthesis and secondary metabolism influence this required ratio.[25] However, LEF produces ATP and NADPH at a ratio of 1.28,[25] causing an additional ATP demand.[29] To modulate the ATP/NADPH ratio, options for alternative electron flows (AEF, Figure 2) are at hand.[30]

- Cyclic electron flow, in which electrons are cycled around PS I involving part of the PETC, but no PS II. It contributes to the *pmf* without forming NADPH. Via one or more enzymes, electrons are transferred from Fd to PQ, from which PS I can be supplied with electrons via Cyt b_6/f . Many possible routes from Fd to PQ are discussed (and dependent on the organism), which most prominently involve the NDH1-complex, PGR5/PGRL1, and the PQ reductase site of Cyt b_6-f .[25, 30]
- In pseudocyclic electron flow, electrons downstream to PS I are transferred back to O_2 via Fd or NADPH. The formed superoxide species is detoxified to H_2O via superoxide dismutase, ascorbate peroxidase, and catalase. Thus, LEF is kept active to power the *pmf*, but electrons (Fd/NADPH) are consumed, leading to an increase of the ATP/NADPH ratio.[25, 31] Pseudocyclic electron flow is also called water-water-cycle, as electrons from water splitting are transferred to O_2 forming water again. This involves proton release on the lumen side and proton removal on the stroma side, which per se

contributes to the *pmf* and an ATP/NADPH ratio increase. Such electron transfer to O₂ also occurs downstream of PS II, which thus also contributes to ATP/NADPH ratio modulation.

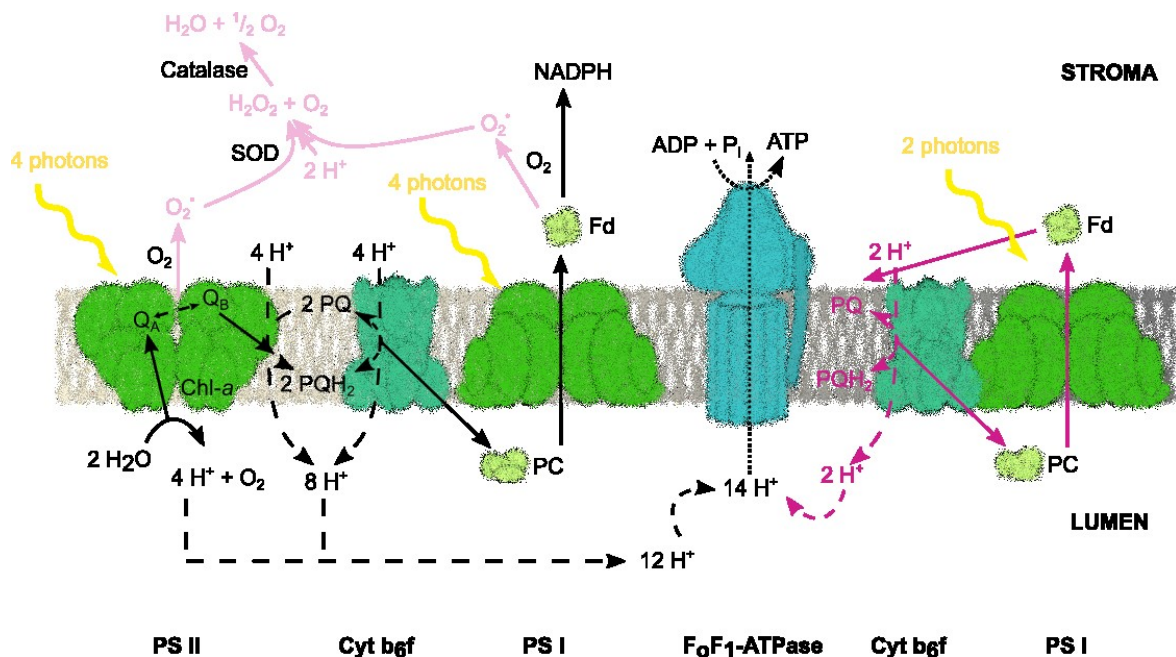


Figure 2: **Linear, cyclic, and alternative electron flow of the photosynthetic light reaction.** In *linear electron transfer* (left part, black arrows), sequential linkage of photosystems II and I (PS II and PS I, green) moves electrons derived from water oxidation along the photosynthetic electron transport chain, finally reducing ferredoxin (Fd, light green) and NADP⁺. Absorption of 8 quanta is required to reduce 2 Fd or NADP⁺ and fuel the proton-motive force (*pmf*) by translocating 12 H⁺ from the stroma to the lumen (dashed black arrows), supported by the Q-cycle of cytochrome b₆f complex (Cyt b₆f, turquoise) increasing the number of translocated H⁺ via plastoquinone (PQ/PQH₂). *Cyclic electron transfer* (right side, pink arrows) cycles electrons around PS I without net reduction of NADP⁺. Instead, electrons from Fd (or NADPH) are transferred to PQ, from which electrons are transferred via Cyt b₆f and plastocyanine (PC, light green) to PS I. With the energy of 2 absorbed quanta, 2 additional H⁺ are translocated from the stroma to the lumen side (dashed pink arrows). *Alternative electron transfer* (light rose arrows): Electron transfer from PS II (here quinones Q_A/Q_B) or Fd to O₂ forms the superoxide radical (O₂[•]), which is detoxified to H₂O₂ + O₂ by superoxide dismutase (SOD) consuming 2 H⁺ per 2 O₂[•]. Catalase converts H₂O₂ to H₂O and ½ O₂. In sum, electrons from water oxidation are transferred back to O₂ to form water in a futile cycle. However, by releasing H⁺ to the lumen and consuming H⁺ in the stroma, AEF contributes to *pmf*. Dotted black arrows: The *pmf* drives the F_oF₁-ATPase (cyan) to generate 3 ATP / 14 H⁺. Figure is combined of and modified from [30] and [32].

The shares of LEF, cyclic, and pseudocyclic electron flow are still debated and obviously highly depend on the cell's demands and thus on environmental conditions.[33] Under non-stress conditions, cyclic electron flow accounts for around 14% of LEF,[25] but values of 35% have also been observed.[34] Roughly, one of five electrons going through PS I have to be cycled,[30] implying a 20% higher flux through PS I than through PS II. In cyanobacteria, however, the PS I:PS II ratio ranges between 5:1 to 2:1,[35] which is necessary, as PS II regeneration after photodamage is much easier than regeneration of PS I. Further, the amount of excitation energy directed PS II or PS I can be modified by the organization of the light-harvesting phycobilisomes to either PS II or PS I, termed state transitions. The regulation of cyclic and pseudocyclic electron flow, as far as known so far, has excellently been reviewed by Nikkanen et al.[24]

1.1.4 The photosynthetic modules have to be regulated to balance source and sink

The supplied energy and reduction equivalents link the light-dependent reaction directly to the nutrient assimilation/CBB. It is not surprising that different regulatory links exist between both photosynthetic modules. One global regulation system is the thioredoxin (Trx) system: Trxs are small (< 100 amino acid) proteins with the reactive motif -Cys-Gly-Pro-Cys-, enabling the buildup of intra- or intermolecular disulfide bridges.[36] Under reductive conditions (i.e., in light), Trx is reduced by ferredoxin-thioredoxin-reductase (FTR) and can activate pivotal photosynthetic enzymes like F_0F_1 -ATPase and CBB-related enzymes like Rubisco activase, GAPDH, fructose-1,6-bisphosphatase, and PRK, enabling a light-induced activation of ATP-generation and the CBB.[37] In general, the redox status of the cell is an important signal for regulation: Sensed and mediated by the redox state of the PQ pool, state transitions and expression of both PS II and PS I are controlled.[38, 39] However, recent studies found that the PQ pool itself is strictly regulated in narrow limits, which emphasizes the importance of excess energy dissipation via terminal oxidases.[40, 41]

Another implicit control is the so-called photosynthetic control: Acidification of the lumen limits oxidation of PQH_2 in the Q-cycle, reducing both proton translocation and photosynthetic electron flow.[18, 23, 42] Additionally, the elevated electric field may promote singlet O_2 production at PS II causing photo-damage, thus limiting the photosynthetic light reaction in a harmful feedback control.[42]

Lately, the importance of regulatory small proteins, like CP12,[43] has been discussed more intensely.[44] Under oxidative/dark conditions, CP12 forms intramolecular disulfide bridges with PRK, forming a protein-protein-complex, which then binds GAPDH, blocking its NADPH-binding. Thus, CP12 simultaneously downregulates two key enzymes of the CBB.[43]

Despite elaborate control of ATP/NADPH ratio and redox status within cells, it occurs that the light reaction and assimilatory processes are not balanced: Under natural conditions, the photosynthetic driving force, i.e., the light availability/intensity or source, often surpasses the sink capacity, i.e., the availability of sinks such as C, N, and S nutrients. Fluctuations in light and nutrient availabilities require an active balancing of energy assimilation (light harvesting, photosynthetic electron flux) and energy demand (nutrient assimilation and biomass formation). To compensate sudden imbalances, dissipation mechanisms like non-photochemical quenching (NPQ) or the above-mentioned pseudocyclic electron flow have evolved.[31, 45, 46] To balance source/sink-ratios on the longer term, variations in PS II-efficiency, Chl-a content, and state transitions, but also Rubisco content have been described.[33, 47, 48] Whereas these mechanisms are indispensable to protect the photosynthetic machinery from photo-inhibition, i.e., light-induced damage of the photosystems, they imply a loss of photosynthetic efficiency. Harvested energy is not used, but dissipated, as not enough energy sinks are available. In photosynthesis research, this is

called the sink hypothesis stating that photosynthetic efficiency is limited by the availability of sinks. In other words, providing appropriate sinks is expected to increase energy conservation and thus photosynthetic efficiency.

1.2 Photo-biotechnology: Exploiting photosynthesis for biotechnology

1.2.1 Photo-biotechnology with cyanobacteria as sustainable option for O₂-dependent biocatalysis

In the last decades, the utilization of microorganisms for biotechnological production processes contributed to an enormous development of the field of biotechnology.[49] Biotechnology today represents an alternative and complement to conventional chemistry as its processes, in general, require less energy, produce less toxic byproducts, and use less harmful reagents, giving them high potential to be environmentally friendlier.[50, 51] While there are numerous processes utilizing enzymes as catalysts or microbes as whole-cell factories, catalyzing redox reaction remains challenging.[52] Redox enzymes depend on co-substrates such as electron carriers and O₂, which constitute the main process limitations.[53] The use of isolated enzymes as catalysts entails high enzyme and cofactor (re)generation costs.[54] In this regard, the use of whole cells as biocatalysts is advantageous: Required cofactors can be biologically regenerated *in situ* at the cost of sacrificial electron donors such as glucose.[55] This bears the inherent challenge that energy mobilization from glucose, i.e., its oxidation and electron transfer to O₂ in respiration, requires additional O₂. Indeed, high O₂ demands often hinder efficient, stable, and cheap redox biocatalysis in heterotrophic cells.[54, 56]

In photo-biocatalysis on the other hand, the photosynthetic apparatus can supply both electrons and O₂ *in situ* from water and sunlight as highly environmentally friendly co-substrates.[57, 58] Phototrophic microorganisms thereby combine this advantage with their self-(re)generation capacity, relying on light, water, and CO₂ as main resources.[59] Compared to heterotrophic organism, challenges for the application of phototrophs and respective scaling include lower growth rates, a less understood metabolism, and poor availability of molecular biology tools, genome scale models, and high-density cultivation options (see also 1.3.1.). Current photo-biotechnology research tries to close these gaps. Besides advantages for electron demanding redox biocatalysis,[59] photosynthesis utilization makes reduced C-compounds, such as glucose, dispensable for both cell maintenance and regeneration of reducing equivalents. This is an important conceptual benefit for different reasons:

- Glucose is an important economic factor in bioprocesses based on heterotrophs; omitting it reduces costs.[60]
- Glucose production requires arable land for culturing of, e.g., sugar cane. In contrast, phototrophs feature a relatively low land use, which is not restricted to arable land.[61]

- For O₂-consuming (oxygenase) reactions, competition for O₂ between respiration and target reactions is completely avoided. In contrast, the catalysts even supplies O₂ for target reactions *in situ*. [57]

In principle, redox biocatalysis can be coupled to photosynthesis in all photosynthetic organisms. However, microbes such as microalgae and especially cyanobacteria constitute the most promising hosts. [59] Advantages of cyanobacteria over microalgae or even plants include i) relatively short generation times, [62] ii) their natural competence, enabling relatively straight-forward genetic modification, [62], iii) the increasing availability of molecular biology tools, [63, 64] and iv) a higher photosynthetic efficiency (see also 1.2.3.). The cyanobacterium *Synechocystis* sp. PCC 6803 (*Synechocystis*), even tipped today as the “green *E. coli*”, [65] is a well-studied model organism not least, because it is a suitable model organism for photosynthesis research. Its genome is fully sequenced. [66] Further species, which have been used for photo-biotechnology are, e.g., *Synechococcus* sp. PCC 7942, [67] *Synechococcus* sp. PCC 7002, [68] and fast-growing strains like *Synechococcus elongatus* UTEX 2973 [69] and PCC 11901 [70] with doubling times of 2.3 and 2.0 h, respectively. Examples for the use of microalgae, like *Chlamydomonas reinhardtii*, for redox biocatalysis are scarce. [71] For a comparison of growth rates and photoproduction rates of phototrophic organisms see also Table 2.

1.2.2 Engineering phototrophic metabolism for whole-cell biocatalysis

Biocatalytic redox reactions depend not only on suitable enzymes, but also on efficient and sustainable redox cofactor supply. To find the optimal electron transfer partner, both the redox potential and the supply rate of this carrier have to be considered. Most commonly, NADH- or NADPH-dependent enzymes are used for electron-demanding reactions. Photosynthetic metabolism provides high supply rates for NADPH and reduced Fd, the primary electron acceptor of photosystem I. Figure 3 displays the PETC and the variety of electron carriers as well as possible homo- and heterologous electron sinks.

The provision of reduced Fd with its relatively low redox potential, [72-74] makes the application of Fd-dependent enzymes in phototrophs promising. Supported by electron transfer via PS I and Fd, specific activities up to $3.4 \pm 0.3 \text{ U g}_{\text{CDW}}^{-1}$ have been achieved. [75] Both enzyme specific and host intrinsic Fds have been found to shuttle electrons, with differing efficiency. [75, 76] Phototrophs contain multiple Fds, with, e.g., at least 9 Fds in the model cyanobacterium *Synechocystis*. [77] This complicates the prediction of electron transfer efficiencies towards Fd-dependent enzymes. NADPH, [78, 79] NADH, [74, 75] flavodoxins or plastoquinones also have the potential to be used as electron donors. Enzymes

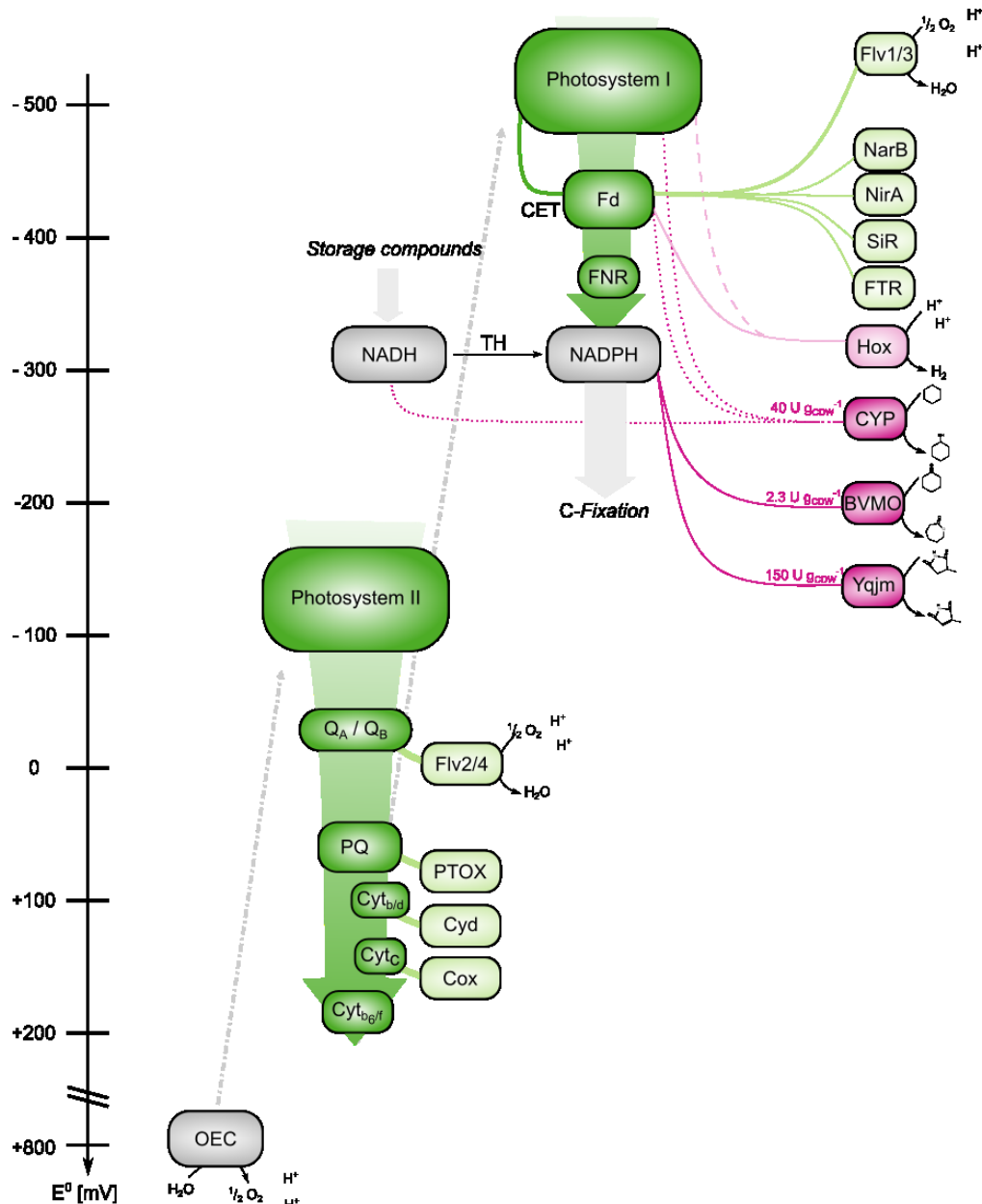


Figure 3: **Tapping the reductive potential of photosynthesis.** Green: components of the photosynthetic electron transport chain (PETC); light green: internal electron sinks; rose: (native) hydrogenase (Hox); pink: representative (recombinant) redox enzymes with maximal specific activities in $\text{U g}_{\text{CDW}}^{-1}$. Electrons derived from water splitting enter the photosynthetic electron transport chain at photosystem II, where energy from light quanta promotes them to a higher excitation state (a more negative potential). This excited state can be used for photochemistry, i.e., the reduction of the primary acceptors (quinones Q_A/Q_B), followed by electron transport over plastoquinone (PQ) and cytochrome b_6/f (Cyt b_6/f) along a gradient of redox potentials. Photosystem I (PS I) again absorbs light energy and constitutes a reducing agent strong enough to transfer electrons to ferredoxin (Fd). Fd-NADPH-reductase (FNR) allocates a big share of electrons from Fd to NADPH, which can be used for C-fixation. Alternatively, electrons can be distributed to N- and S-assimilation (Fd-nitrate-reductase NarB, Fd-nitrite-reductase NirA, and Fd-sulfite-reductase SiR), regulatory elements (e.g., Fd-thioredoxin-reductase FTR), or back to PS I, referred to as cyclic electron transfer (CET). At different points of the PETC, reductive stress can be released by transferring electrons to acceptors like the flavodiiron proteins Flv2/4 and Flv1/3 and respiratory oxidases like the PQ-terminal oxidase PTOX, Cyt b_6/d -oxidase (Cyd), and Cyt c -oxidase (Cox), all of them transferring the electrons back to O_2 . Redox potentials of electron sinks are not drawn to scale. So far, the reductive potential of photosynthesis has been tapped biotechnologically at or downstream of PS I, at the level of Fd (e.g., Hox) or NADPH (e.g., Baeyer-Villiger monooxygenases, BVMO[78]; ene-reductases like Yqjm[79]) or by fusion constructs [80](dashed line). Reductive power for cytochrome P450 monooxygenase (CYP) catalysis could be tapped at the level of PS I, Fd, or NADH derived from storage compounds[74] (dotted lines). In *Synechocystis*, transhydrogenases (TH) can convert NADH to NADPH.

depending on NADPH as a main product of the light reaction thereby benefit from the relatively large pool of and high regeneration rate for NADPH, but may suffer from competition with electron consuming metabolic routes, especially CO₂ fixation and nitrate assimilation.[81] A study investigating the most suitable carrier for a cytochrome P450 monooxygenases (CYPs) showed that i) the type of available electron carrier determines the biocatalytic reaction rate and ii) this rate profits from electron carrier-CYP fusion.[76] Methods to improve intracellular CYP catalysis, including enzyme-, redox-partner-, and substrate engineering recently were nicely reviewed by Li et al.(2020).[82] An improved connection to the PETC has the potential to significantly increase production rates as shown for the linkage of a CYP to the thylakoid membrane.[68] A direct connection to the photosynthetic apparatus is not reported for oxygenases, but allowed a direct electron transfer to hydrogenases, mitigating unwanted electron leakage.[80, 83] As a strategy to avoid intracellular competition for redox equivalents, FNR affinity for Fd can be attenuated, thereby making more Fd available for target reactions, e.g., hydrogen formation catalyzed by Fd-accepting hydrogenases.[21] The PQ pool in principle constitutes another attractive point to tap reducing power from photosynthesis, with native transfer to the terminal oxidase as an example.[41] Its relatively positive redox potential, however, limits the amount of reactions to be potentially fueled by PQH₂.

The implementation of biocatalytic redox reactions in phototrophs mostly constituted an iterative process. Several oxidoreductases like oxygenases,[68, 72, 74, 78] reductases,[79] and hydrogenases[80] have been successfully applied with specific activities up to 150 U g_{CDW}⁻¹ as summarized in Table 1. Interestingly, electron drainage via biotransformation reactions appeared to cause an ATP/NADPH imbalance, (possibly) affecting both the biocatalytic reaction and host metabolism. The combination of pathways relying on C-fixation and reducing power, showed a way to avoid such imbalance.[84, 85] Thus, it is important to consider the balance of sources and sinks. As with heterotrophic microbes, substrate and product inhibition, toxicity, and volatility also have to be considered as engineering targets.[86]

In contrast to cyanobacteria, which have been used in various studies for biocatalysis, examples employing green algae are scarce,[87] which is mostly due to the limited molecular biology toolbox available for such strains. *Chlorella vulgaris* or *Chlamydomonas reinhardtii* were recently applied as whole-cell biocatalysts, using the photosynthetic reduction power for either dehalogenations [88] or aliphatic amine formation via an amine dehydrogenase.[71, 89] The presented examples indicate a limited applicability of phototrophs for NADH-dependent reactions, which only indirectly couple to the photosynthetic light reaction. Application of such enzymes in cyanobacteria/green algae requires either a change in enzymatic cofactor preference,[90, 91] or redirection of electrons towards NADH, as shown for lactate production in *Synechocystis*. [92] Implementation of NADH-dependent nitrate assimilation led to enhanced

NAD(H) turnover, supporting the NADH-evolving target pathways towards butanol products.[93]

Table 1: **Recombinant redox biotransformations in cyanobacteria and microalgae.** Adapted from Jodlbauer et al., 2021 [94] and updated.

Host	Enzyme (origin)	Tapping point	Product	Max. Activity/Scale	Ref
Synechocystis sp. PCC 6803	Yqjm ene reductase (<i>Bacillus subtilis</i>)	NADPH	2-methyl-succinimide	150 U g _{CDW} ⁻¹ 1 mL, 5-30 min 25.7 U g _{CDW} ^{-1 a} 200 mL, 22 h	[79] [95]
	Cytochrome P450 monooxygenase (<i>Acidovorax</i> sp. CHX100)	NADH	Cyclohexanol	39.2 U g _{CDW} ⁻¹ 2 L, 52 h	[74]
	Alkane monooxygenase (<i>Pseudomonas putida</i>)	AlkG, NADH	H-NAME	1.5 U g _{CDW} ⁻¹ 1 mL, 30 min	[58]
	Imine reductase (<i>Streptomyces</i> sp. GF3587)	NADPH	Cyclic amines	21.8 U g _{CDW} ^{-1 a}	[96]
	Cytochrome P450 monooxygenase CYP79A1 and CYP71E1 and glycosyltransferase (<i>Sorghum bicolor</i>)	Fd	<i>p</i> -Hydroxy-phenylacetaloxim Dhurrin	1.0 U g _{CDW} ⁻¹ 0.03 U g _{CDW} ⁻¹	[72]
S. elongatus PCC7942	Alcohol dehydrogenase (<i>Lactobacillus kefir</i>)	NADPH	1-phenylethanol	84 U g _{CDW} ^{-1 a}	[67]
	Cytochrome P450 monooxygenase CYP79A1 (<i>Sorghum bicolor</i>)	Fd	<i>p</i> -Hydroxy-phenylacetaloxim	[26 μM titer with OD ₇₃₀ =2.5] ^b	[68]
Synechococcus sp. PCC 7002	Cytochrome P450 monooxygenase CYP79A1 (<i>Sorghum bicolor</i>)	Fd	<i>p</i> -Hydroxy-phenylacetaloxim	[26 μM titer with OD ₇₃₀ =2.5] ^b	[68]

^a – calculated from substrate consumption

^b – time of biotransformation not available

AlkG – Rubredoxin, H-NAME – ω-hydroxynonanoic acid methyl ester, Fd – Ferredoxin

Besides providing reduction power, the photosynthetic light reaction can supply O₂ and thus overcome one major limitation in the application of oxygenases in heterotrophs. Theoretical calculations indicate that O₂ critically limits applicable concentration of heterotrophic cells and oxygenation productivities,[97] whereas the application of phototrophs completely relieves O₂-supply related issued. For CYP catalysis in cyanobacteria[57] external O₂ supply could even be completely omitted and the reaction be fueled by photosynthesis-derived O₂. Additionally,

an indirect O₂ supply was demonstrated in a mixed species approach, in which phototrophs provided heterotrophic whole-cell biocatalysts with O₂. [98, 99] Furthermore, photosynthetic *in situ* O₂ supply makes application of O₂-dependent enzymes not relying on reduction power conceivable, e.g., alcohol oxidases, amine oxidases, laccases, and dioxygenases. The oxidation of alcohols to aldehydes or ketones by alcohol oxidases is of particular interest for the production of flavors and fragrances. Examples include benzaldehyde (bitter almond), cinnamaldehyde (cinnamon), octanal (citrus), 2-heptanone (banana), ionones (rose), and vanillin (vanilla). [100, 101] Additionally, laccases, which gained interest in recent years, [102] are present in phototrophic species and have the potential to be used for degradation processes. [103, 104]

1.2.3 Efficiency of photosynthesis

When utilizing photosynthesis for biotechnological processes, the conversion efficiency from light to chemical energy is of particular interest. Discussed theoretical maximal values range from 4.5% [8] to 10% [105] of the light stored in dry carbon matter. In reality, dry matter yields of plants only exceptionally exceed 1%, and are estimated to be 0.2% or even lower. [8] Under optimal (= non-natural) growth conditions, cyanobacteria and microalgae, however, show light-to-biomass efficiencies of up to 2%. [47, 106] These differences are plausible considering the more complex organization of plant cells and the fact that plants are multicellular organisms, of which only a part is photosynthetically active.

For biotechnological applications, the desired product is typically not biomass, but bulk or fine chemicals. It is important to note that the solar conversion efficiency decreases with increasing of the product from the photosynthetic light reaction. Two approaches can be distinguished: i) CO₂-valorization for material and energy usage [107-112] and ii) redox biotransformations fueled with electron by the photosynthetic electron chain. [73, 74, 79] For the light-to-product efficiency, there are major questions to be answered:

- i) How efficient does the photo-biocatalyst use the incident light? What are the resulting electron transfer rates (ETRs)?
- ii) At which point can photosynthesis be tapped with what efficiency?
- iii) Which strains or strain character traits are desirable to improve photosynthesis-driven biotechnology?

The light conversion efficiency is maximal at the light saturation point E_k , where incident light is just sufficient to supply the metabolism with the reductive power needed, e.g., for biomass production. In natural environments, phototrophic organisms face a “light usage dilemma”, [113] with the incident light intensity typically being either below or above E_k , impairing overall photosynthetic efficiency. In fact, 82% of the incident PAR reaches the

surface with light intensities above E_k . [113] However, the observation that truncation of light-harvesting antenna increases solar energy conversion efficiency indicates the photosynthetic apparatus being evolved towards efficient light harvest rather than its efficient use. [106]

Within the photosynthetic apparatus, (excess) energy is lost at different levels, often by mechanisms important to protect the apparatus from over-excitation/photo-damage: 1. Depending on their pigmentation, photosynthetic organisms absorb only a share of PAR, expressed as the share of photosynthetically absorbed quanta (Q_{phar}). 2. At PSII, a part of the energy is dissipated via heat or fluorescence and NPQ, which decreases the operative quantum yield at PSII (Φ_{PSII}). Φ_{PSII} can be determined via pulse-amplitude-modulation (PAM) fluorometry and used to calculate the electron transfer rate in PSII. 3. AEF via terminal oxidases and Mehler- or Mehler-type reactions further compromises the light-to-biomass efficiency. As a result, only a fraction of the incident light energy is used for biomass formation or productive (biocatalytic) reactions. To illustrate these theoretical considerations, Table 2 summarizes relevant O_2 evolution, electron supply, and growth rates of phototrophic model microorganisms.

Table 2: Photosynthetic rates of phototrophic model organisms.

Host	O_2 -evolution rate [mol O_2 g $_{\text{Chl a}}$ ⁻¹ h ⁻¹]	e ⁻ supply rate [mol e ⁻ g $_{\text{Chl a}}$ ⁻¹ h ⁻¹]	μ_{max} [h ⁻¹]
<i>Synechocystis</i> sp. PCC 6803	0.34-1.01 ^a [114]	1.08 – 2.16 ^b [115]	0.135 [116]
<i>Synechococcus elongatus</i> UTEX 2973	0.82 [117]	-	0.365 [69]
<i>Chlamydomonas reinhardtii</i>	0.15 ± 0.01 [118]	1.08 ± 0.06 ^c [118]	0.059 [119]
<i>Chlorella vulgaris</i>	0.11 ± 0.01 [120]	0.94 ± 0.02 ^c [120]	0.07 [121]

^a depending on light conditions

^b assessed via NADPH-fluorescence measurements

^c assessed via Chl-a measurements at PS II

μ_{max} – maximal growth rate

Due to the energy losses along the photosynthetic electron transfer chain it is obvious that the closer a reaction is situated to water oxidation at PSII, the higher are electron transfer rates and light use efficiencies. About 50–60% [113] of the light energy can in principle be tapped at PSII or directly downstream to it at the PQ pool, where losses only result from heat (NPQ) and fluorescence dissipation and electron transfer to O_2 via the flavodiiron protein (Flv2/4). Tapping reductive power at PS I or at its acceptor side (via Fd or NADPH) involves further electron losses to respiratory elements, like oxidases or Mehler- and Mehler-type reactions (including Flv1/3). Taken together, these losses account for 30-40%, reducing the light use efficiency to 15-20%. [30, 122] Beside these theoretical efficiencies, the redox potentials of tapped PETC cofactors or electron carriers are of practical importance as reviewed by Mellor et al. [81] Whereas PSII [~ -110 mV in *Synechocystis*, [123]] and PQ [+80 to +110 mV, [124]] feature a

rather low reductive power, final electron carriers like Fd [-430 to -300 mV, [125]] and NADPH [-320 mV], constitute suitable electron donors for redox biocatalysis.

In agreement with these theoretical considerations, potential hosts for light-driven biotechnology require special character traits to ensure powerful and robust processes. High-light- and high-temperature-tolerances are especially important for outdoor applications. Adaptive laboratory evolution (ALE) in combination with systems biology approaches, were successfully applied for *Chlamydomonas*, *Synechocystis*, and *Synechococcus*. [126-130] *Synechocystis*, for instance, was adapted to cope with additional (light) energy on account of a higher light harvesting capacity, [129] auguring well for an effective use of high light intensities. Relatively low growth rates constitute another obstacle for photo-biotechnology (Table 3). Here, the fast growing *Synechococcus elongatus* UTEX 2973 [117] and the recently described *Synechococcus* sp. PCC 11901 [70] represent a significant progress. For the production of fuels or chemicals with (phototrophic) whole-cell factories, solvent tolerance is another desirable trait, for which considerable ALE-based progress recently has been reported for *Synechococcus*. [127]

As mentioned above, phototrophs experience light excess under normal/natural conditions and have evolved multiple mechanisms to dissipate excessive energy. [131, 132] Approaches are needed to avoid such energy loss via overflow valves and to control electron flow. Several studies tackled this aspect in cyanobacteria. Their major protection mechanisms are cyclic electron flow around PSI consuming up to 35% of the photosynthetically captured electrons, [34] flavodiiron proteins, the orange carotenoid protein as main energy dissipater in cyanobacterial antenna systems, and adaptations of the photosynthetic apparatus, e.g., state transitions and antenna sizes. Flavodiiron proteins [133] were targeted in several studies. [45] Knock out strategies increased electron flow and desired product formation. [46, 79] As recently reviewed, numerous mechanisms protect cyanobacteria from photoinhibition, which should be tackled in a holistic approach. [134]

1.3 Barriers and boundaries: Limitations to photo-biotechnology

1.3.1 What withstands application of phototrophic organism for production processes

Several challenges have to be addressed to apply phototrophic organisms for production purposes. Despite the idea of light-driven production has been popular at times during the last decades, photo-biotechnology is a relatively young research field with tremendous developments in the last 10 years. However, it still lacks behind, e.g., conventional biotechnology based on heterotrophs. In the following, important knowledge gaps at different levels are described, as illustrated in Figure 4:

Genetic level. The available molecular toolbox for the genetic modification of cyanobacteria is much less elaborate molecular than the one available for heterotrophs. One example is the availability of Golden Gate modular cloning kits for both yeast[135] and *Escherichia coli*[136] enabling high-throughput strain design. While there are efforts to apply Golden Gate based modular cloning in cyanobacteria,[64] the kits are far from being as broadly applicable or easy to use as their counterparts for heterotrophs. Another example are the clustered regularly interspaced short palindromic repeats (CRISPR)/Cas9 systems being well-established for heterotrophs[137] after its discovery in 2014.[138] Cyanobacteria possess type I and III Cas-systems,[139] but application of CRISPR/Cas9 in cyanobacteria is still scarce, since strong expression of Cas9 results in severe toxicity.[140] Further, one common problem when genetically modifying cyanobacteria is their polyploidy: Cyanobacteria possess multiple copies of their chromosome, requiring tedious sequestration when altering the genome.

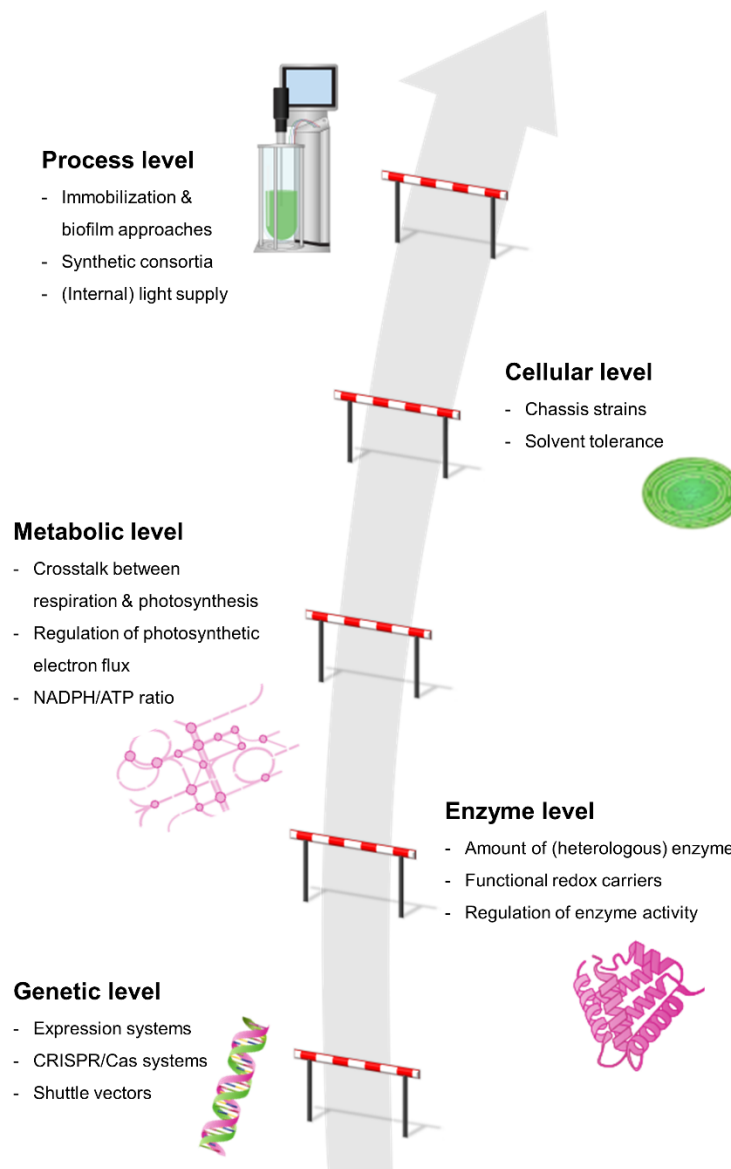


Figure 4: **Limitations to photo-biotechnology.** Feasibility of photo-biotechnological processes is limited due to knowledge gaps at genetic, enzyme, metabolic, cellular and process level.

Despite these challenges, there have been pivotal developments in the last years. In ongoing research, there is a broad effort to develop and, if possible, standardize molecular tools for their use in cyanobacteria.[62] Shuttle vectors for heterologous gene expression have been constructed and characterized.[141, 142] Expression systems, featuring different promoters and ribosomal binding sites have been developed and investigated.[143-147] The availability of the genome sequence of, e.g., *Synechocystis*[66] fostered characterization of native genetic elements as for example transcriptional start sites[148] and the use of CRISPR interference (CRISPRi) in *Synechocystis* has become an important molecular tool.[149, 150]

Protein level. When used as catalysts, suitable host cells need to express (heterologous) genes to produce desired proteins in sufficient amounts. Examples of heterologous proteins levels up to 60% of total cellular protein are known for *E. coli*,[151] whereas heterologous protein levels in cyanobacteria lack far behind. Beside the lack of sufficiently strong expression systems, the structure of the phototrophic metabolism may tolerate less expression-related energetic/metabolic burden. Further, little is known about potential crosstalk of host intrinsic enzymes with desired redox reactions: Are substrates, intermediates, and products interfering with host's proteome? Evidently, regulation of the central carbon and nitrogen metabolism in cyanobacteria is a subject of recent research,[43, 152-155] and regulation mechanisms known from heterotrophs were found to work differently in cyanobacteria.[156] However, some evidence was found that small regulatory proteins, like the above mentioned CP12,[43] play pivotal roles in cyanobacterial regulation circuits.[44]

Especially important for redox biocatalysis, the variety of electron carriers, such as PQ, plastocyanin, ferredoxins, and thioredoxins are of interest, as they constitute possible interaction partners for heterologously expressed oxidoreductases. For instance, *Synechocystis* possesses 9 Fds with different structures and distinct physiological roles,[77] which could potentially be exploited as electron donors for electron consuming reactions. The question, which electron route is used at what efficiency from PS I to heterologous sinks, typically remains unanswered. In this context, it is intriguing that *in vitro* studies showed that *Sorghum bicolor* CYP79A1 was supplied with PS I-derived electrons two times more efficiently by spinach FNR and Fd than by its native components.[157] Another example is CYP105A1 from *Streptomyces griseolus*, which could be supplied with electrons by Fds from tobacco plants, but only at a low rate of about $0.02 \text{ mU g}_{\text{leaf}}^{-1}$. [158] It has yet to be shown that this versatility is a general phenomenon. It will be essential for photo-biotechnology to further investigate such electron routes and optimize them for efficient electron transfer from PS I to heterologous enzymes and finally products.

Metabolic level. Unicellular photoautotrophs need to coordinate both phototrophic and heterotrophic metabolism modes without compartmentalization, this requirement tends to be challenging in cyanobacteria. Thereby, respiration does not only take place in darkness, but

also in light, i.e., photosynthetically active cells.[159] Whereas it is known that the respiratory chain and PETC share common elements, such as the PQ pool and the NDH-1 complex, the detailed regulation and organization is left in the dark, which complicates the development and application of phototrophs for redox biocatalysis. As discussed above, there are forward control mechanisms, based on, e.g., the cell's redox state, to balance electron/energy demands, e.g., by the CBB cycle, and the supply by the light reaction (see 1.1.4.). It is however unclear, in how far the light reaction is demand-driven: Can increased electron demand directly influence photosynthetic electron supply? This question is of vital importance, when aiming to exploit photosynthetically generated reductive power. This brings us back to the sink hypothesis, stating that photosynthetic efficiency is limited by the availability of sinks rather than by the (light) source: The utilization of the light reaction to drive heterologous reactions nowadays is often termed sink engineering, since desired products – constituting C sinks, electron sinks, or both – can potentially optimize photosynthetic efficiency. For C sinks, e.g. lactate synthesis in *Synechocystis*, an increase in carbon assimilation without affecting biomass formation was observed, involving enhanced PS II-efficiency and electron flux through the PETC were found to meet the increased sink demand.[112] However, C sink engineering is always linked to CO₂ uptake and fixation capacities, limiting production rates to values typically below 20 mg g_{CDW}⁻¹ h⁻¹. [160] Also the withdrawal of photosynthetically generated reduction equivalents alone was found to increase photosynthetic efficiency as reflected by enhanced PSII-efficiency,[73, 85, 161] quantum absorption,[161] and electron flux through the PETC.[73, 85, 161] Like carbon sinks, electron sinks can evidently relieve the sink limitation and increase photosynthetic capacity. Grund et al. (2019) investigated physiological differences comparing nitrogen assimilation from NO₃⁻ and NH₄⁺ differing strongly regarding electron demand:[161] NO₃⁻ assimilation involved higher rates not only for the light reaction, but also carbon fixation and growth, obviously enabling a favorable sink/source balance. Taken together, the apparent surplus abundance of reducing power can be considered promising for the coupling of electron consuming biotransformations to the PETC. However, three aspects need detailed investigation: i) the rate/efficiency at which electrons can be withdrawn, ii) the stability of such electron supply, and iii) the effect on cell metabolism and maintenance. Mere electron consumption may for instance disturb the ATP/NADPH balance in the cell. Interestingly, it was shown that ATP consumption can benefit an electron sink, when activated in parallel.[85]

Organism level. Whereas plenty heterotrophic chassis strains are available, the list of phototrophic chassis strains is short and far less optimized/tailor made. For instance, one often required trait is solvent-tolerance of the host strain, which has been screened for or developed in, e.g., *Pseudomonas* [162] or *Saccharomyces cerevisiae*. [163] The tolerance to reactants, organic solvents, or other stressors, like heavy metals, is poorly investigated for cyanobacteria. Further, the combination of enzymes in synthetic cascades (orthogonal pathways) has become

popular in heterotrophic whole-cell biocatalysis, overall increasing atom efficiency, reducing resource and DSP demands and simplifying production steps.[164-166] Up to now, cascade implementation in cyanobacteria is scarce, with the implementation of three enzymes of the dhurrin pathway in *Synechocystis* as a prominent preliminary example.[72]

Process level. For scale-up and industrial implementation of photo-biotechnology, light supply and penetration is a key aspect. Innovative approaches to overcome light limitation have been developed recently,[167-169] including bioreactors with internal illumination,[95, 170] biofilm-based concepts,[171] and cell immobilization approaches.[172, 173] Biofilm reactors enable high surface to volume ratios and thus high biomass concentrations and high light utilization efficiency. Bioreactors with internal light supply enabled to reduce light limitation for suspended cells and a more than two-fold increase in volumetric productivity for photosynthesis-driven 2-methylmaleimide reduction.[95] Further, natural or synthetic phototrophic/heterotrophic consortia recently attracted attention,[174] offering benefits regarding process stability, reaction cascades, cofactor supply, and light utilization.[175] Hoschek et al. demonstrated that a two-species biofilm approach enables a process duration of several weeks for cyclohexane (Chx) hydroxylation at a rate up to $3.76 \text{ g}_{\text{cyclohexanol}} \text{ m}^{-2} \text{ day}^{-1}$ with O_2 provided by cyanobacteria.[98] Substrate and product toxicity constitute another critical factor for industrial application, which can be mitigated by in situ product removal (ISPR) concepts. As an example, tackling substrate and product toxicity and volatility, a two-liquid-phase system has been demonstrated to stabilize a CYP-based photosynthesis-driven hydroxylation process.[74] Despite all these developments, light supply remains the elephant in the room for photo-biotechnology. However, already today, phototrophs constitute a valuable option for high-priced fine chemicals and bioactives, for which low product titers can be accepted.

1.3.2 Scope of this thesis

In the context of the rapidly evolving field of photo-biotechnology, this thesis aims to establish productive light-driven whole-cell redox biocatalysis in cyanobacteria. This includes the application and refinement of molecular biology tools, development and engineering of suitable strains, the testing and optimization of reaction conditions, as well as the description of metabolic states and electron supply capacities. Cyanobacterial strains capable of CYP and BVMO-catalyzed oxyfunctionalizations, are developed and as whole-cell catalysts. The catalyzed reactions represent a suitable proxy for heterologous electron sinks, as they are irreversible and pose an electron pull strong enough to be quantified with methods at hand. The following research questions are addressed in four chapters:

- Which electron routes can be used to couple heterologous redox reactions to the photosynthetic apparatus?
- Which prerequisites must be met for efficient light-driven whole-cell redox biocatalysis in cyanobacteria?
- Which host-intrinsic limitations exist hindering optimal product formation? How can they be overcome?
- At which rate can photosynthesis-derived reduction equivalents be branched off for heterologous redox reactions? Which conditions promote high product yields?
- At which efficiency can the photo-biocatalysts operate with respect to biomass and product formation?

Chapter 2 elucidates how efficiently a heterologous oxygenase, a CYP from *Acidovorax* sp. CHX100, can be linked to cyanobacterial photosynthesis via different host intrinsic and orthogonal electron carriers. **Chapter 3** focuses on the development and optimization of cyanobacterial strains performing Baeyer-Villiger oxidation utilizing the NADPH-dependent BVMO from *Acidovorax* sp. CHX100. It includes promoter studies, characterization of reaction kinetics, and interferences of host enzymes with the target reaction, as well as the development of a process model based on kinetic parameters and a process scale-up to 2L-stirred-tank photo-bioreactors (photo-STRs). In **Chapter 4**, this system is further developed by successfully overcoming the system's main limitation, i.e., product inhibition, through co-expression of a lactonase hydrolyzing inhibitory ϵ -caprolactone (ϵ -Cl). The *in vivo* redox cascade thereby established in cyanobacteria is then characterized regarding process performance and light conversion efficiency in photo-STRs. **Chapter 5** refines the quantitative perspective investigating under which environmental conditions the oxygenase reaction can be supplied with electrons most effectively in growing cells, making use of flat panel reactors and continuous cultivation. The discussion in **Chapter 6** highlights the novel findings of this thesis and puts them into context of photo-biotechnology research today.

2 Enlighting electron routes in oxyfunctionalizing *Synechocystis* sp. PCC 6803

Abstract: Phototrophic microorganisms, like cyanobacteria, are gaining attention as host organisms for biocatalytic processes with light as energy source and water as electron source. Redox enzymes, especially oxygenases, can profit from *in-situ* supply of co-substrates, i.e., reduction equivalents and O₂, by the photosynthetic light reaction. The electron transfer downstream of photosystem I to heterologous electron consuming enzymes in principle can involve NADPH, NADH, and/or ferredoxin, whereas most direct and efficient transfer is desirable. Here, we use the model organism *Synechocystis* sp. PCC 6803 (*Synechocystis*) to investigate, to what extent host and/or heterologous constituents are involved in electron transfer to a heterologous cytochrome P450 monooxygenase from *Acidovorax* sp. CHX100. Interestingly, in this highly active light-fueled cycloalkane hydroxylating biocatalyst, host-intrinsic enzymes were found capable of completely substituting the function of the *Acidovorax* ferredoxin reductase. To a certain extent (20%), this also was true for the *Acidovorax* ferredoxin. These results indicate the presence of a versatile set of electron carriers in cyanobacteria, enabling efficient and direct coupling of electron consuming reactions to photosynthetic water oxidation. This will both simplify and promote the use of phototrophic microorganisms for sustainable production processes.

This chapter has been published in

ChemBioChem, **2023**, e2023000475

Adrian TÜLLINGHOFF, Jörg TOEPEL, and Bruno BÜHLER

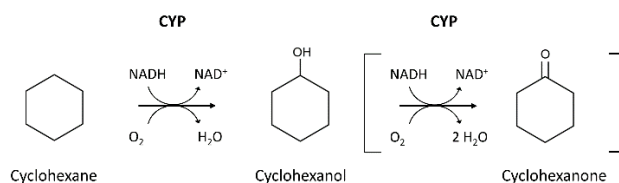
<https://doi.org/10.1002/cbic.202300475>

2.1 Introduction

Sunlight constitutes the central energy source for terrestrial life. The sun today provides more than a thousand-fold of the energy demand of mankind.[8] With photosynthesis, nature invented a process converting light energy to chemical energy in the form of biomass. Cyanobacteria were the first organisms known to perform oxygenic photosynthesis, i.e., using water as electron donor by sequentially linking two photosystems.

Photo-biotechnology seeks to exploit this natural concept to utilize sunlight as abundant energy source to drive productive (bio-)chemical processes. Using phototrophic microorganisms as cell factories, various platform chemicals, such as ethanol,[176] 1-butanol,[177] and glycerol,[109] have been made accessible from CO₂. From an energy economics perspective, this concept surpasses the energy-intensive formation of complex biomass, of which the components then have to be separated/made use of in an again energy-intensive way. In fact, the closer energy demanding processes are coupled to the energy harvesting process, which is the photosynthetic light reaction, the higher becomes the energy efficiency.[8] In this respect, the direct harvesting of high-energy-electrons to drive redox reactions is especially attractive. This allows conversion of externally supplied substrates, reduction of interference with host C-metabolism, and even exploitation of surplus reduction potential not used to fuel rate-limiting C-fixation.[178] It has been shown that heterologous electron-demanding reactions indeed can tap unused potential of photosynthesis by relieving the so-called sink-limitation, which is the limitation of photosynthesis by the lack of available electron sinks.[73, 161]

Among the various electron-consuming enzymes, oxygenases are of special interest for application in cyanobacteria. They require electrons in the form of NADPH, NADH, or reduced ferredoxin (Fd) as well as O₂, which both can be supplied *in situ* by the photosynthetic light reaction,[58] overcoming limitations often encountered in biocatalytic oxyfunctionalizations. Several oxygenases including cytochrome P450 monooxygenases (CYP450s)[68, 72, 74, 84] and Baeyer-Villiger monooxygenases (BVMOs)[179](see also Chapter 3) have been investigated in *Synechocystis* sp. PCC 6803 (*Synechocystis*). Whereas NADPH or NADH typically serve as electron donors,[180] multicomponent oxygenases, as most CYP450s are, also involve electron transfer proteins such as rubredoxin or Fd. The well described cycloalkane-hydroxylating CYP450 system of *Acidovorax* sp. CHX100 (*Acidovorax*) has recently been applied for light-driven oxyfunctionalization of cyclohexane (Chx) in *Synechocystis* (Scheme 1).[74, 98] It consists of three components, a NADH-dependent Fd reductase (FNR_{Av}), a Fd (Fd_{Av}), and an oxygenase (CYP_{Av}), the former two transferring electrons from NADH to CYP_{Av}. [164, 181]



Scheme 1. **Cyclohexane (Chx) oxyfunctionalization catalysed by cytochrome P450 monooxygenase from *Acidovorax* sp. CHX100 (CYP)**. CYP catalyses Chx hydroxylation utilizing O_2 and NADH as co-substrates and shows a minor activity for the overoxidation of cyclohexanol to cyclohexanone (given in brackets).

Fueled by energy from the sun, the photosynthetic light reaction provides water-derived reduction equivalents to a multitude of cellular processes, including carbon fixation as well as nitrogen and sulfur assimilation. In *Synechocystis*, native Fd1 plays a central role in diverting electrons from photosystem I (PS I) to different assimilative and regulative processes,[21] most importantly to ferredoxin-NADP⁺ reductase (FNR_{Syn}) reducing NADP⁺ to the central electron currency NADPH required, e.g., for C-fixation and N-assimilation. Besides the essential and most abundant Fd1, *Synechocystis* possesses 8 other Fds, which can be classified according to the type of their iron sulfur center architecture.[77] These Fds, being functional under specific conditions, provide a high metabolic flexibility. Thereby, they constitute a core part of the diverse set of electron carriers and oxidoreductases required to run the variety of electron demanding pathways in the non-compartmented cyanobacterial cell. This toolset has the potential to make *Synechocystis* – or cyanobacteria in general – exceptionally interesting host organisms for redox biocatalysis with water as a highly sustainable electron source.

In this study, we aim at elucidating the potential of the cyanobacterial redox apparatus to support and simplify light-driven whole-cell redox biocatalysis. Specifically, we investigate if and to what extent FNR and Fds of *Synechocystis* can take over functions of the native redox partners of CYP_{Av}. For this purpose, Chx hydroxylation by CYP_{Av} in the absence of FNR_{Av} and/or Fd_{Av} is investigated in *Synechocystis*.

2.2 Experimental section

2.2.1 Strains, chemicals, and cultivation methods

DNA oligonucleotides, plasmids, and bacterial strains used for cloning procedures are given in the Supporting Information (Table S1). *Synechocystis*[182] was cultivated in 20 or 50 mL BG11 medium[183] with 50 mM 4-(2-hydroxyethyl)-1-piperazinethanesulfonic acid (HEPES), pH 7.2, using 100- or 250 mL baffled shaking flasks with cotton stoppers, respectively. Cultivation conditions were 30°C, 150 rpm (2.5 cm amplitude), 50 $\mu\text{mol}_{\text{photons}} \text{m}^{-2} \text{s}^{-1}$, ambient CO_2 (0.04 %[v/v]), 75% humidity, start $\text{OD}_{750} = 0.06\text{-}0.08$. Plate cultivation was conducted on BG11 agar plates with 1.5-2.0% agar at 30°C and 25 $\mu\text{mol}_{\text{photons}} \text{m}^{-2} \text{s}^{-1}$. If required, kanamycin

(Km) was used at a final concentration of 50 $\mu\text{g mL}^{-1}$. Chx, $\geq 99.8\%$ purity, and cyclohexanol (C-ol), $\geq 99\%$ purity, were purchased from Merck (Darmstadt, Germany), cyclohexanone (C-one), $\geq 99.5\%$ purity, was purchased from Sigma-Aldrich (Steinheim, Germany). All other chemicals were purchased from Carl-Roth GmbH (Karlsruhe, Germany), Merck, or Sigma-Aldrich at the highest purity available.

2.2.2 Cloning and transformation

Standard molecular biology procedures were applied as described.[184] Constructs were based on the replicative pPMQAK1 plasmid[141] containing the Isopropyl- β -D-thiogalactopyranosid (IPTG)-inducible *P_{trc10}* promoter system. For construction of pAH_CYP, pPMQAK1 was digested with *BcuI* FD, followed by the insertion of the CYP_{Av} gene (amplification with primer pair PAH162/ PAH163 using pAH_CYP_FNR_Fd as template, see Table S1) by Gibson cloning. Additionally, a terminator unit (amplification with primers PAH136/PAH137 from pAH_CYP_FNR_Fd) was inserted between the *lacI* operon and the functional CYP operon via digestion with *XbaI* FD and Gibson cloning. For plasmid pAH_CYP_FNR, a one-step strategy was applied: pPMQAK1 was digested with *XbaI* FD and *BcuI* FD, followed by insertion via Gibson cloning of a fragment comprising the terminator unit together with the CYP_{Av} and FNR_{Av} genes (amplification with primers PAH077/PAH164 from pAH_CYP_FNR_Fd). A similar strategy was followed for pAH_CYP_Fd construction: pPMQAK1 was digested with *XbaI* FD and *BcuI* FD and two fragments, comprising i) the terminator unit and the CYP_{Av} gene (primers PAH077/PAH130, template pAH_CYP_FNR_Fd) and ii) the Fd_{Av} gene (primers PAH131/PAH165, template pAH_CYP_FNR_Fd) were inserted.

E. coli DH5 α [185] was transformed with Gibson products via electroporation and correct assembly of plasmids was confirmed via colony PCR and subsequent sequencing. Commercial kits from Macherey-Nagel (Düren, Germany) were used for plasmid DNA extraction and DNA purification.

The strains *Synechocystis* CYP_only, *Synechocystis* CYP_Fd, and *Synechocystis* CYP_FNR (Table S1) were generated by transforming wild type *Synechocystis* with plasmid pAH_CYP, pAH_CYP_FNR, and pAH_CYP_Fd, respectively. For electroporation, cells were grown under standard conditions to an OD₇₅₀ of 0.5-0.7, harvested by centrifugation at 5000 x g and 4°C, and washed and 50 x concentrated in 1 mM HEPES, pH 7.5 (according to[186]). Sixty μl cell suspension were supplied with 0.5-1 μg of plasmid DNA and electroporated (2.5 kV; 5 ms). After 24 h recovery in BG11 under standard conditions, selection was performed at 25 $\mu\text{mol}_{\text{photons}} \text{m}^{-2} \text{s}^{-1}$ on BG11 agar plates containing Km. Transformants grown within 7-10 days were confirmed via colony PCR and sequencing via Genewiz (Azenta, Chelmsford, MA).

2.2.3 Whole-cell activity assays

Cultures of recombinant *Synechocystis* were harvested by centrifugation at 5000 g and 4°C 24 h after induction with 1 mM IPTG and resuspended to a cell concentration of 0.7 - 1 g_{CDW} L⁻¹ in BG11 containing 50 mM HEPES. One ml portions were distributed in 10 ml Pyrex tubes and equilibrated for 10 min at 30°C, 150 μmol_{photons} m⁻² s⁻¹, ambient CO₂ [0.04%], and 200 rpm. Bioconversions were started by adding Chx to a final concentration of 5 mM and stopped after 10 min by quenching with 1 vol diethyl ether containing 0.2 mM *n*-decane as internal standard (for GC analysis). One unit was defined as 1 μmol product formed per min.

2.2.4 In-vitro activity assays

Forty five ml cell culture of recombinant *Synechocystis* strains were harvested by centrifugation at 5000 g and 4°C 24 h after induction with 1 mM IPTG and resuspended in 1.5 ml 100 mM Kpi-buffer, pH 7.5, containing 2 mM phenylmethylsulfonyl fluoride as protease inhibitor. Crude cell extracts were obtained as described in Chapter 3, but with extended centrifugation after cell disruption for 30 min. Enzyme activity was determined based on the decrease in NAD(P)H absorption at 340 nm with a Cary Bio 300 UV-visible spectrophotometer (Varian, Palo Alto, USA) following a described procedure:[187] Assay mixtures of 2 ml total volume in a screw capped cuvette contained 200 μM NAD(P)H and 50-100 μl crude cell extract (0.1-0.3 mg protein) in 100 mM KPi buffer. Assays were initiated by adding 2.5 μl pure Chx and were performed for at least 2 min. Initial activities were calculated from the absorption decrease at 340 nm using a specific absorption coefficient of $\epsilon = 6.22 \text{ mM}^{-1} \text{ cm}^{-1}$ and corrected for the absorption decrease without addition of substrate. One unit of enzyme activity was defined as 1 μmol of NADPH consumed per min.

2.2.5 Analytics

Cell concentrations were assessed by determining OD₇₅₀ in a LibraS11 spectrophotometer (Biochrom, Cambridge, UK). A correlation factor of 0.225 g_{CDW} L⁻¹ per OD₇₅₀ unit was used to calculate cell dry weight (CDW) concentrations.[58] Reactant concentrations were determined by gas chromatography (GC) as described before.[165] See Figure S1 for exemplary calibration curves.

2.3 Results and Discussion

The versatile set of redox components within *Synechocystis* is highly promising for being utilized for light-driven whole-cell redox biocatalysis. In order to investigate, if and to what extent FNR and Fds of *Synechocystis* can substitute functions of the native redox partners of CYP_{Av}, plasmids able to replicate in *Synechocystis* and containing either CYP_{Av} only (pAH_CYP) or in combination with FNR_{Av} (pAH_CYP_FNR) or Fd_{Av} (pAH_CYP_Fd) were constructed (Figure 5). These plasmids were then used to transform *Escherichia coli* DH5α to

confirm successful assembly via colony PCR (Figure S2) and sequencing. Eventually, *Synechocystis* was transformed with these plasmids, yielding the strains *Synechocystis* CYP_only, *Synechocystis* CYP_FNR, and *Synechocystis* CYP_Fd.

In order to test, if electron transfer to the heterologous CYP_{AV} can still be established within *Synechocystis*, several clones of all generated strains were characterized in whole-cell activity assays probing their capability to oxyfunctionalize Chx.

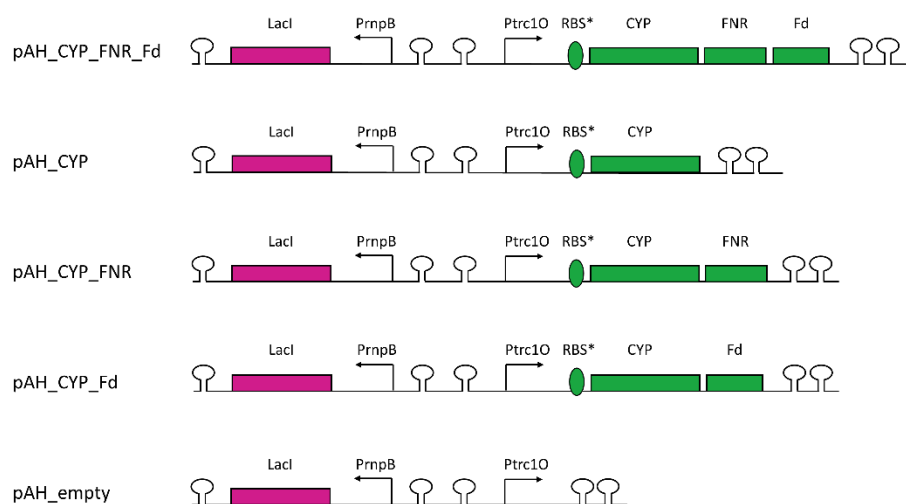


Figure 5: **Inserts on replicative plasmids** comprising different combinations of the three-component CYP450 system of *Acidovorax* sp. CHX100. CYP – cytochrome P450 monooxygenase, Fd – Ferredoxin, FNR – Ferredoxin-NADPH-reductase.

Heterologous expression of the CYP_{AV} alone in *Synechocystis* CYP_only yielded a residual activity of $4.6 \pm 0.8 \text{ U g}_{\text{CDW}}^{-1}$ with the most active clone showing an activity of $5.2 \pm 0.3 \text{ U g}_{\text{CDW}}^{-1}$ (Figure 6A). Thereby, overoxidation of C-ol to C-one made up 2% of overall product formation as observed before with all three genes encoding the three CYP450 components of *Acidovorax* expressed in *Synechocystis*.^[74] The hydroxylation capacity of *Synechocystis* expressing CYP_{AV} without any native electron carrier, although being lower (making up 20%) compared to the presence of all three CYP components of *Acidovorax*, indicates that FNR_{AV} and Fd_{AV} are dispensable for electron transfer to CYP_{AV} in *Synechocystis*.

Obviously, one (or more) intrinsic electron carrier(s), possibly Fds, are able to transfer electrons to CYP_{AV}. A similar phenomenon has been reported for CYP105A1 from *Streptomyces griseolus*, which could be supplied with electrons by Fds from tobacco plants, but only for a low rate of about $0.02 \text{ mU g}_{\text{leaf}}^{-1}$.^[158] This reflects the flexibility of CYP450s regarding accepted electron donor systems.^[188, 189] Fd_{AV}, however, shows a rather low sequence identity to plant-type Fds 1-4 including Fd 1 known to be the major Fd accepting electrons from PS I (Table 3). Fd_{AV} showed the highest identity to the bacterial-type Fd5 of *Synechocystis*, for which, however, the native function is unknown.

Overall, it is noteworthy that the host-intrinsic set of redox carriers can sustain up to 20% of the CYP_{AV} activity achieved with the complete *Acidovorax* system in *Synechocystis*. Specific activities around 5 U g_{CDW}⁻¹ may well suffice for biotransformations providing high value products as the recently reported testosterone hydroxylation with CYP110D1 from *Nostoc* sp. PCC 7120 in *Synechocystis* (with activities of up to 1 U g_{CDW}⁻¹).[190]

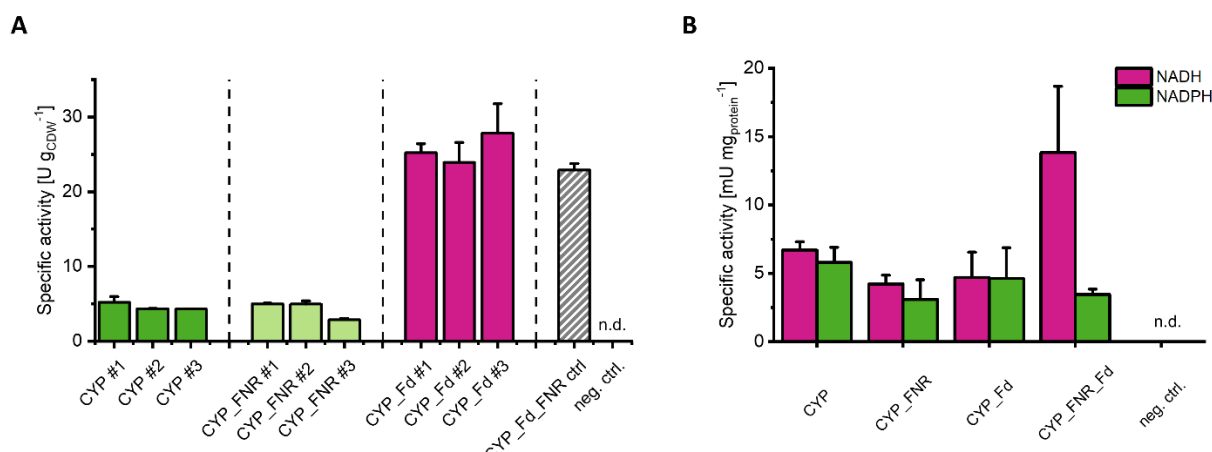


Figure 6: Activity assays with A) whole cells and B) crude cell extracts of recombinant *Synechocystis* containing different combinations of CYP450 components. **A:** Specific activities of *Synechocystis* containing CYP_{AV} alone (green) or in combination with FNR_{AV} (light green), Fd_{AV} (pink), both as positive control (grey striped), or the empty vector as negative control (neg. ctrl., black). Assay conditions: 10 min at 30°C, 150 μmol_{photons} m⁻² s⁻¹, ambient CO₂ [0.04%], and 200 rpm. Numbers refer to different clones. **B:** Activities of crude cell extracts of the same strains assessed via absorption of NADH (pink) or NADPH (green) at 340 nm and referred to the total protein concentration. Depicted are means from ≥3 independent measurements. n.d. – not detected.

The co-expression of the gene encoding FNR_{AV} together with the CYP_{AV} gene in *Synechocystis* CYP_FNR resulted in a specific activity of 4.3 ± 1.2 U g_{CDW}⁻¹ with 4.9 ± 0.1 U g_{CDW}⁻¹ for the best clone (Figure 6A), which is similar to *Synechocystis* CYP_only, indicating that FNR_{AV} cannot efficiently contribute to electron transfer to CYP_{AV} in the absence of Fd_{AV}.

Interestingly, when co-expressing the Fd_{AV} gene together with the CYP_{AV} gene in *Synechocystis* CYP_Fd, a specific activity of 25.6 ± 2.0 U g_{CDW}⁻¹ was measured (27.8 ± 3.9 U g_{CDW}⁻¹ for the best clone, Figure 6A). Thereby, *Synechocystis* CYP_Fd showed an even somewhat higher specific activity than *Synechocystis* CYP_FNR_Fd harboring all three *Acidovorax* components (22.9 ± 0.9 U g_{CDW}⁻¹ in the same biotransformation setup).[74] These data indicate that the FNR_{AV} plays a negligible role in electron transfer to CYP_{AV} in *Synechocystis*.

Matching the observation that the role of native electron transfer components of CYP450s can be taken over by functional homologues, *in vitro* studies revealed that *Sorghum bicolor* CYP79A1 was supplied with PS I-derived electrons two times more efficiently by spinach FNR and Fd than by its native components.[157] Native reductases, like FNR_{Syn} or ferredoxin-thioredoxin reductase (FTR_{Syn}), may well take over the function of FNR_{AV} enabling the high hydroxylation activity (Figure 7, compare also[75]). FNR_{Syn} is known to have many interaction

partners functioning as a hub for the distribution of electrons derived from Fd1,[21] whereas FTR_{Syn} was shown to shuffle electrons between specific Fds (Fd1, Fd7, and Fd9), thereby functioning as a link between different electron routes.[77] Thus, both FNR_{Syn} and FTR_{Syn} may be involved in the efficient electron transfer from PS I to Fd_{Av}. Alternatively, direct electron transfer from PS I to Fd_{Av} may occur (Figure 7).

Table 3: **Native Ferredoxins (Fds) in *Synechocystis***. Based on [77]. HL – high light, BL – blue light, LL – low light, HT – high temperature, LFe – iron starvation, LC – low carbon.

Name	Gene	Type	Conditions for upregulation	Identity to Fd _{Av} ^[a]
Fd1	ssl0020	[2Fe-2S] plant-like	Light, NaHCO ₃	17.5%
Fd2	slI1382	[2Fe-2S] plant-like	Cd, H ₂ O ₂ , HL, BL, UV	12.4%
Fd3	ssl1828	[2Fe-2S] plant-like	BL	23.8%
Fd4	slr0150	[2Fe-2S] plant-like	LL, H ₂ O ₂	18.1%
Fd5	slr0148	[2Fe-2S] bacterial-type	LL, H ₂ O ₂	35.9%
Fd6	ssl2559	[2Fe-2S] bacterial-type	BL	24.4%
Fd7	slI0662	[4Fe-4S]	LFe, HL, LC	11.5%
Fd8	ssr3184	[3Fe-4S][4Fe-4S]	Cd, HL, LC	15.2%
Fd9	slr2059	[4Fe-4S][4Fe-4S]	HL, HT	9.0%

[a] aa identity as determined using the Uniprot alignment tool, see Figure S3.

To shed more light on the electron routes from *Synechocystis* PS I to CYP_{Av}, we performed activity assays with crude cell extracts of the *Synechocystis* strains containing different CYP450 component combinations and used either NADH or NADPH as electron donor (Figure 6B). The overall highest specific activity (12.8 ± 4.8 mU mg_{protein}⁻¹) was expectedly measured for extracts containing all three *Acidovorax* CYP450 components and NADH as their native electron donor. Also extracts with incomplete sets of *Acidovorax* CYP450 components, even with CYP_{Av} alone, enabled functional electron transfer from NADH to CYP_{Av}, although at clearly lower rates. Evidently, *Synechocystis* components partly substitute electron transfer functions of the (missing) native components also in the absence of a functional photosynthetic electron transport chain. Intriguingly, when using NADPH as electron donor, the extracts containing Fd_{Av} did not depict significantly higher specific activities compared to extracts containing CYP_{Av} and FNR_{Av} or CYP_{Av} alone. This questions a dominant contribution of electron transfer via FNR_{Syn} or FTR_{Syn} to Fd_{Av}. High activities for a combination of CYP_{Av} and Fd_{Av} are only observed in intact cells, indicating electron transfer from the photosynthetic electron transport chain, most probably PS I, to Fd_{Av}. The long isoform of FNR_{Syn} can, however, associate to membrane-bound phycobilisomes,[191] which may contribute to the comparably low level of activities found in CYP_{Av} and Fd_{Av} containing cell extracts with NADPH.

The high diversity of CYP450 systems and their electron transport chains attracted the idea of employing non-native electron transport chains for electron supply to CYP450s.[189, 192, 193] Jung et al. showed that the electron transfer via putidaredoxin (CamA) and putidaredoxin reductase (CamB) from *Pseudomonas putida* to CYP135A35 (from *Gordonia alkanivorans*) *in vitro* was 4-times lower compared to an artificial, self-sufficient (one-component) CYP135A35-BM3.[194] Notably, the three-component system with electron transfer via CamA and CamB suited better for whole cells of *E. coli*, reaching a 1.5-times higher yield compared to CYP135A35-BM3.[194] The authors argue that the whole-cell setup benefits the three-component system, as the reduced effective reaction volume in cells enhances electron transfer efficiency. At the same time, uncoupling may be reduced compared to single component systems proposed to suffer from a high electron pressure.[195]

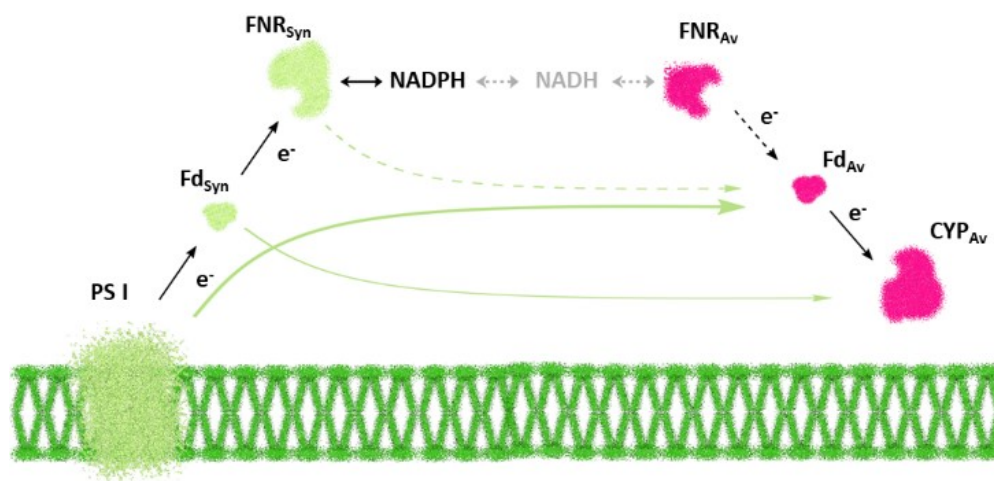


Figure 7: **Possible electron transfer routes to cytochrome P450 monooxygenase (CYP_{Av}) in *Synechocystis* sp. PCC 6803 (*Synechocystis*).** Supplied by the photosynthetic apparatus in the thylakoid membrane (green), electrons (e⁻) are transferred from photosystem I (PS I) via Fd_{Syn} to FNR_{Syn} (all from *Synechocystis*, orange). In the form of NADPH or reduced Fd_{Syn}, e⁻ can be utilized by native electron sinks or by heterologous FNR_{Av} and Fd_{Av} to finally be consumed by CYP_{Av} (all from *Acidovorax*, blue). Straight/dashed orange lines: possible/potential interactions of electron carriers of *Synechocystis* with heterologous electron carriers/sinks. Experimental findings indicate e⁻ transfer from PS I to Fd_{Av}, whereas soluble FNRs (e.g., FNR_{Syn}) show less contribution. To a small extent, *Synechocystis* components, like Fd_{Syn}, appear to directly transfer e⁻ to CYP_{Av}. For details, see main text.

Regarding the electron donor, photosynthesis-driven CYP450 catalysis can be considered of special interest, as water constitutes a highly abundant, cheap, and sustainable electron source. Lately, Mascia et al. reported that light-driven testosterone hydroxylation by *Synechocystis* containing CYP110D1 outcompeted a heterotrophic *E. coli* strain containing CYP110D1 together with the electron carriers CamA and CamB, for an overall specific activity of 1 U g_{CDW}⁻¹. [190] Furthermore, the alkane monooxygenase (AlkBGT), a three-component non-heme diiron enzyme from *P. putida* GPO1, has recently been reported to function in *Synechocystis* independently of its native rubredoxin reductase, but rely on the native

rubredoxin for an activity of $\sim 3 \text{ U g}_{\text{CDW}}^{-1}$, similar to that achieved with all three components.[75] The light-driven whole-cell activities reported in these studies were, however, by far lower than those reached in this study. Further, this study gives new insights about the routes of electrons from water oxidation to heterologous oxygenase subunits in *Synechocystis*. The importance of both heterologous and host intrinsic electron transfer components like Fd_{Av} and $\text{PS I/FNR}_{\text{Syn}}$, respectively, is highlighted. Together with the above described and discussed flexibility of CYP450 and other multicomponent oxygenase systems regarding electron transfer to their oxygenase component, especially in cyanobacteria,[75, 157, 158, 188-190] the findings for the *Acidovorax* CYP450 in this study further reinforce the flexible application of multicomponent oxygenases in cyanobacteria and bring it to another level, especially considering the high levels of specific activities reached.

Redox potentials also play an important role in electron transfer. Depending on their sequence and structure, the reduction potentials of Fds vary. To the best of our knowledge, besides data for Fd1 (-420 mV, [77]), there is no data on redox potentials of other *Synechocystis* Fds available. Whereas plant type Fds typically show reduction potentials around -420 mV, Fds of CYP450s can show considerably higher reduction potentials such as the -240 mV reported for CamA.[196] It is proposed that the redox potential of Fds is not a key factor in supporting CYP450 activity and that other properties such as substrate-induced lowering of P450 heme-iron redox potential also play important roles.[196, 197]

For *Synechocystis* CYP_only and *Synechocystis* CYP_Fd, the expression of less enzyme components reduces the expression burden compared to the three-component system. In this regard, enhanced expression may be achieved with alternative systems, e.g., P_{cpc} , [198] P_{nrsB} , (Chapter 3) P_{Rha} , [199] or stronger expression systems to be developed in future. Strategies to further improve the efficiency of electron transfer from PS I to (heterologous) electron consumers include enzyme anchoring in the thylakoid membrane[68] or fusions of Fd and CYP.[200] Such strategies will benefit from a thorough understanding of the intrinsic Fds and their contribution to heterologous redox biocatalysis. This also holds for light-driven H_2 production based on *Synechocystis* and native[80] or heterologous[201] hydrogenases, as Fds with their strongly negative redox potential constitute highly interesting electron donors to fuel such H_2 formation.

2.4 Conclusion

The presented electron transfer study with *Synechocystis* strains expressing CYP_{Av} either alone or in combination with one of its native electron transfer components FNR_{Av} or Fd_{Av} show that i) CYP_{Av} alone can be supplied with electrons in whole cells of *Synechocystis*, although at a lower rate compared to the native three-component system and that ii) the high

oxyfunctionalization rate of the *Acidovorax* system heterologously expressed in *Synechocystis* can also be achieved with the combination of CYP_{Av} and Fd_{Av}, i.e., without FNR_{Av}, indicating that host intrinsic enzyme systems such as PS I or FNR_{Syn} can efficiently reduce Fd_{Av}. In the light of photo-biotechnology aiming to utilize the energy of the sun for (redox) catalysis, these findings will promote advances in photosynthesis-driven production processes.

3 Maximizing photosynthesis-driven Baeyer-Villiger oxidation efficiency in recombinant *Synechocystis* sp. PCC 6803

Photosynthesis-driven whole-cell biocatalysis has great potential to contribute to a sustainable bio-economy since phototrophic cells use light as only energy source. It has yet to be shown that phototrophic microorganisms, such as cyanobacteria, can combine supply of high heterologous enzyme levels with allocation of sufficient reduction equivalents to enable efficient light-driven redox biocatalysis. Here, we demonstrate that the heterologous expression of a NADPH-dependent Baeyer-Villiger monooxygenase (BVMO) gene from *Acidovorax* sp. CHX100 turns *Synechocystis* sp. PCC 6803 into an efficient oxyfunctionalization biocatalyst, deriving electrons and O₂ from photosynthetic water oxidation. Several expression systems were systematically tested and a *P*_{nrsB}-(Ni²⁺) controlled expression based on a replicative plasmid yielded the highest intracellular enzyme concentration and activities of up to 60.9 ± 1.0 U g_{CDW}⁻¹. Detailed analysis of reaction parameters, side reactions, and biocatalyst durability revealed – on the one hand – a high *in vivo* BVMO activity in the range of 6 ± 2 U mg_{BVMO}⁻¹ and – on the other hand – an impairment of biocatalyst performance by product toxicity and by-product inhibition. Scale-up of the reaction to 2-liter fed-batch photo-bioreactors resulted in a stabilization of the bioconversion over several hours with a maximal specific activity of 30.0 ± 0.3 U g_{CDW}⁻¹, a maximal volumetric productivity of 0.21 ± 0.1 g L⁻¹ h⁻¹, and the formation of 1.3 ± 0.1 g L⁻¹ of ε-caprolactone. Process simulations based on determined kinetic data revealed that photosynthesis-driven cyclohexanone oxidation on a 2-L-scale under high light conditions was kinetically controlled and not subject to a limitation by photosynthesis.

This chapter has been published in

Frontiers in Catalysis, **2022**, 1:780474

Adrian TÜLLINGHOFF, Magdalena B. UHL, Friederike E. H. NINTZEL, Andreas SCHMID, Bruno BÜHLER, and Jörg TOEPEL

<https://doi.org/10.3389/fctls.2021.780474>

3.1 Introduction

Biotechnological processes have been developed since decades to produce materials, chemicals and pharmaceuticals.[49] Compared to standard chemical processes, they in general require less energy due to milder reaction conditions, produce less toxic byproducts, and use less harmful reagents, giving them high potential to be environmentally friendlier. [50, 51] While there are numerous feasible processes using enzymes as catalysts or microbes as whole-cell factories, redox biocatalysis remains challenging.[52] This is due to the dependence of redox enzymes on co-substrates such as electron carriers and O₂. [53] When using isolated enzymes as catalysts, process efficiencies suffer from high enzyme and cofactor regeneration costs.[54] Applying whole cells bears the advantage to employ their metabolism to balance redox demands, e.g., by oxidizing readily available organic compounds to enable electron supply. However, respective costs and high O₂ demands still often hinder efficient, stable, and cheap redox biocatalysis in heterotrophic cell factories.[54, 56]

To overcome these issues, phototrophic microorganisms, such as the model cyanobacterium *Synechocystis* sp. PCC 6803 (*Synechocystis*), are highly attractive host organisms for oxygenases, [68, 74, 78, 202] reductases,[79] and hydrogenases.[80] Their photosynthetic apparatus can be exploited to supply oxygenase reactions not only with reduction equivalents, but also with O₂ from water and sunlight, the most environmentally friendly co-substrates.[58] As whole-cell biocatalysts, cyanobacteria combine this advantage with their self-(re)generation capacity, relying on light, water, and CO₂ as main resources.[59] Yet, phototrophs so far have gathered little attention as biocatalysts for regio-, chemo-, or stereoselective oxyfunctionalizations. Efforts to engineer cyanobacteria, such as introducing a cytochrome P450 monooxygenase (CYP),[73] fusing a cytochrome P450 to a subunit of photosystem I (PS I)[68] or implementing CYP-dependent pathways,[72] remained on proof-of-concept level.

Photosynthesis-driven oxyfunctionalization processes are hampered by a gap of knowledge regarding i) sufficient gene expression,[68] (ii) protein stability and folding, and (iii) co-factor supply. However, these aspects are of special importance to ensure that biocatalysis can be conducted in an efficient, stable, and host-compatible manner. Another hindrance for efficient photo-biotechnology are the high doubling times of cyanobacteria (8-12 h for *Synechocystis*, [62]) and their light-dependency, which limits high-density cultivation and scalability.[203]

High-level expression of heterologous genes in phototrophic organisms suffers from a poorly developed molecular biology tool box compared to typical heterotrophic hosts.[204] Specific characteristics, such as the structure of the RNA-polymerase,[205] promoter types,[141] and a circadian program [206] are fundamental differences to well-studied heterotrophic hosts and often hamper transcriptional engineering.[46, 143] There are, however, pivotal recent developments, such as the design of shuttle vectors [141] and expression studies focusing on

promoters [199, 207] and RBS's,[207], utilized to increase product titers.[208] For detailed perspectives on regulatory systems and promoter types in cyanobacteria, the reader is referred to [147, 209-211].

Recent studies employing oxygenases in *Synechocystis* already showed the accessibility of O₂ and electrons derived from the light reaction.[74] The employment of strictly NADPH-dependent oxygenases, such as cyclohexanone monooxygenase from *Acinetobacter calcoaceticus*, led to rather low activities in *Synechocystis*. [78] This is unexpected as i) sufficient NADPH supply can be assumed under light conditions, with NADPH as main product of the photosynthetic light reaction and ii) high-level NADPH supply was shown recently for a NADPH dependent reductase in *Synechocystis*. [79]

In this study, we aimed to establish and scale efficient NADPH-dependent BVMO biocatalysis driven by light. To this end, we chose a BVMO from *Acidovorax* sp. CHX100 for heterologous expression in *Synechocystis*. This NADPH-dependent BVMO has been shown to exhibit high activity in *Pseudomonas taiwanensis* VLB120 and used for efficient cascade designs. [165, 166] We systematically investigated, how expression levels of the respective gene in *Synechocystis* can be enhanced and investigated the resulting BVMO performance in *Synechocystis*. Further, we examined limitations regarding gene expression, reaction kinetics, and host metabolism. Respective reaction engineering and scaling are shown to enable BVMO catalysis with an efficiency auguring well for future applications of light-driven redox biocatalysis.

3.2 Experimental section

3.2.1 Strains, chemicals and cultivation methods

DNA oligonucleotides, plasmids and bacterial strains used for cloning procedures are given in the Supporting Information (Table S2). *Synechocystis* [182] was cultivated in 20 or 50 mL YBG11 medium [183] with 50 mM 4-(2-hydroxyethyl)-1-piperazinethanesulfonic acid (HEPES), pH 7.2 using 100- or 250 mL baffled shaking flasks with cotton stoppers, respectively. Cultivation conditions were 30 °C, 150 rpm [2.5 cm amplitude], 50 μmol_{photons} m⁻² s⁻¹, ambient CO₂ [0.04 %], 75 % humidity, start OD₇₅₀ = 0.06-0.08. Plate cultivation was conducted on BG11 agar plates with 1.5-2.0 % agar at 30 °C and 25 μmol_{photons} m⁻² s⁻¹. If required, Km was used at a final concentration of 50 μg mL⁻¹. Cyclohexanone (C-one), ≥ 99.5% purity, was purchased from Sigma-Aldrich (Steinheim, Germany). Cyclohexanol (C-ol), ≥ 99% purity, was purchased from Merck (Darmstadt, Germany). All other chemicals were purchased from Carl-Roth GmbH (Karlsruhe, Germany), Merck, or Sigma-Aldrich at the highest purity available.

3.2.2 Cloning and transformation

Standard molecular biology procedures were applied as described by [184]. For construction of pAH059, a fragment coding for the C-terminal *Strep*-tagged *bvmo* gene [165] was amplified from pCom10_Capro [164] via Phusion PCR using the primer pair PAH096/097 and cloned via Gibson assembly [212] into pEERM3_Km, linearized by *Xba*I/*Pst*I-double digestion. For construction of pAH063, the expression cassette of *PrnsB_bvmo_Strep*-tag_terminator was amplified via Phusion PCR using the primer pair BVMO1/2 and cloned via Gibson assembly into pPMQAK1, linearized with *Eco*RI/*Pst*I-double digestion. *Escherichia coli* DH5 α [185] was transformed with Gibson products via electroporation and correct assembly of plasmids was confirmed via colony PCR of transformants and subsequent sequencing. Commercial kits from Macherey-Nagel (Düren, Germany) were used for plasmid DNA extraction and DNA purification.

For electroporation of *Synechocystis*, cells were grown under standard conditions to an OD₇₅₀ = 0.5-0.7 determined with a LibraS11 spectrophotometer (Biochrom, Cambridge, UK), harvested by centrifugation at 5000 x g and 4 °C, washed and 50 x concentrated in 1 mM HEPES, pH 7.5 (according to [186]). Sixty μ l cell suspension were supplied with 0.5-1 μ g of plasmid DNA and electroporated (2.5 kV; 5 ms). After 24 h recovery in YBG11 under standard conditions, selection was performed at 25 μ mol_{photons} m⁻² s⁻¹ on BG11 agar plates containing Km. Transformants grown within 7-10 days were confirmed via colony PCR and sequencing. For chromosomal integration, complete segregation was achieved by iterative plating on selective agar plates with increasing Km concentration.

3.2.3 Protein analysis

Exponentially growing *Synechocystis*_Ni_cBVMO, *Synechocystis*_Ni_pBVMO, and *Synechocystis*_Cu_pBVMO cultures (see Table S2 for strain designations) were harvested by centrifugation at 5000 x g and 4 °C 24 h after induction with defined concentrations of NiSO₄ and concentrated to an OD₇₅₀ = 20 in 1 x TBS (1 mM phenyl-methyl-sulfonyl-fluoride, pH 7.5). Cells were disrupted in a Precellys® homogenizer for 3 cycles á 3 x 30'' with 30'' pause. After centrifugation at 13.300 g and 4 °C for 15 min, the supernatant was used for protein concentration determination via Bradford analysis.[213] Protein abundance was visualized using sodium dodecylsulfate polyacrylamide gel electrophoresis (SDS-PAGE) according to [214], with 3.6 % and 12 % acrylamide in the stacking and in the separation gels, respectively.

3.2.4 Whole-cell activity assays and determination of reaction kinetics

*Synechocystis*_Cu_pBVMO, *Synechocystis*_Ni_cBVMO, and *Synechocystis*_Ni_pBVMO cultures (Table S2) were harvested by centrifugation at 5000 g and 4 °C 24 h after induction with defined concentrations of NiSO₄ and adjusted to a defined cell concentration by re-suspending in YBG11 containing 50 mM HEPES and 10 μ M NiSO₄, pH 7.2, if not stated otherwise. Cells were equilibrated for 10 min to assay conditions. Standard assay conditions

were 30 °C, 200 rpm, 150 $\mu\text{mol}_{\text{photons}} \text{m}^{-2} \text{s}^{-1}$, ambient CO_2 [0.04 %]. The conversion of C-one to ϵ -caprolactone (ϵ -Cl) was started by adding C-one to a final concentration of 5 mM and was stopped after 30 min by either quenching with 1 vol diethylether containing 0.2 mM *n*-decane as internal standard (for GC analysis) or by adding 0.1 vol of acetonitrile (for HPLC analysis).

Table 4: **Conditions and data for *Synechocystis*_Ni_pBVMO-based cylohexaone (C-one) biotransformation** in a 2-L photo STR (Infors AG, Bottmingen, Switzerland).

Parameter	LL LC	HL LC	HL HC
Aeration			
Air [L min^{-1}]	2-0.2 ^a	2-0.2 ^a	2-0.2 ^a
CO_2 [mL min^{-1}]	-	-	20
Light [$\mu\text{mol}_{\text{photons}}^{-2} \text{s}^{-1}$]			
for growth	100	150-200-250 ^b	150-200-250 ^b
for biotransformation	150	700	700
C-one feed [set to $U \text{ g}_{\text{CDW}}^{-1}$]	25	15	30
Biomass conc. ^c [$\text{g}_{\text{CDW}} \text{L}^{-1}$]	0.55 ± 0.09	0.61 ± 0.04	1.02 ± 0.01
Product titer [mM]	11.6 ± 1.0	9.9 ± 1.6	11.5 ± 0.2
	after 27 h	after 25 h	after 27 h

LL – low light, HL – high light, LC – low carbon, HC – high carbon, see text for details.

^a For biotransformation, Air supply was reduced to 0.2 L min^{-1} .

^b Stepwise increase of light intensity during growth.

^c Biomass concentration at the start of the biotransformation, assessed via OD_{750} .

For short-term-assays (30 min), a cell concentration of 0.7 - 1 $\text{g}_{\text{CDW}} \text{L}^{-1}$ was used in a total volume of 1 ml in 10 ml Pyrex tubes. For the investigation of whole-cell kinetics, the cell concentration was reduced to 0.25-0.5 $\text{g}_{\text{CDW}} \text{L}^{-1}$ and the reaction time to 5 min to record initial activities.

Kinetic parameters (V_{max} , K_S , and K_i) were obtained by fitting according to Michaelis-Menten kinetics with substrate inhibition using *OriginPro2019* following equation (1), where V is the specific activity in $U \text{ g}_{\text{CDW}}^{-1}$ and $[S]$ is the substrate concentration.

$$(1) V = \frac{V_{\text{max}} * [S]}{K_S + [S] (1 + \frac{[S]}{K_i})} \quad [U \text{ g}_{\text{CDW}}^{-1}]$$

For competitive and non-competitive inhibitors, K_S and V_{max} in eq. 1 were replaced by K_S' according to equation (2) or V_{max}' according to equation (3), respectively, where $[I]$ and $K_{i,i}$ are the concentration and the inhibition constant of the respective inhibitor.

$$(2) K_S' = K_S * (1 + \frac{[I]}{K_{i,i}}) \quad [\mu\text{M}]$$

$$(3) V_{\text{max}}' = \frac{V_{\text{max}}}{(1 + \frac{[I]}{K_{i,i}})} \quad [U \text{ g}_{\text{CDW}}^{-1}]$$

3.2.5 Production process in a 2-L-stirred tank photo-bioreactor

Whole-cell biotransformations were conducted in a stirred tank photo-bioreactor Labfors 5 Lux (Infors AG, Bottmingen, Switzerland) with 2 L culture volume. Cells were grown for 3-4 days at 30 °C, 2 L min⁻¹ aeration with (high carbon, HC, additional 20 mL min⁻¹ CO₂) or without (low carbon, LC, no additional CO₂), 300 rpm stirrer speed and specific light intensities (for details, see Table 1). Induction with 10 μM NiSO₄ was performed 24 h prior to biotransformation start. During biotransformation, aeration was reduced to 0.2 L min⁻¹ and light intensity was set to low light (LL, 150 μmol_{photons} m⁻² s⁻¹) or high light (HL, 700 μmol_{photons} m⁻² s⁻¹). After pre-conditioning for 30 min, the biotransformation was initiated by starting a continuous feed of 0.25 M C-one in YBG11 medium. Samples were taken at regular time intervals and quenched immediately by adding either 1 vol diethylether or 0.1 vol acetonitrile.

3.2.6 Analytics

The cell concentration was assessed by determining OD₇₅₀ in a LibraS11 spectrophotometer (Biochrom, Cambridge, UK). The previously determined correlation factor of 0.225 g_{CDW} L⁻¹ per OD₇₅₀ unit was used to calculate CDW concentrations.[58] Chl-a concentration was determined as described by [161]. Concentrations of C-ol, C-one, and ε-Cl were determined by gas chromatography (GC) as described before.[165] See Figure S4 for exemplary calibration curves.

Concentrations of 6-hydroxyhexanoic acid (6-HA) were determined by high-pressure liquid chromatography (HPLC) on a Dionex Ultimate 3000 system equipped with an Acclaim® OA column (both Thermo Fisher Scientific, Waltham, MA). The sample was acidified with 1 M HCl to pH 3.0. The mobile phase A consisted of 100 mM sodium sulfate, adjusted with methanesulfonic acid to pH 3. Acetonitrile (>99.95% purity, ProtoChem) was used as mobile phase B. Sample volumes of 10–20 μL were injected, while the flow and the column temperature were kept constant at 0.4 ml min⁻¹ and 60 °C, respectively. The flow profile was as follows: 5 % B for 2 min, 5-30 % B in 6 min, 30-80 % B in 1 min, 80 % B for 1 min, 80-5 % B in 2 min and 5 % B for 5.5 min. Detection was accomplished via a UV detector at 210 nm.

3.2.7 Kinetic bioprocess modeling

For kinetic bioprocess modeling, the *Berkeley Madonna* software (Version 8.3.18) was used. The biotransformation converting C-one to ε-Cl as a product and C-ol as a by-product was described in a kinetic model. The concentration courses for substrate (S', C-one), product (P', ε-Cl), and by-product (B', C-ol) were calculated using equations 4-6

$$(4) S' = F - kB - kP \quad [\text{mM min}^{-1}]$$

$$(5) B' = kB \quad [\text{mM min}^{-1}]$$

$$(6) P' = kP \quad [\text{mM min}^{-1}]$$

with the C-one feed rate F in mM min^{-1} , the reaction rate of the keto reduction k_B (C-ol formation), and of ϵ -Cl formation k_P , described in equations 7 and 8. The reaction rates k_B and k_P were calculated based on determined kinetic parameters (K_s and V_{\max} for keto reduction and K_s , V_{\max} , and $K_{i,C\text{-one}}$ for ϵ -Cl formation); k_P was extended by the competitive inhibition by C-ol and the non-competitive inhibition by ϵ -Cl:

$$(7) k_P = \frac{V_{\max} * [S]}{K_s \left(1 + \frac{[B]}{K_{i,C\text{-ol}}}\right) + [S] \left(1 + \frac{[S]}{K_{i,C\text{-one}}}\right)} * \frac{1}{\left(1 + \frac{[P]}{K_{i,\epsilon\text{Cl}}}\right)} * X \quad [\text{mM min}^{-1}]$$

$$(8) k_B = \frac{V_{\max} * [S]}{K_i + [S]} * X \quad [\text{mM min}^{-1}]$$

with the biomass concentration X in $\text{g}_{\text{CDW}} \text{L}^{-1}$ and the inhibition constants $K_{i,C\text{-ol}}$, $K_{i,C\text{-one}}$, and $K_{i,\epsilon\text{Cl}}$ for C-ol (B), C-one (S), and ϵ Cl (P). See section 4.4 for the exact values chosen for the kinetic parameters.

S, P, and B were initially set to 0 and the parameters X (biomass concentration in $\text{g}_{\text{CDW}} \text{L}^{-1}$) and F (C-one feed rate in mM min^{-1}) were fed into the model according to the respective experiment. The kinetic process model can be found in the supplemental material.

3.3 Results

3.3.1 Plasmid based Ni^{2+} -induced gene expression leads to high levels of active BVMO

In order to systematically analyze different expression strategies in *Synechocystis*, three different strains were constructed: *Synechocystis_Cu_pBVMO* for plasmid-based BVMO gene expression under control of the Cu^{2+} -inducible *PpetE* promoter and *Synechocystis_Ni_pBVMO* and *Synechocystis_Ni_cBVMO* for plasmid- and genome-based BVMO gene expression, respectively, under control of the Ni^{2+} -inducible *PnrsB* promoter. All designed strains were compared in detail regarding protein level and specific C-one to ϵ -Cl conversion activity in short-term assays. Activities of the Ni^{2+} -inducible strains *Synechocystis_Ni_pBVMO* and *Synechocystis_Ni_cBVMO* were found to increase with increasing Ni^{2+} concentration yielding maximum specific activities of 52.2 ± 0.3 ($10 \mu\text{M Ni}^{2+}$) and $23.8 \pm 4.0 \text{ U g}_{\text{CDW}}^{-1}$ ($15 \mu\text{M Ni}^{2+}$), respectively (Figure 8A). The keto reduction of C-one to C-ol was found to occur at a low rate of $0.5 \pm 0.2 \text{ U g}_{\text{CDW}}^{-1}$ (for details, see section 3.3). It is important to note that expression induced by $15 \mu\text{M Ni}^{2+}$ did not significantly affect growth of *Synechocystis_Ni_pBVMO*, whereas this Ni^{2+} concentration slightly affected growth independently of BVMO gene expression (Figure S5). Cu^{2+} -induced *Synechocystis_Cu_pBVMO* yielded a maximal specific activity of $29.7 \pm 0.7 \text{ U g}_{\text{CDW}}^{-1}$ (with $0.5 \mu\text{M Cu}^{2+}$, Figure 8B). Ni^{2+} -inducible systems resulted in tightly regulated expression, whereas the Cu^{2+} -inducible system showed slight leakiness and poor titratability by the inducer concentration. Due to these reasons and the lower activity obtained upon plasmid-based expression, we focused on the Ni^{2+} -inducible system and investigated plasmid- and genome-based expression in more detail. SDS-PAGE analyses of

protein extracts of *Synechocystis_Ni_pBVMO* and *Synechocystis_Ni_cBVMO* showed a distinct band at ~60 kDa, coinciding with the BVMO size (57.8 kDa) (Figure 8C, D). This band intensified with increasing Ni²⁺-concentration and was absent in un-induced cells and cells carrying an empty vector. Densitometric analysis indicated that BVMO accounted for 1.1 ± 0.2% of total soluble protein (TSP) in *Synechocystis_Ni_pBVMO* induced with 10 μM Ni²⁺, a remarkably high value for heterologous expression in *Synechocystis*. Assuming a total protein content of 0.32-0.57 g g_{CDW}⁻¹, [215] the measured specific activity of 52.2 ± 0.3 U g_{CDW}⁻¹ translates into an *in vivo* activity of 7 - 18 U mg_{BVMO}⁻¹ or a k_{cat} of 6.9 - 17.6 s⁻¹ as a rough estimation.

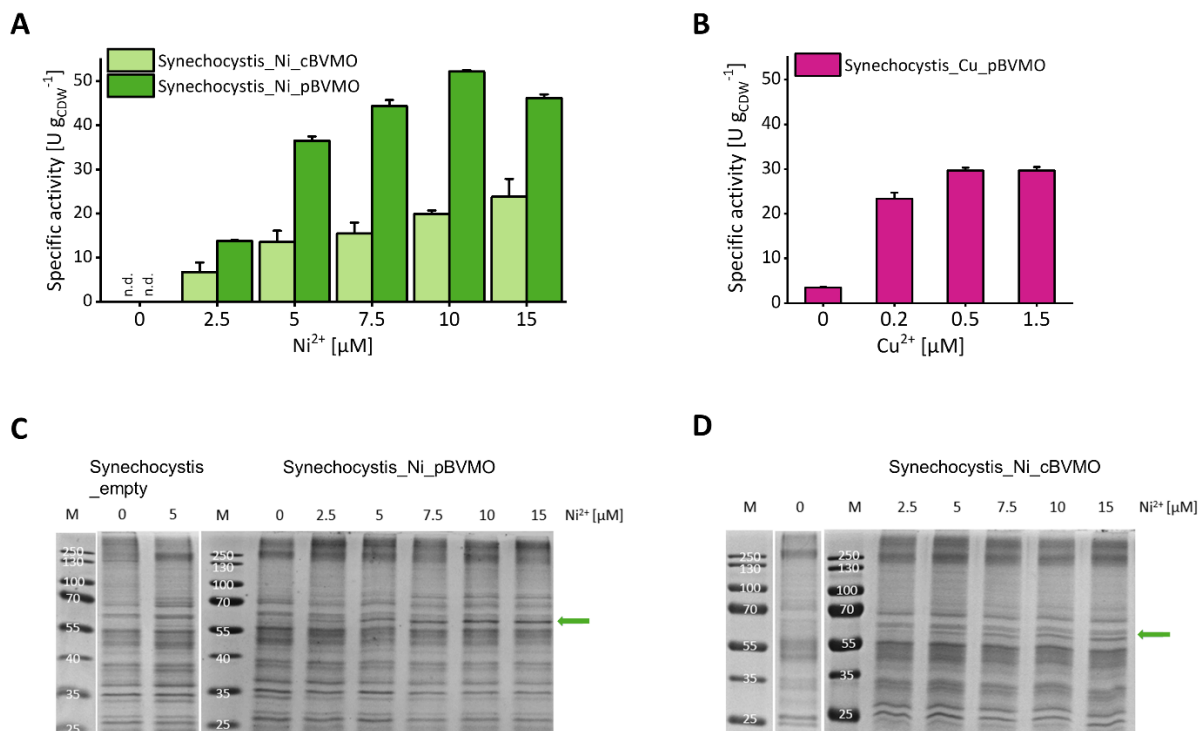


Figure 8: Systematic analysis of Ni²⁺- and Cu²⁺-dependent specific Baeyer-Villiger monoxygenase (BVMO) activities (A,B) and expression levels (C,D) in modified *Synechocystis* strains. BVMO activities of (A) *Synechocystis_Ni_pBVMO* and *Synechocystis_Ni_cBVMO* and (B) *Synechocystis_Cu_pBVMO* determined in short-term assays are given in dependence of the inducer concentration. Depicted are means from ≥2 independent measurements. n.d. not detected; 1 U = 1 μmol product formed min⁻¹. (C,D) SDS-PAGE gels of protein extracts upon Ni²⁺-induced plasmid- and genome-based BVMO gene expression, respectively. Panel C also shows results for extracts of an empty vector control. Numbers above lanes indicate the Ni²⁺-concentrations applied in μM. Arrows indicate BVMO bands [57.8 kDa]; M – Marker (PageRuler™).

In summary, we were able to construct a highly active BVMO-containing *Synechocystis* strain. Our data show that the *PnrsB*-based expression system proved to be a useful tool allowing tight, tunable, and high-level expression. *Synechocystis_Ni_pBVMO* was thus chosen for further characterization of photosynthesis-driven BVMO catalysis.

3.3.2 The BVMO reaction in *Synechocystis* is light-dependent

The BVMO reaction depends on NADPH as electron donor and thus is expected to constitute an artificial electron sink and thus to depend on the major electron source in phototrophs – the

photosynthetic water oxidation. To test, if and to what extent the BVMO reaction in *Synechocystis* depends on incident light, short-term activity assays at light intensities ranging from 0 to 250 $\mu\text{mol}_{\text{photons}} \text{m}^{-2} \text{s}^{-1}$ were performed in medium deficient in organic compounds as potential electron donors. Clearly, specific activities increased with increasing light intensity with the maximal activity of $60.9 \pm 1.0 \text{ U g}_{\text{CDW}}^{-1}$ measured at 150 $\mu\text{mol}_{\text{photons}} \text{m}^{-2} \text{s}^{-1}$ (Figure 9A). With a chlorophyll-*a* (Chl-*a*) content of $11.8 \pm 0.8 \text{ mg}_{\text{Chl-a}} \text{g}_{\text{CDW}}^{-1}$, this activity translates into $5.2 \pm 0.8 \text{ U mg}_{\text{Chl-a}}^{-1}$. Higher light intensities (such as 250 $\mu\text{mol}_{\text{photons}} \text{m}^{-2} \text{s}^{-1}$) led to a slight activity decrease, most likely due to photoinhibitory effects. When blocking electron transfer from PS II to the PQ pool by means of the respective inhibitor 3-(3,4-dichlorophenyl)-1,1-dimethylurea (DCMU) or upon incubation in the dark, residual activities of 13.6 ± 0.3 or $19.0 \pm 0.8 \text{ U g}_{\text{CDW}}^{-1}$ were observed, respectively. These typical background/dark activities are most likely fueled by reducing equivalents derived from storage compounds. We could show that extended periods (up to 16 h) of incubation in the dark or with DCMU, which involves the consumption of storage compounds and thus a reduction of their availability, decreases the activities to 4.7 ± 0.1 and $1.3 \pm 0.2 \text{ U g}_{\text{CDW}}^{-1}$, respectively (Figure 9B). These results clearly indicate a close coupling of the BVMO reaction to the photosynthetic electron transport chain.

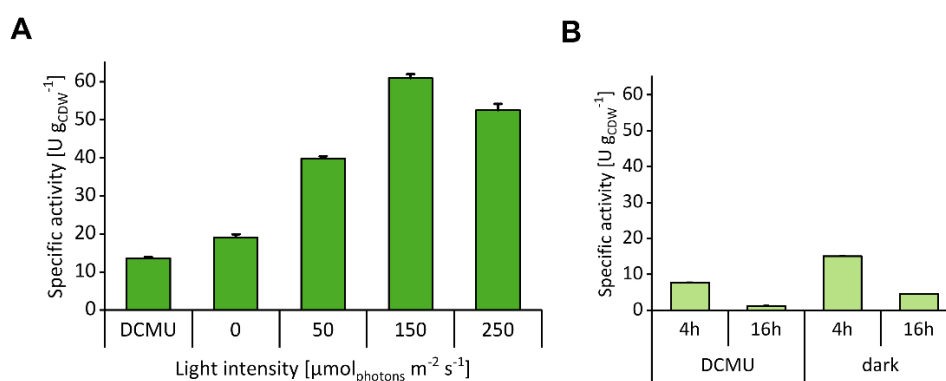


Figure 9: **Specific BVMO-activities of *Synechocystis_Ni_pBVMO* (A) at different light intensities and (B) after extended pre-incubation in absence of photosynthetic water splitting.** (A) Cells were grown under standard conditions and equilibrated at the given light intensities for 1 h before and during the assay. DCMU: Cells were treated with PS II inhibitor DCMU (20 μM final concentration) 1 h before and during the assay and irradiated with 150 $\mu\text{mol}_{\text{photons}} \text{m}^{-2} \text{s}^{-1}$. Specific activities were measured in short-term assays applying a cell concentration of 0.7 - 1.0 $\text{g}_{\text{CDW}} \text{L}^{-1}$. (B) Cells were grown under standard conditions and then equilibrated with DCMU (at 150 $\mu\text{mol}_{\text{photons}} \text{m}^{-2} \text{s}^{-1}$) or in the dark for the given incubation times followed by an activity-assay under the same conditions. Depicted are means and standard deviation of ≥ 3 independent experiments.

3.3.3 Inhibitory effects of substrate and by-product necessitate precise reaction control

To specify the optimal substrate concentration, the reaction kinetics were analyzed for *Synechocystis_Ni_pBVMO* by varying the C-one concentration between 50 μM and 3 mM in 5 min assays. The cells showed Michaelis-Menten-type kinetics with slight substrate inhibition (Figure 10A). Fitting according to Michaelis-Menten kinetics with substrate inhibition gave a reasonable fit and the following kinetic parameters: $K_S = 79 \pm 23 \mu\text{M}$, $V_{\text{max}} = 83.7 \pm 8.0 \text{ U g}_{\text{CDW}}^{-1}$,

$K_i = 4.4 \pm 1.5$ mM. This indicates that the C-one concentration is a critical reaction parameter requiring careful control.

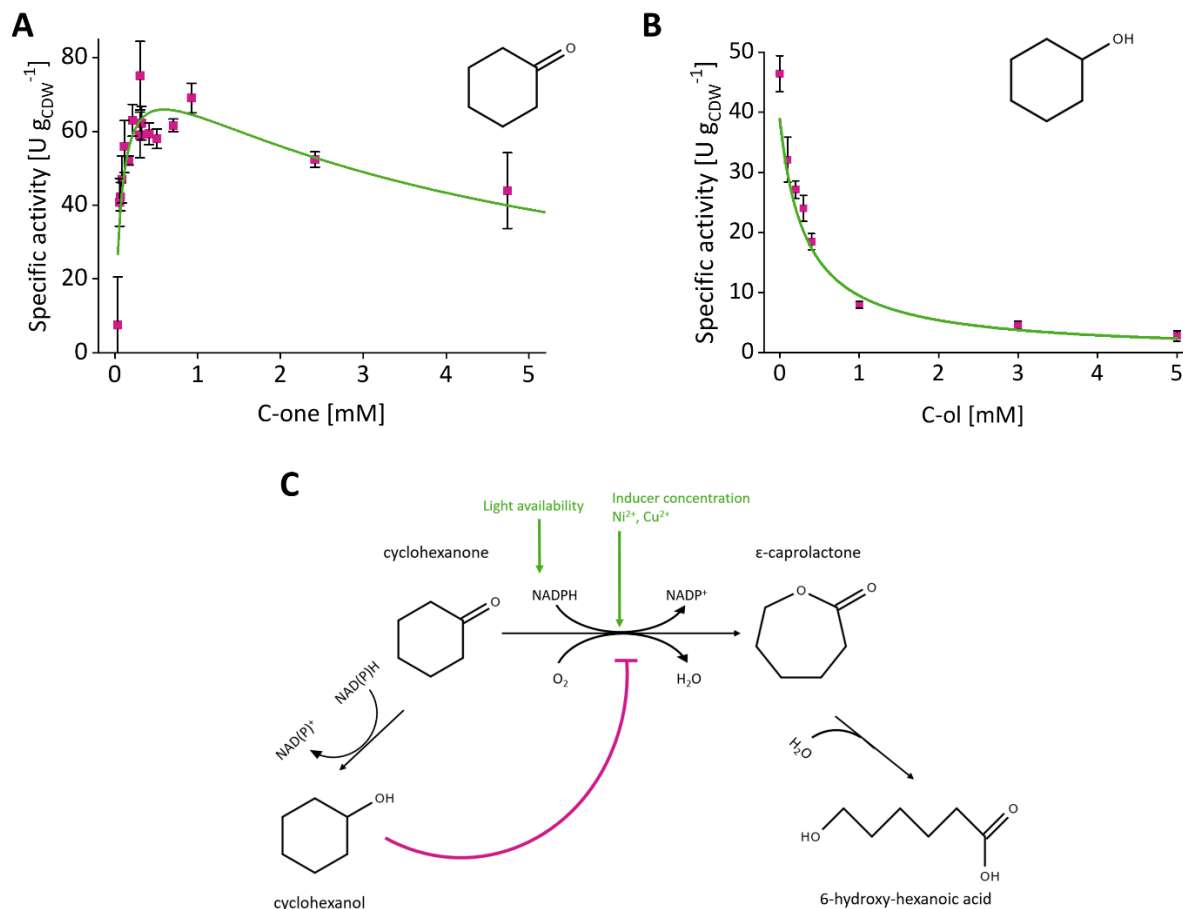


Figure 10: **Kinetic characterization of cyclohexanone (C-one) oxidation by *Synechocystis_Ni_pBVMO*.** (A) Kinetics for C-one oxidation. Kinetic experiments were performed with 1 mL induced cells (0.25 - $0.5\ g_{CDW}\ L^{-1}$) in 10 mL Pyrex tubes. BVMO reactions were started by adding varying amounts of C-one ($50\ \mu M$ to $5\ mM$) to cells equilibrated at standard assay conditions for 10 min and was stopped after 5 min. (B) Effect of cyclohexanol (C-ol) on C-one oxidation activity. Varying amounts of C-ol (0 to $5\ mM$) were added to 1 mL induced cells (0.7 - $1.0\ g_{CDW}\ L^{-1}$) in 10 mL Pyrex tubes. Also here, cells were equilibrated for 10 min and the reaction was started by substrate addition. Reactions were stopped after 30 min. Depicted are mean values and standard deviations from ≥ 2 independent experiments. (C) Reactions and parameters influencing ϵ Cl formation by *Synechocystis*: BVMO-catalyzed conversion C-one into ϵ -Cl; intrinsic alcohol dehydrogenases catalyze C-one reduction to C-ol, which inhibits C-one oxidation. ϵ -Cl is hydrolyzed to 6-HA by intrinsic hydrolases.

C-one oxidation applying whole cells of both heterotrophic [165] and phototrophic hosts [78] has been reported to compete with keto reduction catalyzed by host-intrinsic enzymes, giving rise to C-ol (Figure 10C). This also was true for *Synechocystis_Ni_pBVMO*, which was used for kinetic experiments investigating C-ol formation. Fitting according to Michaelis-Menten kinetics yielded a high K_S of $7.4 \pm 0.6\ mM$ and a comparably low V_{max} of $2.75 \pm 0.15\ U\ g_{CDW}^{-1}$ (Figure S6). Additionally, 6-HA was detected as by-product, which can be ascribed to abiotic hydrolysis of ϵ -Cl (Figure S7). Potential inhibition by these by-products also was tested in activity assays. Whereas 6-HA did not significantly affect C-one oxidation (Figure S9B), C-ol was found to be a strong inhibitor with a K_i of $0.03\ mM$, determined via kinetic fittings as described in section 2.2.4. (Figure 10B), corresponding to a $K_{i,C-ol}/K_{S,C-one}$ ratio of 0.38 . Figure 10C depicts a reaction scheme based on the findings described in this paragraph. Since

intrinsic alcohol dehydrogenase activity can barely be avoided without drastically interfering with host metabolism, high BVMO levels can be considered pivotal to promote ϵ -Cl formation. In this way, low yields due to by-product formation and – even more relevant – inhibition by C-ol can largely be avoided.

3.3.4 Gram-scale ϵ -Cl production in a 2-L photo-bioreactor

To test the long-term stability of C-one oxidation by *Synechocystis_Ni_pBVMO*, we recorded the biotransformation time course in shaking flasks initially containing 5 mM C-one and fed by pulsing the same amount after 1 and 3 h. The 15 mM C-one supplied were completely converted to 14.2 ± 1.5 mM products (ϵ -Cl and 6-HA, Figure S8). Thereby, the initial specific activity of $33 \text{ U g}_{\text{CDW}}^{-1}$ determined for the first hour was found to decrease continuously over time. This decrease can be attributed to C-ol accumulation, reaching a final titer of 0.51 ± 0.07 mM, and intermittently high C-one concentrations leading to enforced substrate inhibition.

In order to test the feasibility of *Synechocystis_Ni_pBVMO* to produce ϵ -Cl in gram scale, this strain was applied in a 2-L stirred-tank photo-bioreactor (photo-STR) providing an efficient O_2 and CO_2 mass transfer and a controlled environment. The latter included the application of a limiting continuous substrate feed to minimize both substrate and by-product inhibition. To establish different source/sink conditions, light intensity (low light, LL: $150 \mu\text{mol}_{\text{photons}} \text{ m}^{-2} \text{ s}^{-1}$ or high light, HL: $700 \mu\text{mol}_{\text{photons}} \text{ m}^{-2} \text{ s}^{-1}$) and CO_2 supply via aeration (low CO_2 , LC: ambient CO_2 or high CO_2 , HC, 1 and 10% CO_2 during growth and biotransformation, respectively) were varied to establish the three source/sink regimes LLLC, HLLC, and HLHC (for details, see Table 4).

After a growth phase of 3-4 days, including induction by adding $10 \mu\text{M NiSO}_4$ 24 h before biotransformation start, C-one feeding was initiated at a fixed rate matching a specifically chosen activity. The first reactor was run with $0.55 \pm 0.09 \text{ g}_{\text{CDW}} \text{ L}^{-1}$ under LLLC and a feed rate set to $25 \text{ U g}_{\text{CDW}}^{-1}$. A final product titer (sum of ϵ -Cl and 6-HA) of 11.6 ± 1.0 mM was reached after 28 h (see Figure 11A). However, 5.4 ± 0.1 mM C-one remained unconverted, as the specific activity strongly decreased within the first hours. A second reactor was set up for HLLC conditions to rule out light limitation as a reason for the decreasing activity. To avoid substrate accumulation, the initial substrate feed rate was adjusted to match an activity of $15 \text{ U g}_{\text{CDW}}^{-1}$ using $0.61 \pm 0.04 \text{ g}_{\text{CDW}} \text{ L}^{-1}$. This led to a prolonged product formation phase, yielding however a slightly lower final product titer of 9.8 ± 1.6 mM after 25 h (Figure 11B). To test, if product formation benefits from higher biomass concentrations, the third photo-STR was conducted using HLHC conditions. These conditions allowed for a 70% higher initial biomass concentration ($1.02 \pm 0.01 \text{ g}_{\text{CDW}} \text{ L}^{-1}$, see Table 1). To increase the C-one conversion rate, substrate supply was set to match $30 \text{ U g}_{\text{CDW}}^{-1}$. Comparable to the previous reactor runs, this pre-set activity of $30 \text{ U g}_{\text{CDW}}^{-1}$ only was met initially and was decreasing in time, resulting in C-one accumulation, requiring adjustment of the C-one feed rate (decrease to 70 % after 4 h and

stop of C-one feed after 8 h, Figure 11C). The final product titer was 11.5 ± 0.2 mM after 27 h, corresponding to a volumetric productivity of 48.6 ± 0.8 mg L⁻¹ h⁻¹ and a product yield of 0.88 (mol_{ε-Cl + 6-HA} mol_{C-one}⁻¹). Thus, all experiments led to similar product titers (9.8-11.6 mM corresponding to 1.12-1.32 g L⁻¹).

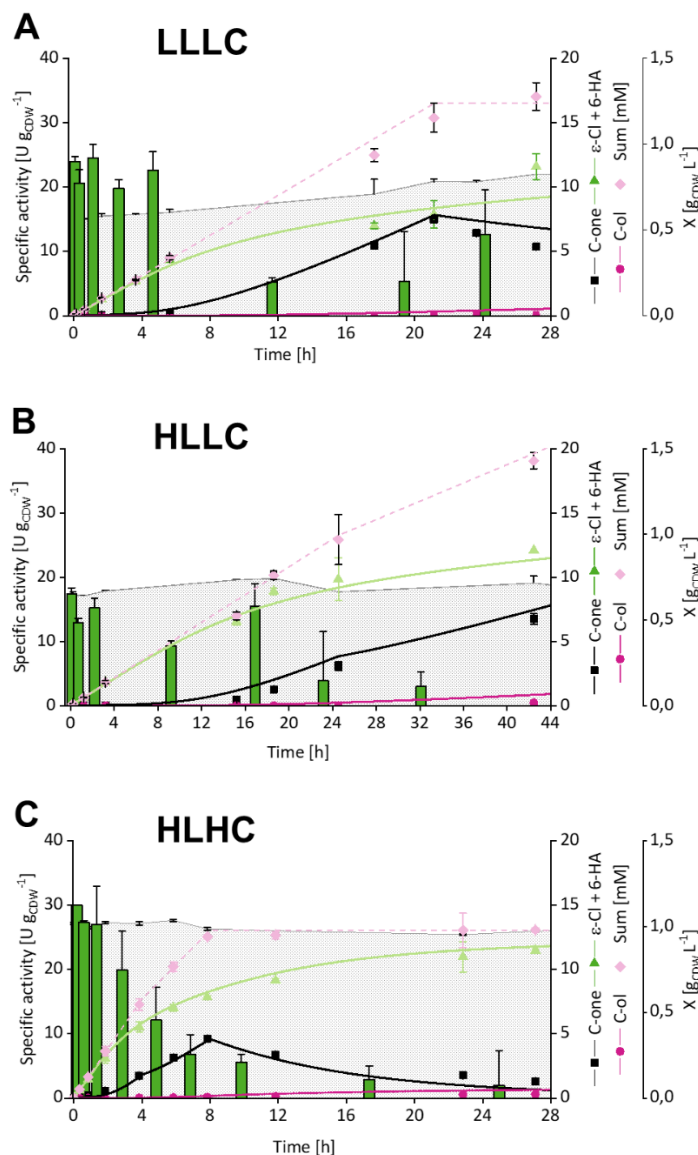


Figure 11: **Photosynthesis-driven cyclohexanone (C-one) oxidation in a 2-L stirred tank photobioreactor under different light and CO₂ regimes.** *Synechocystis*_Ni_pBVMO was grown for 3-4 days and induced with 10 μM NiSO₄. Biotransformations were started 24 h after induction by feeding C-one in a substrate-limited regime, for detailed parameters see Table 1. **(A)** Low light/low carbon (LLLC): C-one was fed at a rate matching a specific activity of 25 U g_{CDW}⁻¹ for 21.5 h with an initial biomass concentration of 0.55 ± 0.09 g_{CDW} L⁻¹. **(B)** High light/low carbon (HLLC): C-one was fed at a rate matching 15 U g_{CDW}⁻¹ for 24.5 h and then at a rate matching 10 U g_{CDW}⁻¹; the initial biomass concentration was 0.61 ± 0.04 g_{CDW} L⁻¹. **(C)** High light/high carbon (HLHC): C-one was fed at a rate matching 30 U g_{CDW}⁻¹ for 4 h, which then was decreased by 30% until 8 h; the initial biomass concentration was of 1.02 ± 0.01 g_{CDW} L⁻¹. Experimental data is given as green bars: specific activity in U (= μmol [ε-caprolactone (ε-Cl) + 6-hydroxyhexanoic acid (6-HA)] min⁻¹) g_{CDW}⁻¹; Black squares: C-one in mM; light green triangles: total product in mM; pink circles: cyclohexanol (C-ol) in mM; rose diamonds: Sum of all analytes in mM. Depicted are mean values and standard deviations from ≥2 technical replicates. Dashed line (blue): Total C-one fed in mM. Straight Lines depict simulated courses of C-one (black), ε-Cl (light green), and C-ol (pink) concentrations obtained via *Berkeley Madonna* software using a model based on determined and fitted kinetic parameters (see text for details).

Irrespective of the applied source/sink conditions, the specific activity decreased in all setups at substrate (C-one) and by-product (C-ol) levels not expected to lead to significant inhibition (Figure 11A-C). The independency of initial specific activities on the applied biomass concentration (varied between 0.55 to 1.02 g_{CDW} L⁻¹) indicates that light availability did not limit the specific activity (Table 1 and Figure 11A-C). This was further confirmed by light intensity variation (250 μmol_{photons} m⁻² s⁻¹ vs 700 μmol_{photons} m⁻² s⁻¹) under otherwise identical conditions as in the HLHC experiment (Figure 11C). This low light high carbon (LLHC) experiment resulted in a similar initial volumetric productivity as in the HLHC experiment corroborating that light did not limit the biocatalytic activity (Table S3). These results indicate that neither inhibition by C-one or C-ol nor photosynthesis limited the biocatalytic activity. Instead, product inhibition may have prevented a more effective and stable conversion. Indeed, ε-Cl was found to compromise BVMO activity in short term assays (Figure S9A). As no product inhibition has been observed on the enzyme level [165], ε-Cl rather inhibits on a physiological level, which can best be described as a non-competitive type of inhibition. With the respective fit (equations 1 and 3), the inhibitory studies yielded a K_{i,ε-Cl} of 0.83 mM.

These findings prompted us to describe the biotransformations by means of a kinetic bioprocess model using Berkeley Madonna software. The model was parametrized using the kinetic data reported in section 4.3, which were derived from fitting according to Michaelis-Menten kinetics with substrate inhibition (equation 1). Taking into account that this approach neglects by-product and product inhibition, which occur, but were not considered for the determination of V_{max} and K_{i,C-one}, these parameters were set to the upper boundaries of the fittings, namely 91 U g_{CDW}⁻¹ and 5.9 mM. The inhibition by ε-Cl observed under assay conditions (Figure S9A, K_{i,ε-Cl} = 0.83 mM) appeared to be less pronounced in bioreactor experiments. Thus, K_{i,ε-Cl} was fitted to bioreactor data resulting in a value of 2.0 mM. This allowed to simulate concentration courses for substrate (C-one), product (ε-Cl + 6-HA), and by-product (C-ol) (depicted as lines in Figure 11A-C) with striking accuracy. This high simulation accuracy obtained with a mere kinetic model, not considering possible influences of light intensity and CO₂ supply variation in the experiments, indicates that C-one conversion was kinetically controlled under the conditions applied, including a physiological effect of ε-Cl, and was not influenced by the tested variation in source/sink regime.

Further, the process model was used to identify optimal process parameters to handle the complex reaction kinetics, namely the feed regime and the biocatalyst concentration. For this purpose, only reaction kinetics were considered, and avoidance of a possible light limitation was assumed. To explore the sensitivity regarding the biocatalyst concentration, values of 0.5, 1, 2 and 5 g_{CDW} L⁻¹ were chosen, being aware that high cell concentrations such as 5 g_{CDW} L⁻¹ would involve light limitation issues in the experimental setup (as further discussed in section 4.3). Thereby, the feed regime applied in the HLHC experiment (Figure 11C) was scaled to

different biocatalyst concentrations (Figure 12A). The highest biomass concentration tested (5 $\text{g}_{\text{CDW}} \text{L}^{-1}$) indeed yielded the highest product titer (17.0 mM), but accumulated C-one (36.9 mM) and C-ol (11.4 mM) in high amounts. To avoid extreme substrate and by-product accumulation and thereby optimize product titer and yield, a more conservative C-one feed was targeted. To this end, an ideal C-one conversion rate was calculated by considering product inhibition only and neglecting substrate and by-product inhibition, reflecting the upper limit of C-one supply which can be handled by the catalyst. This continuously decreasing rate was translated into a feed rate followed by simulation using the kinetic model, again testing different biocatalyst

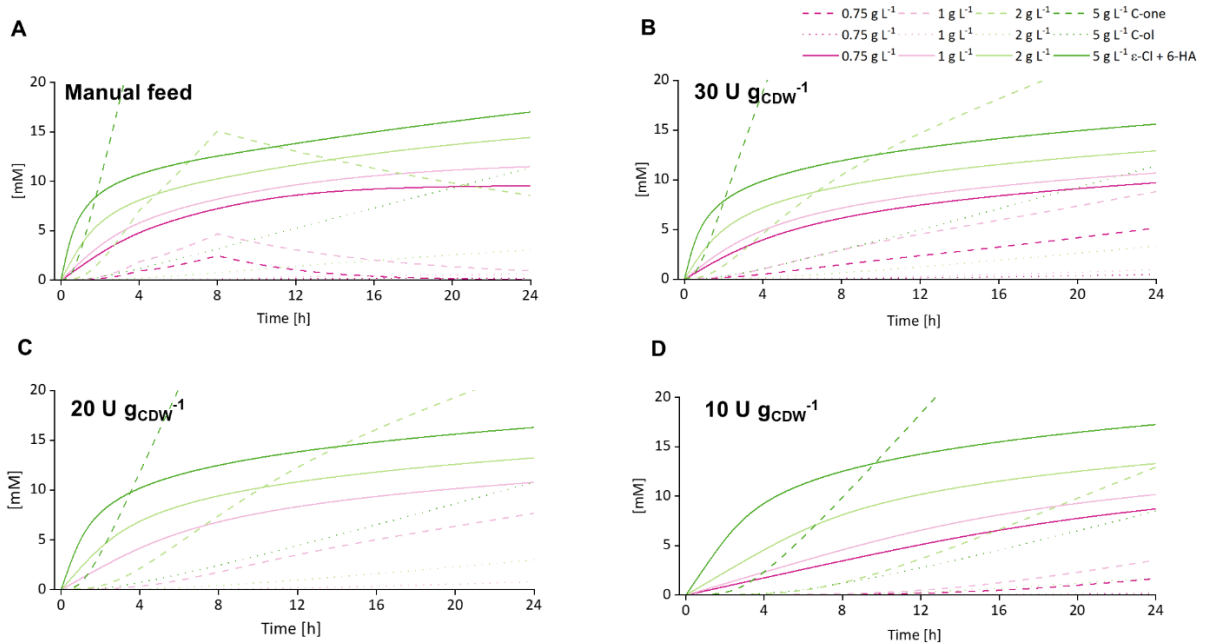


Figure 12: **Simulation and sensitivity analysis of the BVMO process applying the kinetic process model with (A) manual and (B), (C), and (D) optimized feeding regimes, with $30 \text{ U g}_{\text{CDW}}^{-1}$, $20 \text{ U g}_{\text{CDW}}^{-1}$, and $10 \text{ U g}_{\text{CDW}}^{-1}$ respectively.** (A) The feed regime applied for the HLHC reactor (see Figure 4C) was translated to 0.75, 1.0, 2.0, and 5.0 $\text{g}_{\text{CDW}} \text{L}^{-1}$ for a sensitivity analysis regarding the biocatalyst concentration. (B, C, D) An ideal C-one conversion rate based on initial rates of 30/20/10 $\text{U g}_{\text{CDW}}^{-1}$, respectively, was calculated by considering product inhibition only and neglecting substrate and by-product inhibition. This reflects the upper limit of C-one supply which can be handled by the catalyst. The conversion rate was translated into a feed rate, followed by simulations using the kinetic process model with cell concentrations of 0.75, 1.0, 2.0, and 5.0 $\text{g}_{\text{CDW}} \text{L}^{-1}$ (pink, rose, light green, and green lines), to test the system's sensitivity towards the biocatalyst concentration. Depicted are concentrations of C-one, C-ol, and ϵ -Cl in dashed, dotted and straight lines, respectively.

concentrations. Irrespective of the initial feed rate (30, 20 or 10 $\text{U g}_{\text{CDW}} \text{L}^{-1}$, Figure 12B-D), the overall picture remained the same: Higher biocatalyst concentrations (2 and 5 $\text{g}_{\text{CDW}} \text{L}^{-1}$) heavily accumulated C-one and – to a minor extent – C-ol, limiting product formation. Although lower biocatalyst concentrations (0.75 and 1 $\text{g}_{\text{CDW}} \text{L}^{-1}$) suffered less from C-one accumulation and consequential C-ol formation, the final product titer did not exceed 10.7 mM. To conclude, the “optimized” C-one feed regime led to an only moderate increase in final product titer compared to the HLHC experiment (15.5 vs 11.5 mM), but only with 5 times higher biocatalyst concentration and thus to the cost of low biocatalyst-based yield (0.4 vs 1.3 $\text{g}_{\epsilon\text{-Cl} + 6\text{-HA}} \text{g}_{\text{CDW}}^{-1}$) and product yield (0.15 vs 0.88 $\text{mol}_{\epsilon\text{-Cl} + 6\text{-HA}} \text{mol}_{\text{C-one}}^{-1}$). With the same biocatalyst concentration

as in the HLHC experiment, the achieved product titer was even lower (10.7 vs 11.5 mM), which emphasizes the strong impact of the by-product C-ol demanding a more aggressive feed rate decrease. Overall, the reaction system remains intricate, as product titer and yield are not only restricted by product inhibition, but also by the difficult interplay between competitive by-product inhibition and the formation of this by-product: A high substrate concentration can counteract competitive inhibition, but simultaneously increases inhibitor formation. Importantly, assuming the absence of light limitation for higher cell densities did not enable significantly higher product titers than experimentally obtained, reemphasizing that kinetic restrictions are the primary factors limiting the performance of the investigated reaction system.

3.4 Discussion

Photosynthesis is the central biochemical transformation process converting light energy into chemical energy and therefore a highly attractive module for environmentally friendly industrial processes. It can be exploited for biotechnology by making use of photosynthetically active microorganisms such as cyanobacteria.[8, 216] Their capability to fix CO₂ gives rise to the conversion of CO₂ into organic chemicals such as biofuels. [217] *Inter alia*, the production of ethanol,[176] 2,3-butanediol,[218] glycerol,[109] and 1-butanol [219] has been investigated, typically achieving rather low productivities, not exceeding 10 mg L⁻¹ h⁻¹. These processes mainly suffer from low energy efficiency as respective metabolic pathways are linked to carbon fixation and central carbon metabolism, which are evolutionary optimized for biomass formation under given conditions and not explicitly with respect to energy efficiency. One option to increase light-to-product energy efficiency is to link production processes closer to the photosynthetic electron transport chain and thus avoid downstream energy loss.[8]

Following this idea, recent studies focused on the utilization of photosynthesis-derived electrons for redox biocatalysis. The coupling is realized either by directly linking electron consuming enzymes to PS I,[68, 80] or via reduced cofactors produced by the light reaction,[74, 79] e.g., NADPH as in the presented study. This approach is particularly elegant for oxygenation reactions, as not only electron supply but also O₂ supply – often a limiting factor in aerobic large-scale bioprocesses – is realized *in situ* via photosynthetic water oxidation.[57] In this study, the use of a 2-L stirred tank photo-bioreactor setup enabled light-driven ϵ -Cl formation in gram scale within one day exemplifying the potential of this approach.

3.4.1 Enhanced gene expression makes *Synechocystis* an attractive biocatalyst

The development and application of photosynthetically active microorganisms as microbial hosts is still restricted by the limited availability of molecular biology tools and the comparably poor knowledge on cell metabolism and physiology. Here, we investigated different expression systems regarding expression levels and specific activities of BVMO from *Acidovorax* sp.

CHX100 in *Synechocystis*. The Ni²⁺-inducible *PnrsB* promoter system was found to enable high BVMO expression levels and be superior to the Cu²⁺-inducible *PpetE* promoter system in terms of inducibility and expression level, in accordance with previous studies.[207, 220] It is important to note, that the expression level achieved with a promoter depends on the genetic context.[207] The expression levels of up to $1.1 \pm 0.2\%$ of TSP reached in this study are to our best knowledge unprecedented with the *PnrsB* system in *Synechocystis*. Numerous studies have characterized different controllable promoter systems in *Synechocystis*, non-native ones such as the LacI-repressible *Ptrc1O* system,[141] the TetR-regulated L03-promoter,[221] and other *Plac*-variants,[145] as well as native ones, like Cu²⁺-inducible *PpetE* [222] and Ni²⁺-inducible *PnrsB* promoters.[207] However, most studies focused on the optimization of expression systems rather than on designing suitable biocatalysts and use fluorescent proteins as read-out for expression strength. Thus, not much is known about the cellular concentrations of heterologous protein. For catalytically active enzymes, such as dehydrogenases or monooxygenases, [68] constitutive systems, such as the discovered “super strong” promoter *Pcpc560* [146] or the light-inducible promoter *PpsbA* have been applied.[198] They yield high expression levels up to 15 % [146] and 12.6 % [198] of TSP. However, for oxygenase biocatalysis, well-steerable promoter systems are more desirable to control metabolic burden such as ROS formation. They yield lower but still remarkable expression levels of 0.4 % [208] and 1.1% of TSP,[109] of which the latter was met by *Synechocystis_Ni_pBVMO* generated in this study.

With *PnrsB*, plasmid-based expression yielded a 2.6 times higher BVMO level and activity than chromosome-based expression (Figure 8). This difference may be due to a higher copy number of the plasmid compared to the chromosome.[141] It, however, has been reported that the copy number of *pPMQAK1* is comparable to that of the chromosome.[223] Such contradiction has been explained by the observation that both plasmid and chromosome copy numbers vary strongly in *Synechocystis*. [62] This makes chromosomal integration the more laborious method due to the necessity for segregation, whereas the plasmid-based approach can suffer from instability and the necessity for constant antibiotic selection.[54]

The strong correlation of specific BVMO activity and expression level (Figure 8) suggests that the achieved BVMO level still limits the biocatalyst activity. Future advances regarding molecular biology tools for cyanobacteria can be expected to enable even higher biocatalyst activities. Promising candidate expression systems include the recently characterized rhamnose-inducible promoter *Prha* [224] or the vanillate-inducible promoter *PvanCC*. [199]

3.4.2 Photosynthesis-driven BVMO catalysis is hampered by reactant inhibition rather than host metabolism

BVMO containing *Synechocystis* was found to feature a 3.7 times lower apparent uptake constant K_s for C-one ($80 \pm 23 \mu\text{M}$) than *Pseudomonas taiwanensis* VLB 120 containing the

same enzyme ($316 \pm 21 \mu\text{M}$). [187] This indicates a rather efficient substrate mass transfer into the cell. Further, we observed moderate substrate inhibition, an often-encountered effect with BVMOs. [180, 225, 226] The host metabolic background interferes with the biotransformation in terms of C-one reduction to C-ol as reported before, [78] but with a rather low V_{max} ($2.75 \pm 0.15 \text{ mM}$) and a rather high K_s ($7.4 \pm 0.6 \text{ mM}$). More important was the inhibition of BVMO activity by C-ol already at low concentrations ($K_i = 0.03 \text{ mM}$). This is in agreement with published data on heterotrophs containing the same enzyme, [165] indicating an inhibitory effect on the enzyme level. To reduce formation of the (inhibiting) by-product, the introduction of an enzyme for re-conversion of C-ol to C-one could be an interesting solution. [227] Deletion of intrinsic alcohol dehydrogenases constitute another option but may harm cell viability and thus be tedious. Taken together, these data show that controlling substrate concentration is key for efficient photosynthesis-driven BVMO catalysis.

The optimized strain *Synechocystis_Ni_pBVMO* reached a maximal specific activity of $60.9 \pm 1.0 \text{ U g}_{\text{CDW}}^{-1}$. This is around 4 to 5 times lower than published for the heterotrophic host *Pseudomonas taiwanensis* VLB120, [165] which showed significantly higher BVMO expression levels, [187] and features a highly active energy and redox metabolism based on organic acids and sugars. [162] It is, however, noteworthy that the BVMO exhibited a much higher *in vivo* activity in *Synechocystis* than in *P. taiwanensis*, i.e., a 4.6 to 11 times higher k_{cat} ($6.9 - 17.6 \text{ s}^{-1}$ vs 1.5 s^{-1}) [187]. It should be noted that BVMO catalysis in *Synechocystis* appeared not to be limited by the metabolic capacity to supply reduction equivalents as the photo-production of NADPH in *Synechocystis* is in the range of 9-18 U mg Chl-a , [115] which translates to 106-212 $\text{U g}_{\text{CDW}}^{-1}$. Presumably, this limitation was decisive for BVMO catalysis in *P. taiwanensis*. The activities achieved already indicate the great potential of *Synechocystis* as host for energy-dependent biotransformations. Future research efforts to fill knowledge gaps regarding expression systems, other molecular biology tools, and co-factor regeneration can be expected to further improve photosynthesis-driven biotransformation efficiency. [228]

Despite keeping by-product and substrate strictly below inhibiting values, the biocatalyst performance was found to be compromised on the long term. Neither increased light nor CO_2 supply had a positive effect (Figure 11B). Instead, the product $\epsilon\text{-Cl}$ itself was found to affect biocatalyst performance (Figure S9A). Such product inhibition also was the decisive limitation in simulations based on kinetic data, which overall fit well the bioreactor data. Interestingly, product inhibition was not detected with heterotrophic hosts [165] and seems to be *Synechocystis* specific. Effects of $\epsilon\text{-Cl}$ on *Synechocystis* physiology may involve inhibition of metabolism leading to NADPH limitation as discussed below. To address product inhibition, *in situ* product removal technologies can be applied. [229] Whereas two-liquid phase approaches are compromised by the intermediary polarity of the product, solid phase extraction may be a promising, but costly solution. Alternatively, BVMO catalysis can be amended by a lipase [225]

or lactonase [165] reaction to obtain 6-HA which is less problematic in terms of inhibition, but still feasible as a polymer precursor.

3.4.3 Potentials and limitations of photosynthesis-driven redox biocatalysis

The biocatalyst-based yield ($g_{\text{Product}} g_{\text{CDW}}^{-1}$) has been proposed as an important measure for catalyst performance.[180] *Synechocystis_Ni_pBVMO* reached a yield of 1.3 and 1.6 $g_{\text{Product}} g_{\text{CDW}}^{-1}$ in a 2-L photo-bioreactor and in shaking flasks, respectively. A sensitivity analysis based on the kinetic model affirmed a yield of 1.5 $g_{\text{Product}} g_{\text{CDW}}^{-1}$ to be realistic for the used bioreactor setup. This is on the same level as an industry-relevant BVMO-based process with *Escherichia coli* featuring a yield of 1.6 $g_{\text{Product}} g_{\text{CDW}}^{-1}$ for a however more complex product.[230] However, phototrophic processes are not on the same readiness level as heterotrophic biocatalytic processes: It should be noted that the above-mentioned metric neglects the immense differences in cell densities applied. The mentioned *E. coli*-based process uses around 25-times higher biomass concentrations than those applied in this study and thus features a higher volumetric productivity. On the other hand, *Synechocystis*-based biocatalyst production, regeneration, and operation are based on CO_2 as carbon and water as electron source, making the addition of an organic carbon and energy source such as glucose dispensable. Future improvements of reactor design and cultivation strategies, such as the use of capillary biofilm reactor concepts [203, 231] or immobilized cells [232] and internal illumination [95] are expected to push the boundaries of phototrophic cultivation / process operation. Already noteworthy are the initial and 24h- average productivity ($187 \pm 1 \text{ mg L}^{-1} \text{ h}^{-1}$ and $59 \pm 1 \text{ mg L}^{-1} \text{ h}^{-1}$, respectively), ranging among the highest productivities for biotransformations using cyanobacteria. Additionally, the product yield of 0.88 ($\text{mol}_{\text{e-Cl} + 6\text{-HA}} \text{ mol}_{\text{C-one}}^{-1}$) prefigures the high potential of phototrophic hosts for biocatalysis.

The comparably high *in vivo* BVMO activity obtained in this study indicates that – sufficient light supply provided – NADPH can efficiently be withdrawn from phototrophic metabolism to fuel productive reactions. As confirmed by process simulation merely based on whole-cell reaction kinetics, the photosynthesis-based NADPH supply capacity did not limit the biotransformation, with efficient illumination as a prerequisite. The product itself might interfere with NADPH supply at higher concentrations by affecting membrane integrity [233] and thus photosynthetic electron transfer. In contrast, electron consuming redox biotransformations catalyzed by the ene-reductase Yqjm were found to be limited by NADPH availability at activities above $150 \text{ U } g_{\text{CDW}}^{-1}$. [79] By inactivating the flavodiiron proteins Flv1/Flv3, an approach known to reduce electron loss to unproductive O_2 reductions,[46] *Synechocystis* reached specific activities up to $170 \text{ U } g_{\text{CDW}}^{-1}$. It has to be investigated though, if this elevated electron supply can be sustained in the long term.

As oxygenases are prone to uncouple, i.e., reduce O_2 without concomitant substrate oxidation, ROS formation represents another electron sink increasing the electron demand. Further, ROS

formation possibly affects photosynthetic metabolism. [234] Cyanobacteria have evolved different mechanisms to cope with and detoxify reactive oxygen species (ROS), [235] which however involves additional electron/energy investment further increasing the electron demand.

Today, the disposability of electrons from water oxidation, e.g., by water electrolysis, is a field of particular interest, especially for H₂-production. In this context, envisaged light-to-H₂ solutions using cyanobacterial photosynthesis as a transformation module are highly attractive. [80] Success towards this goal relies, beside O₂-tolerance of biocatalysts and high-cell-density cultivation concepts, on the electron supply capacity of photoautotrophic microbes. It is still unclear, if a high electron demand for technically feasible H₂-production can be met by cells still able to sustain themselves. Interestingly, additional electron sinks were shown to increase photosynthetic efficiency and thereby electron fluxes through the photosynthetic apparatus. [161, 236] This observation reinforces the sink-limitation-hypothesis, which states that photosynthesis is rather limited by the availability of electron sinks than by electron (energy) sources. [73] This gives the possibility to tap unused electron supply potential for electron consuming reactions. Limits of and factors influencing electron supply via the photosynthetic light reaction for biotechnological application remain to be investigated. Reductases, such as Yqjm, [79] and oxygenases, such as the cycloalkane hydroxylating cytochrome P450 monooxygenase [74] and the BVMO investigated in this study, have now been established as prominent electron sinks in cyanobacteria and constitute excellent blueprints to decipher the potential of the photosynthetic light reaction as electron source for biotechnological application.

4 Light-driven redox biocatalysis on gram-scale in *Synechocystis* sp. PCC 6803 via an in vivo cascade

The photosynthetic light reaction in cyanobacteria constitutes a highly attractive tool for productive biocatalysis, as it can provide redox reactions with high-energy reduction equivalents using sunlight and water as sources for energy and electrons, respectively. Here, we describe the first artificial light-driven redox cascade in *Synechocystis* sp. PCC 6803 to convert cyclohexanone to the polymer building block 6-hydroxyhexanoic acid (6-HA). Co-expression of a Baeyer-Villiger monooxygenase and a lactonase, both from *Acidovorax* sp. CHX100, enabled this two-step conversion with an activity of up to $63.1 \pm 1.0 \text{ U g}_{\text{CDW}}^{-1}$ without accumulating inhibitory ϵ -caprolactone. Thereby, one of the key limitations of biocatalytic reactions, i.e., reactant inhibition or toxicity, was overcome. In 2 L stirred-tank-photobioreactors, the process could be stabilized for 48 h, forming $23.50 \pm 0.84 \text{ mM}$ ($3.11 \pm 0.12 \text{ g L}^{-1}$) 6-HA. The high specificity enabling a product yield of $0.96 \pm 0.01 \text{ mol mol}^{-1}$ and the remarkable biocatalyst-related yield of $3.71 \pm 0.21 \text{ g}_{6\text{-HA}} \text{ g}_{\text{CDW}}^{-1}$ illustrate the potential of producing this non-toxic product in a synthetic cascade. The fine-tuning of the energy burden on the catalyst was found to be crucial, which indicates a limitation by the metabolic capacity of the cells possibly being compromised by biocatalysis-related reductant withdrawal. Intriguingly, energy balancing revealed that the biotransformation could tap surplus electrons derived from the photosynthetic light reaction and thereby relieved photosynthetic sink limitation. This study shows the feasibility of light-driven biocatalytic cascade operation in cyanobacteria and highlights respective metabolic limitations and engineering targets to unleash the full potential of photosynthesis.

This chapter has been published in

Plant Biotechnology Journal, **2023**, 21 (10), 2074-2083

Adrian TÜLLINGHOFF, Harcel DJAYA-MBISSAM, Jörg TOEPEL, and Bruno BÜHLER,

<https://doi.org/10.1111/pbi.14113>

4.1 Introduction

Photosynthetic microorganisms have gained increasing attention as host organisms for biotechnology.[59] Relying on water, CO₂, and light as the main resources, their phototrophic metabolism has high potential to enable truly sustainable production processes. Especially cyanobacteria have been studied and discussed as work horses for the production of (bulk) chemicals such as ethanol[176], 1-butanol[177], hydrogen (H₂)[80], glycerol[109], to name only a few. Since recently, phototrophic microorganisms are studied for redox biotransformations, thereby making more efficient use of photosynthesis as compared to biomass formation via the direct coupling of biocatalytic electron/energy sinks to energy source utilization, i.e., the photosynthetic light reaction.[8] Redox biotransformations are especially attractive, since the separately added biotransformation substrate does not directly interfere with the hosts C-metabolism.[178, 237] Thereby, these biotransformations function as (external) sinks utilizing photosynthesis-derived energy – in the form of reduction equivalents – that may not be used by the Calvin-Benson-Bassham cycle (CBB) due to its lower turnover capacity compared to the light reaction. Indeed, sink engineering has been shown to relieve sink limitation of the photosynthetic metabolism tapping the unused potential of photosynthesis.[73, 161]

Oxygenases are an especially interesting enzyme class for photo-biocatalysis as the photosynthetic light reaction does not only supply reduction equivalents, but also O₂ *in situ*[58], overcoming typical limitations experienced with heterotrophs, i.e., the addition and efficient utilization of reduction equivalent-delivering co-substrates or O₂ mass transfer.[54] Cytochrome P450 monooxygenases (CYPs)[68, 72, 74, 84] and Baeyer-Villiger monooxygenases (BVMOs)[179](see also Chapter 3) have been applied in the model strain *Synechocystis* sp. PCC 6803 (*Synechocystis*), yielding specific activities up to 39.2 ± 0.7 [74] and 60.9 ± 1.0 U_{g_{CDW}}⁻¹ (Chapter 3) corresponding to volumetric productivities of 2.35 ± 0.04 and 3.40 ± 0.06 mM h⁻¹, respectively.

These studies[74, 179](see also Chapter 3) revealed that the main limitations for light-driven whole-cell redox biocatalysis are i) light availability, ii) metabolic constraints, and iii) reactant toxicity and inhibition. With light being the energy source to drive heterologous redox reactions as well as the host metabolism, it is obvious that light limitation has to be avoided.[95] In a recent study involving a BVMO from *Burkholderia xenovorans*, insufficient light supply was concluded to limit the (light-driven) conversion of cyclohexanone (C-one) to ε-caprolactone (ε-Cl).[179] In our previous study employing a BVMO from *Acidovorax* sp. CHX100 (*Acidovorax*), however, 2.4-fold higher activities were achieved at a larger scale (2 L vs. mL-scale), with product-related effects and not light as the decisive limitation (Chapter 3). As an important metabolic constraint, the ATP:NADPH ratio may be disturbed upon electron

withdrawal for redox biocatalysis. Lately, it has been shown that careful balancing of this ratio by simultaneously applying an ATP sink can benefit redox biocatalysis.[85]

Reactant inhibition and toxicity are well known to impair biocatalyst viability and stability, be it on the metabolic, physiological, or enzymatic level.[180, 225, 226] In fact, product inhibition was found to be the key limitations in the above-mentioned C-one conversion with *Acidovorax* BVMO in *Synechocystis* irrespective of the light- and carbon conditions applied (Chapter 3). With the highly active reductase Yqjm in *Synechocystis*, initial specific activities of up to 170 U g_{CDW}⁻¹ have been reported, but the toxicity of the product 2-methylsuccinimide is arguably thwarting this reaction.[79]

In this study, we constructed an enzyme cascade in *Synechocystis* for the conversion of C-one to non-toxic 6-HA, an equally interesting synthon and polymer building block, thereby minimizing reactant effects on host metabolism. Recently, *Acidovorax* BVMO has been used in *Pseudomonas taiwanensis* VLB120 as part of cascades converting Chx to 6-HA,[165] 6-aminohexanoic acid,[166] and adipic acid,[238] involving an *Acidovorax* lactonase to convert ϵ -Cl to 6-HA, which also was used in this study. So far, enzyme cascades applied in cyanobacteria typically involved native carbon fixation.[160, 239] Examples for enzyme cascades in cyanobacteria making use of non-native substrates and electrons derived from photosynthetic water oxidation are rare. In a proof-of-concept study, Wlodarczyk et al. implemented the dhurrin pathway from *Sorghum bicolor* by expressing two membrane bound cytochrome P450s (CYP79A1 and CYP71E1) and a soluble glycosyltransferase.[72] Vector-based co-expression of all three genes was demonstrated and the process was translated to 8 L photo-bioreactors. The final dhurrin titer of 3.34 mg L⁻¹ was not optimized in the scope of the study. Beside overcoming toxicity-related limitations, the present study aims at elucidating the capacity of and limitations within cyanobacteria for photosynthesis-driven *in vivo* cascades. The approach included the functional co-expression of BVMO and lactonase genes in *Synechocystis* and the evaluation and optimization of the resulting cascade regarding inhibition avoidance as well as conversion rate and product titer.

4.2 Experimental section

4.2.1 Strains, chemicals and cultivation conditions

DNA oligonucleotides, plasmids, and bacterial strains generated and used in this study are given in the supporting information (Table S4). *Synechocystis*[182] was cultivated in 20 or 50 mL BG11 medium[183] with 10 mM 4-(2-hydroxyethyl)-1-piperazinethanesulfonic acid (HEPES), pH 7.5, using 100 or 250 mL baffled shaking flask with cotton stoppers, respectively. Cultivation conditions were 30 °C, 150 rpm (2.5 cm amplitude), 50 $\mu\text{mol}_{\text{photons}} \text{m}^{-2} \text{s}^{-1}$, ambient CO₂ (0.04% [v/v]), and 75% humidity in multitron shakers (Infors, Bottmingen, Switzerland).

Plate cultivation was conducted on BG11 agar plates with 1.5% (w/v) bacto agar at 30 °C and 25 $\mu\text{mol}_{\text{photons}} \text{m}^{-2} \text{s}^{-1}$. If required, chloramphenicol (Cm) was used at a final concentration of 25 $\mu\text{g mL}^{-1}$. C-one, $\geq 99.5\%$ purity, cyclohexanol (C-ol), $\geq 99\%$ purity, and 6-HA, $\geq 95\%$ purity, were purchased from Sigma-Aldrich (Steinheim, Germany), Merck (Darmstadt, Germany), and Acros Organics (Geel, Belgium), respectively. All other chemicals were purchased from Carl Roth GmbH (Karlsruhe, Germany), Merck, or Sigma-Aldrich at the highest purity available.

4.2.2 Cloning and Transformation

Standard molecular biology procedures were applied as described before [184]. Two pSEVA-based vectors were constructed, pAH070, the empty vector control, and pAH073, a replicative plasmid containing the BVMO and lactonase genes from *Acidovorax* sp. CHX100 under control of the Ni^{2+} -inducible *PnrsB* promoter. A modular cloning approach was applied [240, 241], making use of type IIS restriction enzymes, i.e., *Bpil* and *Bsal*, to create a library of different genetic elements and assemble them in the desired way. The applied system is analogous to the previously published CyanoGate, [64] with a reverted order and altered overhangs of the two restriction sites. For details, the reader is referred to [242]. In short, plasmids were assembled in a hierarchical way, i) domesticating genetic information to be implemented to the GoldenGate system syntax as genetic elements (Level 0), ii) assigning positions to genetic elements depending on their function (promoter, gene, terminator, etc.) (Level 1), and iii) combining several units in a pSEVA-based plasmid (Level 2) ready to be transformed into *Synechocystis*. Transfer from one level to another was realized by restriction-ligation cycles (35 cycles of 37 °C for 2 min and 16 °C for 5min, followed by 37 °C, 50 °C, and 80 °C for 5 min each) using *Bsal* FD or *Bpil* FD (Thermo Fischer, Waltham, MA). Assembled plasmid were used for electroporation of *E. coli* DH5 α following standard procedures. [184] After selection with respective antibiotics, positive transformants were grown in lysogeny broth medium, [184] and plasmids were isolated using commercial kits from Macherey-Nagel (Düren, Germany). This procedure was iteratively repeated to finally yield the Level 2 constructs. BVMO and lactonase encoding genes originating from pAH063 (Chapter 3) and pSEVA_6HA, [165] respectively, were domesticated by removing *Bsal* and *Bpil* recognition sites and adding GoldenGate-compatible overhangs via preparative PCR. The PCR products were then used for Level 0 entry. Sequence verification was conducted at Level 0 using the Sanger sequencing service from Azenta (Leipzig, Germany).

For electroporation of *Synechocystis*, cells were prepared as described in Chapter 3. Aliquots of sixty μl freshly prepared cells were supplied with 0.25-1 μg of plasmid DNA and electroporated (2.5 kV; 5 ms; Eporator®, Eppendorf, Hamburg, Germany). The cell suspension was plated onto selective BG11 agar plates containing Cm. Transformants grown within 7-10 days were confirmed via colony PCR. The plasmids pAH070 and pAH073 were used to generate *Synechocystis* ctrl and *Synechocystis* BVMO:Lactonase, respectively.

4.2.3 Whole-cell activity assays and biotransformations

Whole-cell activity assays were conducted as described in Chapter 3, harvesting *Synechocystis* cells 24 h after induction with respective NiSO₄ concentrations by centrifugation at 5,000 g for 10 min. Standard assay conditions were 30 °C, 150 μmol_{photons} m⁻² s⁻¹, 150 rpm, and ambient CO₂ (0.04%[v/v]). After 10 min of equilibration at assay conditions, whole-cell activity assays were started by adding 3 mM C-one and stopped after 30 min by adding 1 vol diethylether containing 0.2 mM n-decane as internal standard for gas chromatography (GC) analysis, or 0.11 vol of acetonitrile for high-pressure liquid chromatography (HPLC). A cell concentration of 0.7-1.0 g_{CDW} L⁻¹ was used in a total volume of 1 mL in 10 mL Pyrex tubes. Assays targeting lactonase activity only were supplied with 3 mM ε-Cl using a reduced cell concentration (0.1-0.2 g_{CDW} L⁻¹) and reaction time (10 min).

Whole-cell biotransformations were conducted in a stirred-tank photo-bioreactor (photo-STR, Labfors 5 Lux, Infors AG, Bottmingen, Switzerland) with 2 L culture volume. Cells were grown for 3-4 days at 30 °C, 2 L min⁻¹ aeration + 20 mL min⁻¹ CO₂, 300 rpm stirrer speed, and given light intensities. Induction with 10 μM NiSO₄ was conducted 24 h prior to biotransformation start. During biotransformation, aeration was reduced to 0.2 L min⁻¹ + 20 mL min⁻¹ CO₂. After pre-conditioning for 30 min, biotransformation was initiated by starting a continuous feed of 0.2 M C-one in BG11 medium at a rate specified in the text. Samples were taken at regular time intervals and quenched immediately by adding either 1 vol diethylether with 0.2 mM n-decane as internal standard or 0.11 vol acetonitrile for GC or HPLC analysis, respectively.

Table 5: **Conditions for cyclohexanone (C-one) biotransformation** with *Synechocystis* BVMO:Lactonase and *Synechocystis* BVMO in 2 L stirred-tank photo-bioreactors.

Strain	<i>Synechocystis</i> BVMO:Lactonase			<i>Synechocystis</i> BVMO
	20 U g _{CDW} ⁻¹	10 U g _{CDW} ⁻¹	0 U g _{CDW} ⁻¹	10 U g _{CDW} ⁻¹
Feed regime ^a	20 U g _{CDW} ⁻¹	10 U g _{CDW} ⁻¹	0 U g _{CDW} ⁻¹	10 U g _{CDW} ⁻¹
Gas input				
air; L min ⁻¹	2-0.2 ^b	2-0.2 ^b	2-0.2 ^b	2-0.2 ^b
CO ₂ ; mL min ⁻¹	20	20	20	20
Light ; μmol _{photons} m ⁻² s ⁻¹				
for growth	100-300-500 ^c	100-300-500 ^c	100-300-500 ^c	100-300-500 ^c
for biotransformation	700-900 ^d	700	700	700
Biomass concentration ^e ; g _{CDW} L ⁻¹	1.16 ± 0.04	0.84 ± 0.02	1.05 ± 0.04	0.79 ± 0.01

^a Substrate feed rate was set to limit specific activities to given values, considering the cell concentrations applied.

^b For biotransformation, air supply was reduced to 0.2 L min⁻¹.

^c Stepwise increase of light intensity during growth

^d Switch to 900 μmol_{photons} m⁻² s⁻¹ after 4 h of biotransformation

^e Biomass concentration at the start of the biotransformation, assessed via OD₇₅₀

4.2.4 Analytics

The cell concentration was assessed by determining OD₇₅₀ in a LibraS11 spectrophotometer (Biochrom, Cambridge, UK). The previously determined correlation factor of 0.225 g_{CDW} L⁻¹ per OD₇₅₀ unit was used to calculate cell CDW concentrations.[58] Chlorophyll-a concentrations were determined as described before.[161] The same is true for the determination C-ol, C-one, and ε-Cl concentrations via GC analysis[243] and 6-HA concentrations via HPLC analysis (see Chapter 3).

4.2.5 Energy balancing

The incident light/input energy converted to product or biomass was estimated via the following two parameters (A) the **quantum yield Φ** relating the product amount to the amount of incident quanta and (B) the **energy yield Y** relating the energy bound in the products to the total energy of the incident light.

A. To have a reasonable physiological unit to relate both biomass (X) and product (P) formation to photosynthetic rates, the quantum demand (Q) for both processes was calculated. For the quantum demand of biomass formation (Q_X), C-fixation and N-assimilation, the two native processes being the main consumers of intracellular reductant, were considered assuming linear electron transfer, i.e., 2 quanta are required to supply 1 electron:

$$(9) Q_X = \left(\frac{\chi_C}{M_C} * 4 + \frac{\chi_N}{M_N} * 8 \right) * 2 \quad [\text{mol}]$$

with χ_C and χ_N being the mass fractions of C and N in total biomass and M_C and M_N as molar masses of C and N. For the assimilation of 1 mol of C from CO₂ and 1 mol of N from NO₃⁻, 4 and 8 electrons are consumed, respectively. The quantum demand for product formation (Q_P) then is

$$(10) Q_P = n_P * 2 * 2 \quad [\text{mol}]$$

with n_P being the amount of product in mol; 2 mol electrons are required for the conversion of 1 mol C-one to ε-Cl, and 2 quanta are required for the supply of 1 electron.

The quantum yields of biomass formation (Φ_X) and of product formation (Φ_P) are defined as

$$(11.1) \Phi_X = \frac{Q_X}{Q_{total}} \quad \text{and} \quad (11.2) \Phi_P = \frac{Q_P}{Q_{total}}$$

with Q_{total} being the total amount of incident quanta.

B. To assess the energy yield (Y) of specific processes, the input and product energies have to be quantified. For the input energy, it has to be considered that the quantum energy (E) depends on its wavelength (λ):

$$(12) E_\lambda = h * \frac{c}{\lambda} * N_A \quad [\text{kJ mol}^{-1}]$$

with the Planck's constant (h), the speed of light (c), and Avogadro's number (N_A).

With a known emission spectrum (Figure S10), the total energy input (E_{PAR}) can be assessed for the photosynthetically active radiation (PAR)

$$(13) E_{PAR} = \int_{400nm}^{700nm} h * \frac{c}{\lambda} * N_A * \frac{I_{\lambda}}{I} d\lambda \quad [\text{kJ}]$$

Based on standard enthalpies of formation in kJ g^{-1} or kJ mol^{-1} , the energy for biomass formation from CO_2 , H_2O , and NO_3^- or product formation can be quantified and related to the input energy to obtain Y_X or Y_P . To quantify the energy flowing into product formation, the energy transferred to the redox currency in phototrophs NADPH upon its formation from NADP^+ , i.e., 220 kJ mol^{-1} , served as a basis.

4.3 Results

In a previous study, we showed that, on bioreactor scale, photosynthesis-driven BVMO-based C-one oxidation is kinetically controlled with product inhibition by ϵ -Cl limiting process stability (Chapter 3). We hypothesized that the coupling of a lactonase efficiently removing ϵ -Cl can relieve this main limitation. Preliminary tests confirmed that 6-HA exhibits a much lower inhibition for *Synechocystis* and, in contrast to ϵ -Cl, did neither inhibit C-one oxidation nor ϵ -Cl hydrolysis (Figure S12). Thus, the cascade biotransformation performance of *Synechocystis* BVMO:Lactonase was tested in a 2 L stirred-tank photo-bioreactor (photo-STR) setup providing efficient O_2 and CO_2 mass transfer in a controlled environment together with a controlled substrate supply.

4.3.1 Functional co-expression of BVMO and lactonase genes

Plasmids pAH070 (empty vector control) and pAH073 (vector containing BVMO and lactonase genes under control of the Ni^{2+} -inducible *PnrsB* promoter) were successfully constructed and introduced into *Synechocystis* to generate the strains *Synechocystis* ctrl and *Synechocystis* BVMO:Lactonase, respectively. Colony PCR verified successful transformation. Functional co-expression of BVMO and lactonase genes in *Synechocystis* BVMO:Lactonase was tested in short term activity assays with both C-one and ϵ -Cl as substrates. Different clones were tested and showed specific activities of up to $63.1 \pm 1.1 \text{ U g}_{CDW}^{-1}$ ($3.1 \pm 0.1 \text{ mM h}^{-1}$) with C-one as a substrate (Figure 13A), 1.2-times higher than activities achieved with *Synechocystis* BVMO (Chapter 3) und identical assay conditions. The only product detected was 6-HA. No intermediary ϵ -Cl was detected. To determine lactonase activities, assays were performed with ϵ -Cl as substrate (Figure 13B). *Synechocystis* BVMO:Lactonase strains showed extremely high specific lactonase activities of up to $2840 \pm 350 \text{ U g}_{CDW}^{-1}$ ($17.6 \pm 2.1 \text{ mM h}^{-1}$), more than one order of magnitude higher than published BVMO activities.[179] (see also Chapter 3) These results illustrate an efficient coupling of both enzymes with BVMO being rate-limiting. In

particular, the efficient ϵ -Cl hydrolysis was promising for the stabilization of BVMO catalysis in process setups.

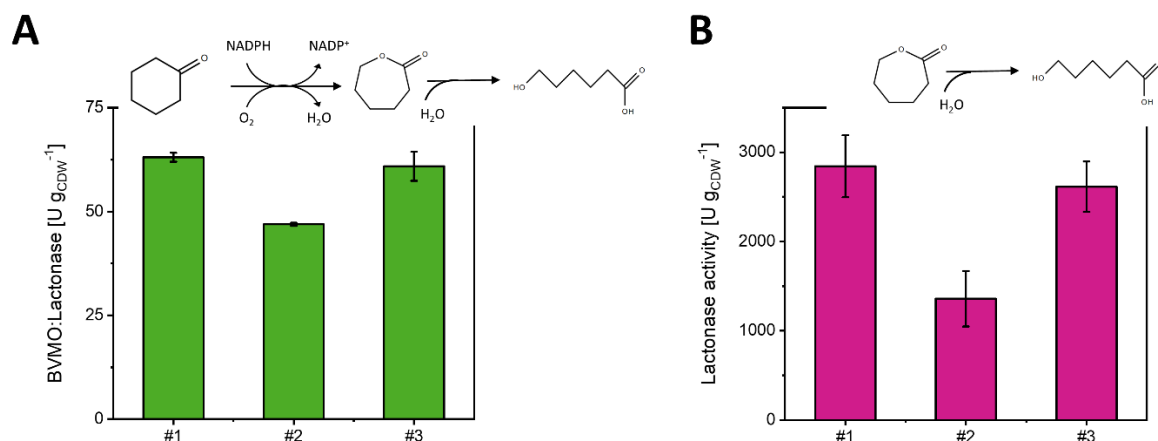


Figure 13: **Specific activities of *Synechocystis* BVMO:Lactonase clones using (A) cyclohexanone and (B) ϵ -caprolactone as substrates.** Short-term activity assays were performed with biomass concentrations of (A) 0.7-1.0 and (B) 0.1-0.2 g_{CDW} L⁻¹ in Pyrex tubes at a light intensity of 150 $\mu\text{mol}_{\text{photons}} \text{m}^{-2} \text{s}^{-1}$. In both cases, 6-HA was the only product detected. Error bars show standard deviations from ≥ 3 technical replicates.

4.3.2 The metabolic capacity of *Synechocystis* appears to limit the redox cascade

To optimally control the substrate concentration, a parameter known to be crucial in this reaction system, a limiting continuous substrate (C-one) feed was applied like in Chapter 3. To avoid any limitation in light or carbon supply, high light (700 $\mu\text{mol}_{\text{photons}} \text{m}^{-2} \text{s}^{-1}$) and high CO₂ (20 mL min⁻¹) conditions were chosen (for details, see Table 2). After growth for 3 days, including induction by adding 10 μM NiSO₄ 24 h before biotransformation start, C-one feeding was initiated at a fixed rate matching 20 U g_{CDW}⁻¹, comparable to the previous one-enzyme-process (Chapter 3). Surprisingly, C-one conversion activity (green bars) decreased right from the start, although inhibiting ϵ -Cl did not accumulate and C-one only began accumulating after 2 h (Figure 14A). Increasing the light intensity to 900 $\mu\text{mol}_{\text{photons}} \text{m}^{-2} \text{s}^{-1}$ (black arrow at 4 h) led to a short increase of the dissolved oxygen concentration (DOC), but not to a recovery of the whole-cell activity, indicating that the light regime was not the main limitation. After 8 h, 6.97 ± 0.37 mM 6-HA was formed with an initial volumetric productivity of 1.48 ± 0.02 mM h⁻¹. C-one accumulation until 8 h of biotransformation can be expected to involve increasing substrate inhibition (K_i : 4.4 ± 1.5 mM, Chapter 3), although not to an extent, which could explain the observed activity decrease. Noteworthy, comparing the two-enzyme process with published data of the one-enzyme-process under comparable conditions reveals a similar activity decrease and an only slightly improved process performance in terms of product titer (12.35 ± 0.14 mM after 28 h vs. 11.5 ± 0.2 mM after 27 h) and average productivity (0.058 ± 0.001 vs 0.049 ± 0.001 g L⁻¹ h⁻¹). (Chapter 3)

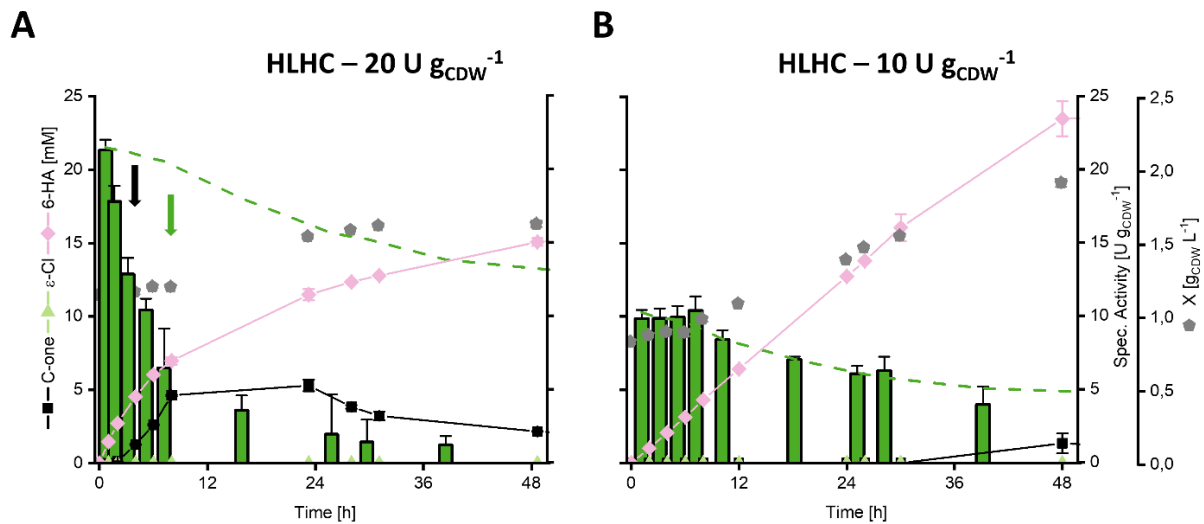


Figure 14: **Photosynthesis-driven two-step cascade in a 2 L photo-STR with different substrate feeding regimes.** *Synechocystis* BVMO:Lactonase was grown for 3 days including 24 h of induction with 10 μM NiSO_4 . Then, biotransformation was started by feeding C-one in a substrate-limited regime matching (A) 20 $\text{U g}_{\text{CDW}}^{-1}$ or (B) 10 $\text{U g}_{\text{CDW}}^{-1}$. For reaction conditions, see Table 2. Cell concentration (grey diamonds), cyclohexanone (C-one, black squares/line), 6-hydroxyhexanoic acid (6-HA, rose diamonds/line), and ϵ -caprolactone (ϵ -Cl, light green triangles/line) concentrations are shown. Specific activities in $\text{U g}_{\text{CDW}}^{-1}$ (green bars) are calculated based on 6-HA formation with the dashed green line giving the maximally achievable activity at the feed rate applied. Black arrow, increase in light intensity to 900 $\mu\text{mol}_{\text{photons}} \text{m}^{-2} \text{s}^{-1}$; green arrow, C-one feed reduction to 25%. Depicted are mean values and standards deviations from ≥ 2 sampling replicates.

As a possible reason for the decreasing biotransformation performance, the capacity of host metabolism may become limiting. Indeed, decreasing DOC levels during the biotransformation indicate a decreasing photosynthetic activity and thus NADPH supply (Figure 15A). To investigate, if a lower burden on metabolism in terms of NADPH withdrawal leads to a stabilization of the biotransformation, a lower conversion rate was established and tested by reducing the substrate feed to a rate enabling 15 $\text{U g}_{\text{CDW}}^{-1}$ while keeping all other parameters unchanged (Figure S13). The decreased substrate supply rate prolonged the stable production phase to more than 8 h with an average volumetric productivity of $1.87 \pm 0.14 \text{ mM h}^{-1}$. After 24 h, however, C-one accumulation was detected, again indicating a capacity limitation and finally leading to substrate inhibition.

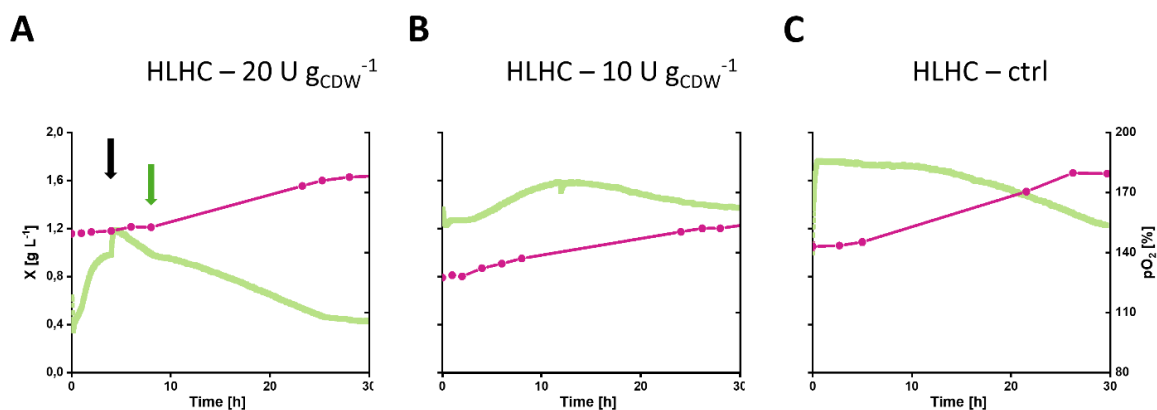


Figure 15: **Biomass concentration (pink) and DOC (light green) courses within different biotransformation setups.** *Synechocystis* BVMO:Lactonase was grown for 3 days including 24 h of induction with 10 μM NiSO_4 . Then, biotransformations were started by feeding C-one in a substrate-limited regime matching (A) 20 $\text{U g}_{\text{CDW}}^{-1}$ or (B) 10 $\text{U g}_{\text{CDW}}^{-1}$. For (C), no substrate was added. Black arrow, increase in light intensity to 900 $\mu\text{mol}_{\text{photons}} \text{m}^{-2} \text{s}^{-1}$; green arrow, C-one feed reduction to 25%.

Motivated by the extended stable production phase, substrate supply was further decreased to $10 \text{ U g}_{\text{CDW}}^{-1}$ in a third photo-STR-experiment (Figure 14B). This moderate biotransformation demand could be met for at least 30 h, leading to the formation of $16.73 \pm 0.92 \text{ mM}$ 6-HA at an average productivity of $0.57 \pm 0.03 \text{ mM h}^{-1}$. The product titer further increased to $23.50 \pm 1.19 \text{ mM}$ 6-HA after 48 h, being twice as high as the one achieved with BVMO only and a higher feed rate (Chapter 3). Interestingly, the cells exhibited high metabolic activity, as indicated by the DOC and growth being comparable to a control without biotransformation (Figure 15B, C). The yield on substrate ($Y_{\text{P/S}} = 0.96 \text{ [mol mol}^{-1}\text{]}$) emphasized efficient and selective conversion of C-one into 6-HA as sole product of the two-step cascade. The biocatalyst-based yield ($Y_{\text{P/X}} = 3.71 \pm 0.21 \text{ g}_{\text{6-HA}} \text{ g}_{\text{CDW}}^{-1}$).

4.3.3 Lactonase is essential to avoid ϵ -Cl inhibition

Yet, the utility of the lactonase to mitigate product inhibition remained unclear: Direct comparison of photo-STR experiments fed for a specific activity of $20\text{-}25 \text{ U g}_{\text{CDW}}^{-1}$ using either BVMO or BVMO:Lactonase strains did not reveal clear differences between the one-enzyme and the two-enzyme approach. These findings question the suggested importance of product limitation by ϵ -Cl and thereby challenge the concept of introducing the lactonase to circumvent product inhibition. Reducing the metabolic burden posed by the biotransformation by a fine-tuned substrate feed may already solve stability issues within the one-enzyme process, as it did for the two-enzyme process.

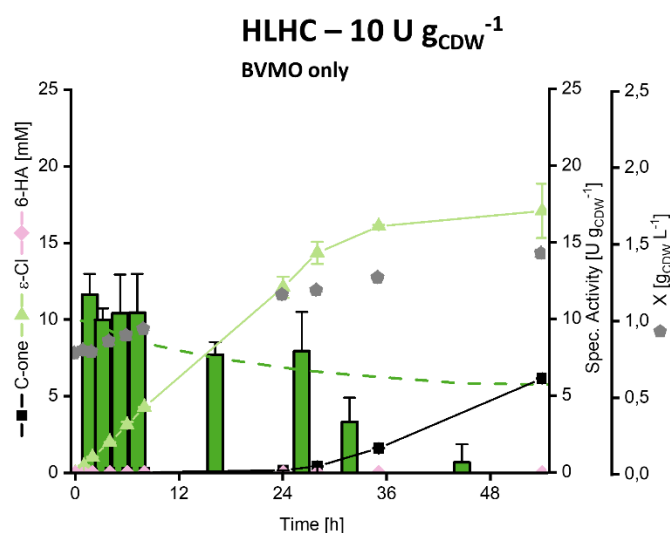


Figure 16: **Photosynthesis-driven one-enzyme process in a 2 L photo-STR with moderate substrate feed regime.** *Synechocystis* BVMO was grown for 3 days including 24 h of induction with $10 \mu\text{M NiSO}_4$. Then, biotransformation was started by feeding cyclohexanone (C-one) in a substrate-limited regime matching $10 \text{ U g}_{\text{CDW}}^{-1}$. For reaction conditions, see Table 2. Courses of cell concentration (grey diamonds), C-one (black squares/line), and ϵ -caprolactone (ϵ -Cl, light green triangles/line) concentrations are shown. Specific activities in $\text{U g}_{\text{CDW}}^{-1}$ (green bars) are calculated based on ϵ -Cl formation with the dashed green line giving the maximally achievable activity at the feed rate applied. Depicted are mean values and standards deviations from ≥ 2 sampling replicates.

To test, if the one-enzyme process actually is hampered by ϵ -Cl accumulation, the process parameters of the ideal reactor run (with a C-one feed rate matching $10 \text{ U g}_{\text{CDW}}^{-1}$) were applied using *Synechocystis* BVMO (Figure 16). For 28 h, the moderate feed could be met by the biocatalyst activity, enabling complete conversion of the fed substrate to ϵ -Cl. However, further increasing product concentrations inhibited C-one conversion and led to a virtually stalled activity after 36 h. Importantly, the ϵ -Cl concentration range, at which inhibition occurred, is in good agreement with concentrations predicted by the published dynamic model based on kinetic data (Chapter 3). Hence, product inhibition was confirmed as key limitation in the one-enzyme-approach irrespective of the substrate feed rate applied.

To conclude, lactonase introduction indeed enabled to overcome limitations imposed by the challenging kinetics of the BVMO-catalyzed reaction in vivo. However, the two-step cascade was found to depend on the metabolic capacity of the host organism. Thus, careful pathway and process design can be considered crucial for successful light-driven biotechnology with the phototrophic metabolism representing a promising engineering target.

4.3.4 Energy balancing reveals unused potential for oxygenase catalysis

Interestingly, *Synechocystis* did not show compromised growth in the 2 L photo-STR, when applying a substrate feed matching $10 \text{ U g}_{\text{CDW}}^{-1}$ (Figure 15B), compared to a control without biotransformation (Figure 15C). This prompted us to perform an energy/redox balancing for the biotransformation phase to unravel how much energy can be withdrawn from the photosynthetic apparatus. For this purpose, the amount of incident light, photosynthetic NADPH/reductant supply, and the electron demands for biomass formation and biotransformation were considered (Table 6). The input energy in kJ was the same for all compared setups (except for the $20 \text{ U g}_{\text{CDW}}^{-1}$ photo-STR experiment, in which light intensity was increased to $900 \mu\text{mol}_{\text{photons}} \text{ m}^{-2} \text{ s}^{-1}$). For translating biomass and product formed (in mg and mM, respectively) into quantum demands (in mmol), theoretical minima were assumed using equations 1 and 2, being aware that experimentally determined quantum demands are slightly higher.[47] On this basis, the quantum efficiencies Φ_x and Φ_P were calculated following eqs. 3.1 and 3.2. To assess the energy yield for biomass formation Y_x , the energy stored in biomass was calculated assuming an energy content of 21.98 kJ g^{-1} , corresponding to the respective combustion energy.[244] As a measure for the energy flowing into product formation, the energy transferred to the redox currency in phototrophs NADPH upon its formation from NADP^+ , i.e., 220 kJ mol^{-1} , served as a basis.

The maximum quantum efficiency for product formation Φ_P (0.070) and the highest light-to-product efficiency (1.8%) were reached in the first hour of the $20 \text{ U g}_{\text{CDW}}^{-1}$ photo-STR experiment, but could not be sustained in the long run. Naturally, both quantum efficiency for product formation Φ_P (0.026) and light-to-product efficiency (0.7%) were lower with reduced substrate feeding, for which, however, a stable activity including substrate depletion was

sustained in the long term. Interestingly, this also was true for the overall quantum efficiency Φ_{total} , which was increased from 0.113 to 0.160, compared to the control experiment, but strongly decreased in the long term with higher substrate feeding.

Table 6: **Energy balancing for the redox cascade run in *Synechocystis* BVMO:Lactonase** cultivated in photo-STRs with different substrate feed rates.

Feed regime ^a		20 U g _{CDW} ⁻¹		10 U g _{CDW} ⁻¹		0 U g _{CDW} ⁻¹	
Time range [h]		0-1	0-31.1	0-1 ^b	0-30.0	0-1 ^b	0-29.7
Incident light							
-	mmol _{quanta}	171	6642	171	5130	171	5073
-	kJ	36	1399	36	1081	36	1069
Growth							
-	Biomass formed mg	35	966	48	1446	46	1211
-	Quantum demand for	16	456	22	682	22	576
Growth, mmol							
Biotransformation							
-	6-HA, mM	1.5	12.8	0.5	16.7	-	-
-	Quantum demand for	12	104	4.4	116	-	-
biotransformation, mmol							
Quantum efficiency, Φ							
-	Φ_X	0.096	0.069	0.131	0.133	0.127	0.113
-	Φ_P	0.070	0.016	0.026	0.026	-	-
-	Φ_{total}	0.166	0.085	0.157	0.160	0.127	0.113
Yield on Light							
-	Y_X , % ^c	2.1	1.5	2.9	2.9	2.8	2.5
-	Y_P , % ^d	1.8	0.4	0.7	0.7	-	-
-	Total, %	3.9	1.9	3.6	3.6	2.8	2.5

^a Substrate feed rate was set to limit specific activities to given values, considering the cell concentrations applied.

^b Data extrapolated for given time ranges

^c Based on 21.98 kJ g_{Biomass}⁻¹ [244]

^d Based on -220 kJ mol_{NADPH}⁻¹

4.4 Discussion

By the establishment of efficient photosynthesis-driven cascade biocatalysis, inter alia to avoid product inhibition, and the evaluation of respective inherent metabolic capacity potentials and limitations within cyanobacteria, this study gives crucial insights for future research and developments in the rapidly evolving field of photo-biotechnology. A two-step cascade was established in *Synechocystis* to convert C-one via ϵ -Cl to 6-HA utilizing a BVMO and a lactonase from *Acidovorax* sp. CHX100. The high activity of the lactonase enabled immediate conversion of ϵ -Cl upon its formation, thereby preventing product inhibition. These results correspond well to results obtained with these enzymes in heterotrophic *P. taiwanensis*

VLB120[165] and are particularly promising, as they illustrate the transferability of engineering principles from heterotrophic to phototrophic chassis strains.

The transfer of the photosynthesis-driven two-step cascade onto a 2 L scale using photo-STRs showed that the avoidance of detrimental ϵ -Cl effects alone did not suffice to stabilize the C-one conversion over an extended period of time (≥ 24 h). The exploited specific activity had to be limited by an appropriate substrate feed regime to enable such stabilization. Energy balancing revealed that the moderate feed regime (enabling $10 \text{ U g}_{\text{CDW}}^{-1}$) translates to the withdrawal of roughly 16% of intracellular reductant. Withdrawing this share appeared to be feasible from a physiological perspective, as not only the biotransformation rate was stabilized, but also biomass formation occurred to the same (or even slightly higher) extent as without biotransformation. However, a higher share of intracellular reductant could only be withdrawn from cellular metabolism for a few hours, followed by a decrease of both biomass formation and bioconversion rates. Obviously, strong and enduring electron withdrawal affected cell physiology. Thus, the high capacity for light reaction-derived electron withdrawal observed on the short term appears to be significantly lower on the long term.

The question arises, why this is the case and what exactly causes the observed limitation and also the observed decrease in reductant supply by the photosynthetic light reaction. One obvious reason may be that reductant supply by photosynthesis is or becomes limited, either due to external factors like light limitation or restricted metabolic/photosynthetic capacity. Previous studies on *Synechocystis* expressing reductant-dependent enzymes elucidated that respective reaction rates are light-dependent[74, 95] (see also Chapter 3), but also showed that light limitation could largely be relieved at high light intensities.[178] In the long term, however, increasing the light intensity did not enable a recovery of decreasing C-one biotransformation activities (Figure 14A). On the other side, photosynthetic metabolism may suffer from a strong reductant withdrawal by electron-demanding biotransformations disturbing the NADPH:ATP balance within the cell.[245] To counteract such an imbalance, cyclic electron transfer can be downregulated. However, when only linear electron transfer is operating, an increasing adenylate energy charge together with an increasing redox ratio in terms of $\text{NADP}^+/\text{NADPH}$ may cause CBB limitation (by NADPH) and/or inhibition. The latter may be mediated by regulators like thioredoxin [37] or small proteins like CP12 [43, 44], which are redox regulated, with the redox state serving as a proxy for light availability.[44] As a consequence, the CBB cycle activity may be significantly decreased upon NADPH withdrawal, in turn reinforcing the NADPH:ATP imbalance due to lacking ATP sink.[246] This then also may harm the photosynthetic machinery, e.g., its regeneration and oxidative stress management, finally leading to a decrease in light reaction rates and thus fostering NADPH limitation.[37, 43, 44, 247] Thus, the NADPH:ATP imbalance caused by extensive NADPH withdrawal may shut down photosynthetic electron supply, resulting in a metabolic stalemate.

One possible way to escape it has been lately reported: It was shown that co-expression of an ATP-sink together with an electron sink could substantially benefit the latter one.[85] Following this hypothesis, a moderate burden would avoid or lead to a weak NADPH:ATP imbalance, which can be endured by the cell without drastic measures, enabling a stable biotransformation. Other strategies to stabilize instabilities encountered with cyanobacteria have recently been reviewed by Guillaume and dos Santos, with the use of genome-scale metabolic models as a promising option to mitigate instability and design stable production strains.[248] Further research is needed to elucidate the occurrence and effects of NADPH:ATP imbalances.

The synergy of biochemical and biocatalyst engineering, including the involvement of a reaction cascade, enabled a stable bioconversion in *Synechocystis* for up to 48 h, reaching a final titer of 23.50 ± 0.84 mM 6-HA, unprecedented for light-driven oxygenase reactions. Besides the excellent specificity ($Y_{P/S} = 0.96 \text{ mol mol}^{-1}$), the high biocatalyst yield of $3.71 \pm 0.21 \text{ g}_{6\text{-HA}} \text{ g}_{\text{CDW}}^{-1}$ illustrates the benefit of a high process stability. Consequently, the presented enzyme cascade outcompetes described photosynthesis-driven oxygenase-based systems regarding both volumetric productivity and final product titer and, thus, holds great promise for future applications of *Synechocystis* as host for photo-biotechnological applications.

However, space-time-yields and final titers still need substantial improvements to make phototrophic microbes commercially applicable as sustainable cell factories. Metabolic engineering, e.g., to balance energy (ATP) and redox demands (NADPH), will play an important role to further increase rates of photosynthesis-driven biocatalysis in *Synechocystis*. [237] A main challenge for efficient scale-up is the typically low cell density in phototrophic cultivation systems, being limited by light input and penetration. Recent developments like internal illumination[95] and capillary biofilm reactors[98] constitute highly attractive concepts to meet this challenge.

The estimation of quantum and light usage efficiencies allows for a quantitative assessment of photosynthesis-driven biocatalysis: Following the calculations for the high C-one feed regime (Table 1), a remarkable share of 40% of intracellularly available reductant was allocated to the biotransformation during the first hour. As discussed above, this high share could not be sustained in the long run. In contrast, the activity limited by a moderate substrate feed, consuming 16.5% of cellular reductant, could be sustained for 30 h, with substantial activity being maintained for at least 48 h without compromising growth. In fact, the biotransformation could be supplied with reduction equivalents in addition without deducting reduction equivalents from growth. Consequently, the biotransformation increased the overall light conversion efficiency (3.6% vs. 2.5%, Table 6). Hence, the biotransformation appeared to be sustained with cellular energy that otherwise would be dissipated and lost from a biotechnological point of view. The sustained quantum efficiency of product formation and the

product yield on light were 2.6 and 0.7%, respectively, representing considerable values, given that both strain and reactor format are far from being optimized for efficient light usage. The overall light conversion efficiency (3.6%) is remarkable in view of the fact that the theoretical maximum conversion efficiency of photosynthesis is debated to lie between 4.5%[8] and 10%[105] and real efficiencies in the range of 1-2%[8, 47, 106]. Strain and reactor engineering augur well to leverage the full potential of photosynthesis-driven redox biocatalysis.

The enzyme cascade described in this study constitutes an excellent model system to investigate physiological responses to a strong electron sink, fulfilling two important criteria: i) It is a tunable reaction, e.g., by substrate supply and/or expression strength, and ii) it allows for a stable conversion for not only hours, but even days. As such it is ideal to study the regulatory processes, e.g., regarding the NADPH:ATP balance, with both omics techniques to investigate effects on the transcript, protein, and metabolome levels and state-of-the-art fluorometry methods to examine photosynthetic apparatus operation. Especially in the light of envisioned bulk chemical production like light-driven H₂ formation, it will be essential to follow up the question, which share of reductant can be withdrawn from cyanobacterial metabolism. The data presented in this study for a fed-batch biotransformation give stimulating insights, but cannot be regarded as quantitative assessment of the photosynthetic capacity, which needs to be investigated in more detail in future.

5 From photons to product – a quantitative study on electron fluxes in oxygenase-active *Synechocystis* sp. PCC 6803

Cyanobacteria provide a highly interesting chassis for the utilization of sun light as energy source for biotechnology. Their metabolism has to balance energy assimilation (*source*) with demand for nutrient assimilation and biomass formation (*sink*). According to the sink hypothesis, extra carbon and electron sinks can increase photosynthetic efficiency by relieving sink limitation. This is of special interest for the implementation of redox biotransformations to tap otherwise unused photosynthetic potential.

We tested physiological responses of the cyanobacterium *Synechocystis* sp. PCC 6803 to the onset of an electron consuming biotransformation under three different sink scenarios, varying light, carbon, and nitrogen source availabilities. A heterologously expressed two-step cascade, i.e., Baeyer-Villiger monooxygenase and lactonase-catalyzed conversion of cyclohexanone via ϵ -caprolactone to 6-hydroxyhexanoic acid, served as a proxy for the decoupling of consumption of photosynthetically generated electrons from biomass formation. Steady state conditions allowed the quantitative assessment of physiological parameters, such as growth rate μ , specific quantum absorption Q_{phar} , and effective quantum yield at photosystem II Φ_{PSII} . Balancing absorbed photons and photosynthetically generated electrons revealed distinct changes in electron flux allocation upon Ni^{2+} -induced expression of heterologous genes and biotransformation initiation under the tested scenarios.

Despite evidence for a high metabolic flexibility, the biotransformation could not be maintained in any of the tested conditions in steady state conditions, most likely due to metabolic or enzymatic instabilities. Sink-limited conditions were found to be best suited to sustainably distribute reductant between growth and biotransformation, whereas sink-replete conditions depicted the highest biotransformation capacity and thus the highest quantum efficiency. The described physiological analysis of an oxygenase-active cyanobacterium is an important cornerstone to optimize phototrophic metabolism for future photo-biotechnological applications.

5.1 Introduction

Phototrophic microorganisms like cyanobacteria have been shown to be interesting hosts for biotechnological processes. Their utilization is motivated by the great promise to unclothe the sun as power supply for production. Making use of their core metabolism, the oxygenic photosynthesis, cyanobacteria are able to form biomass based on sun light, water, and CO₂ as energy, electron, and carbon sources, respectively. Under environmental conditions, the availability of these resources varies: During the day, phototrophic organisms are typically exposed to light intensities above or below the light saturation point (E_k), at which incident light can be used most efficiently for assimilatory processes.[33, 47, 48, 120] Thus, cyanobacteria are forced to constantly balance source and sink utilization and thus energy assimilation (light harvesting, photosynthetic electron flux) and energy demand (nutrient assimilation and biomass formation). To react to sudden imbalances, cyanobacteria possess mechanisms to dissipate energy, with non-photochemical quenching or alternative electron transfer in Mehler-like reactions as the most prominent ones.[45, 46] To balance source/sink ratios on the longer term, state transitions and changes in PSII-efficiency, Chl-*a* content, and Rubisco content are observed.[33, 47, 48] On the one hand, these balancing processes and dissipation mechanisms are protecting the cell from photo-inhibition, i.e., light-induced damage of the photosynthetic apparatus. On the other hand, they encompass an energy loss reducing the overall light conversion efficiency of phototrophs,[8] with photosynthesis operating below its true potential.

To increase conversion efficiency, sink engineering has recently become popular: It is based on the sink hypothesis stating that photosynthetic efficiency can be increased by providing productive pathways as energy/electron sinks making use of surplus photosynthetic energy. In principle, two approaches are pursued: i) **CO₂-based production** of organic chemicals for material and energy use [107-112] and ii) **redox biotransformations** making use of photosynthetic electron supply.[73, 74, 79], (Chapter 3)

CO₂-based production makes use of both the photosynthetic light reaction and CBB to convert/reduce CO₂ to products such as butanol,[107] 2-3 butanediol,[108] glycerol,[109] sucrose,[110, 111] or lactate[112], as reviewed by Angermayer et al. [160]. Utilizing the greenhouse gas CO₂ as carbon source, this strategy sets a basis for truly sustainable processes.

Interestingly, studies on heterologous pathways as carbon sinks in cyanobacteria describe enhanced carbon fixation compared to the respective wild-type strains, [108-110, 112] clearly indicating that cells do not seize their full metabolic potential during ordinary growth and that (carbon) sink engineering can increase photosynthesis efficiency. In a previous study, we showed that, under high-light/low-carbon conditions – arguably reflecting natural conditions,

heterologous lactate synthesis in the cyanobacterium *Synechocystis* sp. PCC 6803 (*Synechocystis*) increased carbon assimilation without affecting biomass formation.[112] To meet the increased sink demand, PSII-efficiency and photosynthesis-derived electron flux were found to be enhanced by 24 and 28%, respectively.[112] CO₂-based production is however tightly linked to CO₂ uptake and fixation capacities, limiting production rates to values typically below 20 mg g_{CDW}⁻¹ h⁻¹. [160]

To achieve higher production rates, the utilization of photosynthesis-derived electrons has gained increasing attention in the last years.[59, 73, 74, 79] This C-independent approach links oxidoreductase-based biotransformations to the light reaction and thereby creates a reductant sink being decoupled from assimilatory routes like the Calvin-Benson-Bassham cycle (CBB).[178] Maximum specific productivities range from 240 and 420 mg g_{CDW}⁻¹ h⁻¹ using cytochrome P450[74] and Baeyer-Villiger monooxygenases,(Chapter 3) respectively, and to 1000 mg g_{CDW}⁻¹ h⁻¹ using ene-reductases (for ~100 g mol⁻¹ products).[79] These numbers demonstrate the high theoretical disposability of photosynthesis-derived electrons for heterologous redox reactions. However, reported production periods range from minutes to a few hours. On the longer term, high electron supply rates could not be maintained, reducing specific activities feasible on the long term (>24 h) to 10-25 U g_{CDW}⁻¹ (corresponding to 60-150 mg g_{CDW}⁻¹ h⁻¹ for ~100 g mol⁻¹ products).[74](see Chapters 3 and 4) Both light limitation [74, 95] and reactant toxicity [74](see Chapter 3) were found to be reasons for decreased photosynthetic electron supply.

Intriguingly, activating extra electron sinks led to an increase of photosynthetic rates, reflected by enhanced photosystem II (PSII) efficiency,[73, 85, 161] quantum absorption,[161] and photosynthesis-derived electron flux.[73, 85, 161] Like carbon sinks, mere electron sinks can evidently relieve the sink limitation and increase photosynthetic efficiency. In a previous study, we examined physiological differences upon nitrogen assimilation from NO₃⁻ and NH₄⁺ strongly differing regarding electron demand [161]: The utilization of NO₃⁻ as N source led to higher photosynthetic rates, which not only promoted electron fluxes, but also carbon fixation and growth, and thus obviously enabled a favorable sink/source balance. Accordingly, an electron consuming biotransformation may also benefit the photosynthetic metabolism by tapping water-derived electrons becoming available in response to upregulated photosynthetic activity. In fact, an orthogonal two-step cascade for the conversion of cyclohexanone (C-one) via ε-caprolactone (ε-Cl) to 6-hydroxyhexanoic acid (6-HA) by means of recombinant Baeyer-Villiger-monooxygenase (BVMO) and lactonase in *Synechocystis* has recently been shown to increase energy conversion efficiencies when the biotransformation substrate was provided as extra electron sink. Furthermore, the rate of electron withdrawal was found to be decisive for metabolic and bioconversion stability, for which a too strong electron sink was detrimental. (Chapter 4)

In the context of photo-biotechnology for light-driven production of both bulk chemicals like polymer precursors and energy carriers like H_2 [21] it is of fundamental interest, how efficient electrons can be withdrawn over a longer time period, i.e., several days or weeks. To answer this question, metabolic prerequisites to stabilize electron withdrawal over extended periods and factors influencing the metabolic robustness have to be investigated.

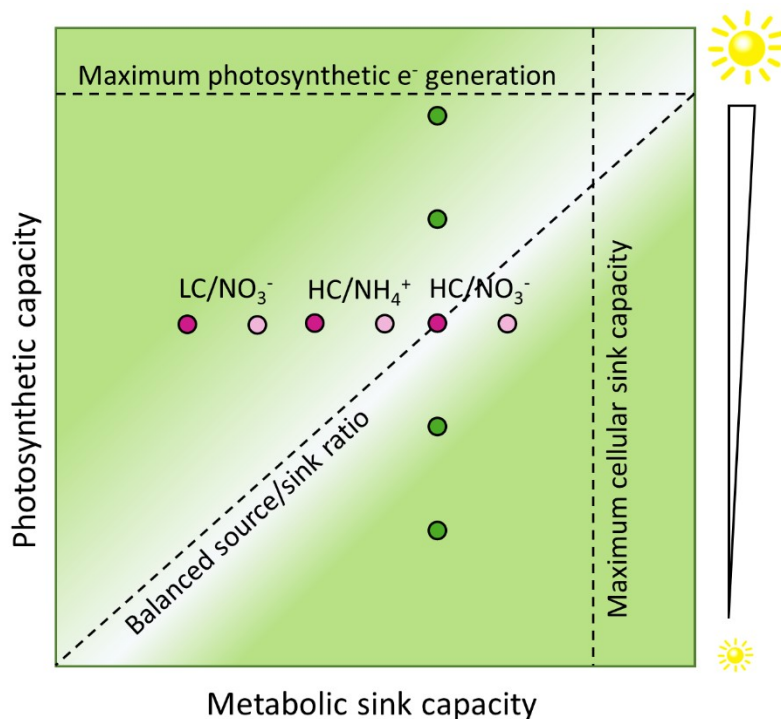


Figure 17: **Source/sink balance in phototrophic organisms.** The capacity for photosynthetic e⁻ provision from water directly depends on light irradiance (y-axis). The generated e⁻ can only be used, when sufficient sinks are available (x-axis) leading to a balanced source/sink ratio. The *green circles* reflect a stepwise increase of light irradiance at a given sink capacity to determine E_k , reflecting optimal source/sink balance. *Magenta circles* reflect the variation of carbon availability (LC – low carbon, HC – high carbon) and nitrogen source (NH_4^+/NO_3^-) at the identified E_k to simulate different sink conditions. *Pink circles* reflect the onset of an e⁻ consuming biotransformation for each sink scenario to increase the sink capacity and investigate physiological responses.

In this study, we used the described two-step cascade in *Synechocystis* as a proxy for an electron sink linked to the photosynthetic light reaction. Physiological and photosynthetic parameters, such as growth, oxygen formation, carbon fixation, PSII-efficiency, and quantum absorbance were assessed during different steady states in continuous cultures. Initially, we increased the available photosynthetic capacity by increasing light irradiance while keeping the sink availability constant. This allowed to screen for a light intensity enabling a balanced source/sink ratio (green circles in Figure 17) and assess the light saturation point (E_k). In a second step, the determined light intensity was used to investigate the effect of different sink scenarios, especially the onset of the electron consuming biotransformation, on the cell physiology (magenta/pink circles in Figure 17). Thereby, we aimed at a holistic insight into the electron flux distribution in a catalytically active cyanobacterium to answer the question to what extent electrons can be decoupled from cyanobacterial growth to fuel desired reactions under different conditions.

5.2 Experimental section

5.2.1 Bacterial strains

A previously designed *Synechocystis* strain co-expressing Baeyer-Villiger monooxygenase and lactonase genes from *Acidovorax* sp. CHX100 (Chapter 4, *Synechocystis* BVMO:Lactonase) and the corresponding wild-type (*Synechocystis*) were maintained as cryo-cultures at -80°C in BG11 medium[183] with 20 % dimethyl sulfoxide and freshly cultivated prior to experiments.

5.2.2 Growth conditions

Synechocystis strains were cultivated described as described in Chapter 4. BG 11 medium supplemented with 10 mM or 5 mM 4-(2-hydroxyethyl)-1-piperazinethanesulfonic acid (HEPES), pH 7.5, was used for shaking flask and bioreactor cultivations, respectively. To enable correct carbon balancing, Na₂CO₃ was omitted. Standard cultivation conditions were 50 μmol photons m⁻² s⁻¹, 30 °C, 75% humidity, and ambient CO₂ levels (0.04% [v/v]) for shaking flask experiments and bioreactor precultures (Multriton; Infors AG, Bottmingen, Switzerland).

Continuous cultivations were conducted in flat-panel (FP) bioreactors (Labfors 5 Lux; Infors AG) as described before[112] with altered standard conditions: 30°C, pH 7.5 (controlled with 1 M HCl and 1 M NaOH), and aeration at 0.5 vessel volume per minute (vvm). To reduce the O₂ share in the aeration gas for precise O₂ evolution measurements, 860 mL min⁻¹ N₂ and 40 mL min⁻¹ pressurized air were premixed in a gas mixing station (GMS150; Photon System Instruments, Drásov, Czech Republic) and fed to the reactor. As second aeration gas, 10 mL min⁻¹ of pure CO₂ or 10% CO₂/90% N₂ for high and low carbon conditions were provided, resulting in 0.6 and 0.12% CO₂ (v/v), respectively. Bioreactors were illuminated by white light LEDs allowing stepless controlling of the incident light intensity. Biomass concentration was kept constant (turbidostat) by feeding fresh medium via a peristaltic pump into the reactor at a rate equaling the specific growth rate under respective conditions. The reactor filling level was kept constant by removing culture broth through a fixed efflux tube at the top of the cultivation vessel. To minimize self-shading and thus ensure even light supply, the cell concentration was kept below 200 mg_{CDW} L⁻¹. For every sink scenario, a new turbidostat bioreactor was started by inoculation from a batch pre-culture.

Feed rate, pH, and pO₂ were monitored online continuously. The following parameters were measured on three different sampling days for each steady state in every sink scenario or at specific time points for all biotransformation phases.

5.2.3 Biomass, Chl-a), and carotenoid concentrations

Biomass concentrations were assessed in terms of cell dry weight (CDW), OD₇₅₀, and cell counts measurements (Multisizer 4E, Beckman Coulter, Brea, CA, USA) as described before

(Chapter 3).[161] The growth rate in continuous mode was determined based on the dilution rate D and changes in biomass concentration (dX) following equation 14:

$$(14) \mu_{1,2} = \frac{dX}{dt} \frac{1}{\frac{X_1+X_2}{2}} + D$$

A new steady state was considered to be reached when the growth rate μ had been kept constant (less than 5 % deviation) for at least three culture volume exchanges. Chlorophyll-*a* (Chl-*a*) and carotenoid extraction was conducted as described by Grund et al.[161] and concentrations were calculated following Zavrel et al.[249]

5.2.4 Carbon fixation and oxygen evolution rates

Carbon fixation and oxygen evolution rates were determined by measuring O_2 and CO_2 concentrations in the IN and OFF gas with BlueInOne sensors (BlueSens, Herten, Germany). Additionally, O_2 concentrations were measured using optical oxygen sensors with temperature correction (FireSting; PyroScience, Aachen, Germany).

5.2.5 Substrate and product concentrations

C-one, C-ol, ϵ -Cl, and 6-HA concentrations were determined as described in Chapter 3. For C-one, C-ol, and ϵ -Cl quantification, samples taken at specific time points were quenched and extracted by adding 1 volume of diethylether containing 0.2 mM n-decane as internal standard, followed by drying over Na_2SO_4 , transfer to gas chromatography (GC) vials, and GC measurement. For 6-HA quantification, samples were quenched by adding 0.11 volumes of acetonitrile and centrifuged. Supernatants were transferred to high-pressure liquid chromatography (HPLC) vials for HPLC measurements.

For continuous cultivations, net variations of analyte concentrations the washed-out analytes between two sampling points (C_{out}) were assessed from measured concentrations via equation 15:

$$(15) C_{out} = \frac{c_1+c_2}{2} D (t_2 - t_1)$$

with D being the dilution rate [in h^{-1}] and c_1 and c_2 the respective analyte concentration [in mM] at time points t_1 and t_2 [in h].

Effective quantum yield of PS II and quantum absorption. The effective quantum yield at PSII (Φ_{PSII}) was measured and calculated as described before[161] using a Multi-Color PAM (MC-PAM) device (Heinz Walz GmbH; Effeltrich, Germany). Chl-*a* excitation was performed at 400 nm in order to minimize excitation of phycobilisomes at higher wavelengths and thus underestimation of Φ_{PSII} . Samples from the bioreactor were transferred instantly into the measuring cuvette of the MC-PAM to determine Φ_{PSII} in the light-acclimated state of the cells. In order to create comparable conditions in the measuring cuvette as in the bioreactor, white actinic light with increasing light intensity was applied to create a light induction curve.

Quantum absorption was measured by a quantum sensor (LI-COR Biosciences; Lincoln, NE, USA) on the backside of the reactor vessel facing towards the light source. Connection of the sensor to the reactor tower enabled online monitoring of the quantum absorption. Even in dilute cell suspensions, self-shading reduces the available light. Hence, determining Φ_{PSII} on the basis of the incident light intensity leads to underestimated values. To correct Φ_{PSII} , an exponential decay of light intensity depending on the horizontal position d [in cm] in the cultivation chamber was assumed (equation 16):

$$(16) I(d) = I_0 e^{-\tau*d} \quad [\mu\text{mol}_{\text{photons}} \text{m}^{-2} \text{s}^{-1}]$$

The decay constant τ can be assessed with a known I_0 and the transmitted light recorded by the quantum sensor on the backside. Φ_{PSII} was corrected following equation 17:

$$(17) \phi_{PSII, \text{corr}} = \overline{\sum_{d=0\text{cm}}^{2\text{cm}} \phi_{PSII}(I(d))}$$

In other words, Φ_{PSII} was determined for different light intensities at specific horizontal positions in the reactor (horizontal dimension is 2 cm), and then averaged to obtain $\Phi_{PSII, \text{corr}}$.

5.2.6 Balancing electron fluxes in cyanobacteria

The maximum electron flux through PS II r_F was calculated from $\Phi_{PSII, \text{corr}}$ determined by PAM-fluorometry and the total absorbed quanta (Q_{phar}) via equation 18:

$$(18) r_F = \Phi_{PSII, \text{corr}} * \frac{Q_{\text{phar}}}{2} \quad [\text{mmol}_e \cdot \text{g}_{\text{CDW}}^{-1} \text{h}^{-1}]$$

taking account for the fact that (at least) 2 quanta need to be absorbed per electron, assuming linear electron transfer. The electron flux to carbon and nitrogen assimilation were defined as r_C and r_N , respectively, and calculated based on equations 19 and 20:

$$(19) r_C = \mu * \frac{x_C}{M_C} * 4 \quad [\text{mmol}_e \cdot \text{g}_{\text{CDW}}^{-1} \text{h}^{-1}]$$

$$(20) r_N = \mu * \frac{x_N}{M_N} * 8 \quad [\text{mmol}_e \cdot \text{g}_{\text{CDW}}^{-1} \text{h}^{-1}]$$

with the specific growth rate μ , the C and N mass fractions x_C and x_N in biomass, respectively, and the molar masses of C and N as M_C and M_N , respectively. The factors 4 and 8 account for the electron demand per assimilated C- and N-atom from CO_2 and NO_3 , respectively.

Based on the product formation rate p , the electron flux to the biotransformation r_{BT} was quantified with equation 21:

$$(21) r_{BT} = p * 2 \quad [\text{mmol}_e \cdot \text{g}_{\text{CDW}}^{-1} \text{h}^{-1}]$$

with 2 mol electrons being required to form 1 mol product.

All alternative electron fluxes were subsumed in r_{AEF} calculated with equation 22:

$$(22) r_{AEF} = r_F - r_C - r_N - r_{BT} \quad [\text{mmol}_e \cdot \text{g}_{\text{CDW}}^{-1} \text{h}^{-1}]$$

5.3 Results

5.3.1 Growth rates are directly dependent on light intensity

To find the optimal light intensity for the setup applied, the light saturation point (E_k) of growing *Synechocystis* was determined in an initial experiment. E_k is defined as the light intensity just sufficient to supply the metabolism with required reductant.[250] Consequently, E_k can be seen as the optimal light intensity, as it marks the point enabling full biological capacity without unnecessary energy losses via dissipation mechanisms. Light penetration and accessibility, but also amount and type of electron sinks depend on the chosen setup and conditions and make E_k system-dependent.

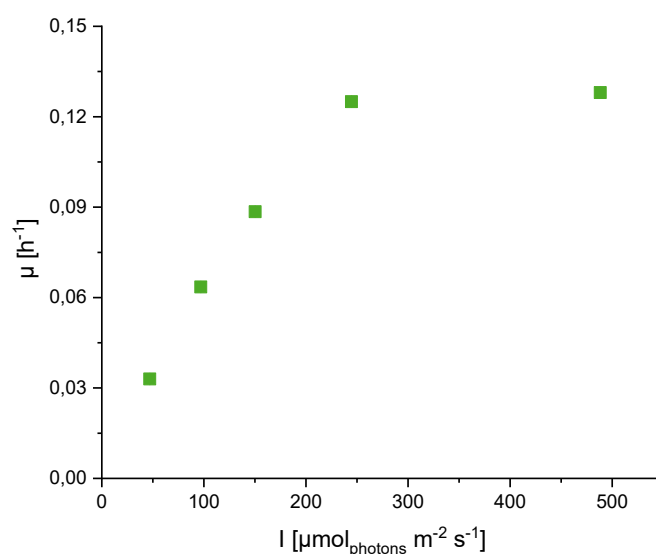


Figure 18: **Dependency of the growth rate on light intensity.** *Synechocystis* cultures were grown in flat panel bioreactors under steady state conditions as described in the Materials and Methods section. For every light intensity, a new steady state was established, including at least three reactor volume exchanges at constant cell density.

In order to determine E_k for our setup, the light intensities 50, 100, 150, 250, and 500 $\mu\text{mol}_{\text{photons}} \text{m}^{-2} \text{s}^{-1}$ were applied during continuous cultivation under high CO_2 conditions (0.6% (v/v) in IN-gas) keeping cell density, aeration, temperature, volume, and pH constant. Between 50 and 150 $\mu\text{mol}_{\text{photons}} \text{m}^{-2} \text{s}^{-1}$, the growth rate μ directly depended on the incident light intensity (I , Figure 18). Higher light intensities did not lead to a proportional increase in μ , indicating the E_k being reached between 200 and 250 $\mu\text{mol}_{\text{photons}} \text{m}^{-2} \text{s}^{-1}$. Notably, high light intensities induced biofilm formation, complicating an accurate assessment of active biomass and thus a correct determination of physiological rates. Conclusively, 150 $\mu\text{mol}_{\text{photons}} \text{m}^{-2} \text{s}^{-1}$ was used for further experiments constituting a compromise between sufficient light input and stable conditions, not inducing rapid biofilm formation.

5.3.2 Strong metabolic electron sinks lead to competition for reductant

The first sink scenario tested was CO₂ in excess (0.6 % (v/v) IN-gas) and NO₃⁻ as N-source. These conditions i) ensured that CO₂ did not limit growth, ii) posed a high electron demand for CO₂ and NO₃⁻ reduction (NO₃⁻ requiring 8 mol e⁻ per mol assimilated N), and iii) can therefore act as light-limited control condition. Our previous study showed that *Synechocystis* BVMO:Lactonase can easily increase photosynthetic rates to meet the increased electron demand for NO₃⁻ instead of NH₄⁺ assimilation.[161] In this sink scenario, *Synechocystis* BVMO:Lactonase grew the fastest of the tested conditions ($\mu = 0.087 \pm 0.003 \text{ h}^{-1}$, Figure 19A), concomitant with the highest measured values for both specific quantum absorption ($Q_{\text{phar}} = 58.2 \pm 3.0 \text{ mmol e}^{-} \text{ g}_{\text{CDW}}^{-1} \text{ h}^{-1}$, Figure 19D) and PS-II efficiency ($\Phi_{\text{PSII}} = 0.536 \pm 0.025$, Figure 19G) thereby maximizing the rate of photosynthetically produced electrons. Upon Ni²⁺-dependent induction of the heterologous BVMO and Lactonase gene expression, μ slightly decreased by 6% to $0.081 \pm 0.002 \text{ h}^{-1}$. Concomitantly, Q_{phar} ($55.2 \pm 2.5 \text{ mmol e}^{-} \text{ g}_{\text{CDW}}^{-1} \text{ h}^{-1}$) and Φ_{PSII} (0.524 ± 0.045) decreased by 5 and 2%, respectively (Table 7).

Upon start of the biotransformation, initiated by supplying C-one in a substrate-limited manner corresponding to an activity of $15 \text{ U g}_{\text{CDW}}^{-1}$, an extra e⁻-sink corresponding to roughly 10% of the overall water oxidation activity was established. Within the first 48 h of the biotransformation, Q_{phar} remained high under high carbon (HC)/NO₃⁻ conditions ($53\text{--}59 \text{ mmol e}^{-} \text{ g}_{\text{CDW}}^{-1} \text{ h}^{-1}$, Figure 19D), indicating constant and high reductant supply. However, as biotransformation and nutrient assimilation are competing for this reductant, a decreased μ of $0.066 \pm 0.001 \text{ h}^{-1}$ was recorded within the first 24 h of biotransformation followed by an abrupt decay to less than 0.04 h^{-1} (Figure 19A). At the same time, the electron demand of the biotransformation could no longer be met, leading to a reduced specific activity, experimentally met by a reduced substrate feed. Finally, substrate accumulated even at the reduced substrate feed (Figure 20A), which – concomitant with still decreasing growth rates – toxifies the cells, making continuous cultivation no longer possible. Low Φ_{PSII} values were detected in this late stage (Figure 19G). In conclusion, in the light- and thus source-limited state, the combined high electron demands of N- and C-assimilation the biotransformation could not be sustained by the photo-biocatalyst in the long-term.

5.3.3 Reduction of N-source-related sink demand via NH₄⁺ provision combined with Ni²⁺-based induction caused physiological stress responses

In a second scenario, the electron demand for cell growth was reduced by using NH₄⁺ instead of NO₃⁻ as sole nitrogen source while supplying CO₂ in excess (0.6 % (v/v) in IN-gas). Thus, a share of 20-25% of e⁻ becomes available compared to scenario I theoretically excelling the demand for the biotransformation. In this scenario, μ ($0.082 \pm 0.004 \text{ h}^{-1}$, Figure 19B), Q_{phar} ($47.6 \pm 3.4 \text{ mmol e}^{-} \text{ g}_{\text{CDW}}^{-1} \text{ h}^{-1}$, Figure 19E), and Φ_{PSII} (0.364 ± 0.022 , Figure 19H) were lower compared to the provision of the e⁻-intensive N source NO₃⁻ as it also has been observed be-

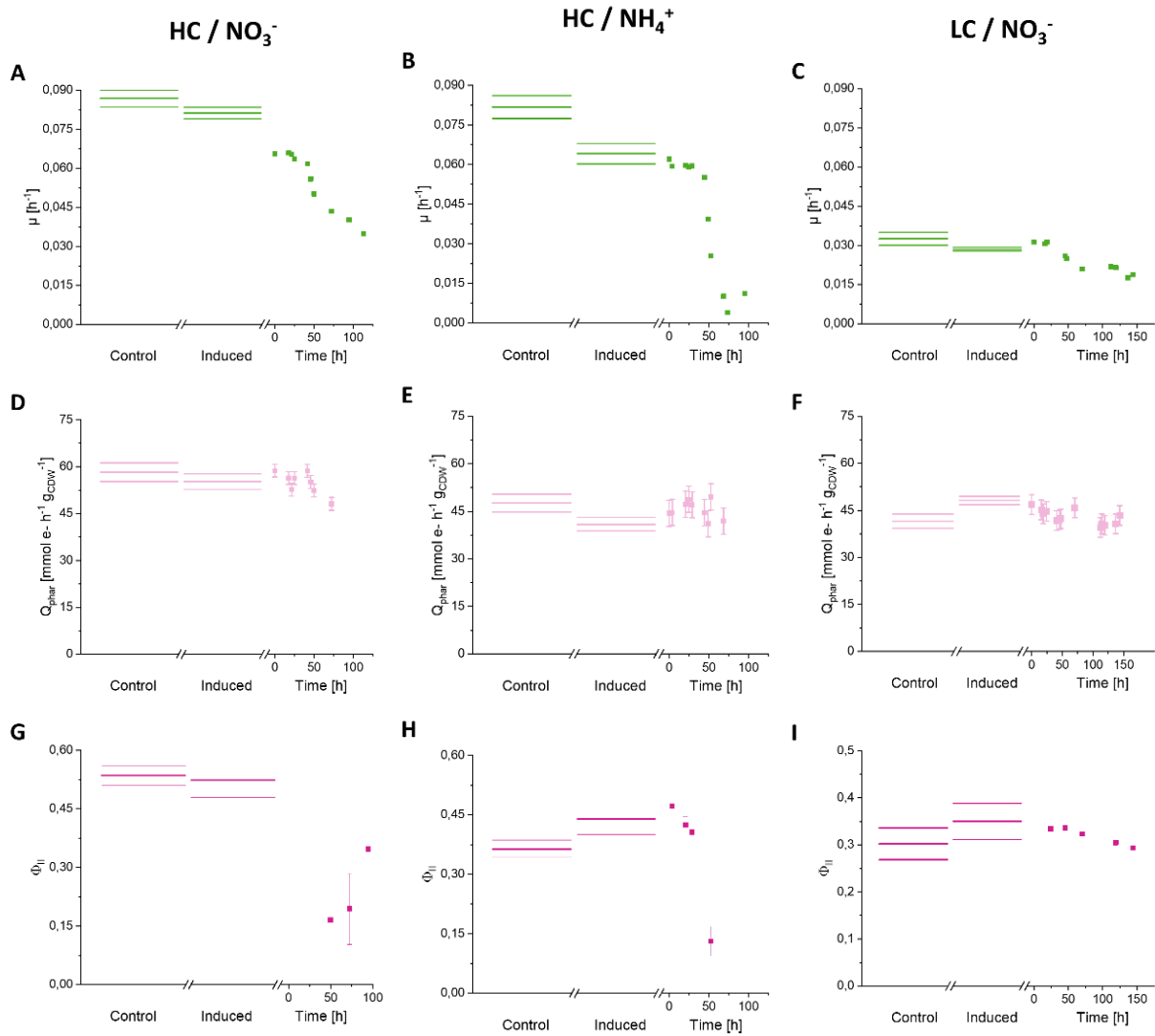


Figure 19: **Growth rate (μ , A-C), specific quantum absorption (Q_{phar} , D-F), and PSII-efficiency (Φ_{PSII} , G-I) in different sink scenarios.** Cultures were grown in flat-panel bioreactors under steady state conditions as described in the experimental section, and different conditions were applied: Scenario I (A, D, G): high carbon (HC)/ NO_3^- , scenario II (B, E, H): HC/ NH_4^+ , scenario III (C, F, I): low carbon (LC)/ NO_3^- . For non-induced (“Control”) and induced (“induced”) conditions, steady states were established, for which means and standard deviations from three different measuring days are given. From the start of substrate feeding, time-specific data points with standard deviations from ≥ 2 technical replica are given with respect to a time scale [in h] on the x-axis.

fore.[161] Interestingly, the growth rate decrease by 22% (to $0.064 \pm 0.004 \text{ h}^{-1}$, Table 7) upon Ni^{2+} - dependent induction of heterologous gene expression was more pronounced than with NO_3^- (6%). Reduction of Q_{phar} by 14% (to $41.0 \pm 2.1 \text{ mmol e}^- \text{ g}_{\text{CDW}}^{-1} \text{ h}^{-1}$) appeared to be counter-acted by a higher Φ_{PSII} (0.439 ± 0.038 , +21%) and was connected with a high alternative electron flux (r_{AEF}), indicating an increased energy demand. Notably, exposure to Ni^{2+} reduced pigment content (Table 7), as can be seen by absorption spectrum shifts (Figure S14), indicating detrimental effects of the Ni^{2+} in combination with NH_4^+ as N source.

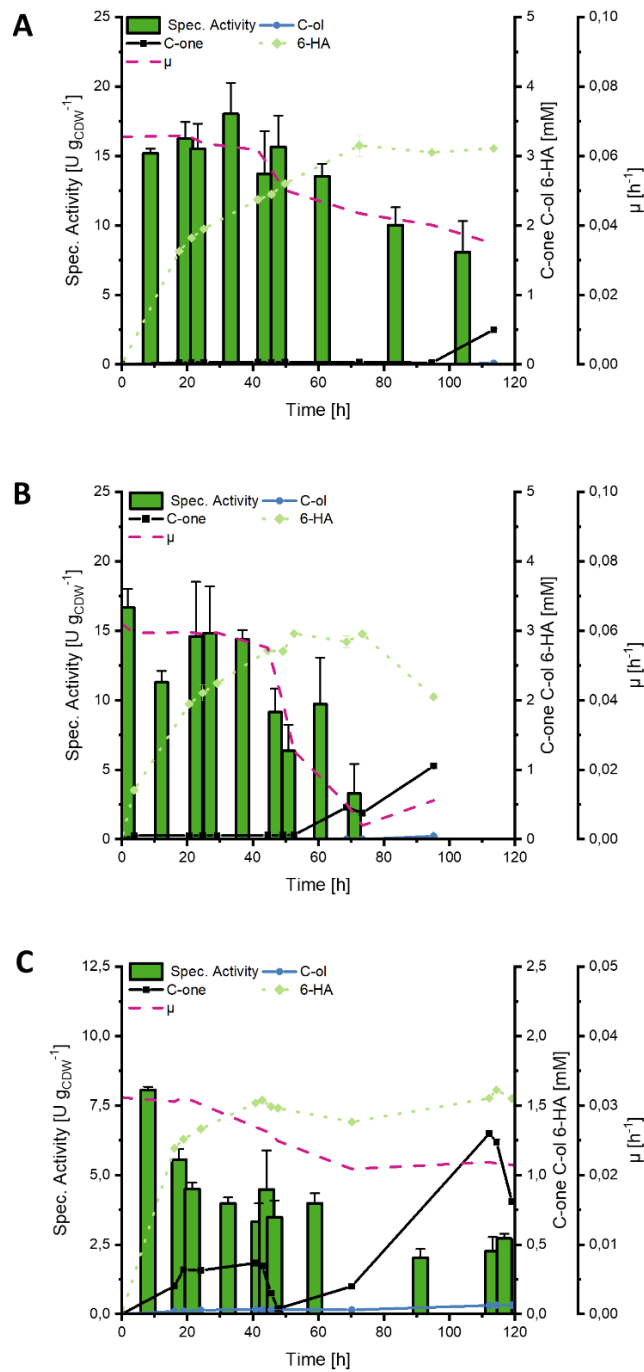


Figure 20: **Bioconversion of C-one to 6-HA in continuous mode under (A) HC/NO₃⁻, (B) HC/NH₄⁺, and (C) LC/NO₃⁻ conditions.** Cultures were grown in flat panel bioreactors under steady state conditions as described in the experimental section. After recording reference and induced steady states, biotransformation was started at $t = 0$ h by continuously feeding C-one into the reactor in a substrate-limited manner. For every condition, a new reactor was started. Concentrations [mM] are given as solid black line/black squares for C-one, dotted light green line/diamonds for 6-HA, and solid blue line/circles for cyclohexanol (C-ol). Dashed magenta lines and green bars represent μ [h⁻¹] and specific activities [U g_{CDW}⁻¹], respectively. Means and standard deviations from ≥ 2 technical replica are given. Mind the different y-axis dimensions in panel C. HC – high carbon, LC – low carbon.

As in scenario I, the electron demanding biotransformation was initiated by substrate supply matching a specific activity of 15 U g_{CDW}⁻¹. Compared to the induced reference, the growth rate slightly decreased (by 3-8%) to 0.059-0.062 h⁻¹ within the first 48 h (Figure 19B). In the same time range, Q_{phar} slightly increased up to 48.8 ± 4.1 mmol e⁻ g_{CDW}⁻¹ h⁻¹ (Figure 19E), while a

slow, but constant decline in Φ_{PSII} was observed (by 14% between 4 and 29 h after biotransformation start, Figure 19H). A sudden decrease of the growth rate to $0.026 \pm 0.003 \text{ h}^{-1}$ 48 h after biotransformation start together with a strong decrease in Φ_{PSII} to 0.131 ± 0.037 at 52.6 h indicated a breakdown of cell metabolism. Like in scenario I, biotransformation performance concomitantly was reduced, leading to substrate accumulation (Figure 20B). Interestingly, growth recovered once biotransformation stalled (from 69 h onwards). In conclusion, although arithmetically possible, the electron surplus due to changing the N source to NH_4^+ could not sustain the oxygenase reaction. Possibly, combined effects of NH_4^+ , Ni^{2+} , and the reaction itself posed too much of a burden to the cellular metabolism in this scenario.

5.3.4 Sink-limited conditions enable long-term biotransformation at reduced rate

As a third, sink-limited scenario, CO_2 input was reduced to a fifth (0.12% (v/v) in IN-gas), while NO_3^- was used as N-source to avoid possible NH_4^+ -related stress. This ensured sink-limitation, as the CO_2 fixation rate thereby was reduced at the same light intensity of $150 \mu\text{mol}_{\text{photons}} \text{ m}^{-2} \text{ s}^{-1}$ potentially enabling the coverage of higher electron demands (see above). The low CO_2 level limited μ to $0.032 \pm 0.002 \text{ h}^{-1}$ under non-induced control conditions (Figure 19C). Both Q_{phar} ($41.5 \pm 2.3 \text{ mmol e}^- \text{ g}_{\text{CDW}}^{-1} \text{ h}^{-1}$, Figure 19F) and Φ_{PSII} (0.302 ± 0.038 , Figure 19I) were relatively low, showing that photosynthesis did not operate at its full capacity as expected for sink-limited conditions. Ni^{2+} -dependent induction of heterologous gene expression caused a 12% growth rate decrease, while both Q_{phar} and Φ_{PSII} increased by 14 and 12%, respectively.

To take account of the assumingly lower electron fluxes under sink-limited conditions, the C-one feed rate was reduced aiming at a specific activity of $5 \text{ U g}_{\text{CDW}}^{-1}$, corresponding to a withdrawal of ca. 10% of overall electron flux. Within the first 24 h of biotransformation, μ remained constant between 0.031 and 0.034 h^{-1} (Figure 19C), while Q_{phar} and Φ_{PSII} slightly decreased by 6 and 4%, respectively, compared to induced conditions (Figure 19F,I). Interestingly, a strong decline of μ after 48 h was not observed with a constant μ of 0.021 - 0.022 h^{-1} between 72 and 120 h. This and the constant Q_{phar} (between 40.6 and $46.8 \text{ mmol e}^- \text{ g}_{\text{CDW}}^{-1} \text{ h}^{-1}$) and Φ_{PSII} (between 0.30 and 0.34) in the same time range indicated a higher metabolic stability upon sink limitation. However, the specific activity nevertheless slowly decreased ($\sim 2.5 \text{ U g}_{\text{CDW}}^{-1}$ after 112 h of biotransformation) leading to C-one accumulation (Figure 20C), which finally also affected μ and Φ_{PSII} and thus continuous cultivation stability.

Electron fluxes in oxygenase-active *Synechocystis* BVMO:Lactonase

In a phototrophic cell, nutrient assimilation, cell growth, and maintenance require reductant and energy supply. The BVMO reaction consumes additional reductant, which disturbs the established source/sink balance. The goal of this study was to quantify electron fluxes in oxygenase-active cyanobacteria to identify main pitfalls and potentials for electron-consuming biotransformations on the long-term.

In order to quantify electron fluxes under different conditions, the electron demand for growth and biotransformation were calculated as follows: Based on nutrient supply, elemental composition of biomass, and growth rate, the assimilation costs were translated into electron fluxes towards carbon fixation (r_C) and nitrogen assimilation (r_N) as main electron sinks. With a sulfur mass fraction of $< 0.5\%$, [251] respective assimilation costs are negligible. The electron flux into product formation (r_{BT}) can be quantified based on the reaction stoichiometry of 2 mol e^- per mol product. Only alternative electron transfer (r_{AEF}), comprising Mehler-like reactions and other dissipative mechanisms, cannot directly be quantified. Instead, the overall photosynthetic electron transfer (r_F) was assessed via PAM-fluorometry as described before. [161] Then, r_{AEF} was defined as the difference between r_F and the sum of all assimilation- and biotransformation-related electron fluxes. Figure 21 depicts the calculated electron fluxes for the three different sink scenarios discussed above.

For both control conditions (non-induced and induced), given data refer to stable steady states, whereas no steady states could be established during biotransformation, and data corresponding to the first 50 h of biotransformation are given (see also Table 7). The overall highest r_F was observed in the growth control under sink-replete conditions (HC/ NO_3^-). Upon Ni^{2+} -induction, r_F decreased by 7%, which agrees well with the growth rate decrease (6%, Figure 19A). Ni^{2+} -effects alone do not explain the growth effects, as control experiments with the wildtype strain show (Table 7, Figure S15). Upon biotransformation, a strong decrease of r_F was observed, going along with an intensified competition for electrons. Consequently, the high growth rate decreased, correlating with the reduced electron flux into C- and N-assimilation. r_{AEF} thereby was strongly reduced.

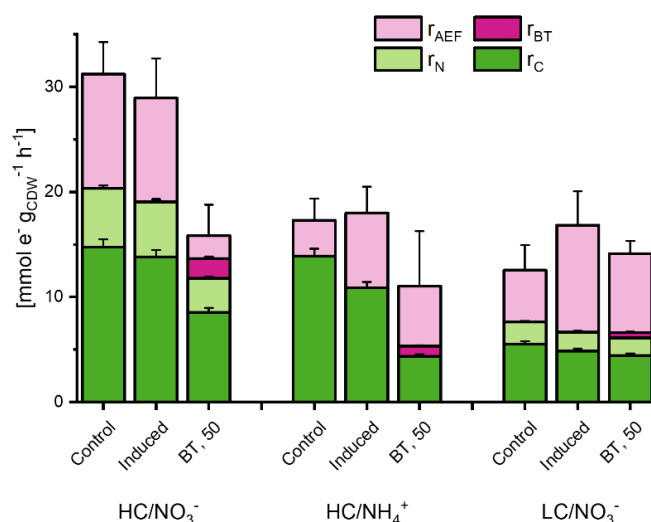


Figure 21: **Electron balancing under HC/ NO_3^- (A), HC/ NH_4^+ (B), and LC/ NO_3^- (C) conditions.** For non-induced (“Control”) and induced conditions (“Induced”) steady state data for electron fluxes are depicted. As no steady state could be established for biotransformation conditions, data recorded 50 h (BT, 50) after the start of substrate feeding are depicted. r_{AEF} , alternative electron flux; r_C and r_N , electron fluxes towards carbon and nitrate assimilation, respectively; r_{BT} electron flux into product formation. Data are depicted as mean values and standard deviations from at least three replicates. See experimental section for details. HC – high carbon, LC – low carbon.

The second scenario with NH_4^+ instead of NO_3^- as N-source relieved the reductant demand for N-assimilation. Thereby, a comparably high growth rate could be maintained (Figure 19B) with only 58% of the r_F observed in sink scenario I and was associated with a very low r_{AEF} (Figure 21). Upon induction, r_F increased by 4%, whereas μ was reduced by 22%, resulting in an increase of r_{AEF} possibly due to expression burden including oxidative stress, which can be caused by uncoupled incomplete O_2 reduction by the BVMO. Upon biotransformation initiation, the r_F was kept constant only for a short time period, before Φ_{PSII} decreased dramatically (see Figure 19E) resulting in a drastic decrease in r_F and consequently in μ .

In the sink-limited scenario, the lowest r_F was observed (Figure 21) correlating with a low Φ_{PSII} (Figure 19I). The electron partitioning, however, scales well with the sink-replete condition (Figure 21). In contrast to that scenario, cells were able to increase r_F (+34%) upon Ni^{2+} -induction in the sink-limited scenario, going along with an only slight decrease of μ by 12%. Only under sink limitation, r_F could be kept high in the first 50 h of biotransformation (-16% compared to induced control conditions). A sink effect of the biotransformation (relieve of sink limitation) was, however, not observed: Neither r_F , nor μ was stably increased during the biotransformation. In fact, from 48 h on, r_F decreased slowly together with μ . Finally, also the specific activity decreased, causing C-one accumulation and, consequently, decrease of both μ and r_F .

1 Table 7: Physiological parameters of *Synechocystis* BVMO:Lactonase and *Synechocystis* wt under different source/sink conditions.

Parameter ^a	HC/NO ₃ ^{-b}			HC/NH ₄ ⁺ ^b			LC/NO ₃ ^{-b}			Wt (HC/NO ₃) ^b	
	Non-induced	Induced	Biotrafo, 50h	Non-induced	Induced	Biotrafo, 50h	Non-induced	Induced	Biotrafo, 50h	- Ni ²⁺	+ Ni ²⁺
D = μ [h ⁻¹]	0.087 ± 0.003	0.081 ± 0.001	0.050 ± 0.004	0.082 ± 0.004	0.064 ± 0.004	0.025 ± 0.003	0.032 ± 0.002	0.028 ± 0.001	0.026 ± 0.001	0.103 ± 0.006	0.102 ± 0.005
X [mg _{CDW} L ⁻¹]	164 ± 7	179 ± 1	162 ± 3	158 ± 2	195 ± 2	176 ± 4	183 ± 16	201 ± 3	208 ± 3	166 ± 2	164 ± 5
C _{Chl-a} [mg _{Chl-a} L ⁻¹]	2.35 ± 0.05	2.55 ± 0.06	-	1.78 ± 0.11	1.94 ± 0.03	1.22 ± 0.10	1.77 ± 0.07	2.22 ± 0.13	1.58 ± 0.08	2.51 ± 0.06	2.59 ± 0.05
Chl-a _{CDW} [μ g _{Chl-a} mg _{CDW} ⁻¹]	14.4 ± 0.3	14.3 ± 0.4	-	11.2 ± 0.8	10.0 ± 0.2	6.9 ± 0.6	9.6 ± 0.4	11.1 ± 0.7	7.6 ± 0.4	15.1 ± 0.4	15.8 ± 0.9
Car _{CDW} [μ g _{Car} mg _{CDW} ⁻¹]	6.95 ± 0.10	7.32 ± 0.14	-	4.03 ± 0.15	5.05 ± 0.02	3.29 ± 0.28	8.42 ± 0.11	8.71 ± 0.64	8.37 ± 0.19	5.36 ± 0.18	5.30 ± 0.30
Q _{phar} [mmol _{e-} g _{CDW} ⁻¹ h ⁻¹]	58.2 ± 3.0	55.2 ± 2.5	58.5 ± 2.1	47.5 ± 2.8	41.0 ± 2.1	41.1 ± 4.1	41.5 ± 2.3	48.1 ± 1.4	42.3 ± 1.5	48.9 ± 4.0	52.2 ± 3.7
Φ_{PSII}	0.54 ± 0.03	0.52 ± 0.05	0.30 ± 0.05	0.36 ± 0.03	0.44 ± 0.04	0.22 ± 0.09	0.30 ± 0.04	0.35 ± 0.04	0.34 ± 0.01	0.56 ± 0.01	0.57 ± 0.02
r _F [mmol g _{CDW} ⁻¹ h ⁻¹]	31.2 ± 3.1	28.9 ± 3.8	15.9 ± 2.9	17.3 ± 2.1	18.0 ± 2.5	11.0 ± 5.2	12.6 ± 2.1	16.8 ± 2.3	14.1 ± 1.2	27.4 ± 2.8	29.6 ± 3.0
r _C [mmol g _{CDW} ⁻¹ h ⁻¹]	14.8 ± 0.7	13.8 ± 0.7	8.5 ± 0.5	13.9 ± 0.7	10.9 ± 0.6	4.3 ± 0.2	5.5 ± 0.3	4.8 ± 0.3	4.4 ± 0.2	17.5 ± 0.9	17.4 ± 0.9
r _N [mmol g _{CDW} ⁻¹ h ⁻¹]	5.6 ± 0.3	5.2 ± 0.3	3.2 ± 0.2	-	-	-	2.1 ± 0.1	1.8 ± 0.1	1.7 ± 0.1	6.7 ± 0.4	6.6 ± 0.3
r _{AEF} [mmol g _{CDW} ⁻¹ h ⁻¹]	10.9 ± 3.1	9.9 ± 3.8	2.2 ± 2.9	3.4 ± 2.1	7.1 ± 2.5	5.7 ± 5.2	4.9 ± 2.1	10.2 ± 2.3	7.5 ± 1.2	3.3 ± 2.8	5.6 ± 3.0
r _{BT} [mmol g _{CDW} ⁻¹ h ⁻¹]	-	-	1.8 ± 0.2	-	-	1.0 ± 0.1	-	-	0.5 ± 0.1	-	-
QE _{6-HA} [%]	-	-	2.3 ± 0.3	-	-	1.3 ± 0.3	-	-	0.8 ± 0.2	-	-
Q _C	31.6 ± 2.9	32.0 ± 1.8	54.9 ± 3.8	27.4 ± 1.7	30.1 ± 1.8	91.6 ± 6.7	60.2 ± 8.3	79.6 ± 5.2	76.1 ± 4.9	22.3 ± 2.1	24.0 ± 1.3

2 ^a D, dilution rate equaling the specific growth rate μ ; X, biomass concentration; C_{Chl-a}, volumetric Chl-a concentration; Chl-a_{CDW} and Car_{CDW}, biomass-specific Chl-a and Carotenoid concentration, respectively; Q_{phar}, rate of photosynthetically absorbed photons, expressed in electrons for purely linear electron transfer (2 photons = 1 e⁻); Φ_{PSII} , effective quantum yield at PS II; r_F, fluorescence-based electron flux at PS II; r_C and r_N, electron fluxes for carbon and nitrate assimilation, respectively; r_{AEF}, alternative electron flux; r_{BT} electron flux into product formation; QE_{6-HA}, quantum efficiency of product formation; Q_C, quantum requirement for carbon fixation.

3 ^b The tested conditions refer to high carbon and nitrate (HC/NO₃⁻), high carbon and ammonium (HC/NH₄⁺), and low carbon and nitrate (LC/NO₃⁻). The wild type was tested under HC/NO₃⁻ conditions. Data are depicted as mean values and standard deviations from at least three replicates. See experimental section for details.

8

5.4 Discussion

To investigate the effects of withdrawing electrons from photosynthesis for light-driven biotransformations, physiological responses in terms of growth rate μ , effective quantum yield at PSII Φ_{PSII} , and specific quantum absorption Q_{phar} of oxygenase-active cyanobacteria were quantified under different sink conditions.

5.4.1 Physiological responses to an extra electron sink depend on source/sink conditions

The expression of the heterologous genes upon Ni^{2+} -induction comes at the expense of reduced growth in all tested scenarios. Previous studies on a similar gene construct estimate the protein level to $1.1 \pm 0.2\%$ of total soluble protein, (Chapter 3) matching the slight growth rate decrease. Under sink-replete conditions (HC/NO_3^-), the lowest growth rate decrease was observed agreeing well with some expression burden. In contrast, the most severe growth effects on *Synechocystis* BVMO:Lactonase in the HC/NH_4^+ scenario cannot be explained by expression burden alone: The $\text{Ni}^{2+}/\text{NH}_4^+$ combination obviously was detrimental causing a doubling of r_{AEF} and thus a high energy demand to the cell. NH_4^+ is known to accelerate light-induced photo-damage of PS II, possibly by destroying the manganese cluster of the oxygen evolving complex. [252, 253] This may restrain electron flux through the photosynthetic electron transport chain (PETC) and thereby limit generation of both ATP and NADPH. At the same time, detoxification mechanisms, like energy-intense Ni^{2+} -exporter systems, and the PS II repair cycle, [254] may be responsible to the observed r_{AEF} increase to meet the increased energy demand. That, however, seems to be a distinct effect with NH_4^+ as N source.

In none of the tested sink scenarios, the two-step biotransformation used as a proxy for electron withdrawal could be stabilized in a metabolic steady state:

1. Under sink-replete conditions, photosynthetic electron supply may be maxed out to satisfy the high electron and energy demands for growth. The biotransformation requires additional e^- from an already constrained metabolic state, distancing the status quo from balance conditions. In this case, competition for electrons is arguably most fierce, causing μ to decrease upon biotransformation initiation. It is, however, not clear, why the reduced μ cannot be kept up and what initially causes both Φ_{PSII} and Q_{phar} to decrease.
2. Regarding the mentioned $\text{Ni}^{2+}/\text{NH}_4^+$ combination, the cell metabolism is stressed due to high detoxification and PS II repair costs. This may prohibit the coverage of an extra e^- sink, either due to toxification/decoupling of electron flux, the extra e^- demand itself or both: Such perturbation of an already fragile state may then have caused the observed rapid decrease in growth and Φ_{PSII} indicating an irreversible metabolic collapse.

3. The comparably lower substrate feed and thus biotransformation rate under sink-limited conditions might well explain the relative stability with μ , Q_{phar} , and Φ_{PSII} remaining roughly constant for about 100 h. However, the expected increase of electron flux through the PETC upon relieve of sink-limitation, was not observed: In fact, higher biotransformation rates seem not to be possible, as substrate started to accumulate already with the low feeding rate applied. It can be speculated that sink-limited conditions, and thereby reduced metabolic turnover, limit biotransformation capacity right from the start.

5.4.2 Stability of oxygenase biocatalysis in a phototrophic metabolism

Over all tested scenarios, the biotransformation was constantly supplied with e^- : This is especially true for the first 24 h of substrate feed, but also in later stages of the experiments, when growth rates already started to decline. Thereby, the cells covered a heterologous e^- sink at the cost of e^- shortage for assimilation processes, and this appeared to affect and reduce growth in all tested scenarios. This is especially surprising for scenario I, in which source-limitation lead to the strongest competition for e^- between assimilatory processes/growth and biotransformation. Enzyme kinetics show a higher NADPH-affinity of native glyceraldehyde-3-phosphate dehydrogenases (GAPDHs; K_M of $40 \pm 3 \mu\text{M}$ for *Thermosynechococcus elongatus*, [43] or $62 \pm 4.5 \mu\text{M}$ for *Synechococcus* PCC 7942, [255]) than of BVMO (K_M of $372 \pm 17 \mu\text{M}$ for NADPH, [187]). Based on NADPH concentrations of $80\text{-}90 \text{ nM OD}^{-1}$, [256] intracellular NADPH levels can be estimated to be around $0.3\text{-}1 \text{ mM}$ (assuming $1\text{-}3 \times 10^7 \text{ cells ml}^{-1} \text{ OD}^{-1}$ and a cell volume of 9 fl), which indicates saturation of both BVMO and GAPDH. Obviously, BVMO was initially limited by substrate availability, operating below its v_{max} ($1.2 \pm 0.1 \text{ U mg}^{-1}$, [187]). In later stages, where both growth and biotransformation were affected by a metabolic imbalance, possibly caused by disordered ATP/NADPH-levels (see below), NADPH limitation may have occurred. While GAPDH is expected to operate at higher rates due to a higher v_{max} ($12.1 \pm 0.5 \text{ U mg}^{-1}$, [43]), overexpression of heterologous BVMO may lead to significantly higher protein levels (Chapter 3) directing e^- to the biotransformation, even in such NADPH-limited conditions.

Instability of the BVMO at low intracellular NADPH/NADP⁺ ratios may be another factor to be considered. CHMO from *Acinetobacter calcoaceticus* was found to be stabilized *in vitro* by the external addition of 0.2 mM NADPH, but not by NADP⁺. [257] In *Synechocystis*, the NADPH/NADP⁺ ratio was found to around 2 under light-irradiated conditions [256], with intracellular pool sizes estimated to be around $0.5\text{-}1.5 \text{ mM}$ [NADPH + NADP⁺]. [115, 256] The NADPH/NADP⁺ ratio is, however, very dynamic and highly susceptible to changes insource/sink conditions, like the onset of an e^- consuming biotransformation. As a result, NADPH-consumption may lead to a low intracellular NADPH/NADP⁺ ratio impairing BVMO stability. To overcome this instability, NADPH excess conditions, promoted, e.g., by high light

supply, may be beneficial. In our setup, however, these conditions caused undesired biofilm formation.

One key parameter expected to change upon withdrawal of electrons from the photosynthetic metabolism is the ATP/NADPH ratio.[29, 258] The requirement of ATP and NADPH in a ratio of 1.5 for C-fixation via the CBB-cycle is not met by linear flux through the photosynthetic electron transport chain, which generates ATP and NADPH in a ratio of about 1.28.[25] Alternative electron transfer routes, like cyclic and pseudocyclic electron flux, can modulate this ratio according to metabolic demands via the uncoupling of ATP generation from NADPH formation.[29, 30] Additional heterologous e^- sinks change the ATP/NADPH demand ratio,[85](see also Chapter 4) possibly even below a value of 1.28, for which compensation mechanisms are not or not sufficiently available in phototrophs. Santos-Merino *et al.* found that introducing an extra ATP sink helps to counteract such perturbation, probably by re-establishing ATP/NADPH demand ratios feasible to be covered by the light reaction.[85] In accordance with these findings, our previous study on the BVMO-based two-enzyme-cascade showed that moderate e^- withdrawal enabled higher long-term stability, while high e^- withdrawal led to a metabolic stalling, probably caused by ATP excess.(Chapter 4) In this context, photorespiration, a natural ATP consuming pathway in phototrophs,[29] might have an alleviative effect. However, low O_2 levels, as applied in the experiments presented in this study, evoke a low share of oxygenation by Rubisco, which may restrict a possible ATP sink role of photorespiration. However, a low r_{AEF} appears mandatory to confine ATP levels. The electron fluxes under HC/NO_3^- conditions indicate exactly this modulation during biotransformation (Figure 21). However, no reduction of r_{AEF} was evident for the other scenarios. For HC/NH_4^+ , r_{AEF} increase upon induction and biotransformation in contrast indicates a high energy demand, as described above. This appeared to destabilize the e^- consuming biotransformation, which may be due to an imbalance of photosynthetic e^- fluxes. As a results, overall electron flux through PETC decreased, most likely due to NH_4^+ -enforced photodamage of PSII.[252, 253] Neither linear electron transfer (for NADPH and ATP generation) nor r_{AEF} (for ATP generation alone) did then suffice to drive biotransformation, detoxification and PS II repair, causing a metabolic collapse. Under sink-limitation, the reduced substrate feed rate posed the lowest e^- burden and thus a comparably faint impact on ATP/NADPH demand ratio. As expected, it could be stabilized for the longest time (see also Chapter 4). To investigate the role of the ATP/NADPH ratio in detail, it will be essential to quantify intracellular levels of adenosine phosphates and NAD(P/H), ideally with recently described methods like LC-MS analysis [256, 259] or *in situ* measurements using fluorescent sensors.[260, 261]

One strategy to increase the availability of reductant and thereby stabilize the biotransformation is the knockout of alternative electron acceptors, like flavodiiron proteins (Flv). The deletion of Flv3 in *Synechocystis*, for instance, inactivated the Flv1/3 couple, which

decreased the ATP/NADPH ratio and increased sucrose production under low light conditions.[46] However, sucrose production was found to still be limited due to carbon flux into PHB.[46] In another study Flv1/3 inactivation was found to increase in vivo activities of NADPH-dependent Yqjm reductase 2-fold.[79] Despite being promising, this intervention into electron fluxes is delicate, as the Flv1/3 couple is an important electron valve and to the proton-motive-force and thus ATP synthesis during dark-light transitions.[24] Thus, its deletion can compromise strain robustness.

5.4.3 Efficient use of light energy for redox biocatalysis

As stated above, the use of light as energy source imposes the necessity of metabolic balancing between source (light) and sinks (assimilatory processes, cell maintenance, biotransformations). In the first place, energy and electron supply depend on the light availability: Up to a certain intensity (E_k), cell growth is proportional to the irradiated light, but this light-dependent increase saturates at higher light intensities, especially at low atmospheric CO_2 levels constituting a sink limitation (Figure 18, see also [114]). While keeping the light source constant at a pre-determined intensity enabling efficient planktonic growth, environmental sink conditions (C source availability, type of N source, expression burden, and biotransformation burden) were varied, which impacted not only growth, but also electron partitioning. Most visibly, the share of r_{AEF} changed dramatically. In *Synechocystis*, dark-interval relaxation kinetics of PS I attributed 35% of total electron flux to cyclic electron transport.[34] This agrees well with our data on *Synechocystis* BVMO:Lactonase, where the share of r_{AEF} under non-induced control conditions with NO_3^- as N source was 35-40%, while the r_{AEF} share was lower (20%) with NH_4^+ as N source. In contrast to PS I-kinetics, in our approach r_{AEF} subsumes all non-linear electron fluxes, i.e. both cyclic electron and pseudocyclic electron fluxes. Upon Ni^{2+} -induced expression of heterologous genes, the share of r_{AEF} increased under all conditions reaching a maximum of 60% under LC/ NO_3^- conditions, which makes the expression burden obvious. These data confirm the frequently presumed flexibility in photosynthetic electron allocation upon changed electron demands/sinks. However, whereas the biotransformation reduced r_{AEF} as expected, also the overall electron flux r_{F} was reduced, which was not expected and compromised growth and in the end also biotransformation.

Previously we reported C fixation efficiency, expressed as quantum requirement for C fixation, Q_c [$\text{mol}_{\text{quanta}} \text{mol}_C^{-1}$], to be an important measure for balanced source/sink conditions.[112] The lowest Q_c (27.4 ± 1.7 , Table 7) under HC/ NH_4^+ conditions indicate this scenario representing the ideal source/sink balance, slightly better than HC/ NO_3^- (31.6 ± 2.9), where arguably light was limiting. Upon biotransformation initiation, Q_c increased in all scenarios, indicating less balanced conditions. For sink-replete conditions (HC/ NO_3^-) introducing an extra sink distances the state further from source/sink balance; together with a r_{F} decrease, likely due to the

unfavorable ATP/NADPH ratio, these imbalances were detrimental. For scenario II, most likely photodamage mediated by NH_4^+ decreased r_F and deflected this state from balanced conditions, increasing Q_c . The comparably high Q_c under sink-limited conditions (60.2 ± 8.3) were increased further upon biotransformation initiation (to 76.1 ± 4.9), contradicting relieve of sink-limitation by the biotransformation. Assumably, e^- withdrawal alone did not benefit the metabolism, but altered ATP/NADPH demand ratios leading to a decrease of r_F .

Interestingly, the highest Q_c under biotransformation co-occurs with the highest QE towards product formation (Table 7), both observed in the HC/NO₃- conditions. In other words, the highest biotransformation capacity was detected under C-replete conditions. This speaks against a direct competition (e.g. for reduction) between C and N assimilation and biotransformation and makes Q_c an important parameter for processes utilizing photosynthetically generated reductant. In agreement with our previous study on the same process, ideal (=high light) conditions for growth were best suited for stable production. (Chapter 4) In the previously described fed-batch process, however, the biotransformation increased overall quantum usage, tapping unused potential of the photosynthetic light reaction. This effect was not observed in the continuous (and light-limited) setup investigated in the present study: Contradicting an expected e^- sink-effect, catalysis did not further increase electron flux, but ran at the expense of electron flux into C- and N-assimilation.

5.5 Conclusion

In the presented study, we could not find conditions to stably maintain the investigated electron demanding biotransformation of cyclohexanone to 6-hydroxyhexanoic acid during continuous cultivation. Yet, the electron balancing approach gave quantitative insights into effects on cell metabolism, especially electron partitioning. Despite being desirable for many envisioned photo-biotechnological processes, it turned out not to be trivial to sustainably tap photosynthetically generated electrons from PS I at high rates. While there is evidence for “pulling” sink effects of (heterologous) electron consumers, the interdependency of electron-demanding biotransformations and photosynthetic growth metabolism as well as respective regulation were found to be of key importance for stable processing and require further investigation. This study shows the importance of carefully considering source/sink balances when aiming at continuous light-driven production in cyanobacteria. In particular, the long-term perspective presented here will be important for possible future photo-biotechnological applications.

6 General Discussion

This section discusses and interconnects the main findings of the studies presented in chapters 2-5 and embeds them in their scientific research context. It will be looked at how the findings can help to overcome main limitations of photo-biotechnology today and tomorrow. The feasibility of photo-biotechnological applications will be critically discussed to illustrate the status of photo-biotechnology and to point out how this thesis contributed to progress in the field.

6.1 Defining boundaries of photo-biocatalysis

To optimize the efficiency of biocatalytic processes, a detailed understanding of its limitations is key.[49] Typical limitations of oxygenase catalysis in whole-cells are:

- Co-substrate limitation like limited supply of reduction equivalents, O₂, or other co-factors.[262, 263]
- Low levels of (heterologous) enzymes limiting the overall conversion rate and low enzyme stability.
- Limitations caused by reactants, like substrate depletion, and reactant inhibitions by substrate, by-product, or product.[52]
- Toxic effects limiting the catalyst viability and, thus, enzyme expression as well as cofactor supply.[264, 265]

Multiple of these limitations can occur simultaneously, with potentially cumulative effects.

From a biotechnological perspective, the so-called window of operation represents a key tool to develop feasible processes.[266] Schrewe et al. defined this window of operation for whole-cell (oxygenase) biocatalysis.[52] In short, the feasibility of biocatalytic processes is determined by downstream processing demands and reactant (mostly product) toxicity, constituting the lower and upper boundaries of feasible product concentrations, and by maximally achievable production rate and catalyst stability, constituting the lower and upper boundaries for accessible reaction times, respectively (Figure 22).

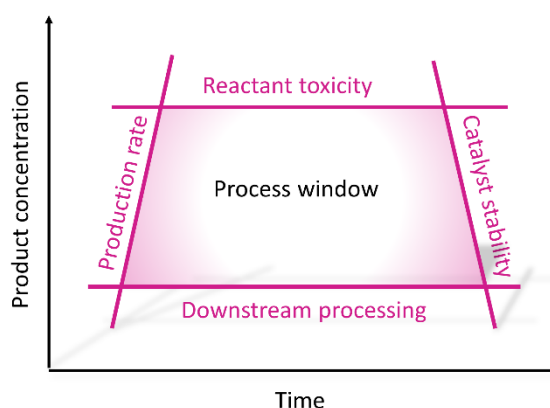


Figure 22: **Window of operation for whole-cell biocatalytic processes.** Reactant toxicity and downstream processing define the upper and lower limit of feasible product concentrations, while the maximally achievable production rate and catalyst stability define the lower and upper boundaries of possible reaction times. Modified from[52].

Deciphering limitations is essential to define this window of operation and to optimize processes accordingly.[49, 195] Thus, the first part of the discussion focuses on different limitations observed and optimized in the presented studies.

6.1.1 Coupling of heterologous enzymes to the photosynthetic apparatus

The implementation of oxygenases in cyanobacterial cells enables the exploitation of the photosynthetic light reaction as supplier of reduction equivalents and O₂. [58] This overcomes respective limitations, but i) leads to a strong dependency on light (see 6.2.) and ii) raises the question, how efficiently heterologous reactions can be coupled to the photosynthetic apparatus via different electron mediators (see Figure 3, Table 1).

Coupling redox enzymes via NADPH enabled the highest specific activities reported so far with the ene-reductase Yqjm from *Bacillus subtilis* (150 U g_{CDW}⁻¹). [79] In Chapters 3 and 4, the utilization of the NADPH-dependent Baeyer-Villiger monooxygenase (BVMO) from *Acidovorax* sp. CHX100 in whole cells of *Synechocystis* was developed and optimized. Specific activities of more than 60 U g_{CDW}⁻¹ were achieved, unprecedentedly high for oxygenase catalysis in phototrophs. Evidently, branching off electrons from photosynthesis via NADPH enables highly efficient electron transfer from the light reaction to (heterologous) electron consumers in *Synechocystis*. Direct dependence of conversion rates on light intensity was observed as described in Chapter 3 (Figure 9A), illustrating the close linkage of the photosynthetic light reaction via NADPH to electron consumers. In this context, it is interesting that glucose was observed to increase specific activities of the otherwise only light-driven Yqjm reductase by a factor of 1.5. [267] This contribution to a NADPH-depending biotransformation indicates a limitation by NADPH regeneration rather than by NADP(H) pool sizes and suggests an even higher potential of electron withdrawal via NADPH. Nevertheless, even with glucose addition, specific activities of 150 U g_{CDW}⁻¹ were not surpassed. [267]

Compared to NADPH-depending reactions, by far lower rates have been reported for NADH-coupled biotransformations in phototrophic microorganisms, e.g., 1.5 ± 0.2 U g_{CDW}⁻¹ for terminal hydroxylation of fatty acid esters in *Synechocystis* [75] (see Table 2). This is not surprising, since NADPH is the main electron currency in phototrophs and NADH turnover via pathways of heterotrophic metabolism like glycolysis and TCA cycle is lower than in heterotrophs. [256, 268-270] However, with a NADH-dependent cytochrome P450 monooxygenase (CYP) system from *Acidovorax* sp. CHX100, light-driven activities of up to 26.3 ± 0.6 U g_{CDW}⁻¹ in aqueous medium and up to 39.2 ± 0.9 U g_{CDW}⁻¹ in optimized two-phase-systems have been reported. [74] This three-component CYP system comprises i) a NADH-dependent ferredoxin-NADPH-reductase (FNR), reducing ii) a ferredoxin (Fd), which delivers electrons to iii) the oxygenase component able to hydroxylate cyclic alkanes. [181] The high specific activity raised the question, how electron coupling *in vivo* is realized and, if native *Synechocystis* components can take over functions of the *Acidovorax* system. Chapter 2 enlightens this issue by expressing the oxygenase component alone or with only one of the components of the native electron transfer chain. Whole-cell activities of up to 5.2 ± 0.3 U g_{CDW}⁻¹ when expressing only the oxygenase component suggest electron supply

via *Synechocystis* components. Interestingly, co-expression of the oxygenase component together with *Acidovorax* Fd restored the whole-cell activities obtained with the complete three-component system ($25.6 \pm 2.0 \text{ U g}_{\text{CDW}}^{-1}$), indicating that *Synechocystis* components can take over the function of *Acidovorax* FNR. It has been reported before that heterologous CYPs can be supplied with electrons by Fd[158] and Fd/FNR[157] systems from phototrophic organisms. However, the high specific activities achieved in Chapter 2 suggest that the whole-cell system enables a close efficient coupling of the photosynthetic electron transport chain (PETC) to heterologous consumers and thus efficient supply of reduction equivalents. To divert reductive power, cyanobacteria possess numerous electron carriers, like Fd, thioredoxin (Trx), plastoquinone (PQ), and redox enzymes such as FNR and ferredoxin-thioredoxin-reductase (FTR), to mediate electron transfer. *Synechocystis*, for instance, harbors 9 Fds, with distinct physiological roles.[77] Chapter 2 demonstrates the applicability of this versatile toolset for electron supply to heterologous oxygenases. Further, evidence for crosstalk between *Synechocystis* PS I and *Acidovorax* Fd was found. The functional network of electron carriers is however far from being completely understood, and detailed knockout studies are required to decipher the crosstalk between *Synechocystis* components and heterologous consumers in more detail. This knowledge is required to optimize and fine-tune electron transfer to heterologous enzymes. E.g., knowledge on the dependence of such electron transfer on the physiological state will help to establish a possibility for an on and off switch of production and thereby enable process control and possibly a stabilization of light-driven redox biotransformations.

Next to the coupling via soluble electron carriers described above, anchoring of (heterologous) redox enzymes in the thylakoid membrane has been described.[68] Membrane anchoring combined with fusing Fd to CYP79A1 was found to increase the hydroxylation rate, most likely due to the close proximity to PS I.[200] In principle, coupling of heterologous redox reactions to the photosynthetic apparatus can also occur earlier in the PETC. In terms of efficient light-usage, branching off electrons upstream of PS I holds great potential, since operating PS II alone potential-wise would suffice heterologous electron supply in many cases. Circumventing quantum-demanding PS I and with it circular electron transfer operation could increase quantum efficiencies dramatically.[8] Functional expression of plastid terminal oxidase from rice in *Synechocystis* showed the principle feasibility of tapping, e.g., the PQ pool.[41] However, the possibly high quantum efficiency comes to the price of lower reductive power: The redox potential of PQ is about +80 to +110 mV[124], which does not suffice to drive the oxygenase reactions described here.

6.1.2 Level of heterologous enzymes and redox carriers in cyanobacteria

In enzyme and whole-cell biocatalysis, limitation by the catalyst, which is the amount of stable and functional enzyme, is very common. This is particularly true for biotechnology with

phototrophs, as the development of strong and reliable expression systems lacks behind (see Figure 4). There are many examples of cyanobacterial whole-cell biocatalysis, for which a low level of heterologous protein is arguably the key limitation[78, 190, 200, 271] or is explicitly named as key parameter for optimization[68, 72, 109, 208]. The used CYP system from *Acidovorax* has been expressed under control of the IPTG-inducible *P_{trc10}* promoter.[74] Specific activity was found to depend on IPTG-concentrations, with modest background activities (around 10 U g_{CDW}⁻¹ without IPTG addition; personal communication by Anna Hoschek) most likely due to leakiness of the promoter system. In the related study, CYP levels were just high enough for detection via sodium dodecylsulfate polyacrylamide gel electrophoresis (SDS-PAGE), while the two electron transfer proteins from *Acidovorax* could not be detected. This strongly indicates a limitation by low protein levels of either CYP or Fd_{AV}, whereas the FNR_{AV} is unlikely to be the bottleneck, as its omission still allowed conversion rates comparable to those achieved with the three component system (see Chapter 2). Hence, conversion rates reported in Chapter 2 with the same expression system are likely also limited by enzyme levels. In Chapter 3, BVMO short-term activities (30 min) of *Synechocystis* whole cells were found to directly depend on Cu²⁺- or Ni²⁺-concentrations when using the *P_{petE}* or *P_{nrsB}* promoter systems, respectively (Figures 8A, B). Further, chromosome-based BVMO gene expression resulted in overall lower whole-cell activities compared to plasmid-based expression, most likely due to a lower chromosome copy number compared to the plasmid copy number.[141] These observations clearly indicate that the expression level (and stability) of BVMO limits initial whole-cell activities.

To increase and fine-tune expression levels of heterologous genes, pivotal progress has been made in recent years: One strategy is the application of modular cloning techniques, employing Type IIS restriction enzymes for Golden Gate cloning.[64] This attempt has been taken up and adapted in our labs for *Synechocystis*, and was already successfully applied, e.g. in Chapter 4. The modular character of this strategy allows for high-throughput testing of native, heterologous, and synthetic components of expression systems, including RBSs, promoters, and other genetic elements. Next, promoter screening will be indispensable, since different genetic sequences were found to show differential expression responses.[207, 272] In this context, Chapter 3 makes an important contribution, comparing *P_{petE}* and *P_{nrsB}* (Cu²⁺ and Ni²⁺-inducible, respectively) regarding expression and activity levels of an oxygenase. However, heavy-metal inducible promoters are not well suited for the envisioned biotechnological use due to high costs and toxicity issues. Alternative promoters, like *P_{rha}* (Rhamnose-inducible) or *P_{vanCC}* (Vanillate-inducible) may be better suited for future applications.[199] Further, the variety of expression vectors (and origins of replication) is still limited in cyanobacteria.[147] Recently, important progress was made with the use of endogenous plasmids of *Synechocystis* as shuttle vectors. In this context, establishing the

BVMO in *Synechocystis* (Chapter 3), made it a suitable cargo gene to demonstrate successful expression from modified endogenous plasmids.[273]

Regarding biotechnological processes, enzyme stability is another crucial factor, especially for oxygenases.[54, 274, 275] The BVMO depicted high and constant activities 24-72 h after induction, illustrating stable expression (Figure S16). However, the biotransformation itself and respective conditions can destabilize enzymes, especially oxygenases with uncoupling as a prominent factor.[54] It has been shown that CHMO is stabilized by external addition of NADPH, but not NADP⁺. [257] Hence, the decreased NADPH/NADP⁺ ratio during biotransformation may affect enzyme stability leading to the observed decrease of specific activities (Figure 11). Yet, as discussed below (6.1.4), a differentiation between a direct NADPH-limitation of the biotransformation and enzyme instability mediated by the lack of NADPH is difficult. In the end, both effects are likely to co-occur.

6.1.3 Control of toxicity and inhibition of oxygenase-based biotransformations

CYP and BVMO from *Acidovorax* feature rather broad substrate spectra.[181, 187] In this thesis, only cyclohexane and cyclohexanone conversions to cyclohexanol and ϵ -caprolactone, respectively, were investigated as model bioconversions to test the performance of these two oxygenases in *Synechocystis*. All four compounds have been shown to severely affect *Synechocystis* cell growth[74] (Chapter 3 and 4). This is due to their intermediate hydrophobicity with partition coefficients between octanol and water ($\log P_{OW}$) between 3.2 (for Chx) and 1.2 (for ϵ -Cl). Compounds with a $\log P_{OW}$ between 1 and 4 are known to easily accumulate in membranes, and thus are considered highly toxic for microbes.[276] Such reactant toxicity as well as possible enzyme inhibitions hamper efficient whole-cell biocatalysis, for which high substrate and especially product concentrations are key for a simple reaction engineering.[277] Even at subtoxic levels, at which biotransformations in Chapters 3-5 were typically conducted, reactants can reduce biotransformation capacity, due to diminished co-factor regeneration upon impairment of metabolism.[264] To handle toxicity issues with *Synechocystis*, Hoschek et al. used a two-liquid phase system with an organic carrier phase serving as substrate reservoir and product sink (*in situ* product removal).[74]

In Chapter 3, we studied how to cope with such inhibitions, focusing on the kinetic characterization of the BVMO reaction and its crosstalk with the host organism. Before, a study on a similar BVMO in *Synechocystis* described the keto reduction of the substrate C-one to C-ol as a side reaction.[78] Besides an unwanted substrate loss impeding selectivity, which was found to be low for the BVMO applied, Chapter 3 detailed the strong inhibition of the target reaction by the by-product C-ol. Whole-cell kinetics revealed a rather unspecific keto reduction ($K_s = 7.4 \pm 0.6$ mM), whereas the K_s for the oxygenation was low ($K_s = 79 \pm 23$ μ M). Further, a

substrate inhibition with an $K_{i,C-one}$ of 4.4 ± 1.5 mM was identified, demonstrating the complexity of the BVMO reaction system in *Synechocystis*. Controlling substrate levels thus was key to overcome several limitations at once, i.e., by-product formation and inhibition as well as substrate inhibition. Conclusively, lab-scale biotransformation in both stirred-tank photobioreactors (photo-STR) (Chapters 3 and 4) and flat-panel (FP) bioreactors (Chapter 5) were conducted in a substrate-limiting regime established via the fine-tuning of the feed rate. Alternatively, host alcohol dehydrogenases, likely catalyzing the keto reduction, could be deleted. This, however, would only prevent by-product formation and inhibition, with potentially detrimental effects on host metabolism. With the continuous feed system, product (ϵ -Cl) titers of up to 11.5 ± 0.2 mM were reached within 27 h. The avoidance of the above-mentioned inhibitions revealed another reactant-mediated limitation, i.e., product inhibition. Whereas enzyme inhibition by ϵ -Cl could be excluded,[165] its solubilization in membranes may hamper photosynthetic electron supply, which thus may limit conversion rates. Product-induced uncoupling may be another mechanism causing inhibition by ϵ -Cl. However, no experimental proof was found for this mechanism.

To overcome ϵ -Cl effects on catalyst performance, an *in vivo* cascade was established, characterized, and applied in *Synechocystis* as described in Chapter 4. A lactonase, being the follow-up enzyme of the BVMO in the degradation pathway of *Acidovorax*, was co-expressed to hydrolyze ϵ -Cl to 6-hydroxyhexanoic acid (6-HA), which is tolerated in far higher concentrations by *Synechocystis* (Figure S11). 6-HA also can serve as monomer for polycaprolactone production[278] or as precursor for adipic acid and 6-amino-hexanoic acid synthesis.[165] The high activity of the lactonase ensured complete conversion of C-one to 6-HA. The combination of a substrate-limited feed regime with the two-step cascade could indeed confine reactant toxicity and inhibition to achieve product (6-HA) titers of up to 23.5 ± 1.2 mM within 48 h, being among the highest ones reached with cyanobacteria. A further increase of conversion rates and product titers was *inter alia* restricted by the metabolic capacity as discussed in the following.

6.1.4 Metabolic capacity for photosynthetic electron supply

The application of oxygenases in cyanobacteria seeks to exploit the photosynthetic metabolism as supplier of electrons (and O_2). The electron supply rate is naturally limited by the capacity of the PETC. Based on fluorescence kinetics, Kauny and Setif estimated a photo-production rate of $530 - 1070 \mu\text{mol}_{\text{NADPH}} \text{mg}_{\text{Chl}} \text{h}^{-1}$ for *Synechocystis*. [115] With a Chl-*a*-content of 1-1.5% (w/w) (Chapters 3-5), this translates into $90 - 270 \mu\text{mol}_{\text{NADPH}} \text{g}_{\text{CDW}}^{-1} \text{min}^{-1}$ ($=U \text{g}_{\text{CDW}}^{-1}$) as an upper boundary for PS-driven redox reactions. With the ene-reductase Yqjm initial specific activities of up to $150 U \text{g}_{\text{CDW}}^{-1}$ have been reported, equaling a consumption of up to 60% of photosynthetically produced reductant.[79] With about $60 U \text{g}_{\text{CDW}}^{-1}$ (Chapter 3 and 4), we achieved the highest specific activity reported so far for oxygenases in phototrophs, both

for BVMO alone and BVMO + lactonase, consuming about 25% of PETC-derived reductant. Overexpression of the small regulatory protein CP12, an inhibitor of the CBB enzymes GAPDH and PRK,[43] may be an interesting option to reduce and increase electron fluxes into C-fixation and towards biotransformations, respectively.[44] This, however, requires further investigations, as results obtained in Chapter 5 indicate that a running CBB fosters redox biocatalysis, questioning the competition between both.

While the achieved initial activities proof the capability of the PETC to provide reduction equivalents at high rates for redox biocatalysis, the question remains, if these rates can be maintained by photosynthetic metabolism in the longer term. Long-term data on light-driven biotransformations are scarce: CYP-catalyzed light-dependent conversion of Chx to C-ol was conducted for 52 h with an average activity of about $10 \text{ U g}_{\text{CDW}}^{-1}$, with a clear activity decrease after 6 h.[74] For the Yqjm reductase, a biotransformation at an average activity $12 \text{ U g}_{\text{CDW}}^{-1}$ was conducted for 22 h with internal illumination ensuring sufficient light supply.[95] The two-step process described in Chapter 4 allowed the systematic investigation of the metabolic capacity to supply (oxygenase-based) biotransformations with electrons. Evidently, a moderate electron demand ($10 \text{ U g}_{\text{CDW}}^{-1}$) ensured constant conversion rates for more than 40 h and, consequently, 1.6-times higher final product titers than higher specific activities ($20 \text{ U g}_{\text{CDW}}^{-1}$), which could be met for only 6 h, after which they decreased significantly (Figure 14). To conclude, there is evidence that the rate for sustainable decoupling of PETC-derived reductant towards redox biocatalysis is limited to about $10\text{-}15 \text{ U g}_{\text{CDW}}^{-1}$. Higher rates can be supplied for a few hours maximally, but inflict reaction stability, and cannot be sustained.

Besides a limitation by the mere capacity of the light reaction, reductant withdrawal for biotransformations may disturb the ATP/NADPH balance within the cell.[245, 258] CET can be downregulated to counteract such an imbalance (as observed in Chapter 5, Figure 21). However, purely linear electron transfer without CET represents the maximum shift of this balance towards reduction power, and a further increase of electron withdrawal can be expected to lead to high ATP/ADP⁺ and low NADPH/NADP⁺ ratios. This imbalance may limit CBB activity, which in turn would reinforce the ATP/NADPH imbalance as the CBB is the major ATP sink.[246] This then also may harm the oxidative stress management within the photosynthetic machinery, resulting in decreased light reaction rates and NADPH regeneration.[37, 43] One possible way to escape this metabolic stalemate caused by extensive NADPH withdrawal is the co-expression of an ATP-sink together with an electron sink.[85] Another way to counteract ATP/NADPH imbalances is the deletion of (native) electron consuming pathways: Flv1/3 deletion was shown to reduce the ATP/NADPH ratio and enhance sucrose production[46] as well as biotransformations catalyzed by Yqjm[79] and BVMO[179], for which conversion short-term rates increased by a factor of 1.5-2. However, long-term consequences of Flv1/3 deletion on biocatalyst stability have not been investigated so far.

Natively, Flv1/3 is an important contributor to the *pmf* and thus ATP synthesis at dark/light transitions,[279] and its deletion might compromise strain robustness.

In the context of future photo-biotechnological applications aiming at reaction times of days or weeks, reductant allocation for assimilatory processes, biomass formation, and cell maintenance on the one side and for product formation on the other side is of essential interest. In this respect, Chapter 4 delivers interesting results: Fed-batch biotransformation did not reduce biomass formation, but tapped otherwise unused potential of the photosynthetic light reaction. This involved improved quantum usage and light-conversion efficiency. Chapter 5 seeks to substantiate this observation by balancing electron fluxes into biomass and product formation under steady state conditions. To alter sink conditions, different C and different N source (e^- intensive NO_3^- vs e^- neutral NH_4^+) availabilities were tested. However, none of the sink scenarios enabled a truly continuous electron withdrawal. Either biotransformation rate or growth decreased dramatically within 50-120 h. While an allocation problem of reductant seems plausible, it cannot be explained, why overall electron fluxes decreased upon biotransformation under all tested conditions. Contradicting these findings, electron flux through the PETC was reported to increase upon activating/adding extra sinks.[73, 85, 112, 161] This sink effect was, however, not observed upon BVMO-based biotransformation, which rather appeared to run at the cost of reduced biomass formation. Nevertheless, Chapter 5 gives important quantitative information on favorable conditions: Sink-limited conditions augur well for long-term, stable electron withdrawal, albeit at lower rates. Sink-replete conditions are suited for high-rate electron withdrawal, albeit for shorter time periods. The observation that a fast growth and high metabolic turnover benefits high conversion rates was consistent over several tested scenarios (Figures 11, 14, 20) and challenges the understanding of a direct competition for reductant. Overall, a promising future engineering should target the maintenance of a high metabolic turnover surpassing growth demands and involving an overflow of electrons (but not ATP), which can be tapped for redox biocatalysis.

In addition to reduction equivalents, oxygenase catalysis also requires O_2 at a stoichiometry of 1 mol O_2 per mol product. O_2 is produced by the photosynthetic light reaction at a ratio of 1 mol O_2 per 4 mol of electrons derived from the oxidation of two water molecules. Hence, O_2 rather than reduction equivalents would be limiting, if the oxygenase was the only consumer. The cell, however, features many electron sinks, while O_2 only is consumed by photorespiration and dark respiration and in Mehler-like reactions.[25, 31] These processes, however, consume only a small share of the produced O_2 making O_2 -limitation unlikely.[25] These considerations are reinforced by the elevated DOC levels over all tested scenarios. Running oxygenase-based biotransformations indeed led to lower DOC levels, which however still surpassed abiotic DOC levels, giving evidence for net O_2 production (Figure 15).

Nevertheless, the fact that reduction equivalents are not the only PETC-derived co-substrates for BVMO (or CYP), may limit their significance for solely electron withdrawing enzymes.

6.2 Light input and usage as critical parameter of photo-biotechnology

After discussing different boundaries of a biocatalytic process and how to overcome respective limitations, with the light reaction as a central module, this section will more deeply discuss the light as a key parameter for photo-biocatalytic processes and how efficiently it can be used for product formation.

6.2.1 Extending the window of operation for photo-biocatalytic processes

The careful control of reactant toxicity and inhibition together with overcoming the detrimental effect of the primary product enabled an 2.8-times increase of product titers, finally reaching $3.1 \pm 0.1 \text{ g L}^{-1}$ of 6-HA (without DSP). This corresponded to a volumetric productivity of $0.07 \text{ g L}^{-1} \text{ h}^{-1}$ over 48 h. Such product titer, productivity, and stability are remarkable for a photosynthesis-driven process. Nevertheless, these numbers are just above or close to minimum requirements for fine chemicals in terms of final product titer ($> 1 \text{ g L}^{-1}$) and volumetric productivity ($> 0.1 \text{ g L}^{-1} \text{ h}^{-1}$), [280] while the product 6-HA can hardly be seen as fine chemical. With boundaries like reactant toxicity (see 6.1.3.) and inherent metabolic capacity (see 6.1.4.), which are already tackled to a large extent, the next step to increase volumetric productivity would be the use of higher catalyst concentrations. To achieve high cell densities with phototrophic microorganisms, efficient supply of both CO_2 and light are key. Sufficient CO_2 supply is realized by CO_2 -enriched aeration or by cultivation systems with membrane-mediated CO_2 supply.[281] Light supply is more complex: Light limitation naturally limits biomass and product formation, as reductant (and energy) generation by the PETC is limited. However, excess light can cause over-reduction of the photosynthetic apparatus, which may destroy the photosystem (photo-damage). In turn, mechanisms protecting the cell from photo-damage compromise efficient quantum usage. Following these consideration, the window of operation requires an extension by a light-axis to describe the boundaries of a photo-biocatalytic process more accurately (Figure 23).

For photo-biocatalytic processes, light penetration is decisive to ensure optimal light conditions for the cells. One option are capillary biofilm reactors, which enabled, based on a high surface to volume ratio, biomass concentrations up to $40 \text{ g}_{\text{CDW}} \text{ L}^{-1}$ in a mixed-species approach and cyclohexane oxyfunctionalization for 31 days in a light-dependent manner.[98] Challenges of this approach include low overall volumes and its scaling. Internal illumination with wireless light emitters ensures an even light distribution to overcome respective limitations of biocatalytically-active suspended cells.[95] However, this approach can rather be seen as

interim solution, as it is electricity driven and not easy to transfer to envisioned outside application driven by sun light.

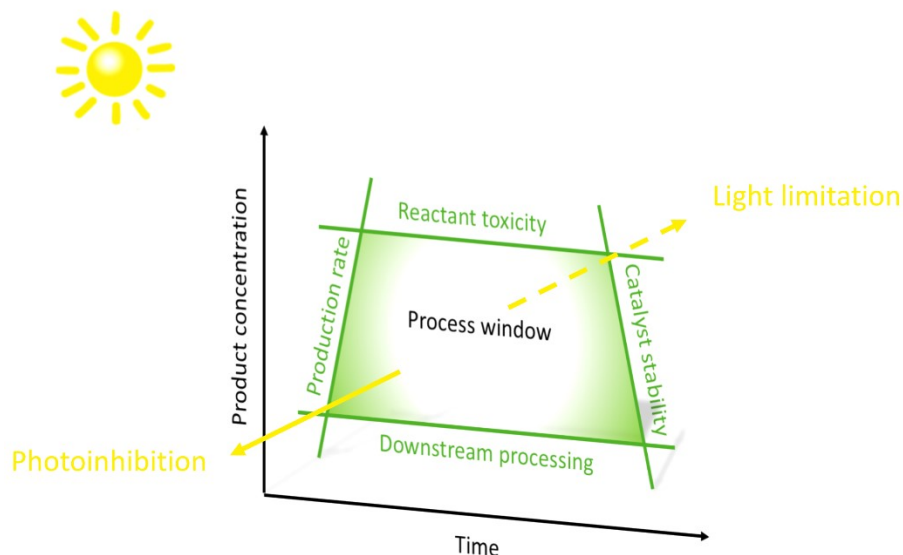


Figure 23: **Extended window of operation for whole-cell photo-biocatalytic processes.** Reactant toxicity and downstream processing demands define the upper and lower limit of the (final) product concentration, while production rate and catalyst stability constitute the lower and upper boundaries in terms of reaction time. Light input can be understood as a third dimension, with excess light reducing quantum efficiency and possibly causing photo-damage (photo-inhibition) and, in contrast, low light intensities compromising catalyst viability, requiring costly energy-harvest optimization, and limiting light-dependent supply of reductant. Hence, both light limitation and light excess limit production rate and catalyst stability. Modified from [52].

6.2.2 Quantum efficiency of photosynthesis-driven product formation

With light being a key limitation of photo-biotechnological processes, its efficient usage by the catalyst is essential. The photon or quantum efficiency constitutes a quantitative measure for light usage and is defined as the amount of productively used photons (e.g., for nutrient assimilation, biomass formation, product formation) divided by the amount of total irradiated photons. There are many studies on quantum usage in both microalgae[47, 48, 118, 120] and cyanobacteria[161],[114]. Via photon balancing for the diatoms *Cyclotella meneghiniana* and *Skeletonema costatum*, Su et al. provided numbers on photosynthetic energy losses to i) fluorescence dissipation and constitutive heat emission (40-45%), ii) non-photochemical quenching (NPQ) (10-13%), iii) alternative electron transfer (7-13%), and iv) photorespiration and dark respiration (15-22%).[122] For the generation of reductant for biomass formation (net O_2 formation), only 16-20% of absorbed quanta are used. In *Synechocystis*, these numbers have not been quantified in comparable depth. While PS II-efficiencies suggest comparable heat and fluorescence losses in the range of 40-60%,[85, 161] NPQ is expected to play a minor role, while the share of alternative electron transfer is considered to be higher[25] (see also

Chapter 5). Hence, a similar quantum efficiency of 20 to maximally 25% can be assumed for biomass formation.

From a biotechnological perspective, the quantum demand of product formation is of interest. The quantum demand is the amount of quanta required for a specific process, be it C fixation, N assimilation, or product formation. Being pioneering in this regard, Chapter 4 puts the quantum efficiency regarding product formation (QE) in numbers. This approach can be extended to all (bioreactor-based) biotransformations presented in Chapters 3-5 (Fig. 6.3). Thereby, the following differences in the biotransformation setups have to be considered: In Chapters 3 and 4, fed-batch biotransformations were conducted in photo-STRs for 24-28 h and 48-52 h, respectively, while, in Chapter 5, continuously cultivated cells were fed with substrate to conduct biotransformation for 50-80 h in FP-bioreactors. In photo-STRs, biotransformations were conducted starting with 0.7-1.1 g_{CDW} L⁻¹, while cell concentrations were kept constant between 0.17 and 0.20 g_{CDW} L⁻¹ in the FP-bioreactors during biotransformation. Next, data from a one-enzyme biotransformation (BVMO only, Chapter 3 and reactor 3 of Chapter 4) are compared to the two-enzyme approach (Chapter 4 and 5). The QE was highest (9.3 ± 0.8%) for cells exposed to the lowest intensity of 150 μmol_{photons} m⁻² s⁻¹ in a photo-STR at relatively high biomass concentrations. This is not surprising, as, upon strong light-limitation, cells are known to maximize energy harvesting.[120, 161] It must be considered that batch-effects, such as mobilization of storage compounds to drive product formation, may lead to an overestimation of QE. Continuous cultivation (without such batch-effects) at 150 μmol_{photons} m⁻² s⁻¹ revealed a 3-times higher QE under C-replete conditions (2.3 ± 0.1%) than under C-limitation (0.7 ± 0.1%). Evidently, higher product formation rates can be supported, when the metabolism operates at higher rates. These observations challenge the generally assumed limitation by the competition for reductant between biomass and product formation, as a substantial amount of quanta was diverted to product formation, even under light-limitation. Interestingly, the 5 higher biomass concentrations in photo-STRs compared to FP-bioreactors depict overall lower (average) specific activities at average, with a cell concentration of 0.17 ± 0.1 g_{CDW} L⁻¹ in the FP-bioreactors yielding the highest specific activity of up to 16.0 ± 0.7 U g_{CDW}⁻¹ in the sink-replete scenarios, respectively. As also reflected by the lower QE, high cell (and thus Chl-*a*) loads lead to less efficient light utilize than lower cell concentrations. Known as “packaging effect” this phenomenon has been described at the cellular level by Wilhelm and Jakob.[47, 282]

The overall quantum efficiency, summing up the quanta used for both nutrient assimilation and product formation, was calculated to 16% with respect to total incident quanta (Chapter 4), whereas the mentioned quantum efficiencies for biomass formation in diatoms (16-20%) refer to absorbed photons (= Q_{phar}).[122] However, the basis is likely comparable, as all incident quanta in the photo-STR-setup used in Chapter 4 are likely to be absorbed by the cells

(cultivated in biomass concentrations $> 1 \text{ g}_{\text{CDW}} \text{ L}^{-1}$ in a cylindrical cultivation vessel). While photorespiration can be suppressed by high CO_2 conditions,[283] losses by fluorescence and heat dissipation or alternative electron fluxes are inevitable, since these processes are either crucial as protective mechanisms against over-reduction/photo-inhibition or as contributors to ATP generation.[30] The quantum efficiency regarding product formation, determined based on photon and electron allocation to different sinks, can be considered a key parameter to quantitatively assess the potential and efficiency of photo-biotechnological processes.

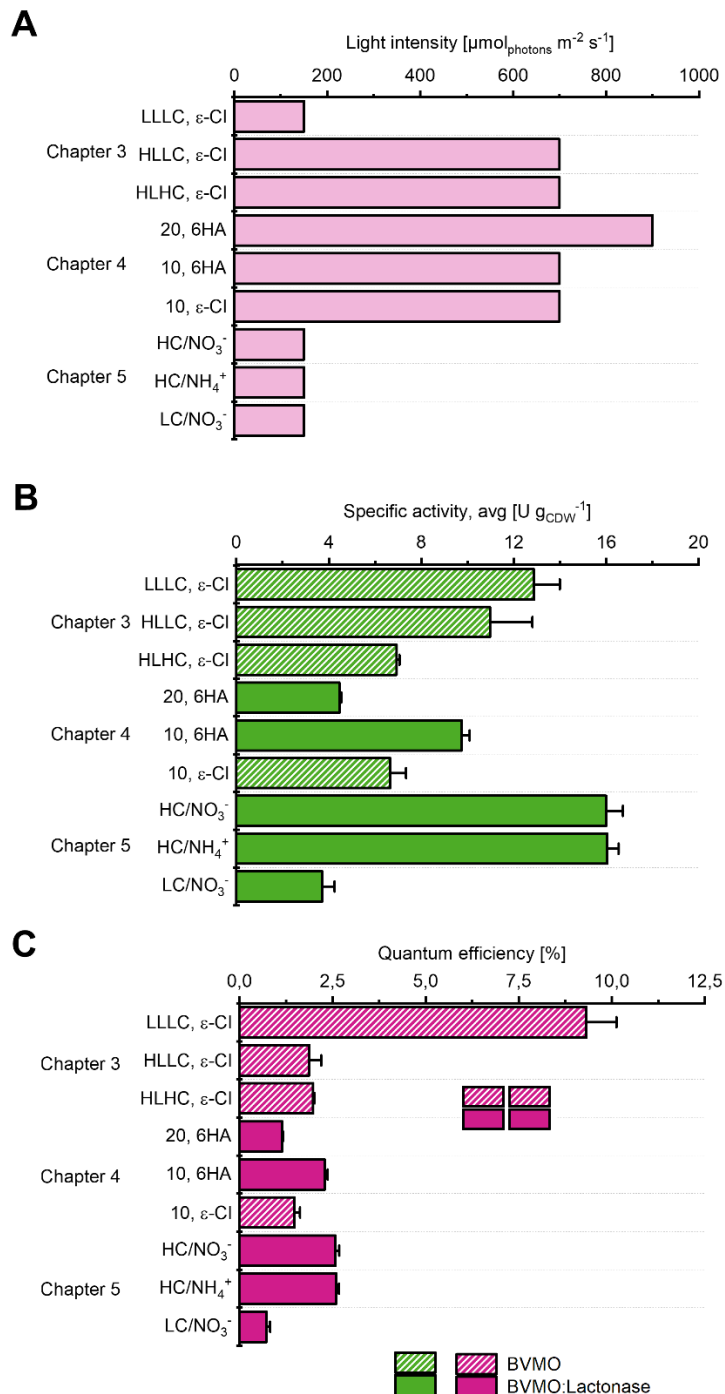


Figure 24: Comparison of (A) light intensity, (B) (average) specific activity, and (C) quantum efficiency of photosynthesis-driven oxygenase-based biotransformations in different reactor formats. In Chapters 3 and 4, biotransformations were conducted in photo-STRs with cell densities of

0.7-1.1 $\text{g}_{\text{CDW}} \text{L}^{-1}$ at biotransformation start using either BVMO (striped bars) or BVMO and lactonase (filled bars). In chapter 5, FP-bioreactors were used for continuous cultivation with cell densities being kept constant between 0.17-0.20 $\text{g}_{\text{CDW}} \text{L}^{-1}$ using BVMO and lactonase (filled bars). For Chapter 4, numbers specify maximal activity in $\text{U g}_{\text{CDW}}^{-1}$ limited by the substrate feed. Reaction times: 24-28h for Chapter 3, 48-52 h for Chapter 4, and 50-80 h for Chapter 5. Reactor conditions: LL – low light ($150 \mu\text{mol}_{\text{photons}} \text{m}^{-2} \text{s}^{-1}$), HL – high light ($700 \mu\text{mol}_{\text{photons}} \text{m}^{-2} \text{s}^{-1}$), LC – low carbon (ambient and 0.12% CO_2 for photo-STR and FP-bioreactors, respectively), HC – high carbon (1% and 0.6% CO_2 for photo-STR and FP-bioreactors, respectively). For Chapter 5, the N source is specified (NO_3^- or NH_4^+).

6.2.3 Optimizing light conversion efficiency

Envisioned photo-biotechnology is prospectively producing energy and materials in a light-dependent way. This raises the question, how efficient phototrophic organisms can convert sunlight to biomass and (energy) products. About 10-15 years ago, biofuel production with microalgae has been intensively discussed.[284, 285] This CO_2 -valorization depends on a relatively low carbon fixation capacity, limiting annual biofuel production rates to 40.000-50.000 L ha^{-1} , assuming a light conversion efficiency of 3% and solar conditions of south Europe.[286, 287] As C-independent concept, exploiting PETC-generated reduction equivalents to drive H_2 -production constitutes a promising alternative.[288, 289] Cyanobacteria, such as *Synechocystis*, [80, 290] but also diazotrophic *Anabaena* sp. and *Nostoc* sp., [291] are discussed as suitable hosts for H_2 -production. To realize this idea and assess the potential of photosynthesis-driven H_2 -production, reliable data on cyanobacterial productivity are required.

In this context, the described oxygenase-systems can serve as proxies for (irreversible) withdrawal of photosynthetically generated reduction equivalents. The efficiency of light usage can be expressed as QE (see above) or light conversion efficiency (also: yield on light). While QE relates the amount of incident quanta to amount of product (or biomass formed), light conversion efficiency sets the total input (light) energy in relation to the energy bound in product (or biomass). Chapter 4 exemplifies this approach: Knowing the spectrum of the light source, the amount of incident quanta can accurately be translated into energy using equations 12 and 13. To calculate the amount of energy bound in product and biomass, we used the Gibbs free energy of NADPH (220 kJ mol^{-1}) and previously determined specific energy stored in *Synechocystis* biomass ($21.98 \text{ kJ g}_{\text{CDW}}$, [244]) as assumptions. The maximally achieved light-to-product efficiency was 0.7% sustained for >30 h in the optimized two-enzyme biotransformation.

One option to increase the light-to-product efficiency may be the direction of reductant flux towards product formation instead of CBB/assimilatory processes. Controlling switches, like the small regulatory protein CP12, will be an important for this purpose.[43] While the overall light conversion efficiency (biomass + product) maximally accounted for 4.4%, the redirection of the entire reductant flux towards product formation is not straight forward. Chapters 4 and 5 consistently indicate a positive correlation of biotransformation rates with metabolic turnover,

including a highly operative CBB cycle. Reductant losses towards assimilatory processes and cell maintenance can be expected to limit light-to-product efficiency. As an option, the (photosynthetically) used light may be extended to far-red light, i.e., wavelengths between 700-750. Among phototrophic microorganisms, specialists use the pigments Chlorophyll-*f* and Chlorophyll-*d* for harvesting energy from far-red light.[292] The potential, however, is limited, as the irradiated energy of this spectral range accounts for 6% of that of total surface radiation (see Figure 1), meaning that the exploitable energy amount would increase by maximally 14%.

6.3 Photo-biotechnology tomorrow – potential of cyanobacterial biotechnology

6.3.1 Cyanobacteria as potential contributors to energy transition?

Economic feasibility is the decisive factor for the application of biotechnological processes. To replace fossil fuels with renewable energy sources, the energy transition implies large land requirements for renewable electricity production causing land-use conflicts.[293, 294] Although photo-biotechnological processes are fueled by cheap and abundant sunlight and do not necessarily require arable land, land-use efficiency of photo-biotechnological processes has to be considered for future applications.

Recently, Bühler et al. presented an idealized concept of decentralized cyanobacterial “white” H₂ production enabling for up to 700 kg H₂ per 100 m² and year, e.g., on a house roof.[289] However, some of the assumptions are very optimistic:

1. The uptime is estimated to be 8 h per day (i.e. 2920 h per year), while a more accurate assessment would be 1600 h of light intensities above E_k , e.g., for Leipzig, per year.[295]
2. The calculation is based on a cell density of 10 g_{CDW} L⁻¹ in a cultivation system with a light path of 4 cm. In contrast, cell densities of 0.16 – 0.2 g_{CDW} L⁻¹ continuously cultivated in reactors with a light path of 2 cm were found to absorb 90-110 μmol_{photons} m⁻² s⁻¹ in order to supply both cell growth and biotransformation with reductive power generated by the PETC (Chapter 5). Thus, even high light intensities of 2000 μmol_{photons} m⁻² s⁻¹ (= 1000 W m⁻², Chapter 1) would not be sufficient to supply these high cell densities in the envisioned reactor format, and either catalyst concentration or the reactor depth have to be reduced.
3. The assumed electron delivery rate can be translated into specific activities of around 50 U g_{CDW}⁻¹ for H₂-production. While the photosynthetic electron supply rate can meet this requirement on short term, our data indicate that on the long-term only 10-15 U g_{CDW}⁻¹ can stably be withdrawn.

Realistic assumptions would be 1600 h of light intensities at or above 1000 μmol_{photons} m⁻² s⁻¹, which suffice to supply 1 g_{CDW} L⁻¹ in a cultivation system with a light path of 4 cm to sustain H₂-

production of a rate of $15 \text{ U g}_{\text{CDW}}^{-1}$. This results in an annual production of 12 kg H_2 per 100 m^2 , which is around 60-times lower than the above mentioned production rate.

For the production of energy carriers such as H_2 , photo-biotechnology has to compete with light-driven processes already in place, as, for instance, photovoltaics. Photovoltaic (PV) cells mainly consist of mono- or polycrystalline silicon, but also substantial amounts of aluminum and other transition metals.[296] In general, cyanobacterial cells require less expensive/scarcely resources: Cultivation can be realized in conventional bioreactors and cultivation media contain (besides water) major nutrients, i.e., N, P, and S sources, and low amounts of trace elements. The use of cheap fertilizer as growth medium was reported for up-scaling experiments and enabled productivities similar to those under controlled laboratory conditions.[72] Recently, *Synechocystis* was demonstrated to grow on human urine (supplemented with trace elements) at decent rates of 0.06 h^{-1} . [297] Assuming that light-to-product efficiencies achieved with oxygenases can be translated to light-to- H_2 efficiencies and can be increased by a factor of 2, e.g., by electron allocation management and deletion of alternative electron sinks, up to 1.5% of incident light energy may realistically be stored in H_2 . Even then, photo-biotechnology would lack behind by a factor of about 10 compared to conventional PV cells with conversion efficiencies of 15-20% [296, 298], translating to 12-16% in the form of H_2 with 80% efficiency for electrolysis. Table 8 compares PV coupled to electrolysis with the described cyanobacterial H_2 production in terms of conversion efficiency, annual production rate, and the technology readiness level (TRL).

Table 8: Comparison of photovoltaic (PV) cells coupled to electrolysis and light-driven H_2 -production with cyanobacteria.

	PV cells & electrolysis	Light-driven H_2 production
		
<i>Uptime</i> [h a ⁻¹]	800 [299] ^a	1600 [295] ^b
<i>Light-conversion efficiency</i>	12-16% [298] ^c	0.7% ^d
<i>Production</i> [100 m ² a ⁻¹]	14.000 kWh (=420 kg) H_2	12 kg H_2 ^e
<i>Energy product</i>	(Electricity), H_2	H_2
<i>Status/TRL</i>	Commercially available	Applied research/TRL 3

^a – full load hours

^b – hours of light intensity above light saturation point E_k

^c – Conversion efficiency regarding H_2 as product

^d – based on Chapters 4 and 5

^e – based on $1 \text{ g}_{\text{CDW}} \text{ L}^{-1}$ in FP-bioreactors (4 cm light path) and $15 \text{ U g}_{\text{CDW}}^{-1}$ specific H_2 - formation rate

TRL – technology readiness level

This line-up arguably compares the incomparable: Commercially available PV cells outcompete photo-biotechnological approaches in both annual production and conversion

efficiency. With light-driven cyanobacterial H₂-production still being in its infancy, conversion rates and efficiencies are not in place yet, but may increase significantly in future. An important milestone is the recent development of an oxygenase-tolerant hydrogenase in *Synechocystis*.^[201] Next, it has to be shown that production rates achieved with oxygenases can be translated to H₂-production rates in cyanobacteria. Further, studies focusing on outside conditions and catalyst durability for months are necessary to prove the feasibility of the white-H₂-approach for, e.g., a house roof. To conclude, photo-biotechnology plays a minor role in terms of energy carriers as of today, but light-driven H₂-production with cyanobacteria constitutes a valuable field of research to achieve a resource-saving and sustainable energy production in future.

6.3.2 Future developments & applications

Being a rather young research field photo-biotechnology lacks behind, e.g., conventional biotechnology based on heterotrophs, at many levels (see 1.3.1). However, as shown in Chapters 2, 3 and 4 and in other studies,^[73, 79, 81, 92, 190] photo-biotechnological processes are already competitive in terms of specific activities. However, volumetric productivities lack behind, as heterotrophic cells can be cultivated in much higher cell densities due to a higher energy flux density. Bound to light as energy source for both catalyst and product formation, light penetration constitutes a key obstacle for bringing photo-biotechnology to higher TRLs. Due to its importance as discussed above (see 6.3.1.), the land-use efficiency is expected to be decisive for (bio-)technological processes and their application potential. Processes based on heterotrophs and renewables typically are land-intensive regarding their supply with organic carbon and energy sources, e.g. glucose. Brandenburg *et al.* estimated that light-driven production of hydroxyproline from CO₂ with cyanobacterial whole cells can reduce land-use by a factor of 10 compared to glucose-based production in *E. coli*.^[300]

Most promising is the use of cyanobacterial catalysts for oxygenase-based processes: Producing both reductant and O₂ *in situ* in a light-dependent manner is highly suited to overcome limitations observed with heterotrophic catalysts.^[58] As discussed above (6.1.4.), the photosynthetic light reaction supplies both co-substrates at high rates and thereby enables high oxygenation rates. While cyanobacterial catalysts might be of special value for oxygenase-based processes, they also shine as hosts for processes catalyzed by other (redox) enzymes, such as reductases^[79] or hydrogenases.^[288] Furthermore, the ability to produce O₂ *in situ* makes cyanobacteria interesting candidates to supply cofactor-independent enzymatic processes with O₂. This feature can also be exploited in microbial consortia to overcome O₂-limitation of (heterotrophic) partner strains.^[301]

The rather limited state-of-the-art volumetric productivities of cyanobacterial processes can be expected to make them first feasible for stereo- and region-specific oxyfunctionalization

reactions yielding high-value fine chemicals. For instance, light-dependent hydroxylation of testosterone to 15 β -hydroxytestosterone by recombinant *Synechocystis* has been reported to feature twice the specific activity than achieved with *E. coli* harboring the same enzyme.[190] While ϵ -Cl and 6-HA production rates reported in Chapters 3 and 4 are noteworthy for light-driven processes, heterotrophic catalysts outcompete *Synechocystis* in terms of volumetric productivity by a factor of 4 to 10.[165, 238] The elaborate implementation of a multi-step cascade in *Pseudomonas* starting from Chx as enabled the production of 6-aminohexanoic acid[166] or adipic acid[238] via the combination of seven enzymatic steps in a one-pot synthesis. Undeniably, photo-biotechnology heading towards this very promising direction, with the *in vivo* redox cascade described in Chapter 4 and the dhurrin pathway[72] representing first examples of presumably many more to come. In this context, studies on artificial scaffolds are encouraging, potentially enabling the organization of several enzymes to improve atom efficiency and overall conversion rates.[302]

While the current chemical and energy industries heavily rely on fossil feedstocks, the overall concept of photo-biotechnology brings about highly sustainable options, relying on renewable energy and electron sources, which may be combined with innovative and state-of-the-art (electro-)chemistry. Morejón et al. recently reported a combined electro-bio-synthesis approach to produce adipic acid from biogenic lignin.[303] The use of biogenic substrate stocks is also applicable in phototrophs to contribute to a (bio-based and sustainable) circular bio-economy.

Focusing on biocatalytic processes, this thesis lays the foundation for the light-driven production not only of fine, specialty, and bulk chemicals, such as polymer precursors, but potentially also of energy carriers. However, the results indicate that photo-biotechnological processes up to now depend on coupled C-fixation to a significant extent. Hence, native pathways can be readily exploited for C-based production of high-value products, such as astaxanthin, a pigment used in food industry.[304, 305] Cyanobacterial strains, such as *Spirulina*, is widely used for food and feed additives[306] and further use of cyanobacteria is to be expected in future.[65] From an light- and cost-efficiency perspective, it is necessary to also make use of the formed biomass with biofertilizer or functional food[307] as attractive options for the dual-use of photo-biotechnological processes. A strong focus on the elucidation of metabolic and regulatory networks including redox and energy balancing will be required to further improve growth-decoupled and efficient usage of photosynthetically generated redox power.

6.4. Conclusions & Outlook

Regarding volumetric productivities and overall product titers, photosynthesis-driven biotechnological processes lack behind conventional biotechnology with heterotrophs, which to date limits their feasibility. For light-driven oxygenase catalysis, this work deciphers limitations in terms of heterologous enzyme levels, reactant inhibition, and reductant supply by the photosynthetic apparatus. Substantial progress was made in detailing electron routes from PS I to a heterologous CYP, overall disclosing a versatile set of electron carriers in *Synechocystis* facilitating electron supply and making this strain a suitable host for light-driven redox biocatalysis. With the introduction of an *Acidovorax* BVMO, a second highly active oxygenase system was established in *Synechocystis* and optimized by increasing expression levels and controlling by-product formation and reactant inhibition. With the development of an artificial *in vivo* cascade in *Synechocystis* by co-expressing a lactonase gene together with the BVMO gene, product inhibition, identified as key limitation, was overcome. The optimized two-enzyme system achieved activities of up to $63.1 \pm 1.0 \text{ U g}_{\text{CDW}}^{-1}$, which is unprecedentedly high for oxygenases in cyanobacteria. With this system, the metabolic capacity of reductant supply was found to limit light-driven redox biocatalysis, especially on the long term.

To increase conversion rates and light usage efficiencies, engineering the photosynthetic metabolism and its regulation to direct electron fluxes towards product formation will be key. Controlling reductant allocation with tools like the small regulatory protein CP12, but also fine-tuning of electron pathways other than the CBB cycle, such as Flv1/3, will be important for balancing intracellular ATP/NADPH levels and with that, sustaining electron consuming biotransformations. To this end, emerging molecular biology tools, tailor-made for cyanobacteria, such as the demonstrated Golden Gate cloning system and CRISPRi approaches to fine-tune expression levels are expected to significantly facilitate respective endeavors. The cascade approach presented in this thesis can only be a start to more elaborate and powerful enzyme cascades in cyanobacteria: Supported by enzyme scaffolding, more sophisticated and efficient conversions can be expected to be linked to and fueled by the photosynthetic apparatus. This progress at the molecular biology level needs to be complemented by biocatalyst and reaction engineering including reactor design to overcome the main limitation of light supply and penetration. In this context, the application of robust and long-living, but also catalytically active biofilms is highly promising. To demonstrate their technical feasibility, the scale-up of photo-biotechnological processes to pilot scale will be decisive to bring presented processes from TRL 3 to TRL 6 or higher.

References

1. Lee, H., et al., Climate Change 2023: Synthesis report. Contribution of working groups I, II and III to the sixth assessment report of the Intergovernmental Climate Change. **2023**, IPCC, Geneva, Switzerland. p. 35-135.
2. Kopp, G. and J.L. Lean, A new, lower value of total solar irradiance: Evidence and climate significance. *Geophys Res Lett*, **2011**. 38(1).
3. Davenport, J. and N. Wayth, Statistical review of world energy. **2023**, Energy institute: London, United Kingdom.
4. Williams, D.R. Earth Fact Sheet. **2023**; Available from: <https://nssdc.gsfc.nasa.gov/planetary/factsheet/earthfact.html>.
5. Wehli, C., Extraterrestrial solar spectrum. **1985**, World Radiation Center: Davos Dorf, Switzerland.
6. Gueymard, C.A., The sun's total and spectral irradiance for solar energy applications and solar radiation models. *Sol Energy*, **2004**. 76(4): p. 423-453.
7. Heldt, H.-W. and B. Piechulla, Pflanzenbiochemie. Vol. 5. **2015**, Berlin Heidelberg: Springer Spektrum.
8. Barber, J., Photosynthetic energy conversion: natural and artificial. *Chem Soc Rev*, **2009**. 38(1): p. 185-96.
9. Fournier, G.P., et al., The Archean origin of oxygenic photosynthesis and extant cyanobacterial lineages. *Proc Royal Soc B*, **2021**. 288(1959): p. 20210675.
10. Falkowski, P.G. and Y. Isozaki, The Story of O₂. *Science*, **2008**. 322(5901): p. 540-542.
11. Gould, S.B., R.F. Waller, and G.I. McFadden, Plastid evolution. *Annu Rev Plant Biol*, **2008**. 59: p. 491-517.
12. Hill, R. and F.A.Y. Bendall, Function of the two cytochrome components in chloroplasts: A working hypothesis. *Nature*, **1960**. 186(4719): p. 136-137.
13. Adir, N., Elucidation of the molecular structures of components of the phycobilisome: reconstructing a giant. *Photosynth Res*, **2005**. 85(1): p. 15-32.
14. Komenda, J., R. Sobotka, and P.J. Nixon, Assembling and maintaining the Photosystem II complex in chloroplasts and cyanobacteria. *Curr Opin Plant Biol*, **2012**. 15(3): p. 245-251.
15. Fromme, P., et al., Structure of photosystems I and II. *C R Chim*, **2006**. 9(2): p. 188-200.
16. Wormit, M. and A. Dreuw, Quantum chemical insights in energy dissipation and carotenoid radical cation formation in light harvesting complexes. *PCCP*, **2007**. 9(23): p. 2917-2931.
17. Renger, G., Oxidative photosynthetic water splitting: energetics, kinetics and mechanism. *Photosynth Res*, **2007**. 92(3): p. 407-425.
18. Malone, L.A., et al., Cytochrome b₆f – Orchestrator of photosynthetic electron transfer. *Biochim Biophys Acta Bioenerg*, **2021**. 1862(5): p. 148380.
19. Cramer, W.A., et al., Transmembrane traffic in the cytochrome b₆f complex. *Annu Rev Biochem*, **2006**. 75: p. 769-90.
20. Amunts, A., O. Drory, and N. Nelson, The structure of a plant photosystem I supercomplex at 3.4 Å resolution. *Nature*, **2007**. 447(7140): p. 58-63.
21. Kannchen, D., et al., Remodeling of photosynthetic electron transport in *Synechocystis* sp. PCC 6803 for future hydrogen production from water. *Biochim Biophys Acta Bioenerg*, **2020**. 1861.
22. Walker, D.A., The Z-scheme-down hill all the way. *Trends Plant Sci*, **2002**. 7(4): p. 183-5.
23. Kramer, D.M., J.A. Cruz, and A. Kanazawa, Balancing the central roles of the thylakoid proton gradient. *Trends Plant Sci*, **2003**. 8(1): p. 27-32.

24. Nikkanen, L., et al., Regulatory electron transport pathways of photosynthesis in cyanobacteria and microalgae: Recent advances and biotechnological prospects. *Physiol Plant*, **2021**. 173(2): p. 514-525.
25. Kramer, D.M. and J.R. Evans, The importance of energy balance in improving photosynthetic productivity. *Plant Physiol*, **2011**. 155(1): p. 70-8.
26. Bassham, J.A., et al., The path of carbon in photosynthesis. XXI. The cyclic regeneration of carbon dioxide acceptor1. *J Am Chem Soc*, **1954**. 76(7): p. 1760-1770.
27. Weissbach, A., B.L. Horecker, and J. Hurwitz, The enzymatic formation of phosphoglyceric acid from ribulose diphosphate and carbon dioxide. *J Biol Chem*, **1956**. 218(2): p. 795-810.
28. Hurwitz, J., et al., Spinach phosphoribulosekinase. *J Biol Chem*, **1956**. 218(2): p. 769-783.
29. Nogales, J., et al., Detailing the optimality of photosynthesis in cyanobacteria through systems biology analysis. *PNAS USA*, **2012**. 109(7): p. 2678-83.
30. Allen, J.F., Cyclic, pseudocyclic and noncyclic photophosphorylation: new links in the chain. *Trends Plant Sci*, **2003**. 8(1): p. 15-19.
31. Asada, K., The water-water cycle in chloroplasts: Scavenging of active oxygens and dissipation of excess photons. *Annu Rev Plant Physiol Plant Mol Biol*, **1999**. 50: p. 601-639.
32. Sachdev, S., et al., Abiotic stress and reactive oxygen species: Generation, signaling, and defense mechanisms. *Antioxidants*, **2021**. 10(2).
33. Mullineaux, C.W., Electron transport and light-harvesting switches in cyanobacteria. *Front Plant Sci*, **2014**. 5: p. 7.
34. Theune, M.L., et al., *In vivo* quantification of electron flow through photosystem I - Cyclic electron transport makes up about 35% in a cyanobacterium. *Biochim Biophys Acta Bioenerg*, **2021**. 1862(3): p. 148353.
35. Luimstra, V.M., et al., Exploring the low photosynthetic efficiency of cyanobacteria in blue light using a mutant lacking phycobilisomes. *Photosynth Res*, **2019**. 141(3): p. 291-301.
36. Schurmann, P. and B.B. Buchanan, The ferredoxin/thioredoxin system of oxygenic photosynthesis. *Antioxid Redox Signal*, **2008**. 10(7): p. 1235-74.
37. Mallén-Ponce, M.J., et al., Depletion of m-type thioredoxin impairs photosynthesis, carbon fixation, and oxidative stress in cyanobacteria. *Plant Physiol*, **2021**. 187(3): p. 1325-1340.
38. Alfonso, M., et al., Redox control of psbA expression in cyanobacteria *Synechocystis* strains. *J Photochem Photobiol B*, **1999**. 48(2): p. 104-113.
39. Allen, J.F., Thylakoid protein phosphorylation, state 1-state 2 transitions, and photosystem stoichiometry adjustment: redox control at multiple levels of gene expression. *Physiol Plant*, **1995**. 93(1): p. 196-205.
40. Schuurmans, R.M., et al., The redox potential of the plastoquinone pool of the cyanobacterium *Synechocystis* species strain PCC 6803 is under strict homeostatic control. *Plant Physiol*, **2014**. 165(1): p. 463-75.
41. Feilke, K., G. Ajlani, and A. Krieger-Liszky, Overexpression of plastid terminal oxidase in *Synechocystis* sp. PCC 6803 alters cellular redox state. *Philos Trans R Soc Lond B Biol Sci*, **2017**. 372(1730).
42. Davis, G.A., et al., Limitations to photosynthesis by proton motive force-induced photosystem II photodamage. *eLife*, **2016**. 5.
43. McFarlane, C.R., et al., Structural basis of light-induced redox regulation in the Calvin-Benson cycle in cyanobacteria. *PNAS USA*, **2019**. 116(42): p. 20984-20990.
44. Brandenburg, F. and S. Klähn, Small but smart: On the diverse role of small proteins in the regulation of cyanobacterial metabolism. *Life (Basel)*, **2020**. 10(12).
45. Allahverdiyeva, Y., et al., Cyanobacterial oxygenic photosynthesis is protected by flavodiiron proteins. *Life (Basel)*, **2015**. 5(1): p. 716-43.
46. Thiel, K., et al., Redirecting photosynthetic electron flux in the cyanobacterium *Synechocystis* sp. PCC 6803 by the deletion of flavodiiron protein Flv3. *Microb Cell Fact*, **2019**. 18(1): p. 189.

47. Jakob, T., et al., A complete energy balance from photons to new biomass reveals a light- and nutrient-dependent variability in the metabolic costs of carbon assimilation. *J Exp Bot*, **2007**. 58(8): p. 2101-12.
48. Wilhelm, C. and D. Selmar, Energy dissipation is an essential mechanism to sustain the viability of plants: The physiological limits of improved photosynthesis. *J Plant Physiol*, **2011**. 168(2): p. 79-87.
49. Schmid, A., et al., Industrial biocatalysis today and tomorrow. *Nature*, **2001**. 409(6817): p. 258-68.
50. Burk, M.J. and S. Van Dien, Biotechnology for chemical production: Challenges and opportunities. *Trends Biotechnol*, **2016**. 34(3): p. 187-190.
51. Bornscheuer, U.T., et al., Engineering the third wave of biocatalysis. *Nature*, **2012**. 485(7397): p. 185-194.
52. Schrewe, M., et al., Whole-cell biocatalysis for selective and productive C-O functional group introduction and modification. *Chem Soc Rev*, **2013**. 42(15): p. 6346-77.
53. Law, H.E.M., et al., Process limitations in a whole-cell catalysed oxidation: Sensitivity analysis. *Chem Eng Sci*, **2006**. 61: p. 6646-6652.
54. Kadisch, M., et al., Maximizing the stability of metabolic engineering-derived whole-cell biocatalysts. *Biotechnol J*, **2017**. 12(8): p. 1600170.
55. Cornelissen, S., et al., Whole-cell-based CYP153A6-catalyzed (S)-limonene hydroxylation efficiency depends on host background and profits from monoterpene uptake via AlkL. *Biotechnol Bioeng*, **2013**. 110(5): p. 1282-92.
56. Baldwin, C.V. and J.M. Woodley, On oxygen limitation in a whole cell biocatalytic Baeyer-Villiger oxidation process. *Biotechnol Bioeng*, **2006**. 95(3): p. 362-9.
57. Hoschek, A., A. Schmid, and B. Bühler, In situ O₂ generation for biocatalytic oxyfunctionalization reactions. *Chem Cat Chem*, **2018**. 10(23): p. 5366-5371.
58. Hoschek, A., B. Bühler, and A. Schmid, Overcoming the gas-liquid mass transfer of oxygen by coupling photosynthetic water oxidation with biocatalytic oxyfunctionalization. *Angew Chem Int Ed Engl*, **2017**. 56(47): p. 15146-15149.
59. Jodlbauer, J., et al., Biocatalysis in green and blue: cyanobacteria. *Trends Biotechnol*, **2021**. 39: p. 875-889.
60. Cheng, M.-H., et al., The costs of sugar production from different feedstocks and processing technologies. *Biofuel Bioprod Biorefin*, **2019**. 13(3): p. 723-739.
61. Brandenburg, F., et al., *Trans*-4-hydroxy-L-proline production by the cyanobacterium *Synechocystis* sp. PCC 6803. *Metab Eng Commun*, **2021**. 12: p. e00155.
62. Heidorn, T., et al., Synthetic biology in cyanobacteria: engineering and analyzing novel functions. *Meth Enzymol*, **2011**. 497.
63. Xia, P.F., et al., Synthetic biology toolkits for metabolic engineering of cyanobacteria. *Biotechnol J*, **2019**. 14(6): p. e1800496.
64. Vasudevan, R., et al., CyanoGate: A modular cloning suite for engineering cyanobacteria based on the plant MoClo syntax. *Plant Physiol*, **2019**. 180(1): p. 39-55.
65. Branco Dos Santos, F., W. Du, and K.J. Hellingwerf, *Synechocystis*: Not just a plug-bug for CO₂, but a green *E. coli*. *Front bioeng biotechnol*, **2014**. 2: p. 36-36.
66. Kaneko, T., et al., Sequence analysis of the genome of the unicellular cyanobacterium *Synechocystis* sp. strain PCC6803. II. Sequence determination of the entire genome and assignment of potential protein-coding regions *DNA Res*, **1996**. 3(3): p. 185-209.
67. Sengupta, A., et al., The effect of CO₂ in enhancing photosynthetic cofactor recycling for alcohol dehydrogenase mediated chiral synthesis in cyanobacteria. *J Biotechnol*, **2019**. 289: p. 1-6.
68. Lassen, L.M., et al., Anchoring a plant cytochrome P450 via PsaM to the thylakoids in *Synechococcus* sp. PCC 7002: evidence for light-driven biosynthesis. *PLoS One*, **2014**. 9(7): p. e102184.
69. Yu, J., et al., *Synechococcus elongatus* UTEX 2973, a fast growing cyanobacterial chassis for biosynthesis using light and CO₂. *Sci Rep*, **2015**. 5: p. 8132.
70. Włodarczyk, A., et al., Newly discovered *Synechococcus* sp. PCC 11901 is a robust cyanobacterial strain for high biomass production. *Commun Biol*, **2020**. 3(1): p. 215.

71. Löwe, J., et al., Providing reducing power by microalgal photosynthesis: a novel perspective towards sustainable biocatalytic production of bulk chemicals exemplified for aliphatic amines. *Sci Rep*, **2018**. 8(1): p. 10436.
72. Włodarczyk, A., et al., Metabolic engineering of light-driven cytochrome P450 dependent pathways into *Synechocystis* sp. PCC 6803. *Metab Eng*, **2015**. 33: p. 1-11.
73. Berepiki, A., et al., Tapping the unused potential of photosynthesis with a heterologous electron sink. *ACS Synth Biol*, **2016**. 5(12): p. 1369-1375.
74. Hoschek, A., et al., Light-dependent and aeration-independent gram-scale hydroxylation of cyclohexane to cyclohexanol by CYP450 harboring *Synechocystis* sp. PCC 6803. *Biotechnol J*, **2019**. 14(8): p. e1800724.
75. Hoschek, A., B. Bühler, and A. Schmid, Stabilization and scale-up of photosynthesis-driven ω -hydroxylation of nonanoic acid methyl ester by two-liquid phase whole-cell biocatalysis. *Biotechnol Bioeng*, **2019**. 116(8): p. 1887-1900.
76. Mellor, S.B., et al., Defining optimal electron transfer partners for light-driven cytochrome P450 reactions. *Metab Eng*, **2019**. 55: p. 33-43.
77. Cassier-Chauvat, C. and F. Chauvat, Function and regulation of ferredoxins in the cyanobacterium *Synechocystis* PCC6803: recent advances. *Life (Basel)*, **2014**. 4(4): p. 666-80.
78. Böhmer, S., et al., Enzymatic oxyfunctionalization driven by photosynthetic water-splitting in the cyanobacterium *Synechocystis* sp. PCC 6803. *Catal*, **2017**. 7(8).
79. Assil-Companiononi, L., et al., Engineering of NADPH supply boosts photosynthesis-driven biotransformations. *ACS Catal*, **2020**. 10(20): p. 11864-11877.
80. Appel, J., et al., Cyanobacterial *in vivo* solar hydrogen production using a photosystem I-hydrogenase (PsaD-HoxYH) fusion complex. *Nat Energy*, **2020**. 5: p. 458-467.
81. Mellor, S.B., et al., Photosynthetic fuel for heterologous enzymes: the role of electron carrier proteins. *Photosynth Res*, **2017**. 134(3): p. 329-342.
82. Li, Z., et al., Engineering cytochrome P450 enzyme systems for biomedical and biotechnological applications. *J Biol Chem*, **2020**. 295(3): p. 833-849.
83. Kanygin, A., et al., Rewiring photosynthesis: a photosystem I-hydrogenase chimera that makes H₂ *in vivo*. *Energy Environ Sci*, **2020**. 13(9): p. 2903-2914.
84. Berepiki, A., et al., Rational engineering of photosynthetic electron flux enhances light-powered cytochrome P450 activity. *Synth Biol*, **2018**. 3(1): p. ysy009.
85. Santos-Merino, M., et al., Improved photosynthetic capacity and photosystem I oxidation via heterologous metabolism engineering in cyanobacteria. *PNAS USA*, **2021**. 118 (11)(11): p. e2021523118.
86. Lin, B. and Y. Tao, Whole-cell biocatalysts by design. *Microb Cell Fact*, **2017**. 16(1): p. 106.
87. Zheng, L., et al., Using algae cells to drive cofactor regeneration and asymmetric reduction for the synthesis of chiral chemicals. *Algal Res*, **2018**. 35: p. 432-438.
88. Khan, S., et al., Enhanced whole-cell biotransformation of 3-chloropropiophenone into 1-phenyl-1-propanone by hydrogel entrapped *Chlorella emersonii* 211.8b. *Biotechnol Lett*, **2021**. 43(12): p. 2259-2272.
89. Gröger, H., Biocatalytic concepts for synthesizing amine bulk chemicals: recent approaches towards linear and cyclic aliphatic primary amines and omega-substituted derivatives thereof. *Appl Microbiol Biotechnol*, **2019**. 103(1): p. 83-95.
90. Park, J. and Y. Choi, Cofactor engineering in cyanobacteria to overcome imbalance between NADPH and NADH: A mini review. *Front Chem Sci Eng*, **2017**. 11(1): p. 66-71.
91. Wang, M., et al., Cofactor engineering for more efficient production of chemicals and biofuels. *Biotechnol Adv*, **2017**. 35(8): p. 1032-1039.
92. Angermayr, S.A., M. Paszota, and K.J. Hellingwerf, Engineering a cyanobacterial cell factory for production of lactic acid. *Appl Environ Microbiol*, **2012**. 78(19): p. 7098-106.
93. Purdy, H.M., B.F. Pflieger, and J.L. Reed, Introduction of NADH-dependent nitrate assimilation in *Synechococcus* sp. PCC 7002 improves photosynthetic production of 2-methyl-1-butanol and isobutanol. *Metab Eng*, **2022**. 69: p. 87-97.

94. Jodlbauer, J., et al., Biocatalysis in green and blue: cyanobacteria. *Trends Biotechnol*, **2021**.
95. Hobisch, M., et al., Internal illumination to overcome the cell density limitation in the scale-up of whole-cell photobiocatalysis. *ChemSusChem*, **2021**. 14(15): p. 3219-3225.
96. Büchsenschütz, H.C., et al., Stereoselective biotransformations of cyclic Imines in recombinant cells of *Synechocystis* sp. PCC 6803. *ChemCatChem*, **2020**. 12(3): p. 726-730.
97. Pedersen, A.T., G. Rehn, and J.M. Woodley, Oxygen transfer rates and requirements in oxidative biocatalysis, in *Comput Aided Chem Eng*, K.V. Gernaey, J.K. Huusom, and R. Gani, Editors. **2015**, Elsevier. p. 2111-2116.
98. Hoschek, A., et al., Mixed-species biofilms for high-cell-density application of *Synechocystis* sp. PCC 6803 in capillary reactors for continuous cyclohexane oxidation to cyclohexanol. *Bioresour Technol*, **2019**. 282: p. 171-178.
99. Heuschkel, I., et al., Data on mixed trophies biofilm for continuous cyclohexane oxidation to cyclohexanol using *Synechocystis* sp. PCC 6803. *Data Brief*, **2019**. 25: p. 104059.
100. Berger, R.G., Biotechnology of flavours - the next generation. *Biotechnol Lett*, **2009**. 31(11): p. 1651-1659.
101. Berger, R.G., Biotechnology as a source of natural volatile flavours. *Curr Opin Food Sci*, **2015**. 1: p. 38-43.
102. Bassanini, I., et al., Biocatalysis with laccases: An updated overview. *Catal*, **2021**. 11(1): p. 26.
103. Afreen, S., et al., A novel multicopper oxidase (laccase) from cyanobacteria: Purification, characterization with potential in the decolorization of anthraquinonic dye. *PLoS One*, **2017**. 12(4): p. e0175144.
104. Liang, Y., et al., Textile dye decolorizing *Synechococcus* PCC7942 engineered with CotA laccase. *Front Bioeng Biotechnol*, **2018**. 6.
105. Bolton, J.R., Photochemical conversion and storage of solar energy. *J Solid State Chem*, **1977**. 22(1): p. 3-8.
106. Melis, A., Solar energy conversion efficiencies in photosynthesis: Minimizing the chlorophyll antennae to maximize efficiency. *Plant Sci*, **2009**. 177(4): p. 272-280.
107. Liu, X., et al., Current advances in engineering cyanobacteria and their applications for photosynthetic butanol production. *Curr Opin Biotechnol*, **2022**. 73: p. 143-150.
108. Oliver, J.W.K. and S. Atsumi, A carbon sink pathway increases carbon productivity in cyanobacteria. *Metab Eng*, **2015**. 29: p. 106-112.
109. Savakis, P., et al., Photosynthetic production of glycerol by a recombinant cyanobacterium. *J Biotechnol*, **2015**. 195: p. 46-51.
110. Ducat, D.C., et al., Rerouting carbon flux to enhance photosynthetic productivity. *Appl Environ Microbiol*, **2012**. 78(8): p. 2660-8.
111. Abramson, B.W., et al., Increased photochemical efficiency in cyanobacteria via an engineered sucrose sink. *Plant Cell Physiol*, **2016**. 57(12): p. 2451-2460.
112. Grund, M., et al., Heterologous lactate synthesis in *Synechocystis* sp. strain PCC 6803 causes a growth condition-dependent carbon sink effect. *Appl Environ Microbiol*, **2022**. 88(8).
113. Wilhelm, C. and H. Wagner, 6 Rate-limiting steps in algal energy conversion from sunlight to products – the role of photosynthesis, in *Photosynthesis*, R. Matthias, Editor. **2021**, De Gruyter: Berlin, Boston. p. 149-174.
114. Zavrel, T., et al., Quantitative insights into the cyanobacterial cell economy. *eLife*, **2019**. 8.
115. Kauny, J. and P. Setif, NADPH fluorescence in the cyanobacterium *Synechocystis* sp. PCC 6803: a versatile probe for in vivo measurements of rates, yields and pools. *Biochim Biophys Acta*, **2014**. 1837(6): p. 792-801.
116. Zavrel, T., et al., Characterization of a model cyanobacterium *Synechocystis* sp. PCC 6803 autotrophic growth in a flat-panel photobioreactor. *Eng Life Sci*, **2015**. 15(1): p. 122-132.

117. Ungerer, J., et al., Adjustments to photosystem stoichiometry and electron transfer proteins are key to the remarkably fast growth of the cyanobacterium *Synechococcus elongatus* UTEX 2973. *mBio*, **2018**. 9(1): p. e02327-17.
118. Langner, U., et al., An energy balance from absorbed photons to new biomass for *Chlamydomonas reinhardtii* and *Chlamydomonas acidophila* under neutral and extremely acidic growth conditions. *Plant Cell Environ*, **2009**. 32(3): p. 250-8.
119. Boyle, N.R. and J.A. Morgan, Flux balance analysis of primary metabolism in *Chlamydomonas reinhardtii*. *BMC Syst Biol*, **2009**. 3: p. 4-4.
120. Wagner, H., T. Jakob, and C. Wilhelm, Balancing the energy flow from captured light to biomass under fluctuating light conditions. *New Phytol*, **2006**. 169(1): p. 95-108.
121. Schuurmans, R.M., et al., Comparison of the photosynthetic yield of cyanobacteria and green algae: Different methods give different answers. *PLoS One*, **2015**. 10(9): p. e0139061.
122. Su, W., T. Jakob, and C. Wilhelm, The impact of nonphotochemical quenching of fluorescence on the photon balance in diatoms under dynamic light conditions. *J Phycol*, **2012**. 48(2): p. 336-46.
123. Allakhverdiev, S.I., et al., Redox potentials of primary electron acceptor quinone molecule (QA)- and conserved energetics of photosystem II in cyanobacteria with chlorophyll a and chlorophyll d. *PNAS USA*, **2011**. 108(19): p. 8054-8.
124. Antal, T.K., et al., Photosynthesis-related quantities for education and modeling. *Photosynth Res*, **2013**. 117(1): p. 1-30.
125. Cammack, R., et al., Midpoint redox potentials of plant and algal ferredoxins. *Biochemical J*, **1977**. 168(2): p. 205-209.
126. Zhang, B., J. Wu, and F. Meng, Adaptive laboratory evolution of microalgae: A review of the regulation of growth, stress resistance, metabolic processes, and biodegradation of pollutants. *Front Microbiol*, **2021**. 12(2401).
127. Srivastava, V., et al., Adaptive laboratory evolution of the fast-growing cyanobacterium *Synechococcus elongatus* PCC 11801 for improved solvent tolerance. *J Biosci Bioeng*, **2021**. 131(5): p. 491-500.
128. LaPanse, A.J., A. Krishnan, and M.C. Posewitz, Adaptive Laboratory Evolution for algal strain improvement: methodologies and applications. *Algal Research*, **2021**. 53: p. 102122.
129. Dann, M., et al., Enhancing photosynthesis at high light levels by adaptive laboratory evolution. *Nat Plants*, **2021**. 7(5): p. 681-695.
130. Mukherjee, B., S. Madhu, and P.P. Wangikar, The role of systems biology in developing non-model cyanobacteria as hosts for chemical production. *Curr Opin Biotechnol*, **2020**. 64: p. 62-69.
131. Muramatsu, M. and Y. Hihara, Acclimation to high-light conditions in cyanobacteria: from gene expression to physiological responses. *J Plant Res*, **2012**. 125(1): p. 11-39.
132. Canonico, M., et al., Gradual response of cyanobacterial thylakoids to acute high-light stress - importance of carotenoid accumulation. *Cells*, **2021**. 10(8): p. 1916.
133. Bao, H., M.R. Melnicki, and C.A. Kerfeld, Structure and functions of orange carotenoid protein homologs in cyanobacteria. *Curr Plant Biol*, **2017**. 37: p. 1-9.
134. Magdaong, N.C.M. and R.E. Blankenship, Photoprotective, excited-state quenching mechanisms in diverse photosynthetic organisms. *J Biol Chem*, **2018**. 293(14): p. 5018-5025.
135. Lee, M.E., et al., A highly characterized yeast toolkit for modular, multipart assembly. *ACS Synth Biol*, **2015**. 4(9): p. 975-986.
136. Moore, S.J., et al., EcoFlex: A multifunctional MoClo Kit for *E. coli* synthetic biology. *ACS Synth Biol*, **2016**. 5(10): p. 1059-1069.
137. Li, Y., et al., Metabolic engineering of *Escherichia coli* using CRISPR-Cas9 mediated genome editing. *Metab Eng*, **2015**. 31: p. 13-21.
138. Doudna, J.A. and E. Charpentier, Genome editing. The new frontier of genome engineering with CRISPR-Cas9. *Science*, **2014**. 346(6213): p. 1258096.

139. Pattharaprachayakul, N., et al., Current understanding of the cyanobacterial CRISPR-Cas systems and development of the synthetic CRISPR-Cas systems for cyanobacteria. *Enzyme Microb Technol*, **2020**. 140: p. 109619.
140. Patel, V.K., et al., Recent progress and challenges in CRISPR-Cas9 engineered algae and cyanobacteria. *Algal Res*, **2023**. 71: p. 103068.
141. Huang, H.H., et al., Design and characterization of molecular tools for a synthetic biology approach towards developing cyanobacterial biotechnology. *Nucleic Acids Res*, **2010**. 38(8): p. 2577-93.
142. Ferreira, E.A., et al., Expanding the toolbox for *Synechocystis* sp. PCC 6803: validation of replicative vectors and characterization of a novel set of promoters. *Synth Biol*, **2018**. 3(1).
143. Camsund, D. and P. Lindblad, Engineered transcriptional systems for cyanobacterial biotechnology. *Front Bioeng Biotechnol*, **2014**. 2: p. 40.
144. Englund, E., et al., Metabolic engineering of *Synechocystis* sp. PCC 6803 for production of the plant diterpenoid manoyl oxide. *ACS Synth Biol*, **2015**. 4(12): p. 1270-8.
145. Thiel, K., et al., Translation efficiency of heterologous proteins is significantly affected by the genetic context of RBS sequences in engineered cyanobacterium *Synechocystis* sp. PCC 6803. *Microb Cell Fact*, **2018**. 17(1): p. 34.
146. Zhou, J., et al., Discovery of a super-strong promoter enables efficient production of heterologous proteins in cyanobacteria. *Sci Rep*, **2014**. 4: p. 4500.
147. Till, P., et al., Regulatory systems for gene expression control in cyanobacteria. *Appl Microbiol Biotechnol*, **2020**. 104(5): p. 1977-1991.
148. Mitschke, J., et al., An experimentally anchored map of transcriptional start sites in the model cyanobacterium *Synechocystis* sp. PCC 6803. *PNAS USA*, **2011**. 108(5): p. 2124-9.
149. Yao, L., et al., Multiple gene repression in cyanobacteria using CRISPRi. *ACS Synth Biol*, **2016**. 5(3): p. 207-212.
150. Yao, L., et al., Pooled CRISPRi screening of the cyanobacterium *Synechocystis* sp. PCC 6803 for enhanced industrial phenotypes. *Nat Commun*, **2020**. 11(1): p. 1666.
151. Francis, D.M. and R. Page, Strategies to optimize protein expression in *E. coli*. *Curr Protoc Protein Sci*, **2010**. Chapter 5(1): p. 5.24.1-5.24.29.
152. Bolay, P., et al., The distinctive regulation of cyanobacterial glutamine synthetase. *Life (Basel)*, **2018**. 8(4).
153. Watzer, B., et al., The signal transduction protein PII controls ammonium, nitrate and urea uptake in cyanobacteria. *Front Microbiol*, **2019**. 10.
154. Kato, N., et al., Dual redox regulation of the DNA-binding activity of the response regulator RpaB in the cyanobacterium *Synechocystis* sp. PCC 6803. *Plant Cell Physiol*, **2022**. 63(8): p. 1078-1090.
155. Gurrieri, L., et al., Calvin–Benson cycle regulation is getting complex. *Trends Plant Sci*, **2021**. 26(9): p. 898-912.
156. Klähn, S., et al., A glutamine riboswitch is a key element for the regulation of glutamine synthetase in cyanobacteria. *Nucleic Acids Res*, **2018**. 46(19): p. 10082-10094.
157. Jensen, K., P.E. Jensen, and B.L. Moller, Light-driven cytochrome P450 hydroxylations. *ACS Chem Biol*, **2011**. 6(6): p. 533-9.
158. O'Keefe, D.P., et al., Plant expression of a bacterial cytochrome P450 that catalyzes activation of a sulfonylurea pro-herbicide. *Plant Physiol*, **1994**. 105(2): p. 473-482.
159. Shimakawa, G., A. Kohara, and C. Miyake, Characterization of light-enhanced respiration in cyanobacteria. *Int J Mol Sci*, **2020**. 22(1).
160. Angermayr, S.A., A. Gorchs Rovira, and K.J. Hellingwerf, Metabolic engineering of cyanobacteria for the synthesis of commodity products. *Trends Biotechnol*, **2015**. 33(6): p. 352-61.
161. Grund, M., et al., Electron balancing under different sink conditions reveals positive effects on photon efficiency and metabolic activity of *Synechocystis* sp. PCC 6803. *Biotechnol Biofuels*, **2019**. 12: p. 43.

162. Volmer, J., et al., Engineering of *Pseudomonas taiwanensis* VLB120 for constitutive solvent tolerance and increased specific styrene epoxidation activity. *Appl Environ Microbiol*, **2014**. 80(20): p. 6539-48.
163. Schalck, T., B.V.D. Bergh, and J. Michiels, Increasing solvent tolerance to improve microbial production of alcohols, terpenoids and aromatics. *Microorganisms*, **2021**. 9(2).
164. Karande, R., et al., Biocatalytic conversion of cycloalkanes to lactones using an in-vivo cascade in *Pseudomonas taiwanensis* VLB120. *Biotechnol Bioeng*, **2018**. 115(2): p. 312-320.
165. Schäfer, L., et al., Rational engineering of a multi-step biocatalytic cascade for the conversion of cyclohexane to polycaprolactone monomers in *Pseudomonas taiwanensis*. *Biotechnol J*, **2020**: p. e2000091.
166. Bretschneider, L., et al., One-pot synthesis of 6-aminohexanoic acid from cyclohexane using mixed-species cultures. *Microb Biotechnol*, **2021**. 14(3): p. 1011-1025.
167. Johnson, T.J., et al., Photobioreactor cultivation strategies for microalgae and cyanobacteria. *Biotechnol Prog*, **2018**. 34(4): p. 811-827.
168. Kirnev, P.C.S., et al., Technological mapping and trends in photobioreactors for the production of microalgae. *World J Microbiol Biotechnol*, **2020**. 36(3): p. 42.
169. Chanquia, S.N., G. Vernet, and S. Kara, Photobioreactors for cultivation and synthesis: Specifications, challenges, and perspectives. *Eng Life Sci*, **2022**. 22(12): p. 712-724.
170. Heining, M., et al., Internal illumination of photobioreactors via wireless light emitters: a proof of concept. *J Appl Phycol*, **2015**. 27(1): p. 59-66.
171. Li, T., M. Strous, and M. Melkonian, Biofilm-based photobioreactors: their design and improving productivity through efficient supply of dissolved inorganic carbon. *FEMS Microbiol Lett*, **2017**. 364(24).
172. Léonard, A., et al., Cyanobacteria immobilised in porous silica gels: exploring biocompatible synthesis routes for the development of photobioreactors. *Energy Environ Sci*, **2010**. 3(3): p. 370-377.
173. Polakovič, M., et al., Progress in biocatalysis with immobilized viable whole cells: systems development, reaction engineering and applications. *Biotechnol Lett*, **2017**. 39(5): p. 667-683.
174. Hays, S.G., et al., Synthetic photosynthetic consortia define interactions leading to robustness and photoproduction. *J Biol Eng*, **2017**. 11(1): p. 4.
175. Weiss, T.L., E.J. Young, and D.C. Ducat, A synthetic, light-driven consortium of cyanobacteria and heterotrophic bacteria enables stable polyhydroxybutyrate production. *Metab Eng*, **2017**. 44: p. 236-245.
176. Gao, Z., et al., Photosynthetic production of ethanol from carbon dioxide in genetically engineered cyanobacteria. *Energy Environ Sci*, **2012**. 5(12): p. 9857-9865.
177. Liu, X.F., et al., Modular engineering for efficient photosynthetic biosynthesis of 1-butanol from CO₂ in cyanobacteria. *Energy Environ Sci*, **2019**. 12(9): p. 2765-2777.
178. Theodosiou, E., et al., Exploitation of hetero- and phototrophic metabolic modules for redox-intensive whole-cell biocatalysis. *Frontiers Bioeng Biotech*, **2022**. 10: p. 855715.
179. Erdem, E., et al., Photobiocatalytic oxyfunctionalization with high reaction rate using a Baeyer-Villiger monooxygenase from *Burkholderia xenovorans* in metabolically engineered cyanobacteria. *ACS Catal*, **2022**. 12(1): p. 66-72.
180. Fürst, M.J.L.J., et al., Baeyer-Villiger monooxygenases: tunable oxidative biocatalysts. *ACS Catal*, **2019**. 9: p. 11207-11241.
181. Salamanca, D., et al., Novel cyclohexane monooxygenase from *Acidovorax* sp. CHX100. *Appl Microbiol Biotechnol*, **2015**. 99(16): p. 6889-97.
182. Stanier, R.Y., et al., Purification and properties of unicellular blue-green algae (order Chroococcales). *Bacteriol Rev*, **1971**. 35(2): p. 171-205.
183. Shcolnick, S., Y. Shaked, and N. Keren, A role for mrgA, a DPS family protein, in the internal transport of Fe in the cyanobacterium *Synechocystis* sp. PCC 6803. *Biochim Biophys Acta Bioenerg*, **2007**. 1767(6): p. 814-819.
184. Sambrook, J. and D.W. Russell, Molecular cloning : a laboratory manual. 3rd ed. **2001**, Cold Spring Harbor, N.Y.: *Cold Spring Harb Lab Press*.

185. Hanahan, D., Studies on transformation of *Escherichia coli* with plasmids. *J Mol Biol*, **1983**. 166(4): p. 557-80.
186. Ludwig, A., et al., Transformation and gene replacement in the facultatively chemoheterotrophic, unicellular cyanobacterium *Synechocystis* sp. PCC6714 by electroporation. *Appl Microbiol Biotechnol*, **2008**. 78(4): p. 729-35.
187. Bretschneider, L., et al., Characterization of different biocatalyst formats for BVMO-catalyzed cyclohexanone oxidation. *Biotechnol Bioeng*, **2021**. 118(7): p. 2719-2733.
188. Munro, A.W., H.M. Girvan, and K.J. McLean, Cytochrome P450-redox partner fusion enzymes. *Biochim Biophys Acta*, **2007**. 1770(3): p. 345-59.
189. Hannemann, F., et al., Cytochrome P450 systems - biological variations of electron transport chains. *Biochim Biophys Acta*, **2007**. 1770(3): p. 330-44.
190. Mascia, F., et al., Light-driven hydroxylation of testosterone by *Synechocystis* sp. PCC 6803 expressing the heterologous CYP450 monooxygenase CYP110D1. *Green Chem*, **2022**. 24(16): p. 6156-6167.
191. Thomas, J.C., et al., A second isoform of the ferredoxin:NADP oxidoreductase generated by an in-frame initiation of translation. *PNAS USA*, **2006**. 103(48): p. 18368-73.
192. Bell, S.G., et al., A cytochrome P450 class I electron transfer system from *Novosphingobium aromaticivorans*. *Appl Microbiol Biotechnol*, **2010**. 86(1): p. 163-75.
193. Liu, X., et al., Three pairs of surrogate redox partners comparison for Class I cytochrome P450 enzyme activity reconstitution. *Commun Biol*, **2022**. 5(1): p. 791.
194. Jung, E., et al., Production of omega-hydroxy palmitic acid using CYP153A35 and comparison of cytochrome P450 electron transfer system in vivo. *Appl Microbiol Biotechnol*, **2016**. 100(24): p. 10375-10384.
195. van Beilen, J.B., et al., Practical issues in the application of oxygenases. *Trends Biotechnol*, **2003**. 21(4): p. 170-7.
196. Lewis, D.F. and P. Hlavica, Interactions between redox partners in various cytochrome P450 systems: functional and structural aspects. *Biochim Biophys Acta*, **2000**. 1460(2-3): p. 353-74.
197. Chiliza, Z.E., J. Martínez-Oyanedel, and K. Syed, An overview of the factors playing a role in cytochrome P450 monooxygenase and ferredoxin interactions. *Biophys Rev*, **2020**. 12(5): p. 1217-1222.
198. Wang, B., et al., A genetic toolbox for modulating the expression of heterologous genes in the cyanobacterium *Synechocystis* sp. PCC 6803. *ACS Synth Biol*, **2018**. 7(1): p. 276-286.
199. Behle, A., et al., Comparative dose-response analysis of inducible promoters in cyanobacteria. *ACS Synth Biol*, **2020**.
200. Mellor, S.B., et al., Fusion of ferredoxin and cytochrome P450 enables direct light-driven biosynthesis. *ACS Chem Biol*, **2016**. 11(7): p. 1862-9.
201. Lupacchini, S., et al., Rewiring cyanobacterial photosynthesis by the implementation of an oxygen-tolerant hydrogenase. *Metab Eng*, **2021**. 68: p. 199-209.
202. Lassen, L.M., et al., Redirecting photosynthetic electron flow into light-driven synthesis of alternative products including high-value bioactive natural compounds. *ACS Synth Biol*, **2014**. 3(1): p. 1-12.
203. Hoschek, A., et al., Mixed-species biofilms for high-cell-density application of *Synechocystis* sp. PCC 6803 in capillary reactors for continuous cyclohexane oxidation to cyclohexanol. *Bioresour Technol*, **2019**. 282: p. 171-178.
204. Berla, B.M., et al., Synthetic biology of cyanobacteria: unique challenges and opportunities. *Front Microbiol*, **2013**. 4: p. 246.
205. Imamura, S. and M. Asayama, Sigma factors for cyanobacterial transcription. *Gene Regul*, **2009**. 3: p. 65-87.
206. Johnson, C.H. and S.S. Golden, Circadian programs in cyanobacteria: adaptiveness and mechanism. *Annu Rev Microbiol*, **1999**. 53: p. 389-409.
207. Englund, E., F. Liang, and P. Lindberg, Evaluation of promoters and ribosome binding sites for biotechnological applications in the unicellular cyanobacterium *Synechocystis* sp. PCC 6803. *Sci Rep*, **2016**. 6: p. 36640.

208. Sebesta, J. and C.A.M. Peebles, Improving heterologous protein expression in *Synechocystis* sp. PCC 6803 for alpha-bisabolene production. *Metab Eng Commun*, **2020**. 10: p. e00117.
209. Gale, G.A.R., et al., Emerging species and genome editing tools: future prospects in cyanobacterial synthetic biology. *Microorganisms*, **2019**. 7(10).
210. Immethun, C.M. and T.S. Moon, Synthetic gene regulation in cyanobacteria, in Synth Biol Cyano, W. Zhang and X. Song, Editors. **2018**, Springer Singapore: Singapore. p. 317-355.
211. Gordon, G.C. and B.F. Pflieger, Regulatory tools for controlling gene expression in cyanobacteria. *Adv Exp Med Biol*, **2018**. 1080: p. 281-315.
212. Gibson, D.G., et al., Enzymatic assembly of DNA molecules up to several hundred kilobases. *Nat Methods*, **2009**. 6(5): p. 343-5.
213. Bradford, M.M., A rapid and sensitive method for the quantitation of microgram quantities of protein utilizing the principle of protein-dye binding. *Anal Biochem*, **1976**. 72: p. 248-54.
214. Laemmli, U.K., Cleavage of structural proteins during the assembly of the head of bacteriophage T4. *Nature*, **1970**. 227(5259): p. 680-5.
215. Zavrel, T., P. Ocenaseva, and J. Cerveny, Phenotypic characterization of *Synechocystis* sp. PCC 6803 substrains reveals differences in sensitivity to abiotic stress. *PLoS One*, **2017**. 12(12): p. e0189130.
216. Angermayr, S.A., et al., Energy biotechnology with cyanobacteria. *Curr Opin Biotechnol*, **2009**. 20(3): p. 257-63.
217. Gao, X., et al., Cyanobacterial chassis engineering for enhancing production of biofuels and chemicals. *Appl Microbiol Biotechnol*, **2016**. 100(8): p. 3401-13.
218. Oliver, J.W.K., et al., Cyanobacterial conversion of carbon dioxide to 2,3-butanediol. *PNAS USA*, **2013**. 110(4): p. 1249.
219. Atsumi, S., W. Higashide, and J.C. Liao, Direct photosynthetic recycling of carbon dioxide to isobutyraldehyde. *Nat Biotechnol*, **2009**. 27(12): p. 1177-80.
220. Liang, F., et al., Engineered cyanobacteria with enhanced growth show increased ethanol production and higher biofuel to biomass ratio. *Metab Eng*, **2018**. 46: p. 51-59.
221. Huang, H.H. and P. Lindblad, Wide-dynamic-range promoters engineered for cyanobacteria. *J Biol Eng*, **2013**. 7(1): p. 10.
222. Briggs, L.M., V.L. Pecoraro, and L. McIntosh, Copper-induced expression, cloning, and regulatory studies of the plastocyanin gene from the cyanobacterium *Synechocystis* sp. PCC6803. *Plant Mol Biol*, **1990**. 15 (4): p. 633-42.
223. Jin, H., et al., Construction of a shuttle vector using an endogenous plasmid from the cyanobacterium *Synechocystis* sp. PCC6803. *Front Microbiol*, **2018**. 9: p. 1662.
224. Kelly, C.L., et al., A rhamnose-inducible system for precise and temporal control of gene expression in cyanobacteria. *ACS Synth Biol*, **2018**. 7(4): p. 1056-1066.
225. Scherkus, C., et al., Kinetic insights into ε-caprolactone synthesis: Improvement of an enzymatic cascade reaction. *Biotechnol Bioeng*, **2017**. 114(6): p. 1215-1221.
226. Schmidt, S. and U.T. Bornscheuer, Baeyer-Villiger monooxygenases: From protein engineering to biocatalytic applications. *Enzymes*, **2020**. 47: p. 231-281.
227. Bayer, T., et al., In Vivo Synthesis of Polyhydroxylated Compounds from a “Hidden Reservoir” of Toxic Aldehyde Species. *ChemCatChem*, **2017**. 9(15): p. 2919-2923.
228. Hitchcock, A., C.N. Hunter, and D.P. Canniffe, Progress and challenges in engineering cyanobacteria as chassis for light-driven biotechnology. *Microb Biotechnol*, **2020**. 13(2): p. 363-367.
229. Dafoe, J.T. and A.J. Daugulis, In situ product removal in fermentation systems: improved process performance and rational extractant selection. *Biotechnol Lett*, **2014**. 36(3): p. 443-60.
230. Woo, J.M., et al., Improving catalytic activity of the Baeyer-Villiger monooxygenase-based *Escherichia coli* biocatalysts for the overproduction of (Z)-11-(heptanoyloxy)undec-9-enoic acid from ricinoleic acid. *Sci Rep*, **2018**. 8(1): p. 10280.
231. Karande, R., et al., Segmented flow is controlling growth of catalytic biofilms in continuous multiphase microreactors. *Biotechnol Bioeng*, **2014**. 111(9): p. 1831-40.

232. Vajravel, S., et al., Towards sustainable ethylene production with cyanobacterial artificial biofilms. *Green Chem*, **2020**. 22(19): p. 6404-6414.
233. Sikkema, J., J.A. de Bont, and B. Poolman, Mechanisms of membrane toxicity of hydrocarbons. *Microbiol Rev*, **1995**. 59(2): p. 201-22.
234. Nishiyama, Y., S.I. Allakhverdiev, and N. Murata, Inhibition of the repair of photosystem II by oxidative stress in cyanobacteria. *Photosynth Res*, **2005**. 84(1-3): p. 1-7.
235. Latifi, A., M. Ruiz, and C.C. Zhang, Oxidative stress in cyanobacteria. *FEMS Microbiol Rev*, **2009**. 33(2): p. 258-78.
236. Zhou, J., et al., Introducing extra NADPH consumption ability significantly increases the photosynthetic efficiency and biomass production of cyanobacteria. *Metab Eng*, **2016**. 38: p. 217-227.
237. Toepel, J., et al., Cyanobacteria as whole-cell factories: current status and future perspectives. *Curr Opin Biotechnol*, **2023**. 80: p. 102892.
238. Bretschneider, L., et al., Rational orthologous pathway and biochemical process engineering for adipic acid production using *Pseudomonas taiwanensis* VLB120. *Metab Eng*, **2022**. 70: p. 206-217.
239. Miao, R., et al., Current processes and future challenges of photoautotrophic production of acetyl-CoA-derived solar fuels and chemicals in cyanobacteria. *Curr Opin Chem Biol*, **2020**. 59: p. 69-76.
240. Engler, C., R. Kandzia, and S. Marillonnet, A one pot, one step, precision cloning method with high throughput capability. *PLoS One*, **2008**. 3(11): p. e3647.
241. Weber, E., et al., A modular cloning system for standardized assembly of multigene constructs. *PLOS ONE*, **2011**. 6(2): p. e16765.
242. Lupacchini, S., et al., The activity of an O₂-tolerant hydrogenase recombinantly expressed in *Synechocystis* sp. PCC 6803 is controlled by fine-tuned gene expression in combination with sink and source availability. *Plant Biotechnol*.
243. Schäfer, L., R. Karande, and B. Bühler, Maximizing biocatalytic cyclohexane hydroxylation by modulating Cytochrome P450 monooxygenase expression in *P. taiwanensis* VLB120. *Front Bioeng Biotechnol*, **2020**. 8: p. 140.
244. Touloupakis, E., B. Cicchi, and G. Torzillo, A bioenergetic assessment of photosynthetic growth of *Synechocystis* sp. PCC 6803 in continuous cultures. *Biotechnol Biofuels*, **2015**. 8: p. 133.
245. Erdrich, P., et al., Cyanobacterial biofuels: new insights and strain design strategies revealed by computational modeling. *Microb Cell Fact*, **2014**. 13: p. 128.
246. Cano, M., et al., Glycogen synthesis and metabolite overflow contribute to energy balancing in cyanobacteria. *Cell Reports*, **2018**. 23(3): p. 667-672.
247. Ogawa, T., K. Suzuki, and K. Sonoike, Respiration interacts with photosynthesis through the acceptor side of photosystem I, reflected in the dark-to-light induction kinetics of chlorophyll fluorescence in the cyanobacterium *Synechocystis* sp. PCC 6803. *Front Plant Sci*, **2021**. 12: p. 717968.
248. Guillaume, M.C. and F. Branco Dos Santos, Assessing and reducing phenotypic instability in cyanobacteria. *Curr Opin Biotechnol*, **2023**. 80: p. 102899.
249. Zavřel, T., M.A. Sinetova, and J. Červený, Measurement of chlorophyll a and carotenoids concentration in cyanobacteria. *Bio-protocol*, **2015**. 5(9): p. e1467.
250. Ritchie, R.J., Fitting light saturation curves measured using modulated fluorometry. *Photosynth Res*, **2008**. 96(3): p. 201-215.
251. Touloupakis, E., et al., Effect of high pH on growth of *Synechocystis* sp. PCC 6803 cultures and their contamination by golden algae *Poteroiochromonas* sp. *Appl Microbiol Biotechnol*, **2016**. 100(3): p. 1333-1341.
252. Drath, M., et al., Ammonia triggers photodamage of photosystem II in the cyanobacterium *Synechocystis* sp. strain PCC 6803. *Plant Physiol*, **2008**. 147(1): p. 206-15.
253. Dai, G.Z., B.S. Qiu, and K. Forchhammer, Ammonium tolerance in the cyanobacterium *Synechocystis* sp. strain PCC 6803 and the role of the psbA multigene family. *Plant Cell Environ*, **2014**. 37(4): p. 840-51.

254. Aro, E.M., I. Virgin, and B. Andersson, Photoinhibition of photosystem II. Inactivation, protein damage and turnover. *Biochim Biophys Acta Bioenerg*, **1993**. 1143(2): p. 113-134.
255. Tamoi, M., et al., Enzymic and molecular characterization of NADP-dependent glyceraldehyde-3-phosphate dehydrogenase from *Synechococcus* PCC 7942: resistance of the enzyme to hydrogen peroxide. *Biochem J*, **1996**. 316 (Pt 2)(Pt 2): p. 685-90.
256. Tanaka, K., et al., Quantification of NAD(P)H in cyanobacterial cells by a phenol extraction method. *Photosynth Res*, **2021**. 148(1-2): p. 57-66.
257. Goncalves, L.C.P., et al., Mutagenesis-independent stabilization of class B flavin monooxygenases in operation. *ASC*, **2017**. 359(12): p. 2121-2131.
258. Kugler, A. and K. Stensjö, Optimal energy and redox metabolism in the cyanobacterium *Synechocystis* sp. PCC 6803. *NPJ Syst Biol Appl*, **2023**. 9(1): p. 47.
259. Lu, W., et al., Extraction and quantitation of nicotinamide adenine dinucleotide redox cofactors. *Antioxid Redox Signal*, **2018**. 28(3): p. 167-179.
260. Tao, R., et al., Genetically encoded fluorescent sensors reveal dynamic regulation of NADPH metabolism. *Nat Methods*, **2017**. 14(7): p. 720-728.
261. Tantama, M., et al., Imaging energy status in live cells with a fluorescent biosensor of the intracellular ATP-to-ADP ratio. *Nat Commun*, **2013**. 4: p. 2550.
262. Bühler, B., et al., NADH availability limits asymmetric biocatalytic epoxidation in a growing recombinant *Escherichia coli* strain. *Appl Environ Microbiol*, **2008**. 74(5): p. 1436-46.
263. Bühler, B.S., A. J. J and B.S. Witholt, A., Analysis of two-liquid-phase multistep biooxidation based on a process model: Indications for biological energy shortage. *OPRD*, **2006**. 10(628-643).
264. Kuhn, D., et al., Subtoxic product levels limit the epoxidation capacity of recombinant *E. coli* by increasing microbial energy demands. *J Biotechnol*, **2013**. 163(2): p. 194-203.
265. Kadisch, M., et al., Maximization of cell viability rather than biocatalyst activity improves whole-cell omega-oxyfunctionalization performance. *Biotechnol Bioeng*, **2017**. 114(4): p. 874-884.
266. Woodley, J.M. and N.J. Titchener-Hooker, The use of windows of operation as a bioprocess design tool. *Bioprocess Eng*, **1996**. 14(5): p. 263-268.
267. Barone, G.D., et al., Towards the rate limit of heterologous biotechnological reactions in recombinant cyanobacteria. *Biotechnol Biofuels Bioprod*, **2023**. 16(1): p. 4.
268. Ito, S., N. Koyama, and T. Osanai, Citrate synthase from *Synechocystis* is a distinct class of bacterial citrate synthase. *Sci Rep*, **2019**. 9(1): p. 6038.
269. Pelroy, R.A., R. Rippka, and R.Y. Stanier, Metabolism of glucose by unicellular blue-green algae. *Arch Microbiol*, **1972**. 87(4): p. 303-322.
270. Angermayr, S.A., et al., Exploring metabolic engineering design principles for the photosynthetic production of lactic acid by *Synechocystis* sp. PCC6803. *Biotechnol Biofuels*, **2014**. 7: p. 99.
271. Lindberg, P., S. Park, and A. Melis, Engineering a platform for photosynthetic isoprene production in cyanobacteria, using *Synechocystis* as the model organism. *Metab Eng*, **2010**. 12(1): p. 70-9.
272. Mutalik, V.K., et al., Quantitative estimation of activity and quality for collections of functional genetic elements. *Nat Methods*, **2013**. 10(4): p. 347-353.
273. Opel, F., et al., Generation of synthetic shuttle vectors enabling modular genetic engineering of cyanobacteria. *ACS Synth Biol*, **2022**. 11(5): p. 1758-1771.
274. Schrewe, M., et al., Whole-cell biocatalysis for selective and productive C-O functional group introduction and modification. *Chem Soc Rev*, **2013**. 42(15): p. 6346-77.
275. Bertelmann, C., et al., Efficiency aspects of regioselective testosterone hydroxylation with highly active CYP450-based whole-cell biocatalysts. *Microbial Biotechnology*, **2023**. n/a(n/a).
276. Sikkema, J., J.A. de Bont, and B. Poolman, Interactions of cyclic hydrocarbons with biological membranes. *J Biol Chem*, **1994**. 269(11): p. 8022-8028.

277. Julsing, M.K., et al., Outer membrane protein AlkL boosts biocatalytic oxyfunctionalization of hydrophobic substrates in *Escherichia coli*. *Appl Environ Microbiol*, **2012**. 78(16): p. 5724-33.
278. Williams, C.K., Synthesis of functionalized biodegradable polyesters. *Chem Soc Rev*, **2007**. 36(10): p. 1573-1580.
279. Nikkanen, L., et al., Regulatory electron transport pathways of photosynthesis in cyanobacteria and microalgae: Recent advances and biotechnological prospects. *Physiol Plant*, **2021**.
280. Julsing, M.K., et al., Heme-iron oxygenases: powerful industrial biocatalysts? *Curr Opin Chem Biol*, **2008**. 12(2): p. 177-86.
281. Bähr, L., A. Wüstenberg, and R. Ehwald, Two-tier vessel for photoautotrophic high-density cultures. *J Appl Phycol*, **2016**. 28(2): p. 783-793.
282. Wilhelm, C. and T. Jakob, Balancing the conversion efficiency from photon to biomass. *Microalgal Biotechnology: Potential and Production*, ed. P. Clemens and W. Christian. **2013**, Berlin, Boston: *De Gruyter*.
283. Ehlers, I., et al., CO₂-driven suppression of photorespiration in C3-plants over the 20th century detecting long-term metabolic shifts using isotopomers. *PNAS USA*, **2015**. 112(51): p. 15585-15590.
284. Schenk, P.M., et al., Second generation biofuels: high-efficiency microalgae for biodiesel production. *Bioenergy Res*, **2008**. 1(1): p. 20-43.
285. Stephens, E., et al., Future prospects of microalgal biofuel production systems. *Trends Plant Sci*, **2010**. 15(10): p. 554-64.
286. Weyer, K.M., et al., Theoretical maximum algal oil production. *Bioenergy Res*, **2010**. 3(2): p. 204-213.
287. Wijffels, R.H. and M.J. Barbosa, An outlook on microalgal biofuels. *Science*, **2010**. 329(5993): p. 796-799.
288. Redding, K.E., et al., Advances and challenges in photosynthetic hydrogen production. *Trends Biotechnol*, **2022**.
289. Bühler, K., et al., Biocatalytic production of white hydrogen from water using cyanobacteria. *Photosynthesis*, ed. R. Matthias. **2021**, Berlin, Boston: *De Gruyter*.
290. Appel, J., et al., Cyanobacterial in vivo solar hydrogen production using a photosystem I–hydrogenase (PsaD-HoxYH) fusion complex. *Nat Energy*, **2020**. 5(6): p. 458–467.
291. Toepel, J., et al., Photosynthesis driven continuous hydrogen production by diazotrophic cyanobacteria in high cell density capillary photobiofilm reactors. *Bioresour Technol*, **2023**. 373: p. 128703.
292. Chen, M. and R.E. Blankenship, Expanding the solar spectrum used by photosynthesis. *Trends Plant Sci*, **2011**. 16(8): p. 427-431.
293. Gawel, E., et al., The future of the energy transition in Germany. *Energy Sustain Soc*, **2014**. 4(1): p. 15.
294. Tröndle, T., Supply-side options to reduce land requirements of fully renewable electricity in Europe. *PLOS ONE*, **2020**. 15(8): p. e0236958.
295. Wilhelm, C. and H. Wagner, Rate-limiting steps in algal energy conversion from sunlight to products. *Photosynthesis*, ed. R. Matthias. **2021**, Berlin, Boston: *De Gruyter*.
296. Shoro, G.M., D.M. Akbar Hussain, and D. Sera. Photovoltaic System in Progress: A Survey of Recent Development. in *Communication Technologies, Information Security and Sustainable Development*. **2014**. Cham: Springer International Publishing.
297. Canizales, S., et al., Cyanobacteria cultivation on human urine for nutrients recovery. *Algal Res*, **2023**. 71: p. 103064.
298. Green, M.A., et al., Solar cell efficiency tables (Version 60). *Progress Photovolt: Res Appl*, **2022**. 30(7): p. 687-701.
299. Gebauer, M., Energiespeicherkonzepte und ihre Nutzungsmöglichkeiten unter Berücksichtigung einer optimalen Sektorenkopplung, in *Fak05*. **2023**, RWTH Aachen University: Aachen.
300. Brandenburg, F., et al., Trans-4-hydroxy-L-proline production by the cyanobacterium *Synechocystis* sp. PCC 6803. *Metab*, **2021**. 12: p. e00155.

301. Gao, H., et al., Applications of synthetic light-driven microbial consortia for biochemicals production. *Bioresour Technol*, **2022**. 351: p. 126954.
302. Zedler, J.A.Z., et al., Self-assembly of nanofilaments in cyanobacteria for protein co-localization. *ACS Nano*, **2023**.
303. Morejón, M.C., et al., Integrated electrosynthesis and biosynthesis for the production of adipic acid from lignin-derived phenols. *Green Chem*, **2023**. 25(12): p. 4662-4666.
304. Shimada, N., et al., Astaxanthin production in a model cyanobacterium *Synechocystis* sp. PCC 6803. *J Gen Appl Microbiol*, **2020**. 66(2): p. 116-120.
305. Diao, J., et al., Tailoring cyanobacteria as a new platform for highly efficient synthesis of astaxanthin. *Metab Eng*, **2020**. 61: p. 275-287.
306. Habib, A.B. and M. Parvin. Review on culture, production and use of *Spirulina* as food for humans and feeds for domestic animals and fish. **2008**.
307. Chittora, D., et al., Cyanobacteria as a source of biofertilizers for sustainable agriculture. *Biochem Biophys Rep*, **2020**. 22: p. 100737.

**Selbstständigkeitserklärung gemäß § 5 (4) Promotionsordnung der
Naturwissenschaftlichen Fakultäten I, II und III der Martin-Luther-Universität
Halle-Wittenberg**

Hiermit erkläre ich, Adrian Tüllinghoff, dass ich die vorliegende Dissertation selbstständig und ohne fremde Hilfe verfasst habe, dass keine anderen als die von mir angegebenen Quellen und Hilfsmittel verwendet und die den Werken wörtlich oder inhaltlich entnommenen Stellen als solche kenntlich gemacht worden sind.

Die Dissertation habe ich in der gegenwärtigen bzw. in einer anderen Fassung noch keiner Prüfungsbehörde vorgelegt.

Leipzig, 14.01.2024

Appendix

Curriculum Vitae

Education

05/2019 – 12/2023	Dissertation at the Helmholtz-Centre for Environmental Research (UFZ) Leipzig, under supervision of Prof. Bruno Bühler
10/2016 – 05/2019	Master of Science, Biochemistry, MLU Halle-Wittenberg, <i>Grade 1,0</i>
08/2018 – 04/2019	Master Thesis, Technical University Chalmers, Gothenburg, Sweden, “Development of a CRISPR/Cas9-based multicopy gene integration method to engineer industrial yeast strains for cellobiose fermentation”
10/2012 – 08/2016	Bachelor of Science, Biochemistry, Leipzig University, <i>Grade 1,2</i>
03/2016 – 08/2016	Bachelor Thesis, Helmholtz-Centre for Environmental Research (UFZ) Leipzig, “Generation of PHB-negative mutants of methylotrophic bacteria”
08/2011 – 07/2012	Voluntary service in a parish in Gothenburg, Sweden
07/2011	Abitur at Gymnasium Hammonense, Hamm <i>Grade 1,0</i>
Leipzig, 14.12.2023	

Publications

- 2023 **Tüllinghoff, A.**, Toepel, J., Bühler, B.: „Enlightening electron transfer routes in oxyfunctionalizing *Synechocystis* sp. PCC 6803” in ChemBioChem, e2023000475
- 2023 **Tüllinghoff, A.**, Djaya-Mbissam, H., Toepel, J., Bühler, B.: „Light-driven redox biocatalysis on gram-scale in in *Synechocystis* sp PCC 6803 via an in vivo cascade” in Plant Biotechnol J, 21 (10): 2074-2083
- 2022 Opel, F., Siebert, N.A., Klatt, S., **Tüllinghoff, A.**, Hantke, J.G., Toepel, J., Bühler, B., Nürnberg, D.J., Klähn, S.: “Generation of synthetic shuttle vectors enabling modular genetic engineering of cyanobacteria” in ACS Synth Biol, 11 (5): 1758-1771
- 2022 Theodosiou, E., **Tüllinghoff, A.**, Toepel, J., Bühler, B.: „Exploitation of hetero- and phototrophic metabolic modules for redox-intensive whole-cell biocatalysis” in Front Bioeng Biotechnol, 10: 855715
- 2022 **Tüllinghoff, A.**, Uhl, M.B., Nintzel, F.E.H., Schmid, A., Bühler, B., Toepel, J.: “Maximizing photosynthesis-driven Baeyer-Villiger oxidation efficiency in recombinant *Synechocystis* sp. PCC 6803“ in Front Catal, 1:780474
- 2019 Hoschek, A., Toepel, J., **Hochkeppel, A.**, Karande, R., Bühler, B., Schmid, A.: „Light-dependent and aeration-independent gram-scale hydroxylation of cyclohexane to cyclohexanol by CYP450 harboring *Synechocystis* sp. PCC 6803” in Biotechnol J, 14: 1800724

Conference contributions

09/2023	Cyano2023 , Kassel, Germany	Oral presentation
06/2023	Biotrans 2023 , La Rochelle, Frankreich	Poster presentation
09/2022	Cyano2022 , Leipzig, Germany	Organisation
07/2022	Pharma research day , 2022, Halle, Germany	Oral presentation
06/2022	14th Workshop on Cyanobacteria , East Lansing (MI), USA	Poster presentation
03/2022	VAAM Conference 2022 , Düsseldorf/remote	Poster presentation
03/2020	VAAM Conference 2020 , Leipzig, Germany	Poster presentation

Supplementary Material

Table S1	Used oligonucleotides, plasmids and strains I	125
Figure S1	Calibration curves for Cyclohexane, cyclohexanol, and cyclohexanone	127
Figure S2	Colony PCR of generated <i>Synechocystis</i> strains	128
Figure S3	Alignment of <i>Synechocystis</i> Fds1-6 to Fd _{AV}	129
Table S2	Used oligonucleotides, plasmids and strains II	130
Sequence	Sequence of <i>Synechocystis</i> _Ni_pBVMO	131
Script	Script for dynamic modeling using <i>Berkeley Madonna</i> software	132
Figure S4	Calibration curves for GC-quantification	133
Figure S5	Effect of different Ni ²⁺ concentrations on growth of <i>Synechocystis</i> _empty (A) and <i>Synechocystis</i> _Ni_pBVMO (B)	134
Figure S6	Characterization of keto reduction in <i>Synechocystis</i> _wt	135
Figure S7	Abiotic ϵ -caprolactone hydrolysis at different pH	136
Figure S8	Long-term stability of BVMO-reaction in <i>Synechocystis</i> _Ni_pBVMO	137
Figure S9	Effect of ϵ -caprolactone (A) and 6-hydroxyhexanoic acid (B) on BVMO activity in <i>Synechocystis</i> _Ni_pBVMO	138
Table S3	Comparison of low light and high light conditions for a BVMO biotransformation	139
Table S4	Used oligonucleotides, plasmids and strains III	140
Figure S10	Emission spectrum of LED unit from used photo-STR	141
Figure S11	Effect of 6-hydroxyhexanoic acid (6-HA) on growth of <i>Synechocystis</i> BVMO:Lactonase	142
Figure S12	Effect of 6-HA on conversion of cyclohexanone to 6-hydroxyhexanoic acid (6-HA)	143
Figure S13	Photosynthesis-driven two-enzyme process in a 2 L-photo-STR with substrate feed regime matching 15 U g _{CDW} ⁻¹	144
Figure S14	Specific absorption shifts upon Ni ²⁺ -induction under HC/NO ₃ ⁻ , HC/NH ₄ ⁺ , and LC/NO ₃ ⁻ conditions	145
Figure S15	Electron balancing with <i>Synechocystis</i> wildtype without and with 5 μ M NiSO ₄	146
Figure S16	Induction-time dependent BVMO stability in <i>Synechocystis</i> _Ni_pBVMO	147

Table S1: **Used oligonucleotides, plasmids and strains I.**

Oligo name	Sequence	Function	
PAH077	GGGAGGTATTGGACCGCATTGAACTCTAGTATATAA ACGCAGAAAGGCC	Construction primer, Term_CYP(_FNR) unit	
PAH130	TGGTGATGCGGCACTCGGCCGCGTATGAAATCAGG CATTGATCCGGACTGGC	Construction primer, Term_CYP unit	
PAH131	GATTCATACGCGGCCGAGTGCCGCATCAC	Construction primer, FD unit	
PAH136	TTCCACAGCAATGGCATCCT	Construction primer, terminator unit	
PAH137	TCCAGCGGAATCGAATAGGC	Construction primer, terminator unit	
PAH162	GTGGAATTGTGAGCGGATAACAATTCACACATAC	Construction primer, CYP unit	
PAH163	CTGAGCCTTTCGTTTTATTTGATGCCTGGTATCAGG CATTGATCCGGAC	Construction primer, CYP unit	
PAH164	GAGCCTTTCGTTTTATTTGATGCCTGGTATCAGGCC GCCAGCGCCTTTG	Construction primer, Term_CYP_FNR unit	
PAH165	GACTGAGCCTTTCGTTTTATTTGATGCCTGGTATC	Construction primer, FD unit	
SPAH024	AACGCGAAGTAATCTTTTCG	Sequencing primer	
SPAH030	CAGGGGAGGTATTGGACC	Sequencing primer	
SPAH033	GGCGAGACCTTCAACTGGG	Sequencing primer	
Plasmid name	Characteristics	Function	Reference
pAH_CYP	pPMQAK1_Ptrc1O_CYPonly		This work
pAH_CYP_FNR	pPMQAK1_Ptrc1O_CYP_FNR		This work
pAH_CYP_Fd	pPMQAK1_Ptrc1O_CYP_Fd		This work
pAH_CYP_FNR_Fd	pPMQAK1_Ptrc1O_CYP_FNR_Fd	Three component plasmid, template	[74]
pAH_empty	pPMQAK1_Ptrc1O	Empty vector	[74]
Strain	Characteristics	Reference	
<i>E. coli</i> DH5 α	<i>supE44, ΔlacU169 (80lacZ, ΔM15) hsdR17 recA1 endA1 gyrA96 thi-1 relA1</i>	[185]	
<i>Synechocystis</i>	Wild-type	[182]	
<i>Synechocystis</i> CYP_only	<i>Synechocystis</i> sp. PCC 6803 containing plasmid pAH_CYP	This work	
<i>Synechocystis</i> CYP_FNR	<i>Synechocystis</i> sp. PCC 6803 containing plasmid pAH_CYP_FNR	This work	
<i>Synechocystis</i> CYP_Fd	<i>Synechocystis</i> sp. PCC 6803 containing plasmid pAH_CYP_Fd	This work	

Appendix

<i>Synechocystis</i> CYP_FNR_Fd	<i>Synechocystis</i> sp. PCC 6803 containing plasmid pAH_CYP_FNR_Fd	[74]
<i>Synechocystis</i> control	<i>Synechocystis</i> sp. PCC 6803 containing plasmid pAH_empty	[74]

All oligonucleotides were ordered from Eurofins scientific, Luxembourg.

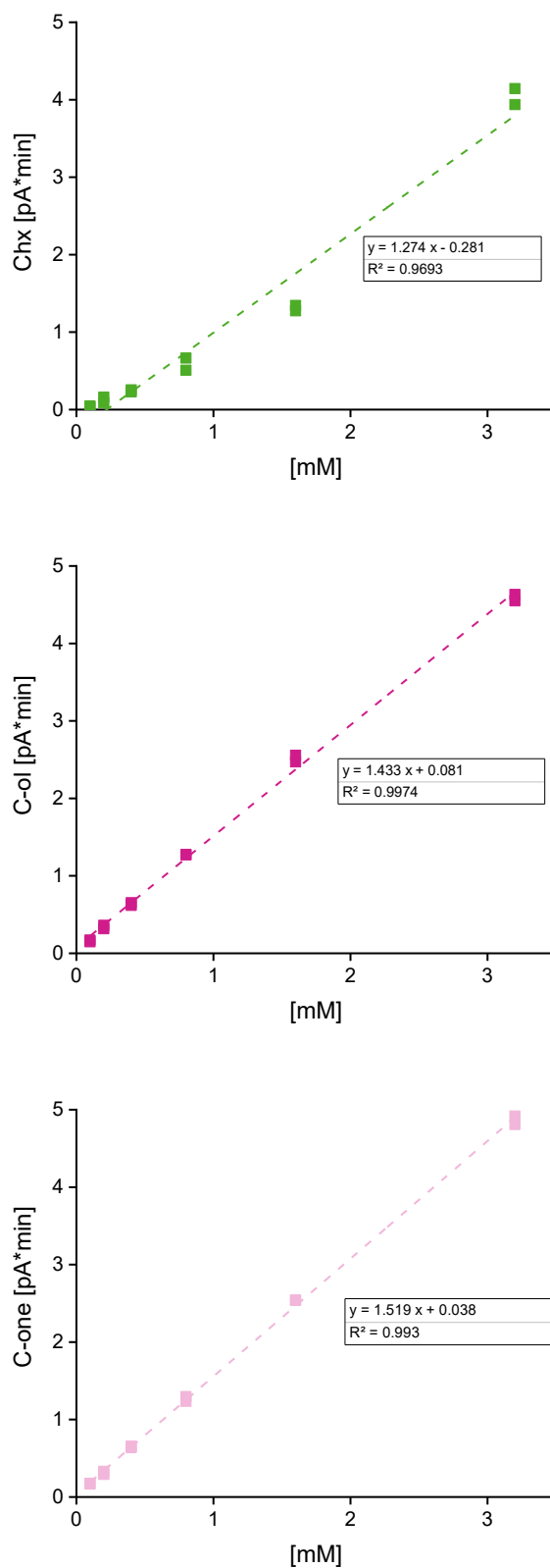


Figure S1: **Calibration curves for Cyclohexane (Chx), cyclohexanol (C-ol), and cyclohexanone (C-one).** Formula of the linear regression and R² is given in the graph.

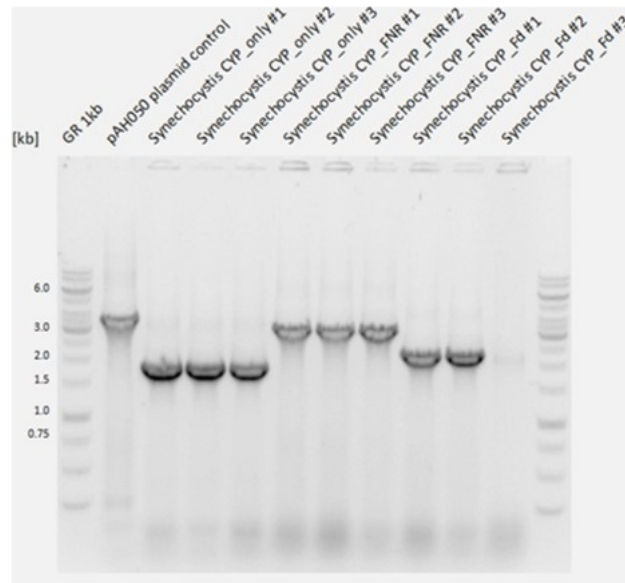


Figure S2: **Colony PCR of generated *Synechocystis* strains.** Expected band sizes: 3.4 kb for pAH_CYP_FNR_Fd (plasmid control), 1.6 kb for *Synechocystis* CYP_only, 2.7 kb for *Synechocystis* CYP_FNR, and 2.1 kb for *Synechocystis* CYP_Fd.

Table S2: **Used oligonucleotides, plasmids and strains II.**

Oligo name	Sequence	Function	
PAH096	ACAAATTCCCAATTTAGTGGAGGTTACTAGATGAAAAAAA CCCAACATCTGG	Construction primer	
PAH097	TCGTTTTATTTGATGCCTGGCTGCACTATTTTTCGAACTG CGGGTGGCTCCAAGCGCTCTGGAATACGAAACCCTCG	Construction primer	
BVMO1	AGCTTTCGCTAAGGATGATTTCTGGTTCACCAGCAAAA TTCG	Construction primer	
BVMO2	CCTTGCCCTTTTTTGCCGACTGCATATAAACGCAGAAA GGCC	Construction primer	
BVMO 3	AGCTTTCGCTAAGGATGATTTCTGGGAAGGGATAGCAA GCTAATTTTTATG	Construction primer	
BVMO 4	TAACCTCCACTAACTTCTTGCGATTGTATC	Construction primer	
BVMO 5	ATCGCCAAGAAGTTAGTGGAGGTTACTAGATG	Construction primer	
sBVMO1	AAAGGGAATAAGGGCGACAC	Sequencing primer	
sBVMO2	GAGCTTTGTCTATTGCTACTCC	Sequencing primer	
sBVMO3	AACGCGAAGTAATCTTTTCG	Sequencing primer	
Plasmid name	Characteristics	Function	Reference
pEERM3_Km	Integrative vector, <i>Km^R</i>	Backbone for pAH059	[144]
pCom10_Capro	pCom10-derived, harbouring <i>bvmo</i> gene	Template for BVMO	[164]
pPMQAK1	Replicative vector, <i>Km^R</i> , <i>Amp^R</i>	Backbone for pAH063	[141]
pAH059	pEERM3_PnrsB_ <i>bvmo</i>	Integrational shuttle vector	This work
pAH063	pPMQAK1_PnrsB_ <i>bvmo</i>	Episomal shuttle vector	This work
pAH064	pPMQAK1_PpetE_ <i>bvmo</i>	Episomal shuttle vector	This work
Strain	Characteristics	Reference	
<i>E. coli</i> DH5alpha	<i>supE44</i> , Δ <i>lacU169</i> (80 <i>lacZ</i> , Δ M15) <i>hsdR17</i> <i>recA1 endA1 gyrA96 thi-1 relA1</i>	[185]	
<i>Synechocystis</i>	Wild-type	[182]	
<i>Synechocystis</i> _empty	Control strain, <i>KmR</i> inserted into neutral site I	This work	
<i>Synechocystis</i> _Ni_cBVMO	<i>Synechocystis</i> , PnrsB_ <i>bvmo</i> _T _{double} <i>KmR</i> inserted in neutral site I	This work	
<i>Synechocystis</i> _Ni_pBVMO	<i>Synechocystis</i> containing plasmid pAH063	This work	
<i>Synechocystis</i> _Cu_pBVMO	<i>Synechocystis</i> containing plasmid pAH064	This work	

All oligonucleotides were ordered from Eurofins scientific, Luxembourg.

Sequence: **Sequence of *Synechocystis*_Ni_pBVMO.**

Consensus sequence from reads with sBVMO1, sBVMO2 and sBVMO3. *Red, italic – PnrsB promoter, Red, bold – RBS**, *blue, bold – BVMO gene sequence, black, bold – T_{double} Terminator.*

TTCCTTTTTTCATATTATTGAAGCATTATCAGGGTTATTGTCTCATGAGCGGATACATATTTGAATG
TATTTAGAAAAATAAACAAATAGGGGTTCCGCGCACATTTCCCCGAAAAGTGCCACCTGACGTCT
AAGAAACCATTATTATCATGACATTAACCTATAAAAATAGGCGTATCACGAGGCAGAATTTTCAGAT
AAAAAAAATCCTTAGCTTTTCGCTAAGGATGATTTCTGGTTCCACCAGCAAAATTCGCATCGCCTCT
GCCTTTTTTATAACGGTCTGATCTTAGCGGGGGAAGGAGATTTTCACCTGAATTTTCATACCCCTT
TGGCAGACTGGGAAAATCTTGGACAAATTCCTCAATTTAGTGGAGGTTACTAGATGAAAAAACCC
AACATCTGGACGCCATCGTCATCGGTGCCGGCTTTGGCGGCATGTACATGCTGAAAAAGCTGC
GTGACGAGCAGGGCCTGAAAGTGCGCGTCTTTGACAAGGCCGGCGGGCTGGGCGGCACCTGG
TACTGGAACCGTTACCCCGCGCGCTCTCCGACACCGAGAGCTTTGTCTATTGCTACTCCTGGG
ACAAAGAGCTGCTGCAAGAGATGCACATCACACGCGCTATGTGACGCAGCCGCAAATTTCTGT
CGTACCTGGAGCATGTGGCCGACCGCCACAACCTGCGCCCCGACATCCAGCTCAACACCGGC
ATCACCGCCGCCACTTCAACGAAGCCACCAACCTGTGGGAAGTGAAAACCGACACCGGCGA
GGCCTACACCGCCAATTCCTGGTGACCGCGCTGGGCCTGCTCTCGGCCACCAACGTCCCCAA
GATCAAGGGGCTCGACACCTTCCAGGGCGAGTGGCTGCACACCGGCAACTGGCCCGAAGGCG
TGCAATACGACGGCAAGCGCGTGGGCGTGATTGGCACGGGCTCCACCGGCACCCAGGTCATC
ACCGCCATTGCGCCCAAGGTCGAGCACCTGACGGTATTCCAGCGCTCGCCCCAGTACAGCGTG
CCCGTGGGCAACGGCCCGGTACGCCCCGAATACGTGGCAGAGGTGAAGAAGAACTACGACGA
GATCTGGGAGCAGGTGAAGGGCTCGGTGGTGGCCTTTGGCTTCAAGGAGAGCACCGTGTCCG
CCATGAGCGTGTGGAAGAAGAGCGCCAGGCCGTGTTCCAGAAAGCCTGGGACAACGGCGGT
GGTTCCGCTTCATGTTTCGAGACCTTCTGCGACATCGCCACCGATGAGCGCGCCAACAAGGCG
GCGCAAGACTTCATCCGCAGCAAGATTGCCGAAATCGTCAAGGACCCCGAGACGGCACGCAA
GCTCATGCCGCAAGACCTGTACGCCAAGCGCCCGCTGTGCGACAGCGGCTACTACGCCACCT
ACAACCGGCCAATGTGCGATCTGGTTCGATGTCAAGGCCAACCAGATTGTGCAAATCACCCCA
AGGGCGTCAAACCACCGATGGCGTGGAGCACGAACTGGACATGCTGATTTTTGCCACTGGCT
TTGACGCGGTGGATGGCAACTACACCAAGATCGACATCCGTGGCCGCAATGGCCTGACGATTC
AAGAGCAGTGAAATCAGGCCCTAGCAGCTACATGGGCGTGGCCAATGCCAACTTCCCCAAC
ATGTTTCATGGTGTGTTGGGCCCAACGGCCCCTTACCAACCTGCCACCGGCCATCGAGAGCCAG
GTCGAGTGGATTGCCGCGCTGATCAAGGATGTGAACGCCAAGGACCTGAAAACCGTGGAGGC
CACCACCGCCCGCAAGCCGGCTGGACCAAGACCTGCCAGGACATCGCCAACATGACGCTGT
TCCCCAAGGCCGACTCCTGGATTTTTGGCGCAAACATCCCCGGCAAACCAACACCGTGTACT
TCTACATGGCGGGCCTGGGTGCTTACCGGCAAGAGCTGTGCGCGGTGCAAAACAAGGGTTAC
GAGGGTTTCGTATTCCAGAGCGCTTGGAGCCACCCGCAGTTCGAAAAATAGTGCAGCCAGGCAT
CAAATAAACGAAAGGCTCAGTCGAAAGACTGGGCCTTTTCGTTTTATCTGTTGTTTGTCCGGTGA
ACGCTCTCTACTAGAGTCACACTGGCTCACCTTCGGGTGGGCCTTTCTGCGTTTATATGCAGTC
CGGCAAAAAGGGCAAG

Script: **Script for dynamic modeling using *Berkeley Madonna* software.**

METHOD RK4

STARTTIME = 0
STOPTIME= 1440
DT = 0.001
DTOUT= 2

Mass Balances

$S' = F + G - kB - kP$; Cyclohexanone
 $B' = kB$; Cyclohexanol
 $P' = kP$; Product
 $F = \text{IF TIME} \geq t1 \text{ then } 0 \text{ else } f1$
 $G = \text{IF TIME} \geq t2 \text{ then } 0 \text{ else } f2$

Initial Conditions

INIT S=0 ; C-one
INIT B=0 ; C-ol
INIT P=0 ; Product

Kinetics

$kP = v_{max} * S / (K_s + B / k_1 * K_s + S + S * S / k_0) * 1 / (1 + P / k_2) * X$; BVMO reaction with inhibition
 $kB = 0.002 * S / (7.420 + S) * X$; keto reduction

Constants

$X = 1.02$; biomass [g L⁻¹]
 $t1 = 240$
 $t2 = 480$
 $f1 = 0.3 * 0.032 * X$; C-one feed 1 before 4h, mmol L⁻¹ min⁻¹
 $f2 = 0.7 * 0.032 * X$; C-one feed 2 before 8h, mmol L⁻¹ min⁻¹
 $v_{max} = 0.091$; mM min⁻¹
 $K_s = 0.079$; mM
 $k_0 = 5.4$; C-one inhibition, mM
 $k_1 = 0.00237$; C-ol inhibition, mM
 $k_2 = 2.0$; e-CL inhibition, mM

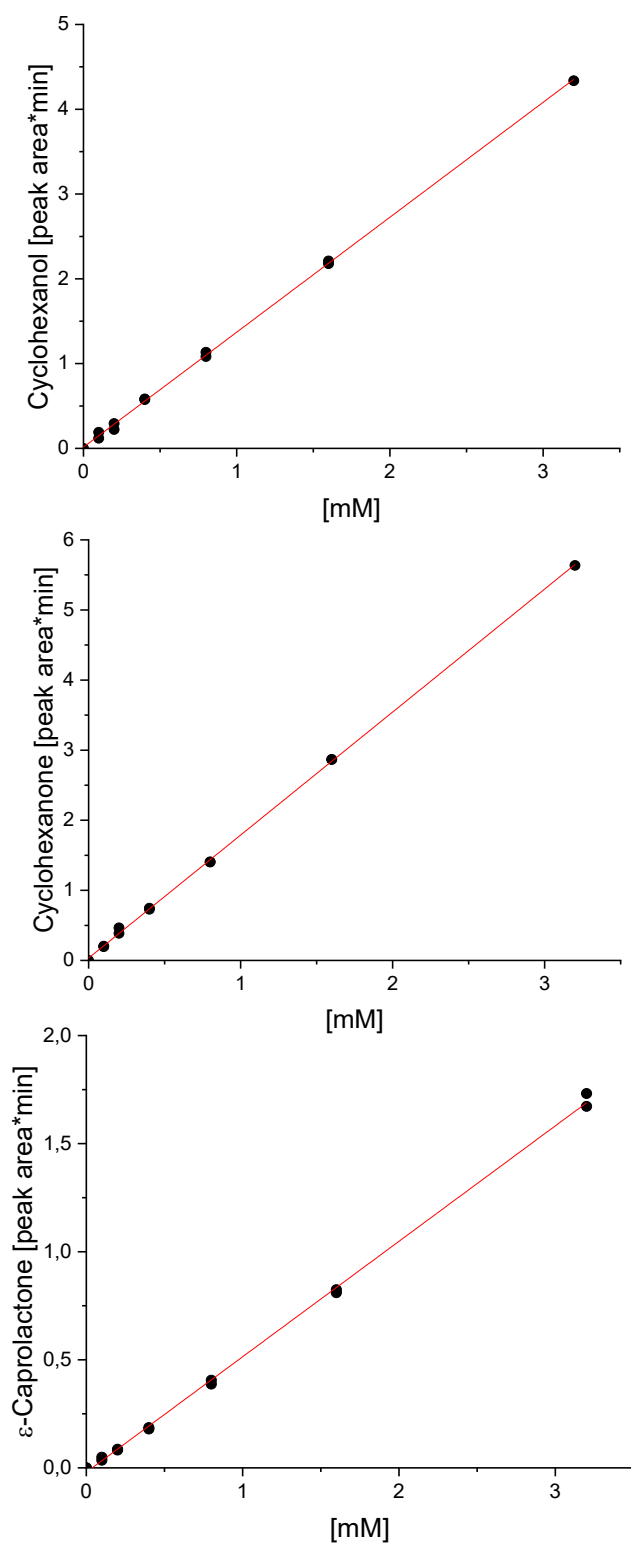


Figure S4: **Calibration curves for GC-quantification** of cyclohexanol, cyclohexanone and ϵ -caprolactone. For details, see experimental section (Chapter 3).

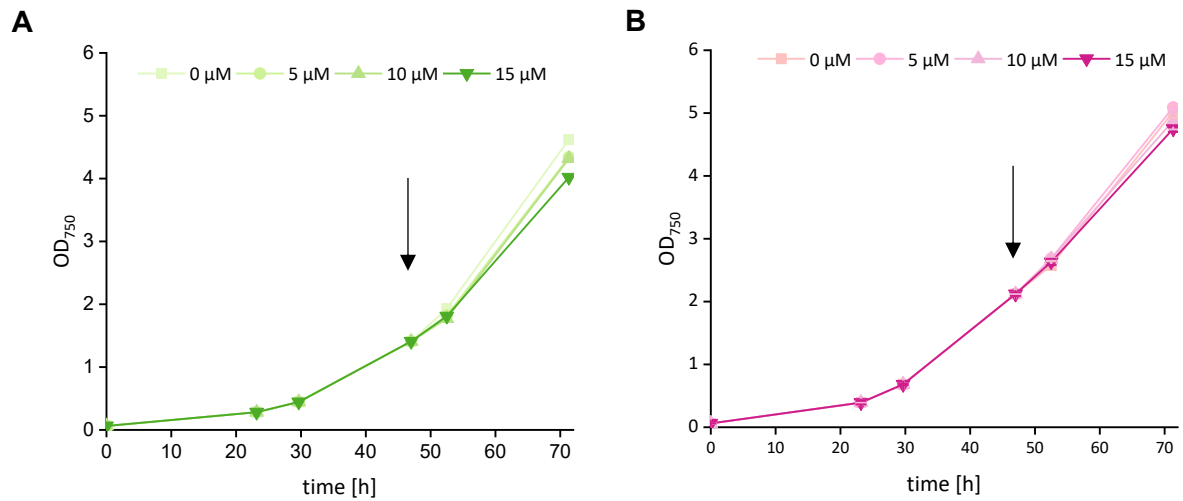


Figure S5: **Effect of different Ni²⁺ concentrations on growth of *Synechocystis_empty* (A, green) and *Synechocystis_Ni_pBVMO* (B, pink).** Ni²⁺ was added after 48h of growth (black arrow). *Synechocystis_empty* harbouring a kanamycin resistance gene inserted into neutral site I was used as a control to differentiate between sole Ni²⁺ effects and (additive) BVMO expression effects. Cells were cultivated at 30 °C, 50 μmol_{photons} m⁻² s⁻¹ 2% CO₂. Error bars represent SD (n=2).

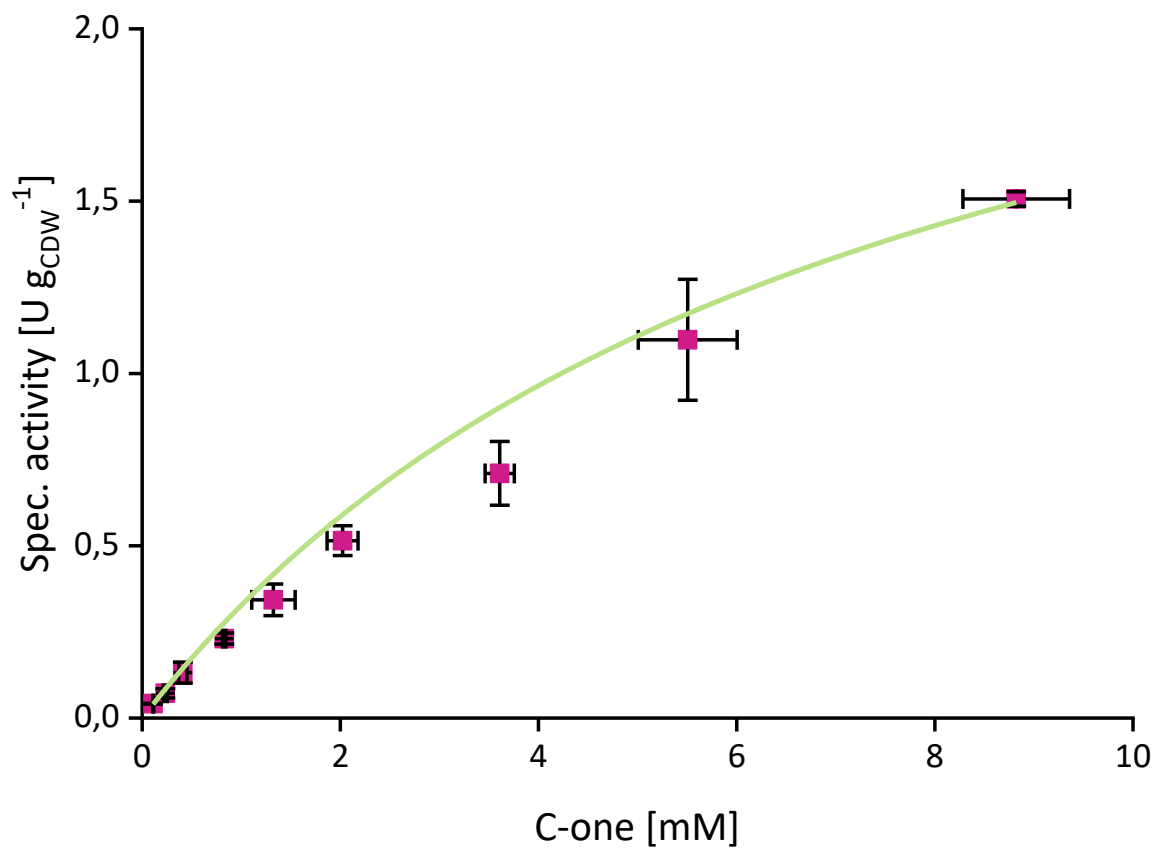


Fig S6: **Characterization of keto reduction in *Synechocystis_wt.*** Experiments were conducted as short-term assays with varying cyclohexanone (C-one) concentration. Conditions: $1 \text{ g}_{\text{CDW}} \text{ L}^{-1}$, 30min, 0...10 mM cyclohexanone. $K_s=7.4 \pm 0.6 \text{ mM}$; $v_{\text{max}} = 2.75 \pm 0.15 \text{ U g}_{\text{CDW}}^{-1}$

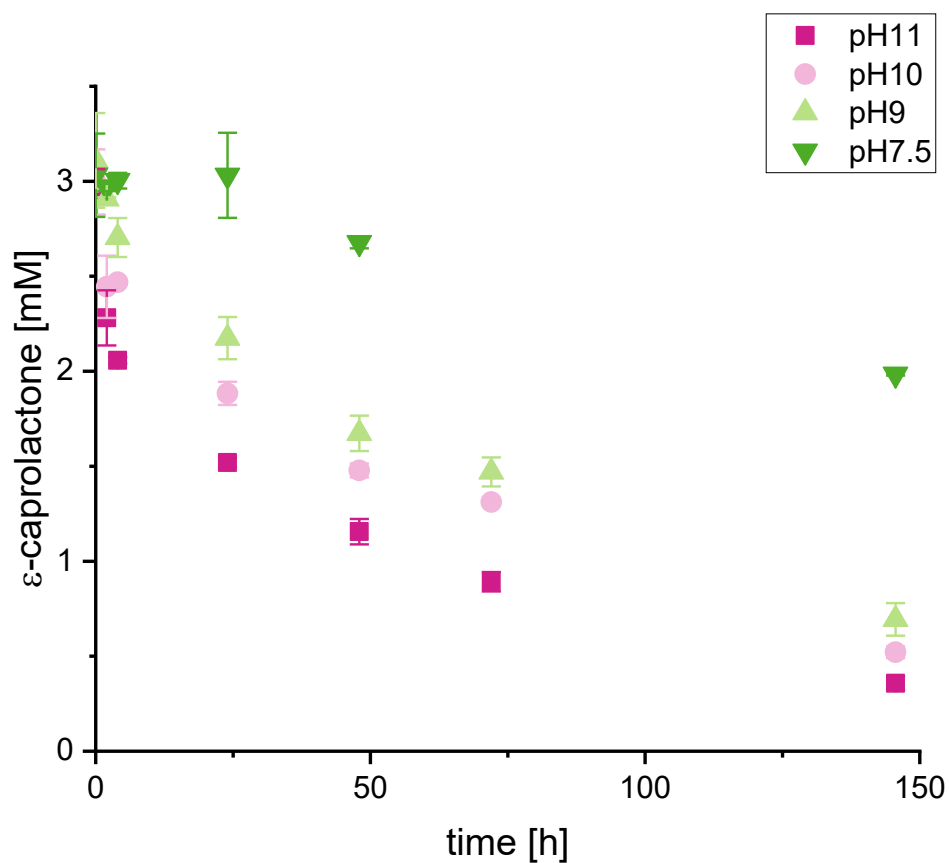


Fig S7: **Abiotic ϵ -caprolactone hydrolysis at different pH.** 3 mM ϵ -caprolactone was added to YBG11 medium adjusted to the given pH (11, 10, 9 and 7.5, which is the used standard medium), incubated under assay-like conditions and product hydrolysis was followed by lactone quantification via gas chromatography.

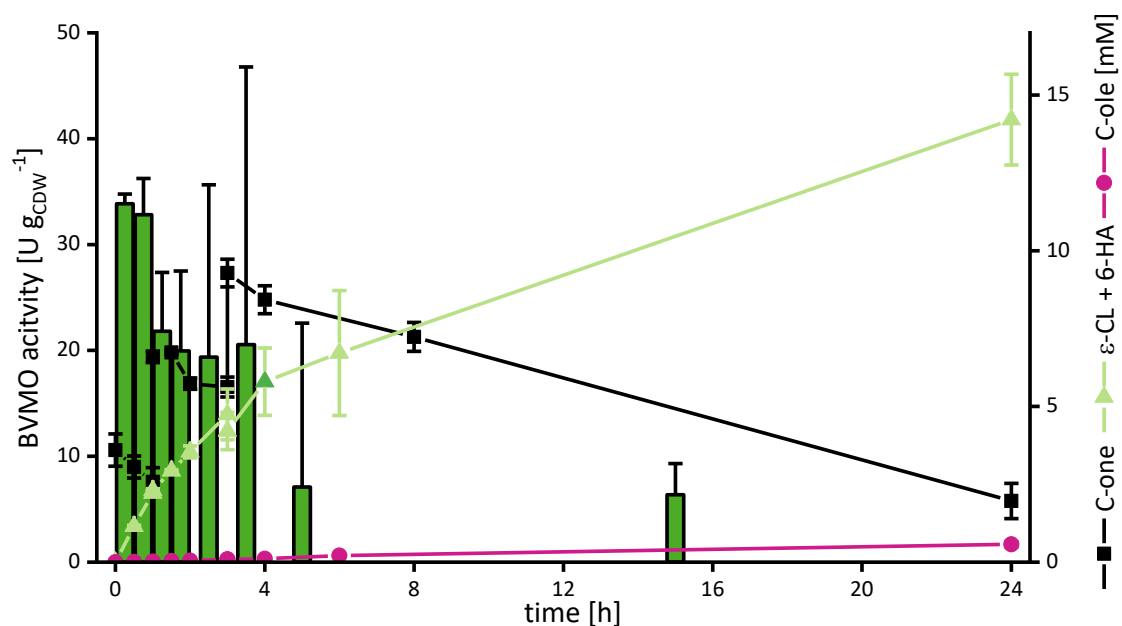


Figure S8: **Long-term stability of BVMO-reaction in *Synechocystis_Ni_pBVMO***. Green bars: BVMO activity, calculated in U ($=\mu\text{mol} [\epsilon\text{-caprolactone } (\epsilon\text{-Cl}) + 6\text{-hydroxyhexanoic acid } (6\text{-HA})] \text{ min}^{-1} \text{ g}_{\text{CDW}}^{-1}$); Squares/black line: cyclohexanone (C-one); Triangles/green line: total product [$\epsilon\text{-Cl} + 6\text{-HA}$]; circles/pink line: cyclohexanol (C-ol). Assays were conducted using 20 mL cell suspension in 100 mL screw-capped shaking flasks at standard conditions. 5 mM C-one was fed initially and after 1 and 3 hrs. All data derived from ≥ 2 biological and ≥ 2 technical replicates.

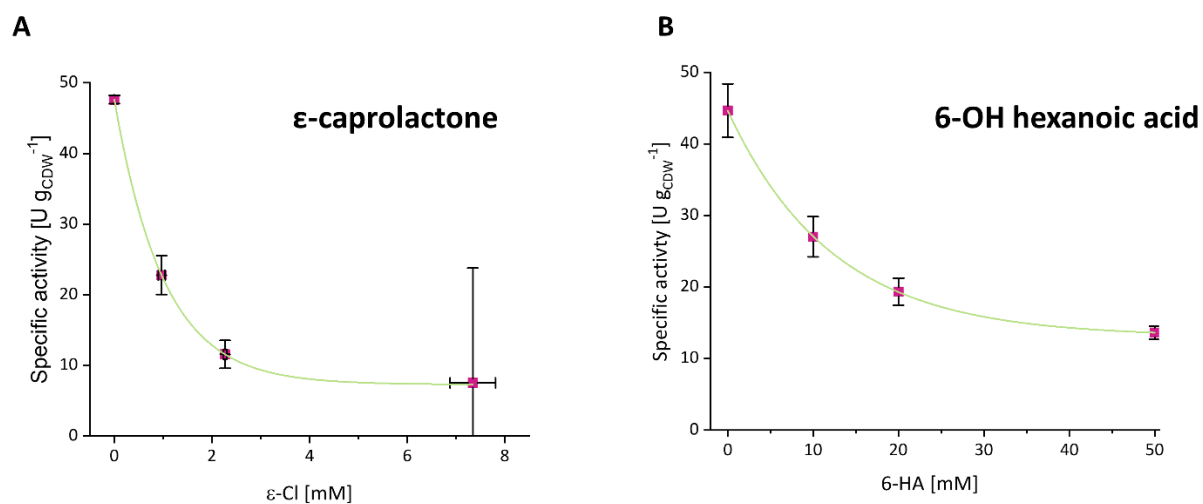


Figure S9: **Effect of ϵ -caprolactone ($\epsilon\text{-Cl}$) (A) and 6-hydroxyhexanoic acid (6-HA) (B) on BVMO activity in *Synechocystis_Ni_pBVMO*.** Product inhibition was tested in whole-cell assays (30min), with defined concentrations of $\epsilon\text{-Cl}$ or 6-HA added prior to the assay. BVMO activity, in U ($=\mu\text{mol} [\epsilon\text{-Cl} + 6\text{-HA}] \text{min}^{-1} \text{g}_{\text{CDW}}^{-1}$) was calculated from the product formed during the assay. All data derived from ≥ 2 biological and ≥ 2 technical replicates.

Table S3: **Comparison of low light and high light conditions for a BVMO biotransformation** in a 2-L photo STR (Infors AG, Bottmingen, Switzerland)

Parameter	HL HC	LL HC
Aeration		
Air [$L \min^{-1}$]	2-0.2 ^a	2-0.2 ^a
CO ₂ [$mL \min^{-1}$]	20	20
Light [$\mu mol_{photons} m^{-2} s^{-1}$]		
for growth	150-200-250 ^b	100-175-250 ^b
for biotransformation	700	250
C-one feed [set to $U g_{CDW}^{-1}$]	30	30
Biomass conc. ^c [$g_{CDW} L^{-1}$]	1.02 ± 0.01	1.00 ± 0.03
Initial vol. productivity [$g L^{-1} h^{-1}$]	0.174 ± 0.022	0.186 ± 0.002

LL – low light, HL – high light, LC – low carbon, HC – high carbon

^a For biotransformation, Air supply was reduced to 0.2 \min^{-1} .

^b Stepwise increase of light intensity during growth.

^c Biomass concentration at the start of the biotransformation, assessed via OD₇₅₀.

Table S4: Used oligonucleotides, plasmids and strains III.

Oligo name	Sequence	Function	
Fw1_BVMO	AAAGGTCTCGGATGAAAAAACCCAACATCTGG	Construction primer	
Fw2_BVMO	AAAGGTCTCGTGCGACATCGCCACCGATGA	Construction primer	
Fw1_Lactonase	AAAGGTCTCGGATGATAGTGGAGGTTACTAGATG GGCACCTCACCCAATCC	Construction primer	
Fw2_Lactonase	AAAGGTCTCGTGACCTACAAGTCGGAAGTG	Construction primer	
Fw3_Lactonase	AAAGGTCTCGCATGCAGCACGTATCCCGTTCC	Construction primer	
Rev1_BVMO	AAAGGTCTCGCGCAGAAGGTTTTCGAACATG	Construction primer	
Rev2_BVMO	AAAGGTCTCGCTTTTCTATTTTTCGAACTGCGGGTG	Construction primer	
Rev1_Lactonase	AAAGGTCTCGGTCACGTCCTCGGGCTCGAG	Construction primer	
Rev2_Lactonase	AAAGGTCTCGCATGCCGTCACCACCGACAG	Construction primer	
Rev3_Lactonase	AAAGGTCTCGCTTTTCAGGCGCGCTTGAACCAC	Construction primer	
sBVMO1	AAAGGGAATAAGGGCGACAC	Sequencing primer	
sP_110_fw	AATGCAGCTGGCACGACAGG	Sequencing primer	
sP_105_rev	AAAGGTCTCGCTTTTACGCCCGCCCTG	Sequencing primer	
Plasmid name	Characteristics	Function	Reference
pAH063	pPMQAK1_PnrsB_bvmo	Template	Chapter 3
pSEVA_6HA	pSEVA_CL1, <i>lactonase</i> gene from <i>Acidovorax</i> sp. with RBS*	Template	[165]
pGGC_Lvl0	Level 0 Entry vector (#0)	Entry vector	Unpublished data
pGGC_Lvl0_bvmo	Level 0 vector with <i>bvmo</i> gene	Construction	This work
pGGC_Lvl0_lactonase	Level 0 vector with <i>lactonase</i> gene	Construction	This work
pGGC_Lvl0_PnrsB	Level 0 vector with PnrsB (#8)	Construction	Unpublished data
pGGC_Lvl1_Pos3	Level 1 entry vector, Pos. 3 (#3)	Entry vector	Unpublished data
pGGC_Lvl1_Pos4	Level 1 entry vector, Pos. 4 (#4)	Entry vector	Unpublished data
pGGC_Lvl1_Pos5	Level 1 entry vector, Pos. 5 (#5)	Entry vector	Unpublished data
pGGC_Lvl1_PnrsB_2.3	Level 1 PnrsB in Pos. 2.3 (#17)	Construction	Unpublished data
pGGC_Lvl1_EL1-2	Level 1 Endlinker 1→2 (#40)	Construction/Linker	Unpublished data
pGGC_Lvl1_EL6-7	Level 1 Endlinker 6→7 (#44)	Construction/Linker	Unpublished data
pGGC_Lvl1_Tdouble_5	Level 1 Tdouble in Pos. 5	Construction	This work
pGGC_Lvl1_bvmo_3	Level 1 <i>bvmo</i> in Pos 3	Construction	This work
pGGC_Lvl1_lact_4	Level 1 <i>lactonase</i> in Pos 4	Construction	This work
pGGC_Lvl2	pSEVA351, Entry vector (#208)	Backbone	Unpublished data
pAH070	Level 2, empty vector control	Transformation	This work
pAH073	Level 2, <i>bvmo</i> and <i>lactonase</i>	Transformation	This work
Strain	Characteristics	Reference	
<i>E. coli</i> DH5alpha	<i>supE44, ΔlacU169 (80lacZ, ΔM15) hsdR17 recA1 endA1 gyrA96 thi-1 relA1</i>		
<i>Synechocystis</i> sp. PCC 6803	Wild-type	[182]	
<i>Synechocystis</i> sp. PCC 6803 BVMO	<i>Synechocystis</i> containing plasmid pAH063	Chapter 3	
<i>Synechocystis</i> sp. PCC 6803 BVMO:Lactonase	<i>Synechocystis</i> containing plasmid pAH073	This work	
<i>Synechocystis</i> sp. PCC 6803 ctrl	<i>Synechocystis</i> containing plasmid pAH070, empty vector ctrl	This work	

All oligonucleotides were ordered from Eurofins scientific, Luxembourg.

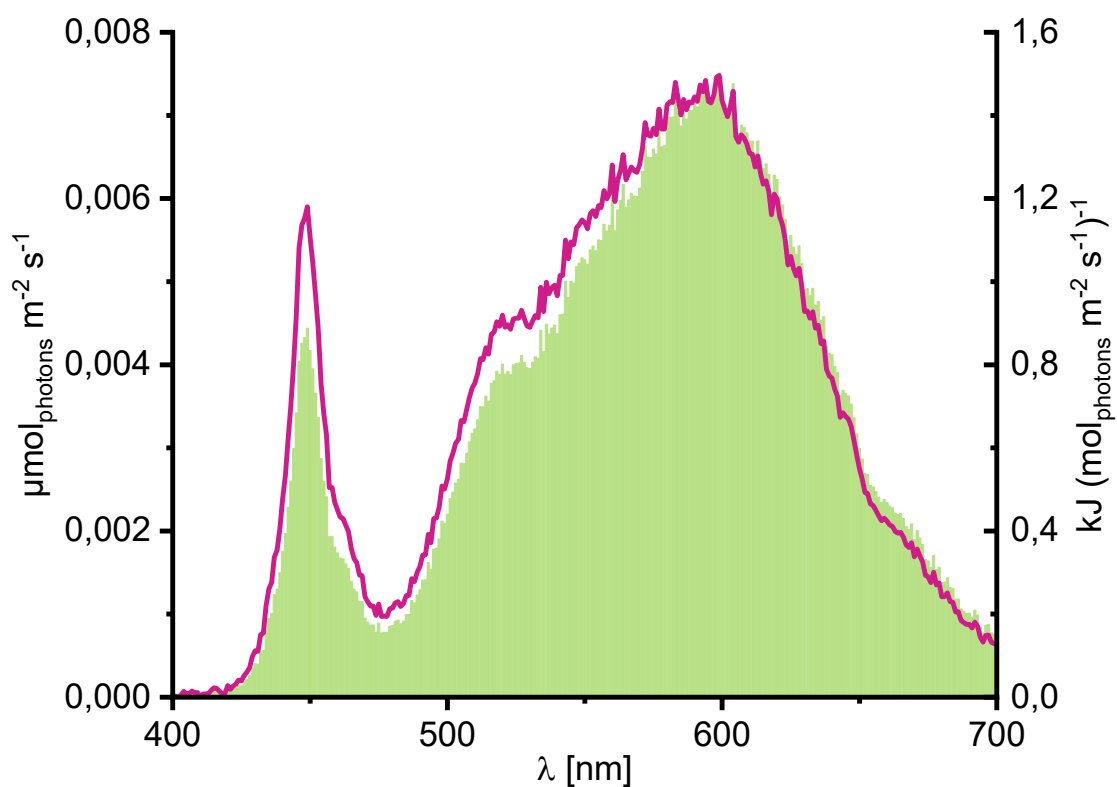


Figure S10: **Emission spectrum of LED unit from used photo-STR** (Infors AG, Bottmingen, Switzerland). Light green: Light intensity in $\mu\text{mol}_{\text{photons}} \text{m}^{-2} \text{s}^{-1}$, normalized to an intensity of 1. Pink: Energy input in kJ per $\mu\text{mol}_{\text{photons}} \text{m}^{-2} \text{s}^{-1}$. The emission spectrum was recorded with a spectroradiometer (Tristan 4.0, m-u-t GmbH, Wedel, Germany) applying an intensity of $10 \mu\text{mol}_{\text{photons}} \text{m}^{-2} \text{s}^{-1}$.

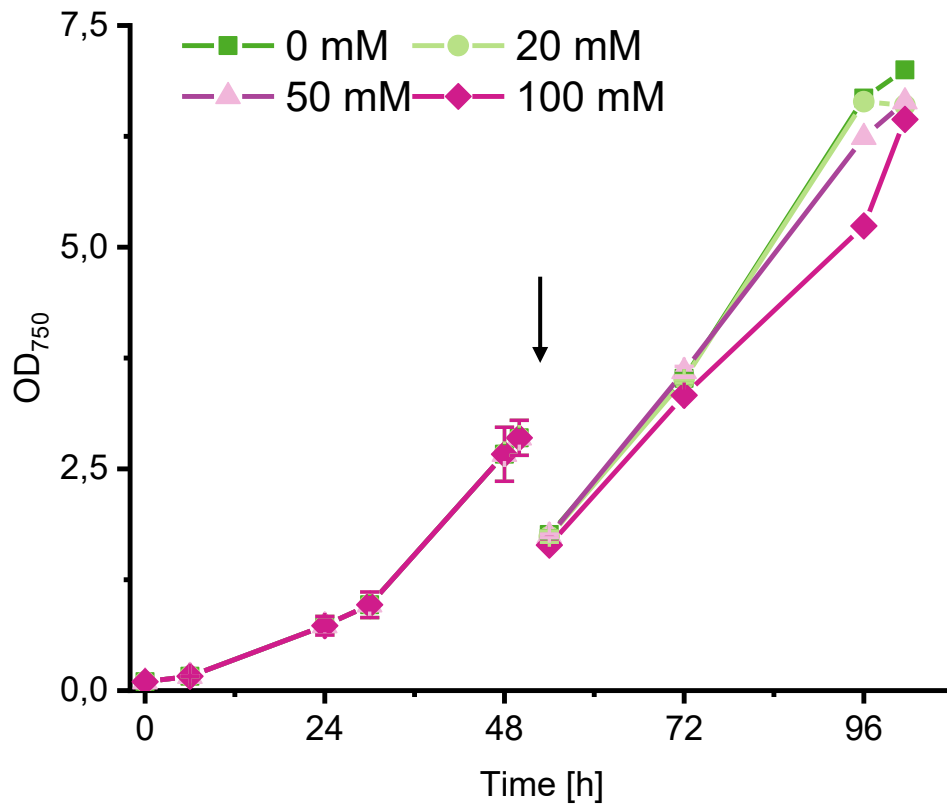


Figure S11: **Effect of 6-hydroxyhexanoic acid (6-HA) on growth of *Synechocystis* BVMO:Lactonase.** Different concentrations of 6-HA (in BG11, buffered to pH=7.5 with NaOH), were added to cultures growing in shakings flask, $50 \mu\text{mol}_{\text{photons}} \text{m}^{-2} \text{s}^{-1}$, 2% CO₂. Black arrow: Time point of 6-HA addition. Depicted are means from ≥ 2 technical replicates.

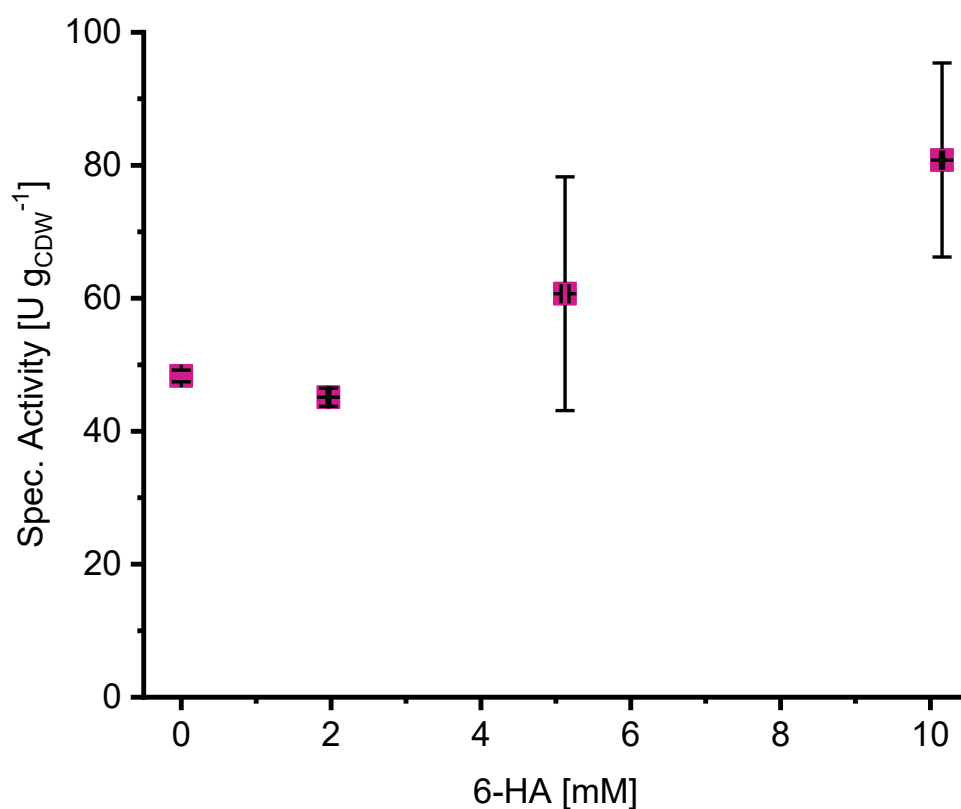


Figure S12: **Effect of 6-HA on conversion of cyclohexanone to 6-hydroxyhecanoic acid (6-HA).** Short-term-assays were conducted with $1.05 \pm 0.01 \text{ g}_{\text{CDW}} \text{ L}^{-1}$ under standards assay conditions. 0, 2, 5, and 10 mM 6-HA were added to the cells prior to equilibration to assay conditions, 10 min before starting the assay by adding 3 mM cyclohexanone. Specific activities were calculated based on the increase of 6-HA during 30 min assay time. Depicted are means from ≥ 2 technical replicates.

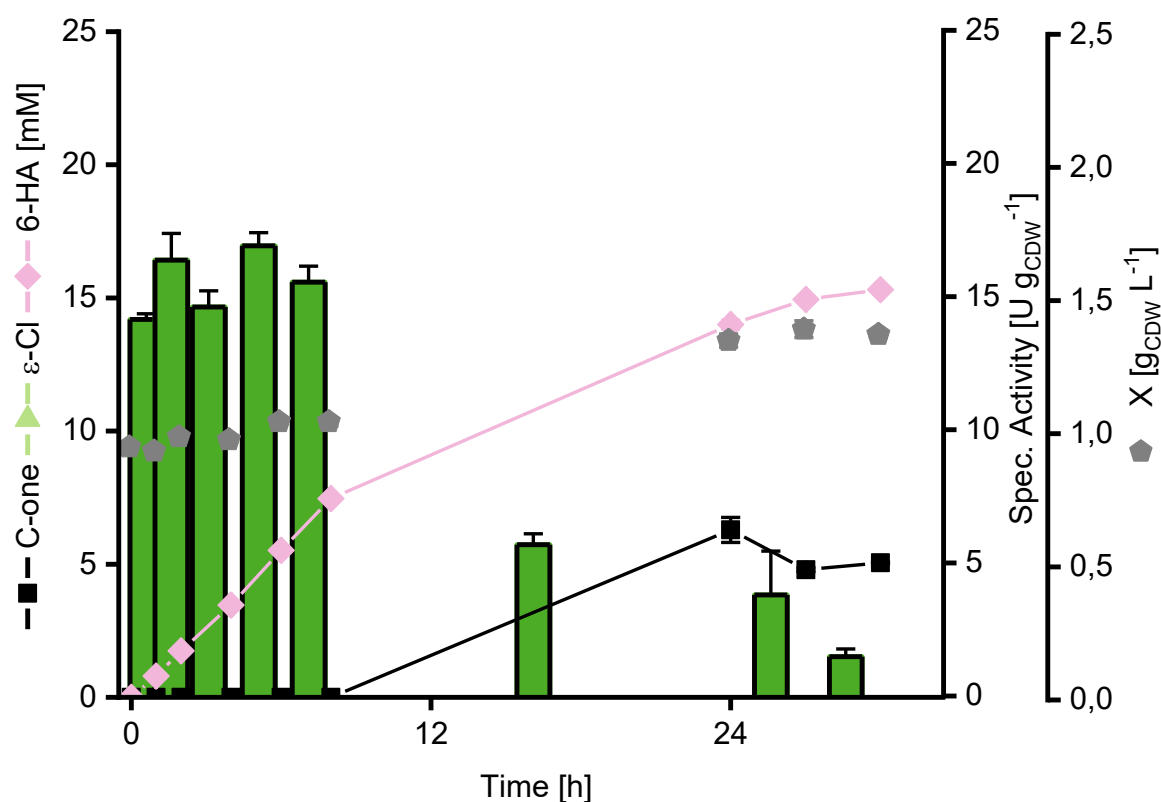


Figure S13: **Photosynthesis-driven two-enzyme process in a 2 L-photo-STR with substrate feed regime matching $15 \text{ U g}_{\text{CDW}}^{-1}$.** *Synechocystis* BVMO was grown for 3 days and induced with $10 \mu\text{M NiSO}_4$. Biotransformation was started 24 h after induction by feeding cyclohexanone (C-one) in a substrate-limited regime matching $15 \text{ U g}_{\text{CDW}}^{-1}$. Courses of cell concentration (grey diamonds), C-one (black squares/line), and 6-hydroxyhexanoic acid (6-HA, rose diamonds/line) concentrations are shown. Specific activities in $\text{U g}_{\text{CDW}}^{-1}$ (green bars) are calculated based on 6-HA formation. Depicted are mean values and standards deviations from ≥ 2 sampling replicates.

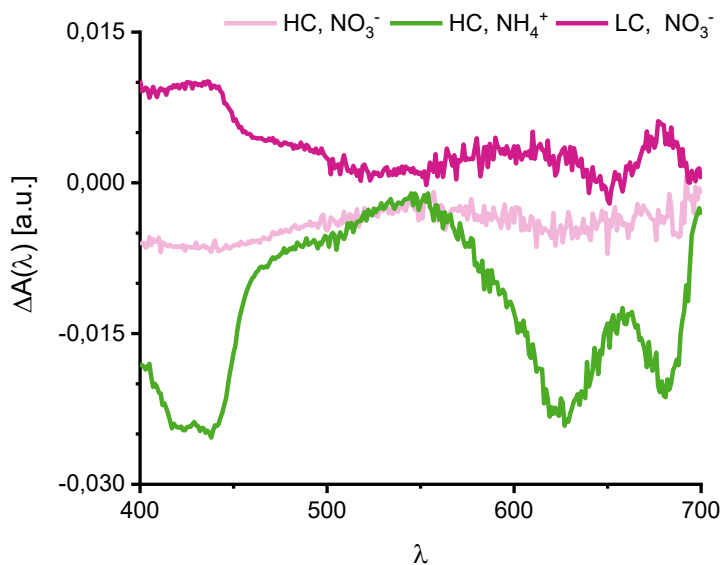


Figure S14: **Specific absorption shifts upon Ni^{2+} -induction under HC/ NO_3^- (pink), HC/ NH_4^+ (green), and LC/ NO_3^- (magenta) conditions.** Absorption spectra were recorded in a GENESYS 150 UV/VIS spectrophotometer (Thermo Fischer Scientific, Waltham, USA) from 700 to 400 nm in one nm intervals. Absorption was normalized to biomass concentration. The depicted $\Delta A(\lambda)$ depicts the change in absorption upon Ni^{2+} induction.

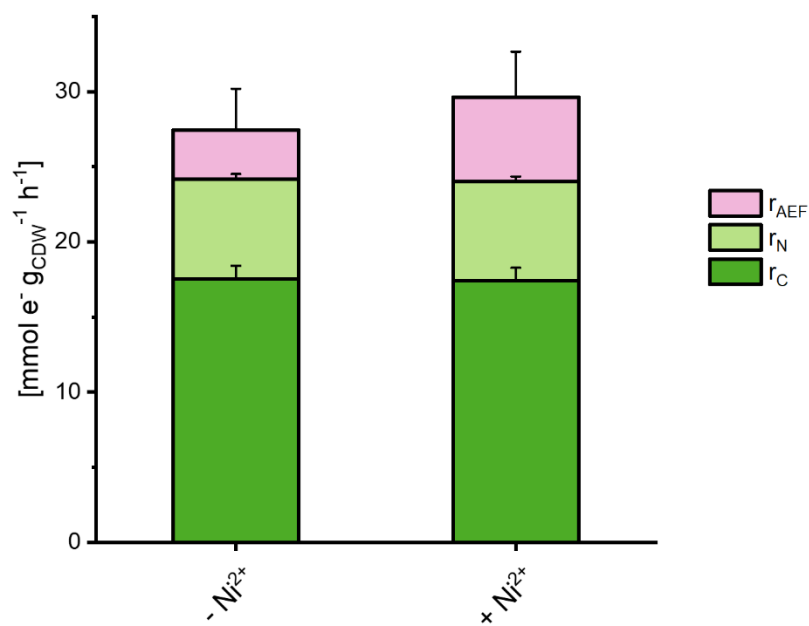


Figure S15: **Electron balancing with *Synechocystis* wildtype without (- Ni²⁺) and with (+ Ni²⁺) 5 μ M NiSO₄.** Steady state data for electron fluxes und HC/NO₃⁻ conditions are depicted. r_{AEF} , alternative electron flux; r_C and r_N , electron flux for carbon and nitrate assimilation, respectively; r_{BT} electron flux into product formation. Data are depicted as mean values and standard deviations from at least three replicates. See experimental section (Chapter 5) for details.

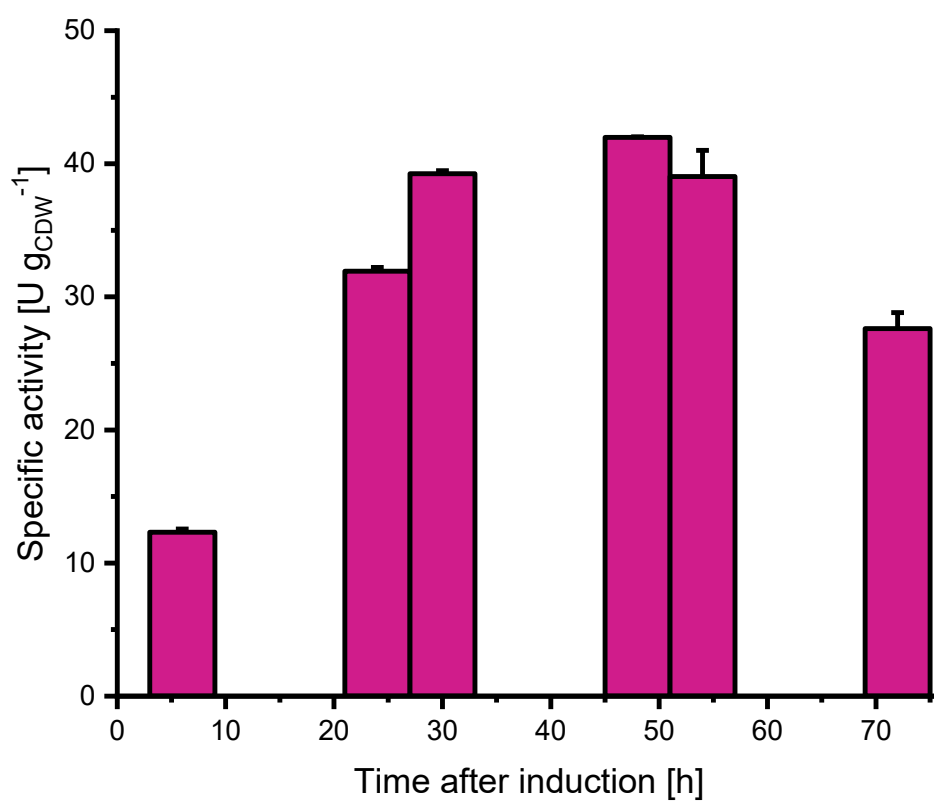


Figure S16: **Induction-time dependent BVMO stability in *Synechocystis_Ni_pBVMO***. BVMO activity was tested in short-term assays with whole-cells of *Synechocystis_Ni_pBVMO* 6, 24, 30, 48, and 72 h after induction of with 10 μM NiSO_4 . Data are depicted as means from ≥ 3 technical replica. 1 U = 1 μmol product formed per min.